16 State House Station
Augusta, Maine 04333

MaineDOT

Transportation Research Division

Technical Report 14-06

Advanced Bridge Safety Initiative

Task 1: Development of Improved Analytical Load Rating Procedures for Flat-Slab Concrete Bridges – A Thesis and Guidelines

Final Report – Task 1, August 2012

Technical Report Documentation Page

1. Report No. ME 14-06	2.	3. Recipient's Accession No.	
4. Title and Subtitle DEVELOPMENT OF IMPROVED ANALYTICAL LOAD RATING PROCEDURES FOR FLAT-SLAB CONCRETE BRIDGES – A Thesis and Guidelines		5. Report Date 2010 6.	
7. Author(s) Timothy J. Poulin Bill Davids, Ph.D., P.E.		8. Performing Organization Report No.	
9. Performing Organization Name and Address University of Maine		10. Project/Task/Work Unit No. Project 017666.00 Task 1 11. Contract © or Grant (G) No. Contract # 20100506*5729	
12. Sponsoring Organization Name and Address Maine Department of Transportation 16 State House Station Augusta, Maine 04333		13. Type of Report and Period Covered 14. Sponsoring Agency Code	
15. Supplementary Notes			

16. Abstract (Limit 200 words)

Current AASHTO provisions for the conventional load rating of flat slab bridges rely on the equivalent strip method of analysis for determining live load effects, this is generally regarded as overly conservative by many professional engineers. As a result there are a significant number of slab bridges in Maine that are (or will be) posted for reduced truck weights, when in reality such postings may not be necessary.

The objective of this study is to verify a program called SlabRate which was created using MATLAB, a numerical computing tool and explore the potential benefits of using it over the conventional strip width method. SlabRate computes the rating factors for simply-supported, continuous flat slab bridges using finite element analysis (FEA). The verification includes creating parallel models of identical bridges in both SlabRate and the commercial software, and comparing the maximum moments and locations of those moments due to a variety of live and dead loads. These models were used to assess SlabRate's finite-element implementation and verify the assumptions that are used in SlabRate. In addition to using commercial software to verify SlabRate, live load testing of a reinforced flat-slab concrete bridge was done, these results were then compared with the predictions of SlabRate. To explore the potential benefits of using SlabRate over the conventional strip width, twenty existing bridges were load rated using both. Twenty one different truck configurations were analyzed, these include AASHTO's design and legal trucks, along with AASHTO's specialized hauling vehicles and MaineDoT's rating trucks.

The results from comparing SlabRate to commercial models and the live load test showed that its finite element implementation is correct for evaluating simply-supported and continuous flat slab bridges. It was also concluded that SlabRate can be reliably used to load rate flat slab bridges having skew angles of 20° or less. Only fourteen bridges of the original twenty bridges met this criteria, of which seven would have rating factors above one using SlabRate while below one using the conventional strip width method.

17. Document Analysis/Descriptors Concrete slab bridges, load rating, finite element analysis		18. Availability Statement	
19. Security Class (this report)	20. Security Class (this page)	21. No. of Pages 286	22. Price

DEVELOPMENT OF IMPROVED ANALYTICAL LOAD RATING PROCEDURES FOR FLAT-SLAB CONCRETE BRIDGES

By

Timothy J. Poulin

B.S. University of Maine, 2010

A THESIS

Submitted in Partial Fulfillment of the

Requirements for the Degree of

Master of Science

(in Civil Engineering)

The Graduate School

The University of Maine

August, 2012

Advisory Committee:

William G. Davids, Professor of Civil Engineering, Advisor

Roberto A. Lopez-Anido, Professor of Civil Engineering

Eric Landis, Professor of Civil Engineering

DEVELOPMENT OF IMPROVED ANALYTICAL LOAD RATING PROCEDURES FOR FLAT-SLAB CONCRETE BRIDGES

By: Timothy J. Poulin

Thesis Advisor: Dr. William Davids

An Abstract of the Thesis Presented
in Partial Fulfillment of the Requirements for the
Degree of Master of Science
(in Civil Engineering)
August, 2012

The Maine Department of Transportation (MaineDoT) is responsible for 2,723 bridges and minor spans, of which 271 are in poor condition and 226 are structurally deficient. The MaineDoT estimates that 288 bridges are at risk of closure or weight restrictions in the next decade. A MaineDoT report titled “Keeping Our Bridges Safe” estimates that funding for bridge replacement and rehabilitation needs to be increased from 70 million per year to 130 million per year to ensure bridge safety and minimize bridge restrictions or closures. Current AASHTO provisions for the conventional load rating of flat slab bridges rely on the equivalent strip method of analysis for determining live load effects, this is generally regarded as overly conservative by many professional engineers. As a result there are a significant number of slab bridges in Maine that are (or will be) posted for reduced truck weights, when in reality such postings may not be necessary.

The objective of this study is to verify a program called SlabRate which was created using MATLAB, a numerical computing tool and explore the potential benefits of using it over the conventional strip width method. SlabRate computes the rating factors

for simply-supported, continuous flat slab bridges using finite element analysis (FEA). The program allows for the definition of a variety of bridge configurations such as span length and width, skew angle, slab thickness etc. A user-friendly graphical user interface has been developed for SlabRate to allow rapid model creation and the review of load rating results. The verification includes creating parallel models of identical bridges in both SlabRate and the commercial software, and comparing the maximum moments and locations of those moments due to a variety of live and dead loads. These models were used to assess SlabRate's finite-element implementation and verify the assumptions that are used in SlabRate. In addition to using commercial software to verify SlabRate, live load testing of a reinforced flat-slab concrete bridge was done, these results were then compared with the predictions of SlabRate. To explore the potential benefits of using SlabRate over the conventional strip width, twenty existing bridges were load rated using both. Twenty one different truck configurations were analyzed, these include AASHTO's design and legal trucks, along with AASHTO's specialized hauling vehicles and MaineDoT's rating trucks.

The results from comparing SlabRate to commercial models and the live load test showed that its finite element implementation is correct for evaluating simply-supported and continuous flat slab bridges. It was also found that the assumptions inherent in SlabRate were also verified, these assumptions were pinned supports, linear elasticity, and small deformations. It was also concluded that SlabRate can be reliably used to load rate flat slab bridges having skew angles of 20° or less. Only fourteen bridges of the original twenty bridges met this criteria, of which seven would have rating factors above one using SlabRate while below one using the conventional strip width method.

ACKNOWLEDGEMENTS

I would like to thank my advisor Bill Davids for his guidance and support throughout this research and thesis writing process. I would like to thank the rest of my committee for their valuable input. This research was aided by the knowledge and labor of staff members at the AEWC.

Funding that made this research possible was provided by Maine Department of Transportation.

TABLE OF CONTENTS

LIST OF TABLES

LIST OF FIGURES

CHAPTER 1. INTRODUCTION

1.1. Project Background

Following the I-35 Minnesota bridge failure, Governor Baldacci issued an Executive Order directing the Maine Department of Transportation (MaineDoT) to review Maine's bridge inspection and programming. The Advanced Bridge Safety Program has been designed to address selected recommendations from the MaineDoT report titled *Keeping Our Bridges Safe* (MaineDoT 2007). The MaineDoT is responsible for 2,723 bridges and minor spans, of which 271 are in poor condition and 226 are structurally deficient. Nine percent of Maine's bridges are over 81 years old and 37% are over 61 years old. The MaineDoT (2007) estimated that 288 bridges are at risk of closure or weight restrictions before 2017. Closing or restricting a bridge places additional hardships on Maine people and Maine companies. The MaineDoT struggles to balance public safety and socioeconomic concerns when faced with bridge closure and load restriction decisions. On the other hand, the cost of replacement or rehabilitation needed to keep such a bridge open to all traffic is extraordinary.

Keeping Our Bridges Safe (MaineDoT 2007) concluded that between 30 and 40 bridges need to be replaced during the decade 2007 - 2017 to reduce additional bridge closures or restrictions. With additional rehabilitation costs, the report estimates that funding for bridge replacement and rehabilitation needs to be increased from $70M/year to $130M/year to ensure bridge safety and minimize bridge restrictions or closures. Subsequent to the report, the Legislature increased funding substantially but short of meeting the needs. They are relying on MaineDoT to continue to find innovations to address this significant problem.

A significant portion of the MaineDoT's bridge inventory that may not have sufficient load-carrying capacity consists of flab slab concrete bridges. Current AASHTO provisions for the conventional load rating of slab bridges rely on the equivalent strip method of analysis for determining live load effects (AASHTO 2008), which has been shown to be conservative compared to more advanced analysis methods (Jáuregui et al. 2007, 2010; Menassa et al. 2007) and also compared to field live load testing (Amer et al. 1999, Saraf 1998). As a result, there are a significant number of slab bridges in Maine that could require posting for reduced truck weights, when in reality such postings may not be necessary. Recent research by Jáuregui et al. (2007, 2010) examined this issue, and found that an 11% - 26% increase in live load capacity for a multi-span slab bridge was justified based on advanced analysis.

The research reported in this thesis supports a larger project designed to assess the safety of flat slab brides in Maine using advanced analysis methods, and to develop non-proprietary methods of strengthening these bridges with fiber-reinforced polymer materials.

1.2. Objective of Thesis

As part of the larger project, the finite element program SlabRate was developed using MATLAB (MathWorks 2009) by Professor William G. Davids, PhD, PE, for the load rating of simply-supported and continuous flat slab bridges. This thesis will present the verification studies performed with SlabRate. These studies include using commercial software to assess SlabRate's finite-element implementation and verify the assumptions that are used in SlabRate. This thesis also presents the results of live load testing of a

reinforced flat-slab concrete bridge, and compares the live load test results with the predictions of SlabRate.

This thesis also explores the potential benefits of using finite-element analysis instead of the equivalent strip method for load rating of flat slab bridges. This will be done by load rating twenty existing bridges using both the equivalent strip method and SlabRate. By using higher-level analysis, it is expected that the rating factors will be less conservative leading to bridges not having to be weight restricted or closed. The following sections will discuss in more detail what is contained in each chapter of this thesis.

1.2.1. Chapter 2: FE Methodology

Chapter 2 outlines how SlabRate works and the underlying code used in the program. It will also include the convergence studies done for SlabRate for both skewed and non-skewed bridges to determine necessary levels of mesh refinement. Independent modeling using commercial finite-element software to verify SlabRate's underlying finite element solver is also addressed. The modeling used both the ANSYS software (ANSYS 2009) and Abaqus software (Abaqus 2009). The ANSYS models provide the verification of the program under the same assumptions used in SlabRate. This is done to verify the implementation of finite element analysis. The Abaqus models explore the verification of the assumptions that were used to create SlabRate.

1.2.2. Chapter 3: Load Rating of Existing Flat-Slab Concrete Bridges

In Chapter 3 twenty existing flat slab concrete bridges will be load rated using both the conventional strip width method (AASHTO 2008) and the SlabRate program.

The conventional strip width method is currently being used by MaineDoT for load rating procedures. The results from both will then be presented and compared to each other to show the benefits of using finite element analysis in load rating existing bridges. The rating factors along with the live load moments will be presented for AASHTO's design and legal loads (AASHTO 2010) and Maine legal loads.

1.2.3. Chapter 4: Field Load Test

The purpose of Chapter 4 is to compare the results from a non-destructive live load test of Bradford Bridge #3430 to the results predicted by finite-element analysis. The chapter will provide details on the live load test, including the equipment used and the resulting strains and a comparison of those results to finite-element model predictions. Twenty-two strain gauges were used during the live load test. Tests were performed for four separate loading cases, with three of those cases being run twice to assess repeatability of results, leading to seven separate live load tests.

1.2.4. Chapter 5: Effect of Skew Angle on FE-Based Load Rating

The finite-element analysis and load ratings detailed in Chapter 3 of this thesis consider only longitudinal bending moments. However, as skew angle increases, the transverse and torsional bending moments become more significant, which may lead to lower rating factors. This is discussed further in Chapter 5. Models are created in Abaqus (Abaqus 2009) for bridges with skews ranging from 0° to 40°. Applied moments and capacities are then calculated for different failure planes taking into consideration the effect of the longitudinal, transverse and torsional moments. Minimum rating factors are then computed and compared to the rating factors when only the longitudinal bending

moment is considered. The goal of this chapter is to provide limitations, if any, to skew angles when considering only longitudinal moments when load rating a slab bridge.

1.2.5. Chapter 6: Conclusions and Recommendations

This chapter provides an overview of important results, conclusions obtained from results, and the future work that could be done to improve the topics discussed in this thesis.

CHAPTER 2. FE METHODOLOGY

2.1. Introduction

The finite element program SlabRate was created using MATLAB (MathWorks 2009) by Professor William G. Davids, PhD, PE, for the load rating of simply-supported and continuous flat slab bridges with one to five spans. SlabRate automatically generates multiple lanes of live loading, allows the definition of a variety of dead loads, and generates a summary of load rating results in an Excel file as well as detailed ASCII text file output for each rating vehicle. A user-friendly graphical user interface was also developed that allows rapid model creation and the review of load rating results.

After SlabRate was developed, the solutions it created had to be verified using commercial software to ensure that the underlying finite-element code is correct. This was done by creating parallel models of identical bridges in both commercial finite element software and SlabRate and comparing the maximum moments and location of those moments due to a variety of live and dead loads.

This chapter will outline how SlabRate works and the underlying code along with the independent modeling with commercial software done to verify SlabRate's underlying finite element solver. The modeling used both ANSYS software (ANSYS 2009) and Abaqus software (Abaqus 2009). It will also include the convergence studies done for SlabRate for both skewed and non-skewed bridges.

2.2. SlabRate FE Software

SlabRate was created to take in any geometry for flat slab bridges with five or less spans and calculate the minimum rating factors based on finite element analysis. To allow

the straightforward analysis for multiple truck positions and a variety of dead loads at any position on the bridge, moment influence coefficients are generated for each node in the model. Using the nodal influence coefficients, moments due to a load at any point in the model may then be easily computed. The mesh is triangulated using a Delaunay triangulation to permit a point load at any point on the deck surface to be easily distributed to the three nodes defining the triangle in which the point load lies. In turn, this allows a uniform patch load to be treated as the sum of a large number of smaller point loads with no need for the finite element mesh and the load patch to be coincident.

SlabRate's graphical user interface is used to input the bridge properties, define the loads, define the mesh and provides the results. The first tab where the bridge properties are defined includes span length, width, slab thickness, curb widths, slab reinforcement and concrete properties, (see Figure 2.1). The second tab is where the loads are defined and is shown in Figure 2.2. The truck definitions are defined using ASCII text files and are loaded in this tab. Curb, rail and wearing surface loads are also described here along with load factors. The third tab is where the meshing parameters are defined and where the analysis is started as seen in Figure 2.3. The final tab is where results of the analysis are displayed and can be seen in Figure 2.4. These results include contour plots for dead and live load moments along with contour plots for rating factors, along with the location of the minimum rating factors for each truck that was specified.

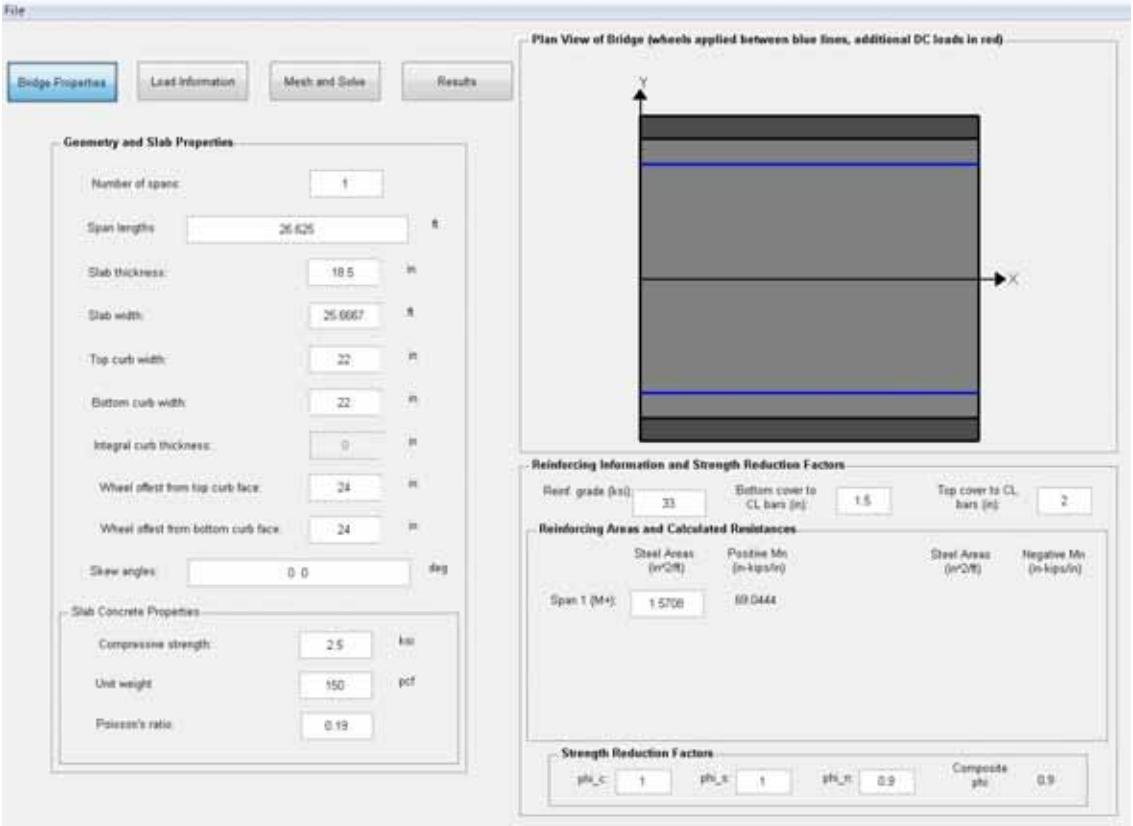

Figure 2.1 – SlabRate's graphical user interface bridge properties tab

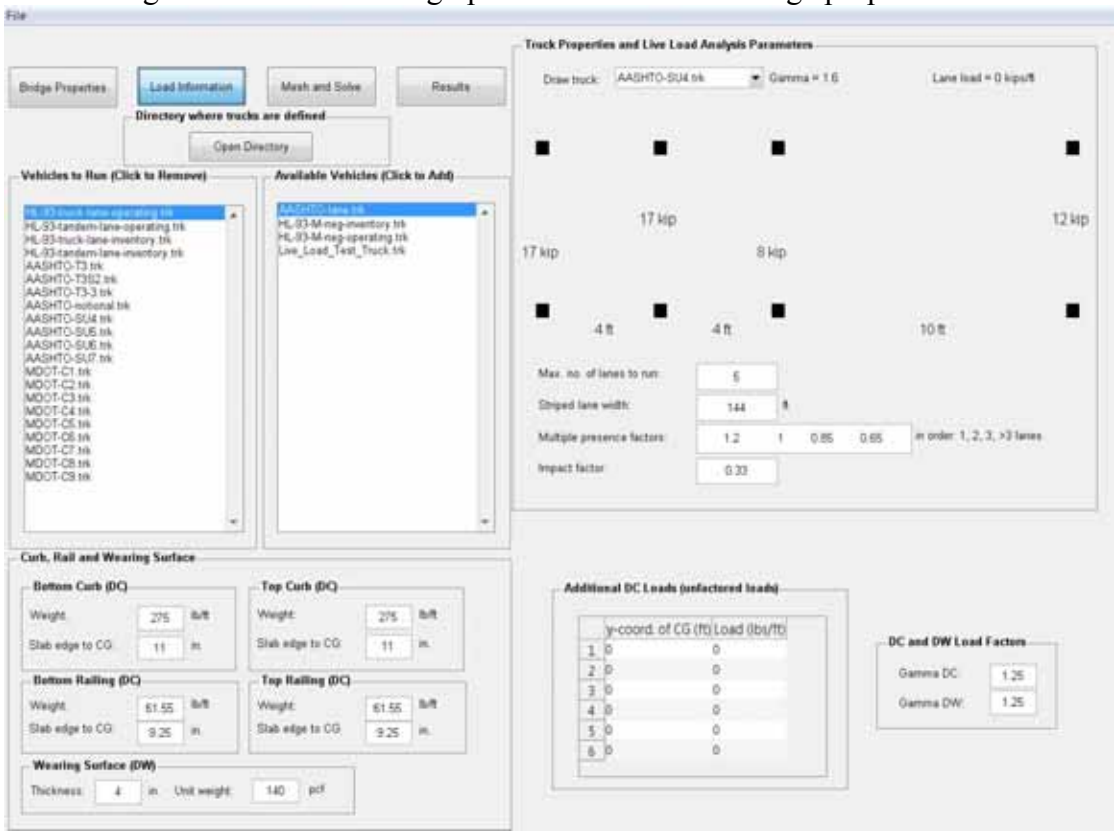

Figure 2.2 - SlabRate's graphical user interface load information tab

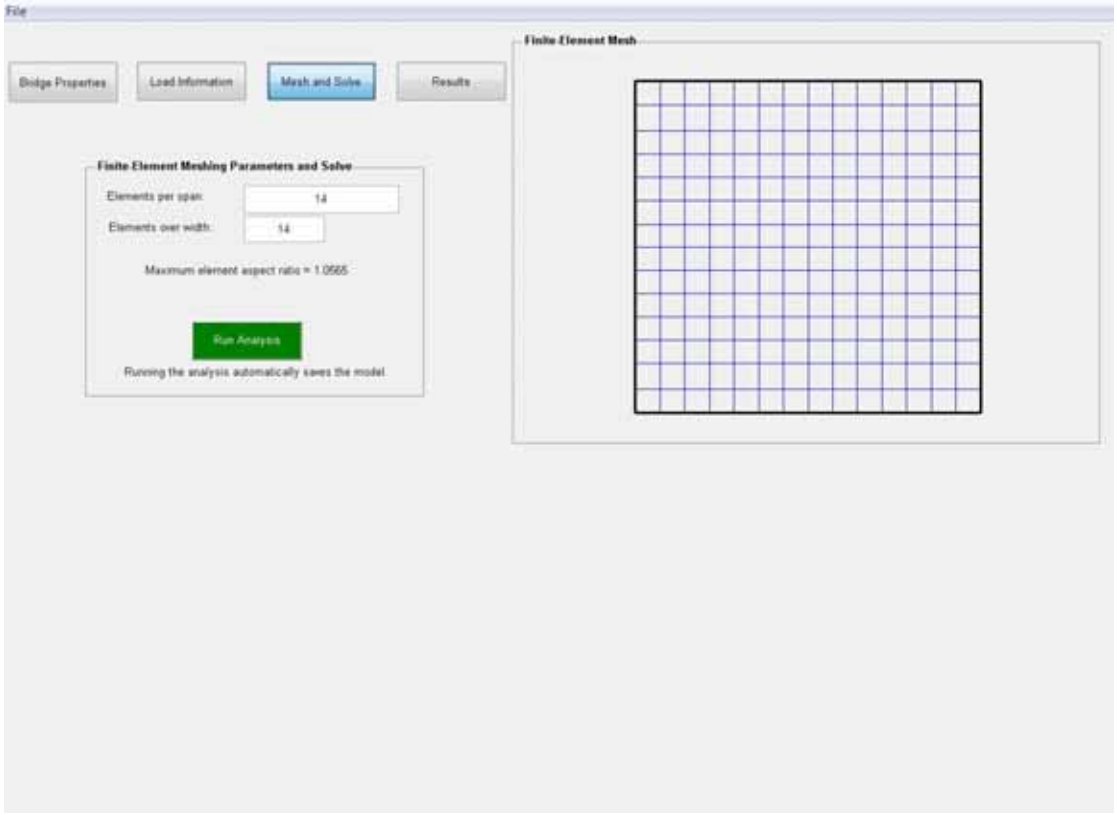

Figure 2.3 - SlabRate's graphical user interface mesh and solve tab

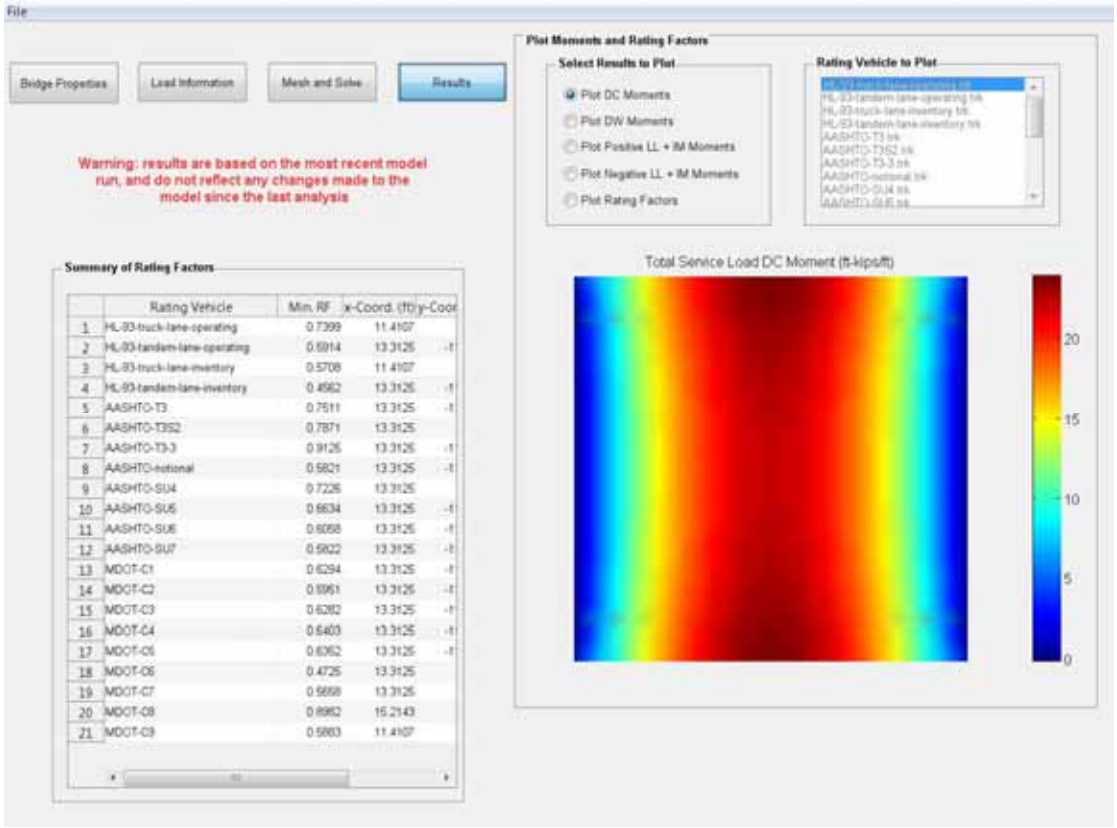

Figure 2.4 - SlabRate's graphical user interface results tab

Dead loads are treated as uniform pressures or uniform line loads. In addition to slab self-weight, the wearing surface, curbs and railings are explicitly considered. Any number of additional uniform line loads can be specified to account for interior barriers, utilities, etc.

Live loads can consist of a truck and a lane load. The maximum number of lanes that will fit on the traveled width is automatically computed, and the bridge is analyzed from one to this maximum number of loaded lanes. Each lane is positioned at multiple locations along the span and across the bridge, including positioning lanes as close as possible to the top and bottom curbs. The truck direction is always left-to-right, but the axle order is automatically run both as defined for the truck and reversed to capture the effect of different travel directions. When loading multiple lanes for a bridge with non-skewed abutments, adjacent trucks are assumed to be in the same x-position. For bridges with skewed abutments, the x-position of adjacent trucks is varied along the span based on the abutment skew angles, which produces larger moments in the slab. Truck axles that do not contribute to the maximum load effect may be either considered or dropped at the option of the user.

Each wheel load is treated as a 25.4 cm x 50.8 cm uniform pressure, which is divided into an 8x16 grid of squares. The uniform pressure acting over each of these 128 squares is then converted to an individual point load, and the moments produced by each point load are determined using pre-computed influence coefficients as detailed previously.

Lane loads are treated as uniform loads acting over a 3.05 m loaded width positioned transversely within each lane to maximize their effect. Load patterns are

automatically generated where all possible combinations of alternate spans are loaded to maximize positive moment, and adjacent spans plus alternate spans are loaded to maximize negative moments at interior piers.

2.2.1. General Assumptions

Four major assumptions were used when developing SlabRate's finite element code. These assumptions are linear elasticity, small deformations, pinned supports and the consideration of only longitudinal bending moments. The assumption of linear elasticity is conservative when computing moments, and these structures do experience small deformations and strains. However, the supports may not be truly pinned, and the slab might lift off part of one or both supports under live loading. This will be examined further in section 2.2.4 with the use of commercial software. The assumption that only longitudinal bending moments must be considered when assessing bridge capacity is discussed more in Chapter 5.

2.2.2. Mesh and Element Types

The underlying finite element model relies on an 8-noded, shear deformable plate element. This element is described in detail in Bhatti (2006). Quadratic shape functions are used for element displacements. To avoid shear locking, the shear contributions to the element stiffness matrix are under-integrated using 2x2 Gaussian quadrature; 3x3 Gaussian quadrature is used for integrating the bending contributions to the element stiffness matrix. An isoparametric element formulation allows the use of non-rectangular elements, which are required when modeling bridges with skewed supports. After solving

for displacements and computing the corresponding moments in each element, nodal averaging of the moments is automatically performed.

The finite element mesh is uniform, although different numbers of elements in the traffic direction may be used for each span (see Figure 2.5 for a plan view of mesh of a 4-span bridge). A single element width is usually assumed under each curb and a single element width is generally used between the face of each curb and the nearest wheel line. (More element widths under the curbs and between the curb face and nearest wheel line may be used to maintain good element aspect ratios when a large number of elements are used.) The global coordinate system used in the model definition and in model output has its origin centered on the left-most pier, with *x* positive to the right and *y* positive upward as shown in Figure 1. Pinned supports are assumed at all piers.

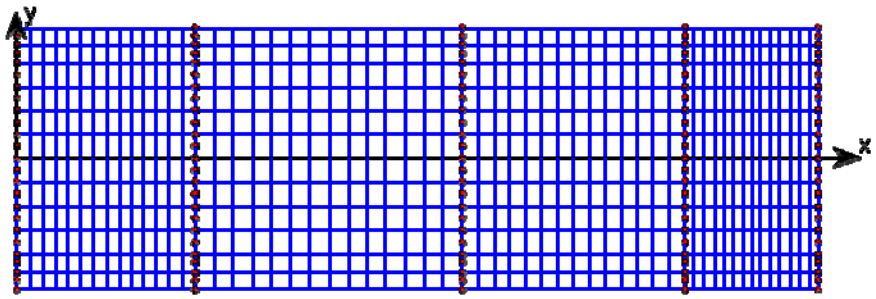

Figure 2.5 - Mesh of four-span continuous slab bridge

2.2.3. SlabRate Convergence Studies

Before any finite element load ratings were completed, a mesh refinement study was done to determine how many elements are needed in both the longitudinal and transverse directions for both skewed and non skewed bridges. A mesh size needs to be found such that the rating factors, live load moments and dead load moments have converged to a relatively constant value. The more elements that are used in the analysis

the more precise the results will be; however adding elements increases the computational time. The reason for convergence studies is to ensure that the results have converged to relatively consistent values without incurring excess computation time.

2.2.3.1. Non-Skewed Bridge

Two bridges were used for the convergence study of non-skewed bridges: Argyle Township Bridge #3827 and Levant Bridge #5253. The bridge characteristics used in this convergence study can be seen in Table 2.1. A concrete compressive strength of 17.23 MPa and steel reinforcing yield strength of 227 MPa were used for both bridges. An elastic modulus of 19640 MPa was also used for both bridges along with a Poisson's ratio of 0.19 and a unit weight of concrete of 2400 kg/m^3. The rail weights were modeled as a constant distributed load, determined by finding the maximum moment due to the real rail weights than computing the constant distributed load that would provide the same maximum moment.

Table 2.1 – Bridge characteristics for bridges used in the convergence study for non-skewed bridges for SlabRate

Bridge	Argyle Township #3827	Levant Bridge #5253
Span Length (m)	6.664	8.115
Bridge Width (m)	8.434	7.824
Slab Thickness (m)	0.406	0.470
Wearing Surface Thickness (m)	0.102	0.102
Moment Resistance (kN-m / m)	288.7	307.12
Rail Weights (kN/m) (Top / Bottom)	2.810 / 2.810	0.898 / 0.898
Top Curb Height / Width (m)	0.330 / 0.343	0.305 / 0.559
Bottom Curb Height / Width (m)	0.330 / 0.343	0.305 / 0.559
Striped Lane Offset (m) (Top / Bottom)	0.914 / 1.041	0.610 / 0.610

2.2.3.1.1. Mesh Study for Argyle Bridge #3827

The live load moments on the Argyle Township Bridge #3827 are shown in Figure 2.6 and Figure 2.7 below. An HL-93 truck and tandem, along with lane loads, were used in the analysis. The number of longitudinal elements tested in this convergence study ranged from 6 to 22 elements in increments of 4 elements. For each of the different longitudinal meshes sizes the number of the transverse elements also ranged from 6 to 22.

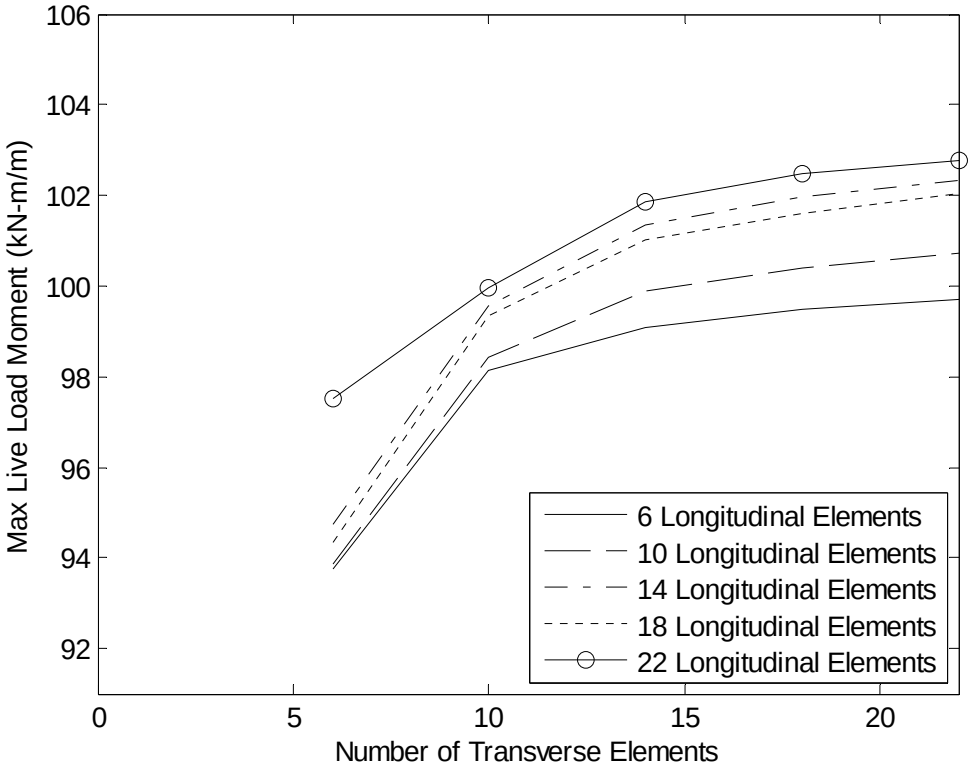

Figure 2.6 - Effects on max live load moment with an increase in mesh elements under HL-93 truck and lane load for Argyle Township Bridge #3827

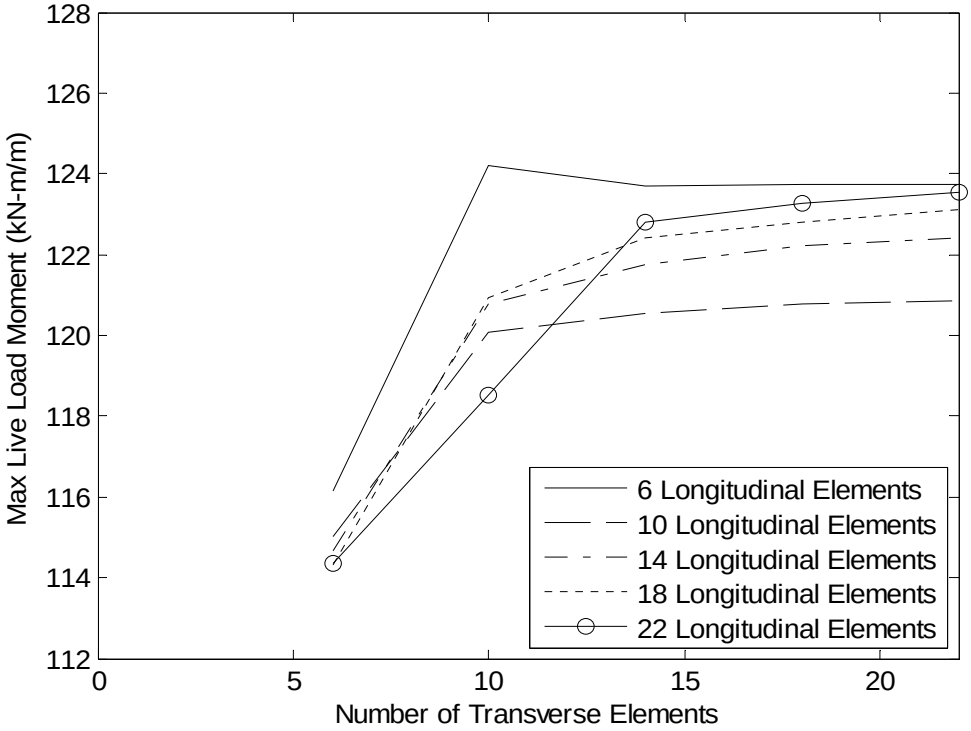

Figure 2.7- Effects on max live load moment with an increase in mesh elements under HL-93 tandem and lane load for Argyle Township Bridge #3827

As seen in Figure 2.6 and Figure 2.7, both the number of longitudinal and transverse elements have an effect on the maximum live load determined from the FEA model SlabRate. The graphs show that the live load moment for both HL-93 truck and tandem, both with lane load, converge to a relatively constant value at 14 longitudinal and 14 transverse elements. A difference in live load moment of 2.3% and 1.6% are seen from 6 to 14 longitudinal for HL-93 truck and HL-93 tandem loads respectively, both with 14 transverse elements. Only a 0.5% and 0.8% difference from 14 to 22 longitudinal elements was seen for HL-93 truck and tandem load, respectively. There is a 7.0% difference for HL-93 truck load and 6.2% difference for HL-93 tandem load while going from 6 to 14 transverse elements while 14 longitudinal elements are used, and only 1.0% and 0.5% differences are seen between 14 and 22 transverse elements.

Figure 2.8 – Figure 2.13 show the rating factors for Argyle Township Bridge #3827 for the HL-93 truck and tandem live loads for different mesh sizes. The rating factors for both loading cases for both inventory and operating follow the same pattern as the live load moments. They also show that the rating factors converge to a relatively constant value when 14 longitudinal and 14 transverse elements are used. This is because the dead load moments are remaining relatively constant irrespective of mesh refinements, so changes in live load moment are the primary driver of changes in the rating factor. Analyses of several bridges – both skewed and non-skewed – provide similar results, and therefore the remainder of the convergence studies will examine only live load moments.

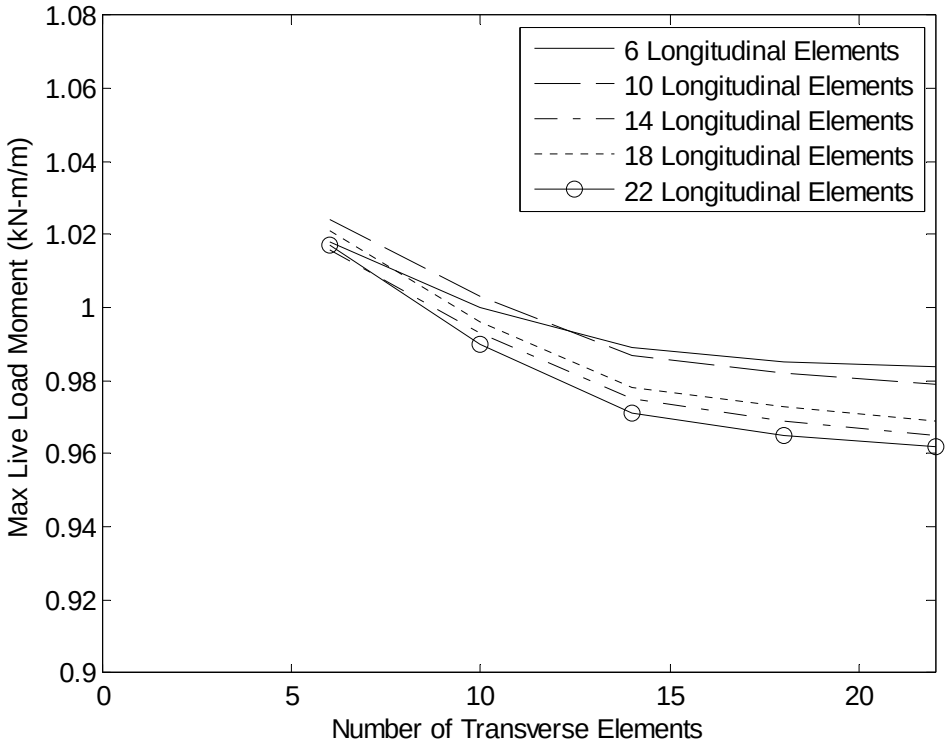

Figure 2.8 - Effects on inventory rating factor with an increase in mesh elements under HL-93 truck and lane load for Argyle Township Bridge #3827

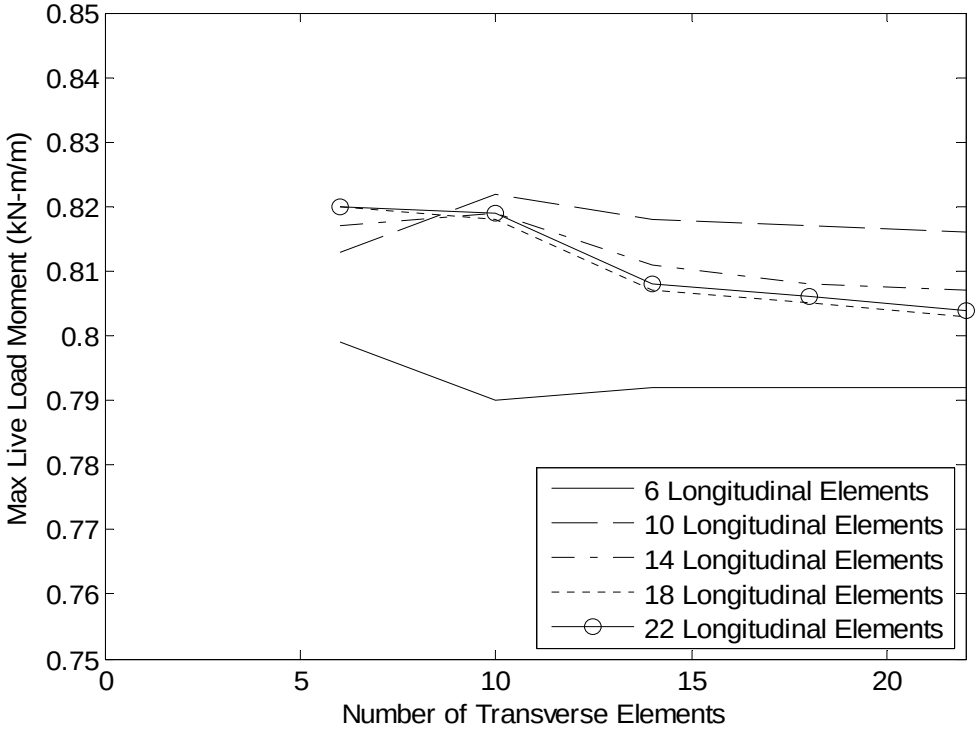

Figure 2.9 - Effects on inventory rating factor with an increase in mesh elements under HL-93 tandem and lane load for Argyle Township Bridge #3827

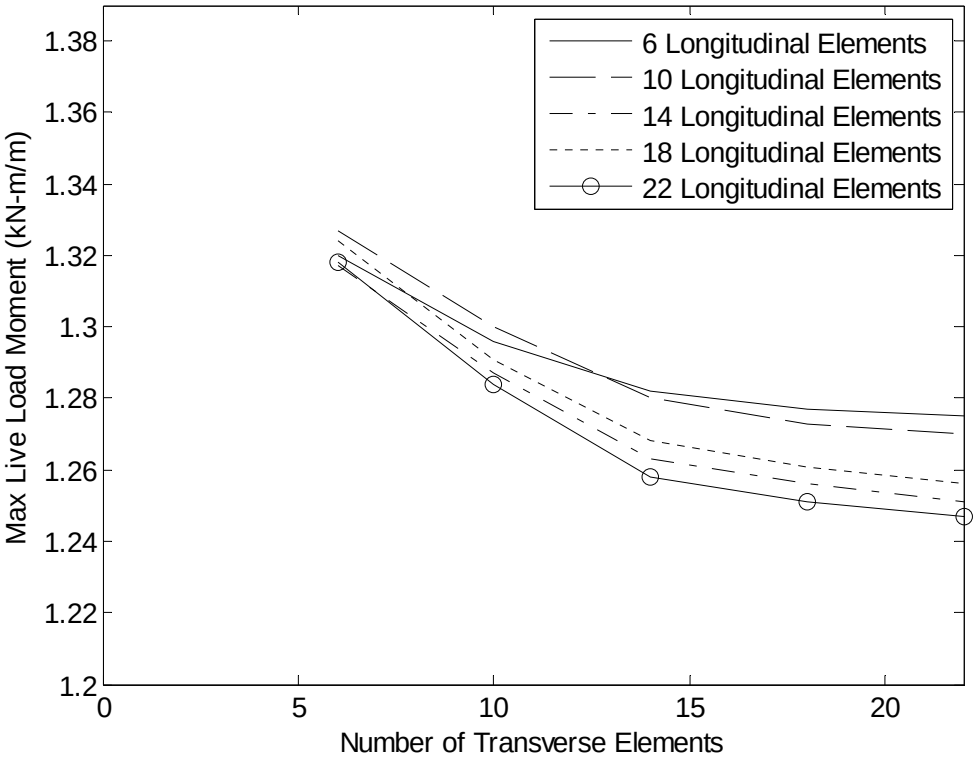

Figure 2.10 - Effects on operating rating factor with an increase in mesh elements under HL-93 truck and lane load for Argyle Township Bridge #3827

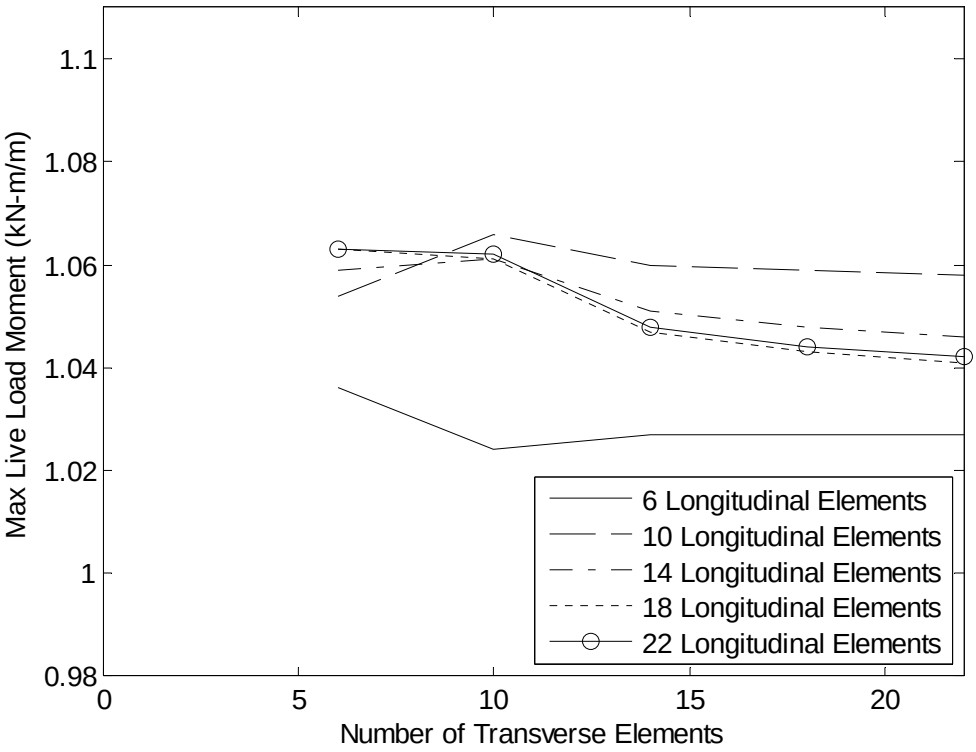

Figure 2.11- Effects on operating rating factor with an increase in mesh elements under HL-93 tandem and lane load for Argyle Township Bridge #3827

2.2.3.1.2. Mesh Study for Levant Bridge #5253

Levant Bridge #5253 maximum live load moments follow the same pattern as Argyle Bridge #3827, Figure 2.12 and Figure 2.13 show the maximum live load moments for Levant Bridge #5253. The bridge appears to converge to a relatively constant value when 10 longitudinal and 10 transverse elements are used. Since Argyle Bridge #3827 converged to a relatively constant value while using 14 longitudinal and 14 transverse elements, the study will show the difference up to and after using 14 elements. Levant Bridge #5253 sees a difference in live load moment of 9.2% and 2.5% when increasing from 6 to 14 longitudinal for HL-93 truck and HL-93 tandem respectively, both including lane load. While only a 1.4% and 0.3% difference for HL-93 truck and HL-93 tandem load respectively while increasing the number of longitudinal elements from 14 to 22. When increasing the number transverse elements from 6 to 14 an increase of 7.0% and 6.2% in live load moment was seen for HL-93 truck and tandem loads respectively. While only a 1.3% and 0.9% difference were seen between 14 and 22 transverse elements.

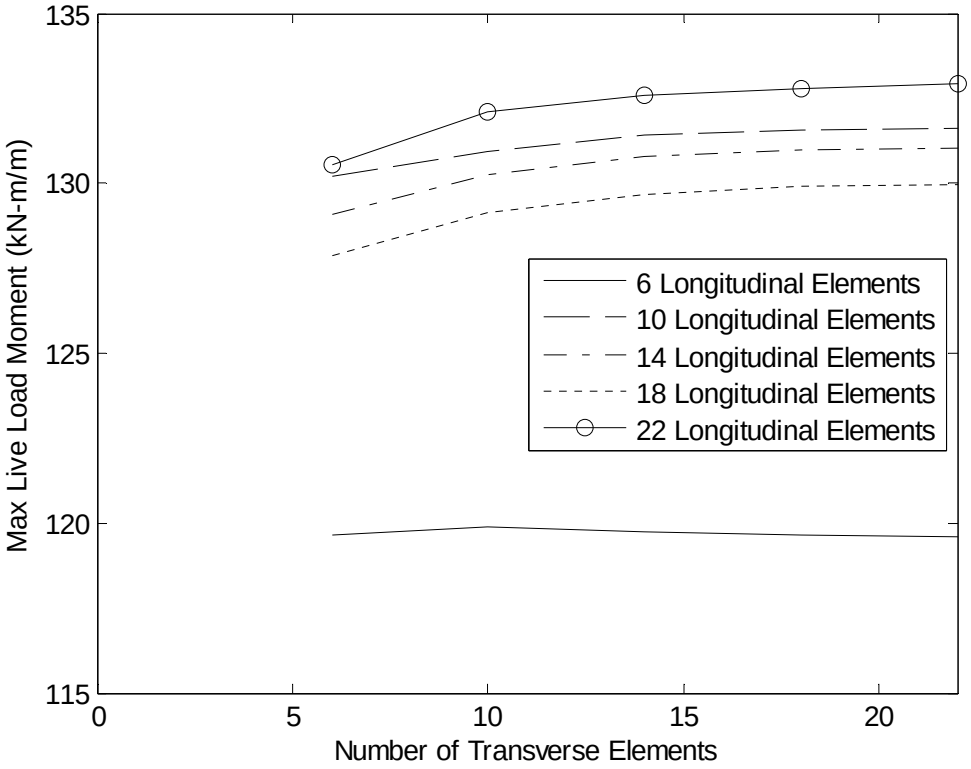

Figure 2.12 - Effects on max live load moment with an increase in mesh elements under HL-93 truck and lane load for Levant Bridge #5253.

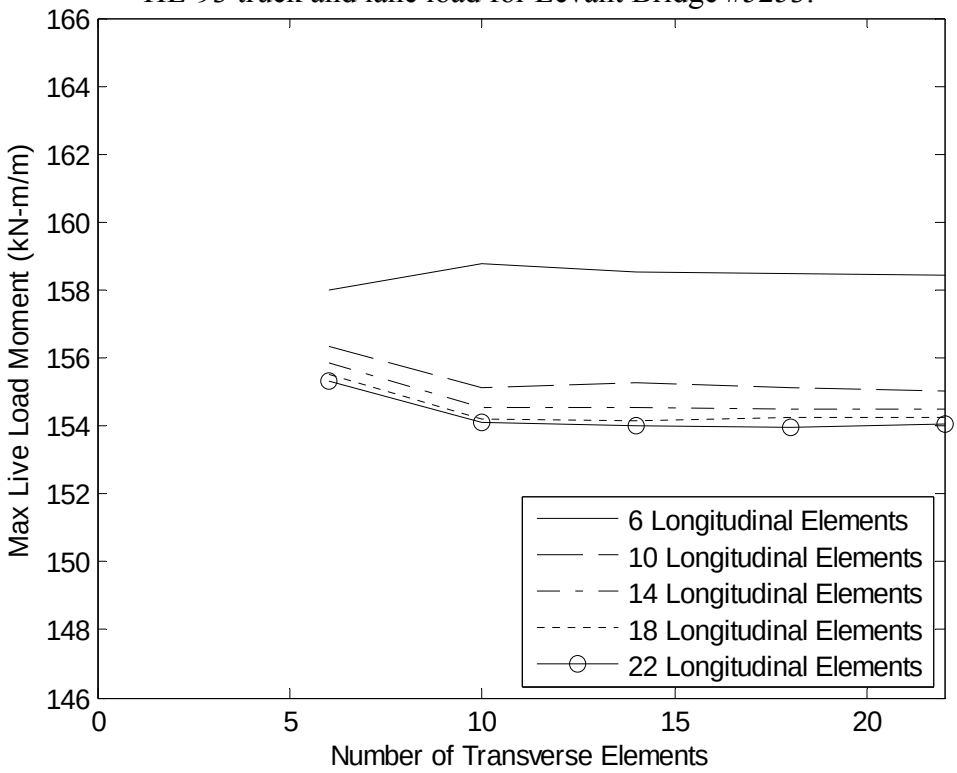

Figure 2.13 - Effects on max live load moment with an increase in mesh elements under HL-93 tandem and lane load for Levant Bridge #5253.

2.2.3.1.3. Mesh Recommendation for Non-Skewed Bridges

From this study and more testing that was done using SlabRate it was found that the number of both longitudinal and transverse elements has an effect on live load moments and rating factors. For final results the mesh should consist of at least 14 longitudinal and 14 transverse elements. Fewer elements can be used for initial analyses to decrease the computational time and estimate an initial rating factor, but is not recommended to use those results for the final rating. For particularly long or wide bridges (structures with a large planar aspect ratio), the number of elements in either the longitudinal or transverse directions may need to be increased to maintain element aspect ratios less than or equal to three and ensure good element accuracy.

Figure 2.14 and Figure 2.15 below show the recommended mesh sizes for Levant Bridge #5253 and Argyle Township Bridge #3827.

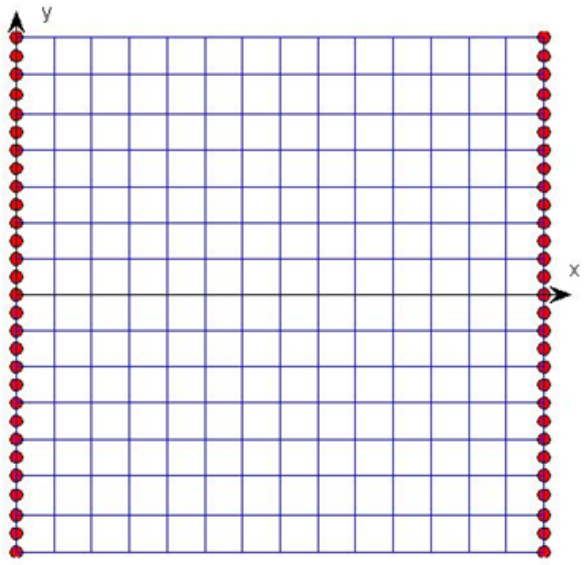

Figure 2.14 – Levant Bridge #5253 recommended finite element mesh, 14 longitudinal elements and 14 transverse elements.

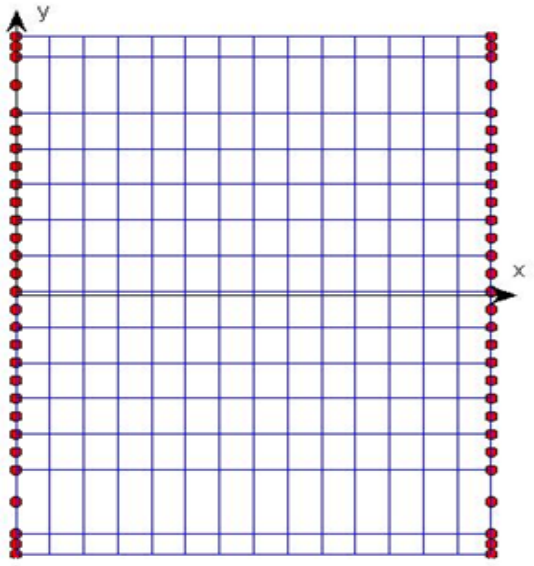

Figure 2.15 – Argyle Township Bridge #3827 recommended finite element mesh, 14 longitudinal elements and 14 transverse elements.

2.2.3.2. Skewed Bridge

Two different bridges, each with two separate skew angles, were analyzed to determine the required degree of mesh refinement in both the longitudinal and transverse direction for skewed bridges. The bridges that were analyzed were a modified Brewer Bridge #5638, at skew angles of 45° and 20°, and Carmel Bridge #5191, at skew angles of 45° and 30°.

2.2.3.2.1. Mesh Study for Modified Brewer Bridge #5638

The Brewer Bridge span length is 7.042 m from centerline to centerline of the supports and the bridge width is 11.43 m. The slab thickness is 0.349 m, with reinforcing providing a moment resistance of 314.66 kN-m/m along with a wearing surface thickness of 0.051 m. To keep the bridge symmetric for simplicity, the bridge curb widths were

taken as 1.067 m, the smaller of the two curb widths of the actual bridge, with a curb height of 0.305 m. The edge of lane offset from the curb was taken as 0.610 m, and rail weights were not used for simplicity. An elastic modulus of 19640 MPa was used along with a Poisson's ratio of 0.19 and a unit weight of 2400 kg/m^3 was used for the concrete. Two separate skew angles were used, 45° and 20° (45° is the skew of the actual bridge).

Design Loads, HL-93 truck and tandem along with lane loads, were used in the analysis. The live load moments of the Brewer Bridge with a 45° for different mesh sizes are shown in Figure 2.16 and Figure 2.17 for HL-93 truck and tandem loads.

The mesh sizes that were used are 14 to 20 longitudinal elements with an increment of 2 elements. A range of 10 to 52 transverse elements were also used in the study. The number of longitudinal and transverse elements was always taken as even so there is a node at the center of the bridge.

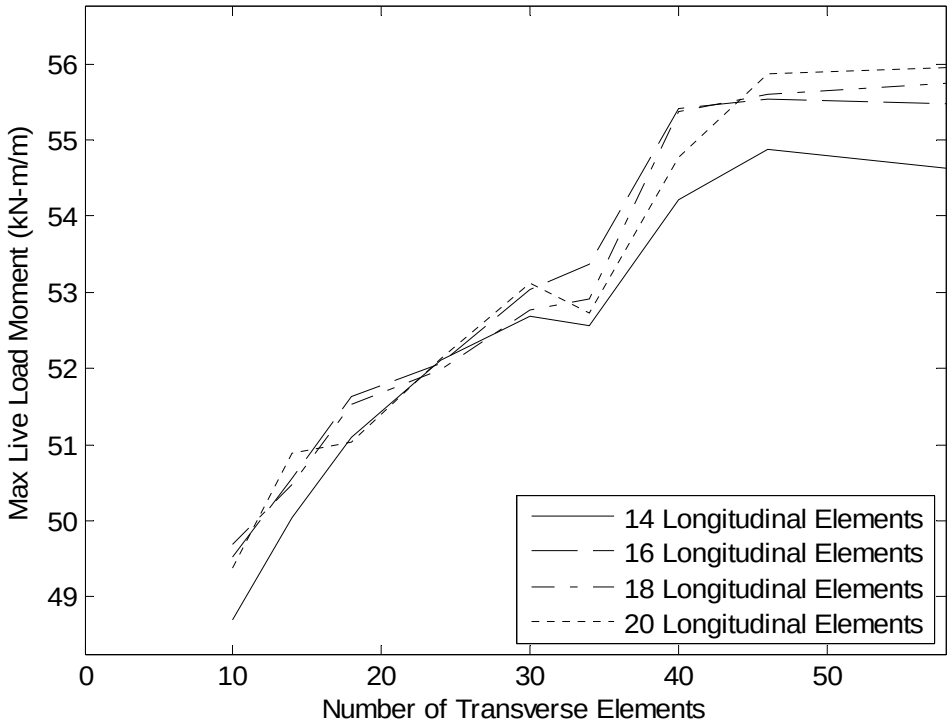

Figure 2.16 - Effects on max live load moment with an increase in mesh elements under HL-93 truck and lane load for Brewer Bridge #5638, skew of 45°

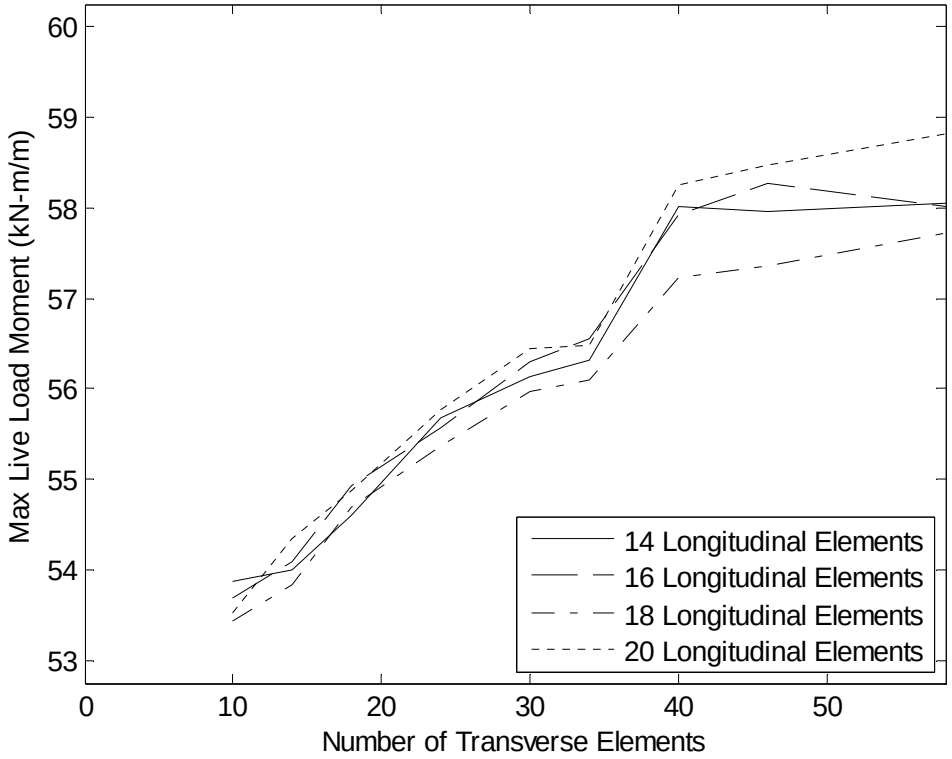

Figure 2.17 - Effects on max live load moment with an increase in mesh elements under HL-93 tandem and lane load for Brewer Bridge #5638, skew of 45°

As the graphs show, the number of longitudinal elements has minimal affect on the maximum live load moment, an average of 1.4% and 0.6% increase from the smallest to the largest live load moment for HL-93 truck load and HL-93 tandem load respectively. The number of transverse elements has a much greater affect on the max live load moments. As seen from the graph the moment starts to converge to a relatively constant value at 40 transverse elements. The live load moment increases by an average of 11.4% for the HL-93 truck and 7.9% for the HL-93 tandem going from 10 to 40 transverse elements while only a 0.9% and 0.5% increase from 40 to 52 elements.

The Brewer Bridge was also analyzed with a skew angle of 20° while keeping all other aspects of the bridge the same. The results for the live load moments for different mesh sizes are shown below in Figure 2.18 and Figure 2.19.

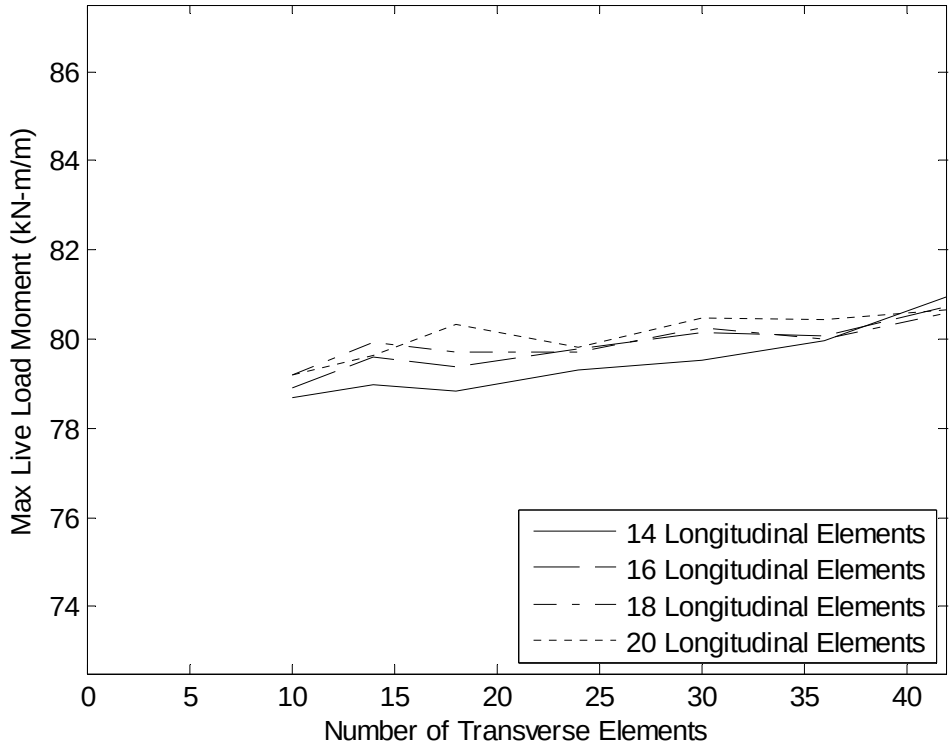

Figure 2.18 - Effects on max live load moment with an increase in mesh elements under HL-93 truck and lane load for Brewer Bridge #5638, skew of 20°

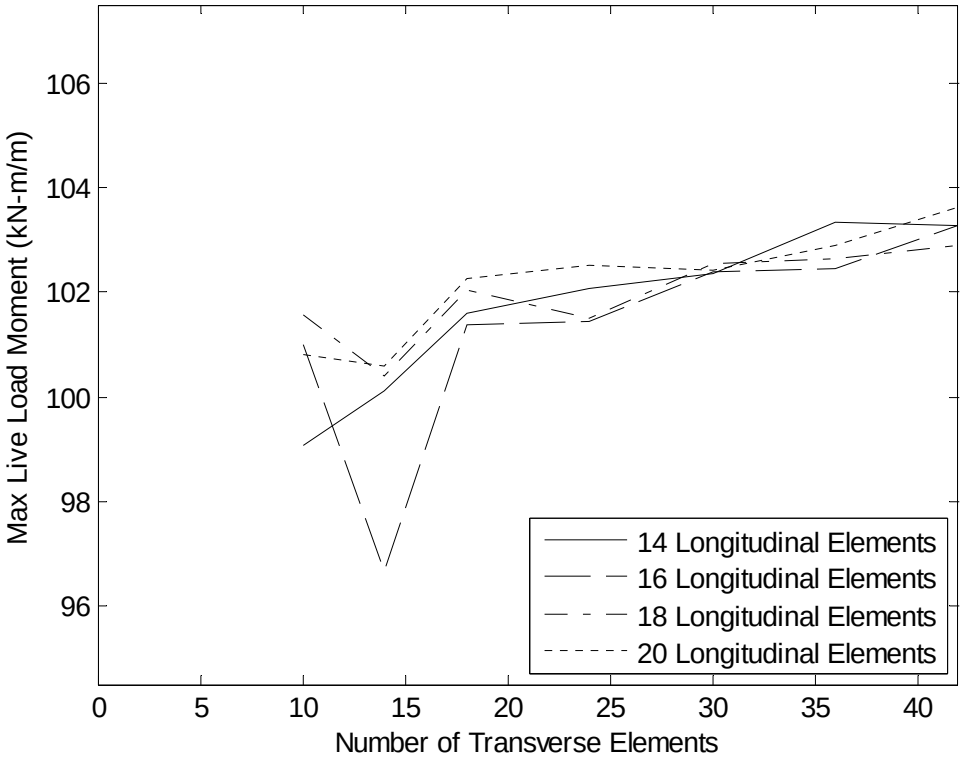

Figure 2.19 - Effects on max live load moment with an increase in mesh elements under HL-93 tandem and lane load for Brewer Bridge #5638, skew of 20°

With a decrease in a skew angle it was found that the effects of mesh refinement decreased significantly. The average percent increase in live load moment from 10 transverse elements to 42 transverse elements is 1.7% and 2.0% for HL-93 truck and HL-93 tandem respectively. Also the average percent increase from the smallest live load moment to the largest live load moment for the same number of transverse elements are 0.9% for HL-93 truck load and 1.5% for HL-93 tandem load. The 20° skew leads to the convergence of the moments with a smaller amount of elements in comparison to the 45° skew.

2.2.3.2.2. Mesh Study for Carmel Bridge #5191

The Carmel Bridge span length is 10.16 m from centerline to centerline of the supports and a bridge width of 7.80 m. The slab thickness is 0.559 m deep, with reinforcing to provide a moment resistance of 468 kN–m/m with a wearing surface of 0.102 inches. The width of the bridge curbs were taken as 0.330 m, with a curb height of 0.305 m. The edge of lane offset from the curb was taken as 0.711 m for the top curb and 0.914 m for the bottom curb, and rail weights of 99.0 kN/m were placed 0.133 m from each edge of the slab. An elastic modulus of 19640 MPa was used along with a Poisson's ratio of 0.19 and a unit weight of 2400 kg/m^3 was used for the concrete.

The same loads were applied to the Carmel Bridge as were applied to the Brewer Bridge (HL-93 truck load and a HL-93 tandem load). Both of these loads include the design lane live load. The live load moments for the actual Carmel Bridge with a skew of 30° are shown in Figure 2.20 and Figure 2.21 for different mesh sizes.

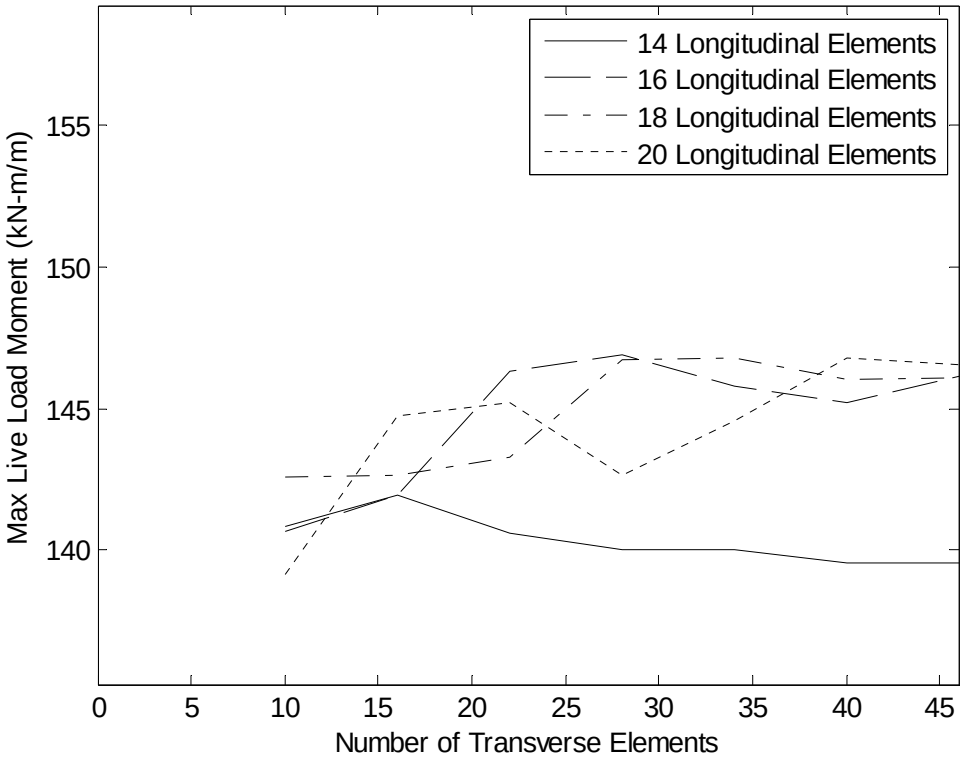

Figure 2.20 - Effects on max live load moment with an increase in mesh elements under HL-93 truck and lane load for Carmel Bridge #5191, skew of 30°

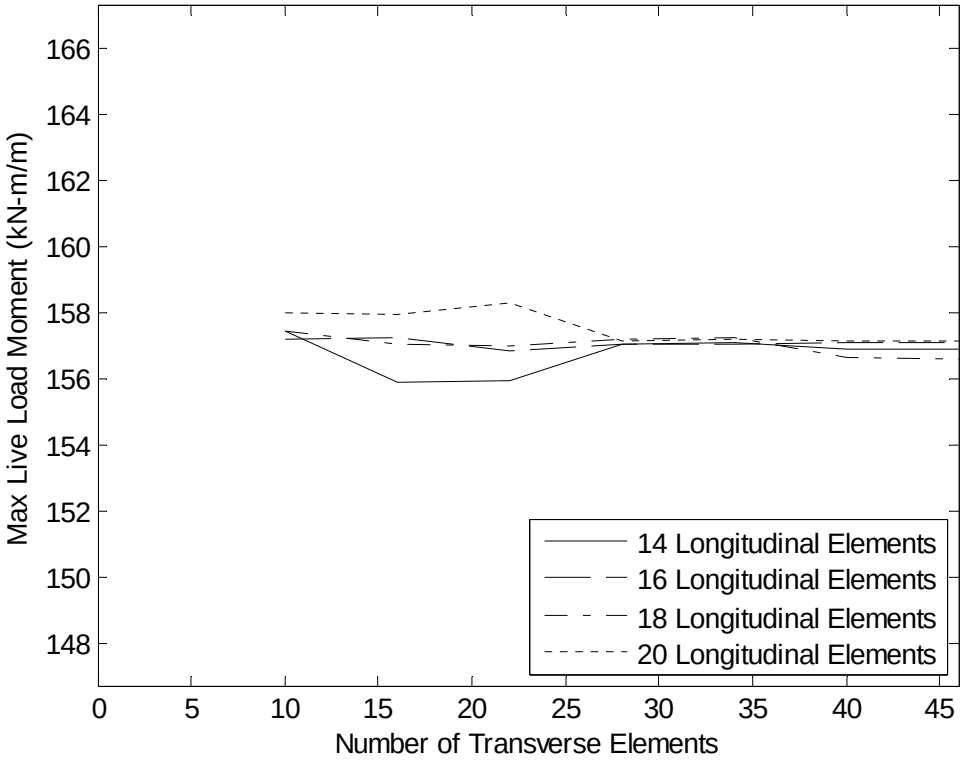

Figure 2.21 - Effects on max live load moment with an increase in mesh elements under HL-93 tandem and lane load for Carmel Bridge #5191, skew of 30°

Effects on the live load moment due to different size meshes for the Carmel Bridge #5191 with a 30° skew seem to be somewhat inconsistent. While looking at the 14 longitudinal elements for the HL-93 truck load, the live load moment decreases as more transverse elements are added, a 0.9% decrease from 10 transverse elements to 40 transverse elements. This does not follow the normal pattern of all the other bridges with different numbers of longitudinal elements; all others see an increase in live load moment while increasing the amount of transverse elements. The mesh configurations with 16, 18 and 20 longitudinal elements all follow the same pattern as all other bridges by increasing and converge to a relative maximum live load moment as more elements are added. The relative maximum live load for Carmel Bridge #5191 with a skew of 30° under HL-93 truck and lane load is 146.1 kN-m/m an average increase of 3.9% from 14 transverse to 40 transverse elements. The HL-93 tandem load seems to have already converged to a constant value by 10 transverse elements for all longitudinal mesh configurations, an average change of -0.2% from 10 to 40 transverse elements.

Carmel Bridge #5191 was also analyzed under a 45° skew while keeping all the other characteristics of the bridge the same. The results of the SlabRate live load moments with different mesh size are shown in Figure 2.22 and Figure 2.23.

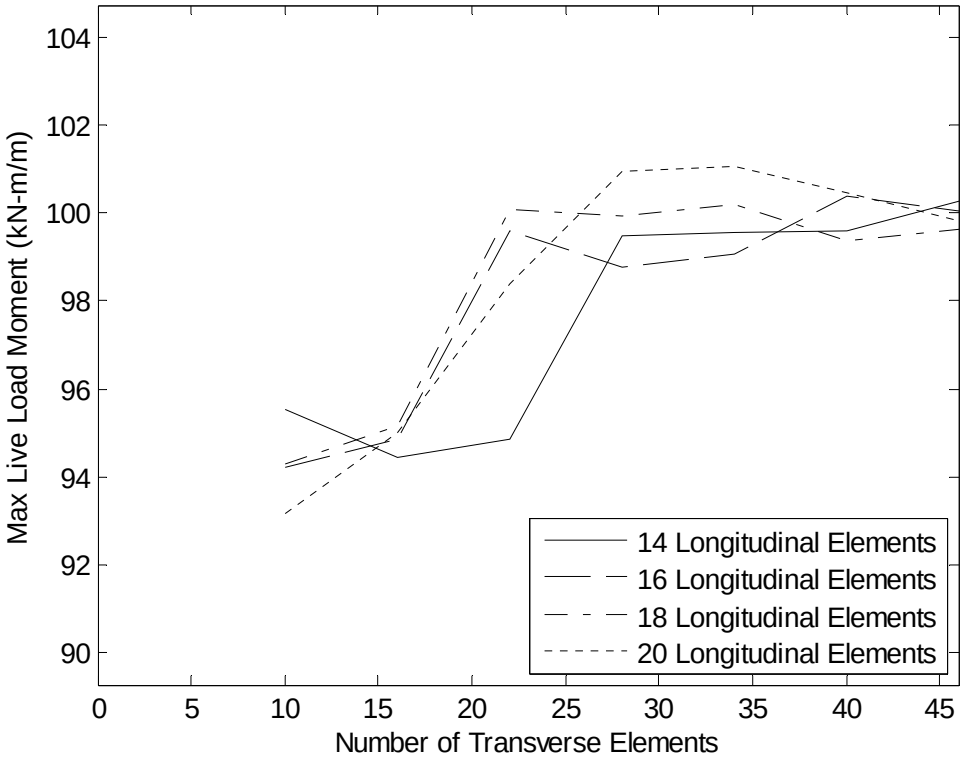

Figure 2.22 - Effects on max live load moment with an increase in mesh elements under HL-93 truck and lane loads for Carmel Bridge #5191, skew of 45°

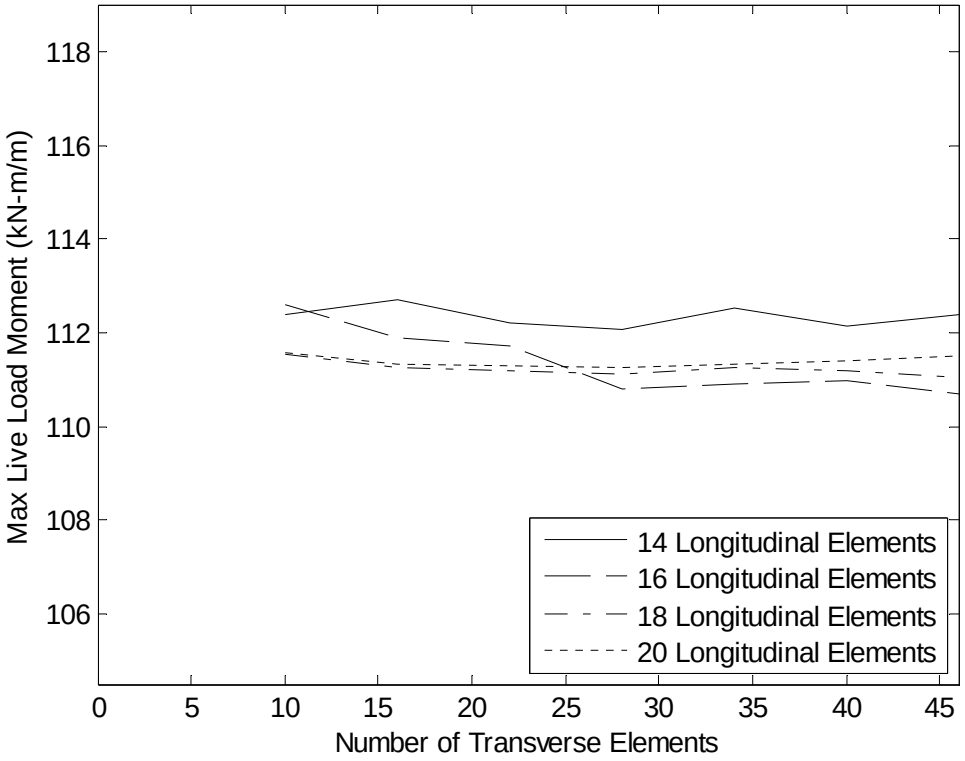

Figure 2.23 - Effects on max live load moment with an increase in mesh elements under HL-93 tandem and lane load for Carmel Bridge #5191, skew of 45°

Carmel Bridge #5191 with a skew of 45° follows the same pattern as with a 30° skew. The HL-93 truck load requires more elements to converge to a relatively constant value than the HL-93 tandem load. The HL-93 truck converges at 28 transverse elements when 14 longitudinal elements are used and 22 transverse elements when more than 14 longitudinal elements are used. The HL-93 truck shows an average increase of 5.9% from 10 transverse elements until the number of transverse elements needed to converge to a relatively constant value, 28 transverse elements for 14 longitudinal elements and 22 transverse elements for 16, 18 and 20 longitudinal elements. After the values appear to converge to a relatively constant number an increase of 0.8% is seen from that point up to 46 mesh elements. These results indicate that the model converges to a constant value around 22 transverse elements. The 14 longitudinal meshes converged later but it might be closer to the 22 transverse elements if more mesh sizes were analyzed. The HL-93 tandem load does not show any increase in live load moment due to an increase in the number of elements. An average 0.6% change from 10 to 40 transverse elements shows that the HL-93 tandem load converges quickly.

2.2.3.2.3. Mesh Recommendation for Skewed Bridges

When considering how skew affects the finite element analysis code SlabRate, it was found that the amount of transverse elements significantly affects the live load moments and thus the rating factors. All the results showed that the number of longitudinal elements had a lesser effect on the rating factors and moments. It was also found that with an increase of skew angle more transverse elements are needed to have the moments and rating factors converge to a constant value. Additionally, the width of

the bridge also seems to have an effect on the live load moments and the rating factors. This is likely because the Brewer Bridge is 11.43 m wide while the Carmel Bridge is only 7.80 m wide, and the rating factors and live load moments for the Brewer Bridge took more transverse elements to converge, around 40 with a skew angle of 45°, while the Carmel Bridge with a skew angle of 45° only needed about 22 transverse elements to converge to a constant value. Based on the analyses conducted here, the recommended mesh size is a minimum of 14 longitudinal and 40 transverse elements when there is a significant skew angle in the bridge. A mesh size of 14 longitudinal and 14 transverse elements can be used for a bridge width no skew.

Smaller skew angles may be accommodated with intermediate levels of mesh refinement. Figure 2.24 and Figure 2.25 show the recommended finite element meshes for Brewer Bridge #5638 with a 45 degree skew and Carmel Bridge #5191 with a 30 degree skew, the actual skews of the bridges. Another factor that must be considered when constructing the mesh is the element aspect ratio, which in general should be between 1:1 and 3:1. Particularly long or wide slab bridges may require more refined meshes than those used here to ensure that this aspect ratio is not exceeded.

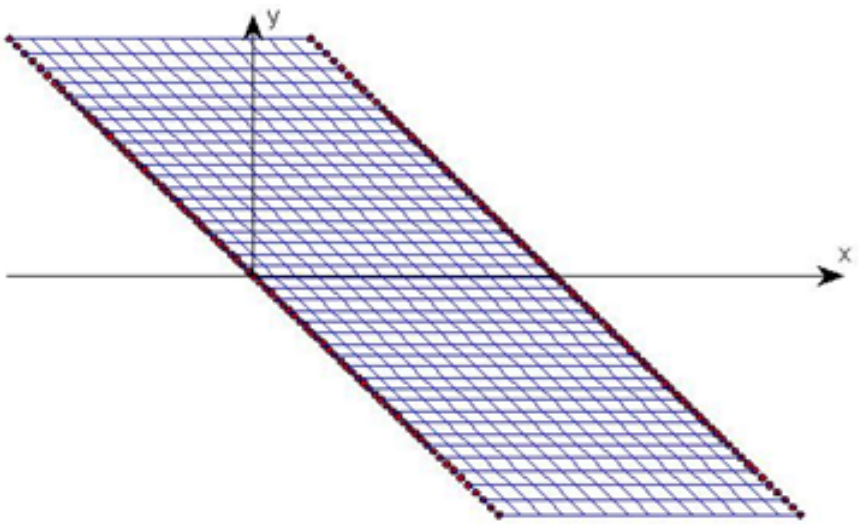

Figure 2.24 – Brewer Bridge #5638 recommended finite element mesh, 14 longitudinal elements and 40 transverse elements

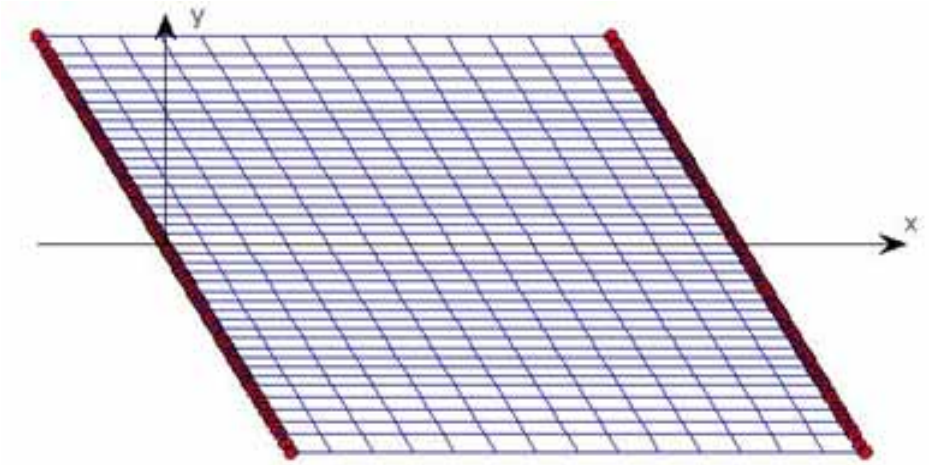

Figure 2.25 – Carmel Bridge #5191 recommended finite element mesh, 14 longitudinal elements and 40 transverse elements

2.2.4. Comparison of SlabRate with Commercial Finite Element Software

After SlabRate was developed, the solutions it created were verified using commercial software to ensure that the underlying finite-element code is correct. This was done by creating parallel models of identical bridges using both commercial finite element software and SlabRate and comparing the maximum moments and location of those moments due to a variety of live and dead loads. Two different commercial finite

element programs were used ANSYS (ANSYS 2009) and Abaqus (Abaqus 2009). Convergence studies were done for each commercial finite element program, and the models were also checked against known analytical solutions to verify the solutions of the models.

2.2.4.1. Modeled Bridge Characteristics

Models for three separate bridges were created in ANSYS. These bridges were Brewer Bridge #5638, Carmel Bridge #5191 and Levant Bridge #5253. The characteristics for these bridges are shown below in Table 2.2. These bridges were chosen because they capture a wide range of bridge skews (45°, 30° and 0° for the Brewer Bridge, Carmel Bridge and Levant Bridge, respectively). These bridges were also used in prior convergences studies conducted with SlabRate.

The Abaqus models only examined two separate bridges, Brewer Bridge #5638 and Levant Bridge #5253, whose characteristics are in Table 2.2. The reason for only comparing two bridges instead of three is since the purpose of the Abaqus models was to primarily examine the support lift-off, it was found that the two extremes skew angles (45° and 0°) could be examined. If neither of those bridges experienced a significant change in results, it could then be assumed that an intermediate skew angle (30°) would also not experience a change in results.

Table 2.2 – Bridge model characteristics

Bridge	Brewer #5638	Carmel #5191	Levant #5253
Span (Centerline to Centerline) (m)	7.04	10.16	8.12
Width (m)	11.43	7.77	7.82
Skew Angle	45	30	0
Slab Thickness (m)	0.349	0.559	0.470
Wearing Surface Thickness (m)	0.051	0.102	0.102
Moment Resistance (kN-m/m)	314.7	468.0	307.1
Rail Weight (kN / m) Top/ Bottom	1.889 1.889	1.959 1.959	0.898 0.898
Top Curb Width/ Height (m)	1.816 0.308	0.305 0.330	0.305 0.559
Bottom Curb Width/ Height (m)	1.054 0.295	0.305 0.330	0.305 0.559

2.2.4.2. Creation of ANSYS Models

The ANSYS (ANSYS 2009) models were used to verify that SlabRate provides accurate solutions given the modeling assumptions of linear elasticity, and small deformations. ANSYS was used for these models since they were easily created using input text files and straightforward to modify for different bridge characteristics and truck positions.

2.2.4.2.1. Simple ANSYS Model vs. Analytical Solution

Initially a simple model was created using ANSYS for a problem with a known analytical solution to ensure that ANSYS was being used properly. The model that was created was a simply-supported plate with a length of 100 cm, a width of 10 cm, a

thickness of 3.42 cm, an elastic modulus of $1x10^{10}$ Pa and a Poisson's ratio of 0.1. A load of 210 N was applied to the center of the plate and distributed evenly over the width.

Equation 2.1 – Equation 2.3 were used to calculate the analytical solution for maximum internal moment, maximum deflection and maximum stress.

$$M_{\max} = \frac{PL}{4} \qquad \text{Equation 2.1}$$

$$\Delta_{\max} = \frac{PL^3}{48EI} \qquad \text{Equation 2.2}$$

$$\sigma_{\max} = \frac{M_{\max}}{S\left(1-\nu^2\right)} \qquad \text{Equation 2.3}$$

Where:

M_{max} = maximum moment

P = total applied load

L = span

Δ_{max} = maximum deflection

E = elastic modulus

I = moment of inertia

σ_{max} = maximum stress

S = section modulus

ν = Poisson's ratio

The same geometry and loading were used to create a model in ANSYS. The model uses SHELL281 elements, which are 8-noded shell elements that use quadratic shape functions without reduced integration and also incorporate the effects caused by shear. These elements were used as they are the closest element to the elements used in

SlabRate. SlabRate elements are shear deformable plate elements that use quadratic shape functions to determine element displacements as well as rotations, but are under-integrated to prevent shear locking. The ANSYS model was meshed with an element edge length of 1 cm along both the length and the width of the elements. Figure 2.26 below shows the meshed model with the applied loads and boundary conditions.

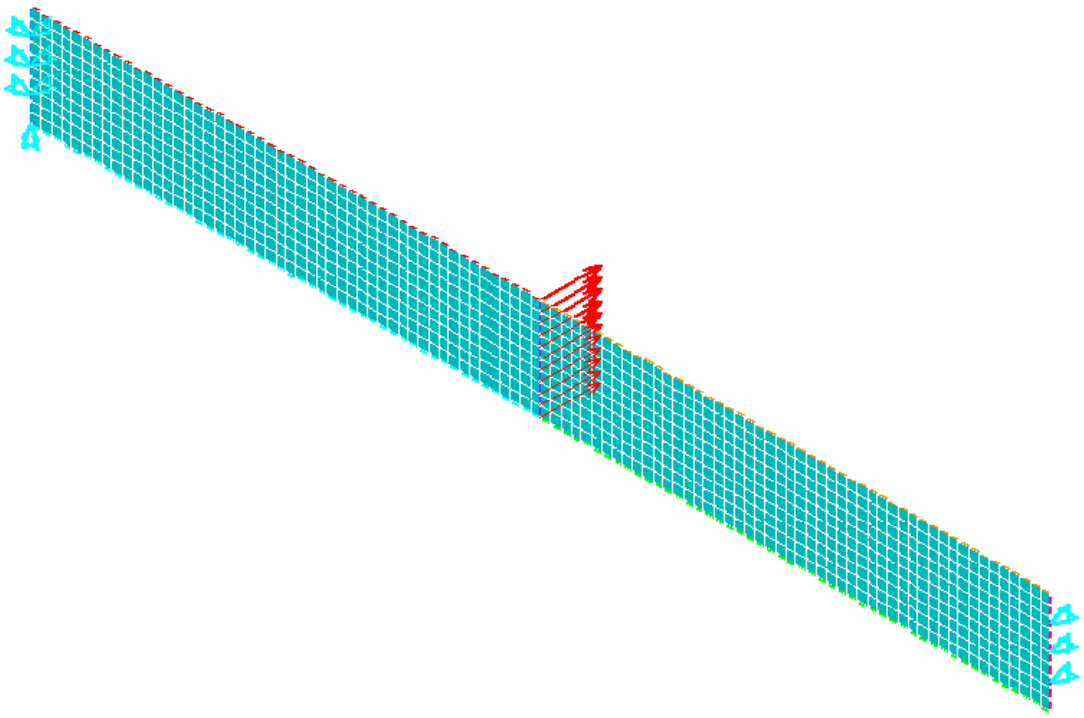

Figure 2.26 – Loading, geometry and mesh of the model created using ANSYS

The solutions for both the analytical solutions and ANSYS model along with the percent difference between the analytical solution and the ANSYS model are shown below in Table 2.3.

Table 2.3 – Analytical and ANSYS solutions for the maximum moment, deflection and stress

	Analytical Solution	ANSYS	Percent Difference
M_{max} (N-cm)	5250	5222	0.53%
Δ_{max} (cm)	0.1312	0.1314	0.15%
σ_{max} (N / cm^2)	271.95	271.66	0.11%

As the results show the values generated by ANSYS correspond very well with the results provided by the analytical solution, with a maximum difference of 0.52%. This demonstrates that the ANSYS model results are being interpreted correctly.

2.2.4.2.2. Dead Load Convergence Study

Convergence studies were done for each of the ANSYS bridge models before comparing the ANSYS models to SlabRate to ensure that the model-predicted maximum moment converged to a nearly constant value. The dead load convergence studies for all three of the bridges were done with all the dead loads applied including the weight of the slab, curbs, rails and the wearing surface. The element edge length is the length and width of each of the 8-noded shell elements used to mesh the model. The minimum element edge length for these models was 3.81 cm; when the element edge length was decreased beyond this point the maximum number of elements allowed by ANSYS was exceeded, as an academic version of the software was used. The total number of elements corresponding to the 3.81 cm edge length were 32300, 31470 and 24740 for the Brewer, Carmel and Levant bridges, respectively. Figure 2.27 – Figure 2.29 show the results for the dead load convergence studies.

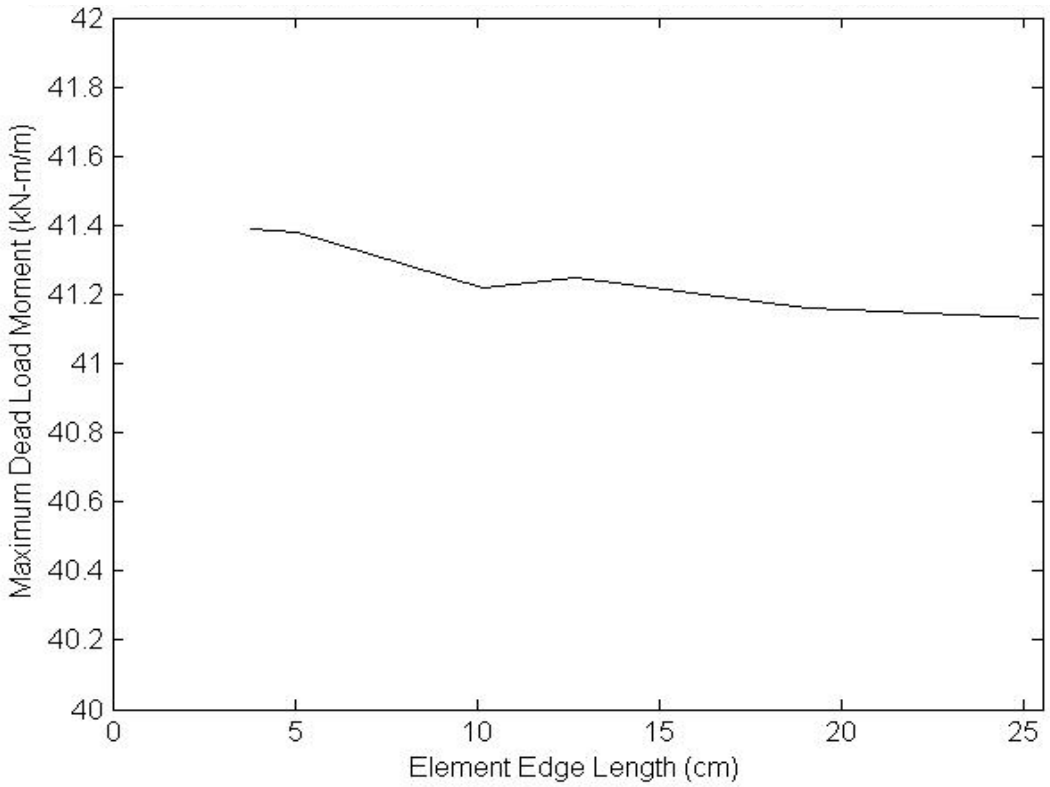

Figure 2.27 - Maximum moment values based on the element edge length while only dead loads are applied for Brewer Bridge #5638

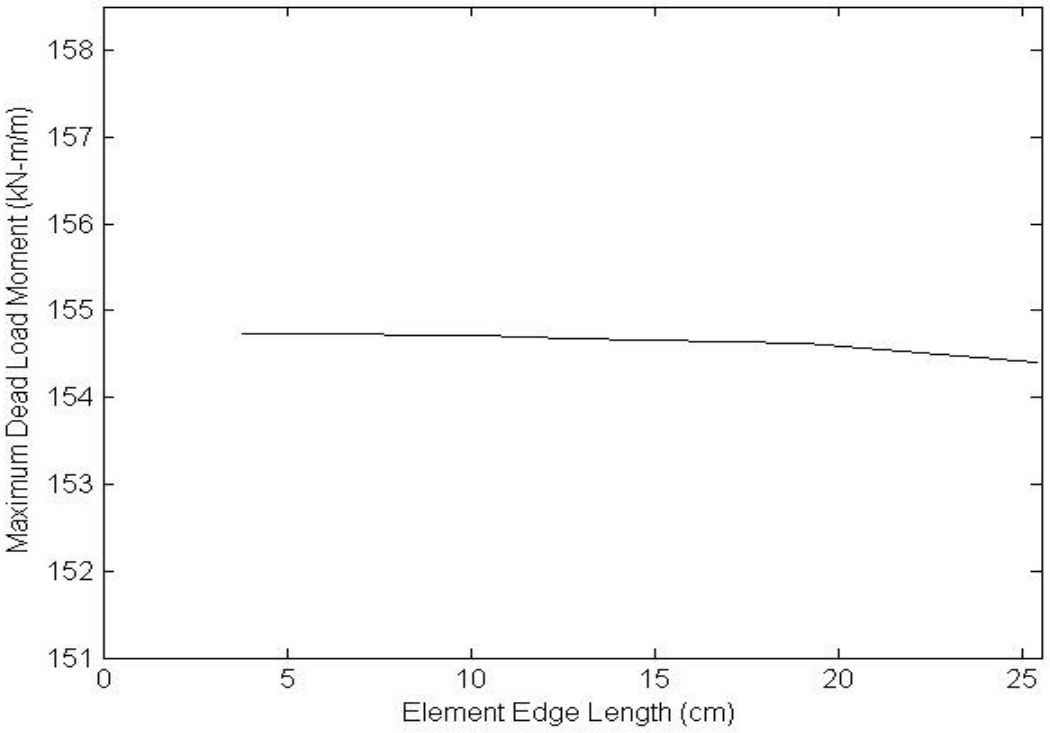

Figure 2.28 - Maximum moment values based on the element edge length while only dead loads are applied for Carmel Bridge #5191

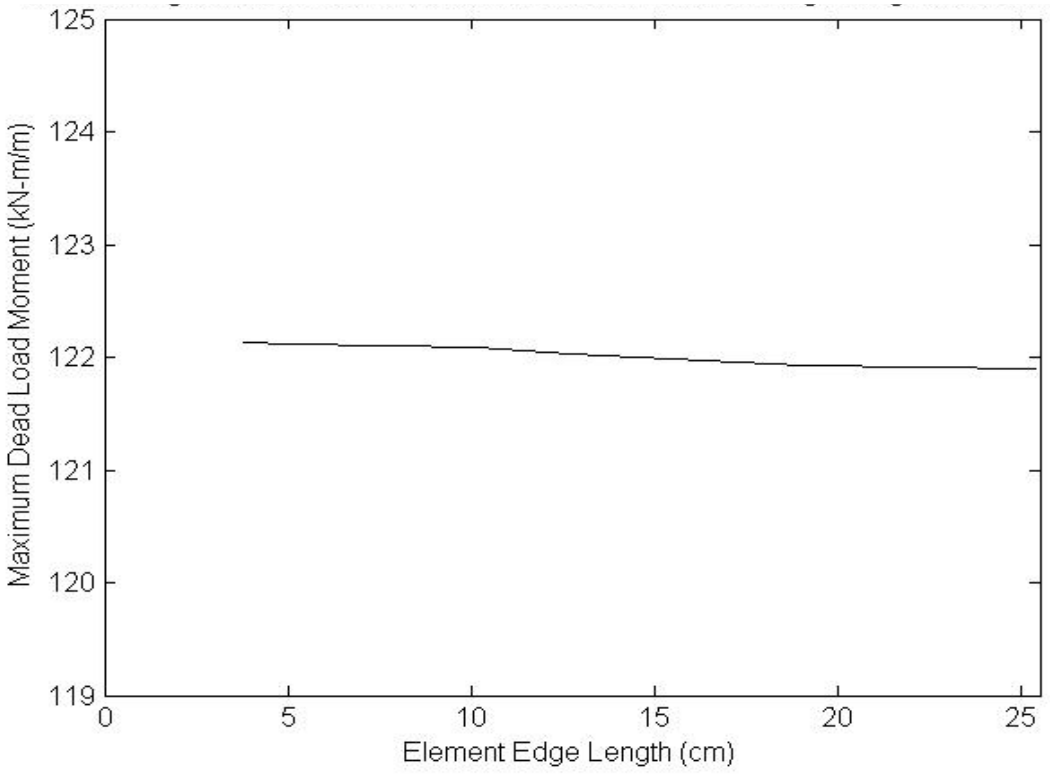

Figure 2.29 - Maximum moment values based on the element edge length while only dead load are applied for Levant Bridge #5253

Figure 2.27 – Figure 2.29 all have a vertical scale range of ±2.5% of the maximum moment value. Each of the plots show that the dead load models converge to an essentially constant value before an element edge length of 25.40 cm. Brewer Bridge #5638 had the largest percent difference between the 3.81 cm and 25.40 cm edge length, however that difference was only 0.6%. The other two bridges had percent differences of only 0.2% respectively.

2.2.4.2.3. Live Load Convergence Study

The live load convergence studies were done with the HL-93 Truck when the top tire of the middle axle was placed at the center of the bridge and the truck faced left. Therefore the center and back axles (axles right of the center) on the bridge weigh 145

kN while the front wheels (wheels left of the center) weigh 35 kN. Below in Figure 2.30 – Figure 2.32 are the models that were used for the live load convergence study with the truck and boundary conditions applied for each bridge. Each of the figures shows a mesh with an element edge length of 5.08 cm. The maximum moment values for different element edge lengths can be seen in Figure 2.33 – Figure 2.35.

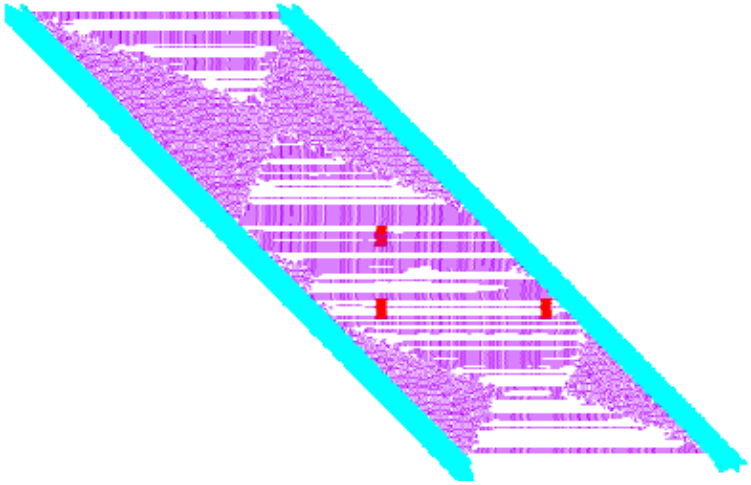

Figure 2.30 – Brewer Bridge #5638 with HL – 93 truck and boundary conditions applied

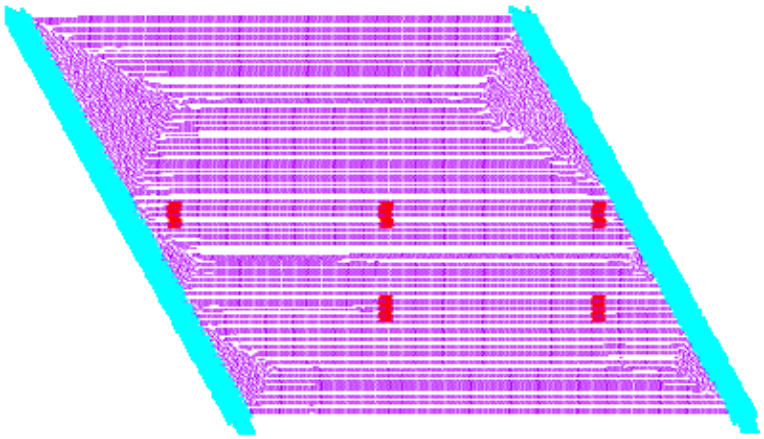

Figure 2.31 – Carmel Bridge #5191 with HL – 93 truck and boundary conditions applied

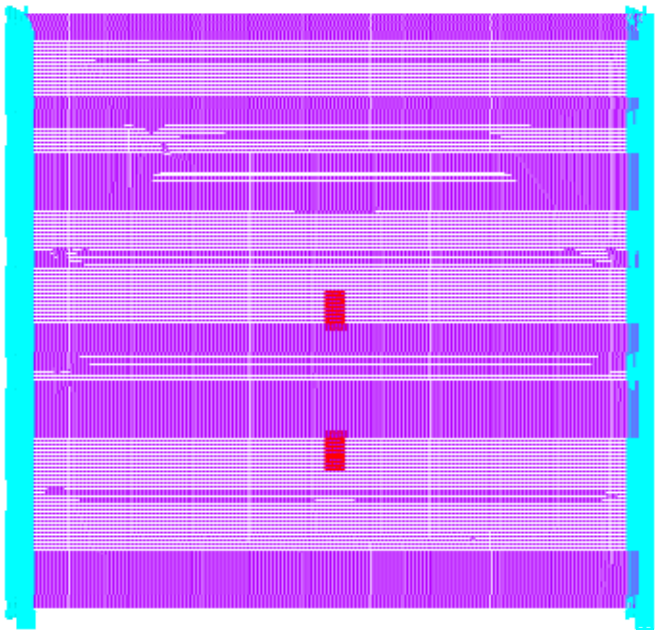

Figure 2.32 – Levant Bridge #5253 with HL–93 truck and boundary conditions applied

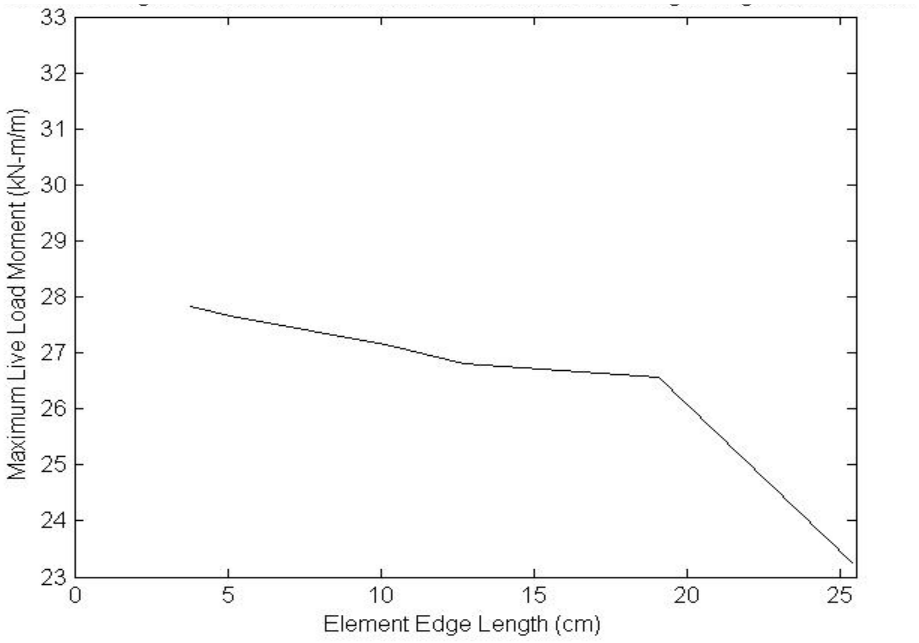

Figure 2.33 - Maximum moment values based on the element edge length while only live loads are applied for Brewer Bridge #5638

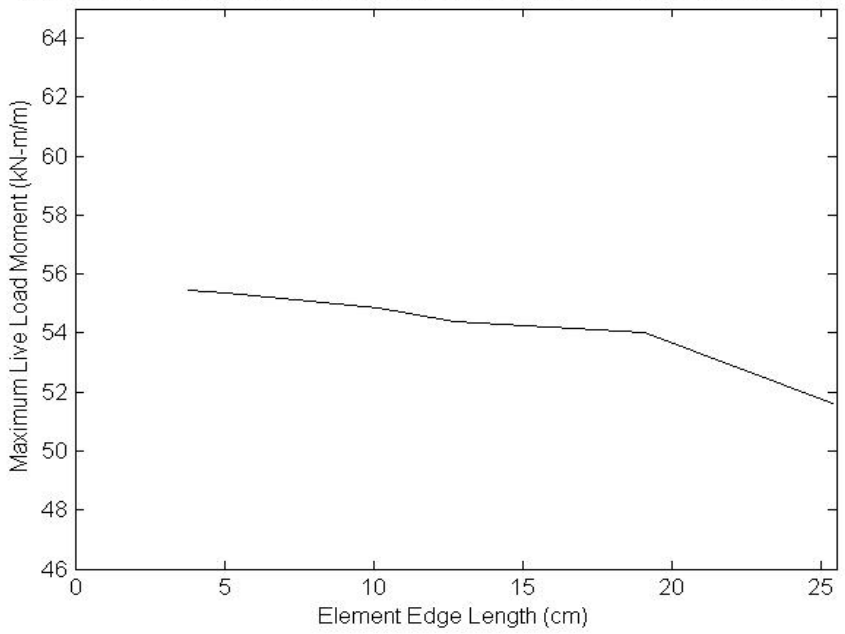

Figure 2.34 - Maximum moment values based on the element edge length while only live loads are applied for Carmel Bridge #5191

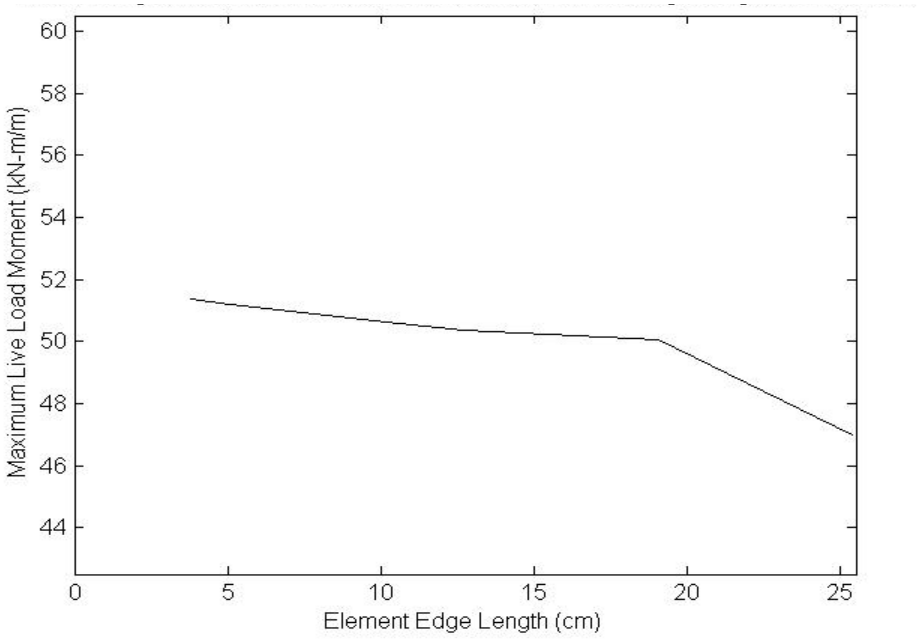

Figure 2.35- Maximum moment values based on the element edge length while only live load are applied for Levant Bridge #5253

Figure 2.33 – Figure 2.35, all have a vertical scale ranging from ±17.5% of the maximum live load moment for each bridge. As seen from the figures the models show a large increase in moment going from an element edge length of 25.40 cm to 19.05 cm

(12.4%, 4.4% and 6.1% for the Brewer Bridge, Carmel Bridge and Levant Bridge respectively). After this initial jump all of the models seem to have converged to a relatively constant value. There was a 4.6%, 2.6% and 2.5% increase going from an element edge length of 19.05 cm to 3.81 cm for the Brewer, Carmel and Levant bridges respectively.

2.2.4.2.4. Element Edge Length Recommendation

After both of the convergence studies were done it was determined that an element edge length of 5.08 cm would be used based on the live load convergence study results, which required more elements to converge in comparison to the dead load models. The 5.08 cm element edge length was deemed the best because live load moments were within 0.5% of the model maximum moments using the maximum number of elements. The models with an element edge length of 5.08 cm were also chosen because they took considerably less time to run compared to the model with an element edge length of 3.81 cm.

2.2.4.3. Comparison of SlabRate and ANSYS Model

After completion of the convergence studies, the ANSYS models were then compared to the results of SlabRate finite element models for each of the three bridges. The SlabRate program used the recommended mesh size of 14 longitudinal and 14 transverse elements for non-skewed bridges (Levant Brdige #5253) and 14 longitudinal and 40 transverse elements for skewed bridges (Brewer Bridge #5638 and Carmel Bridge #5191) based on the initial convergence studies reported earlier in this section 2.2.3.

Dead loads and live loads were compared separately just as they were in the convergence studies.

2.2.4.3.1. Dead Load Comparison

First the dead load moments were compared. The results for both the ANSYS models and SlabRate for different combinations of dead loads are shown below in Table 2.4 – Table 2.6. Figure 2.36 – Figure 2.38 show the moment contour plots for both ANSYS and SlabRate when all the dead loads are applied to each of the bridges.

Table 2.4 – Max moment due to dead load for ANSYS and SlabRate for Brewer Bridge #5638

Dead Load Applied	ANSYS Model (kN-m/m)	SlabRate (kN-m/m)	Percent Difference (%)
Slab	23.72	23.70	0.05
Slab and Curb	37.75	37.42	0.86
Slab, Curb and Rail	40.39	40.09	0.73
Slab, Curb, Rail and Wearing Surface	41.38	41.04	0.81

Table 2.5 - Max moment due to dead load for ANSYS and SlabRate for Carmel Bridge #5191

Dead Load Applied	ANSYS Model (kN-m/m)	SlabRate (kN-m/m)	Percent Difference (%)
Slab	123.70	123.76	0.05
Slab and Curb	130.31	130.26	0.04
Slab, Curb and Rail	135.81	135.64	0.12
Slab, Curb, Rail and Wearing Surface	154.74	154.62	0.08

Table 2.6 - Max moment due to dead load for ANSYS and SlabRate for Levant Bridge #5253

Dead Load Applied	ANSYS Model (kN-m/m)	SlabRate (kN-m/m)	Percent Difference (%)
Slab	93.79	94.10	0.33
Slab and Curb	104.08	104.33	0.24
Slab, Curb and Rail	106.40	106.63	0.22
Slab, Curb, Rail and Wearing Surface	122.12	122.43	0.25

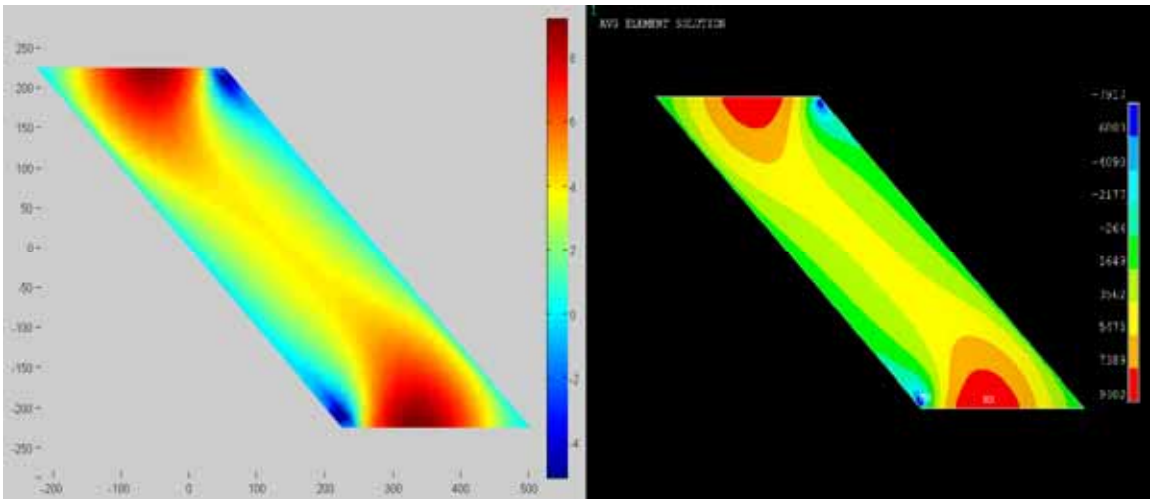

Figure 2.36 – Moment contour plots with all dead loads applied for Brewer Bridge #5638
Left: SlabRate **Right**: ANSYS model

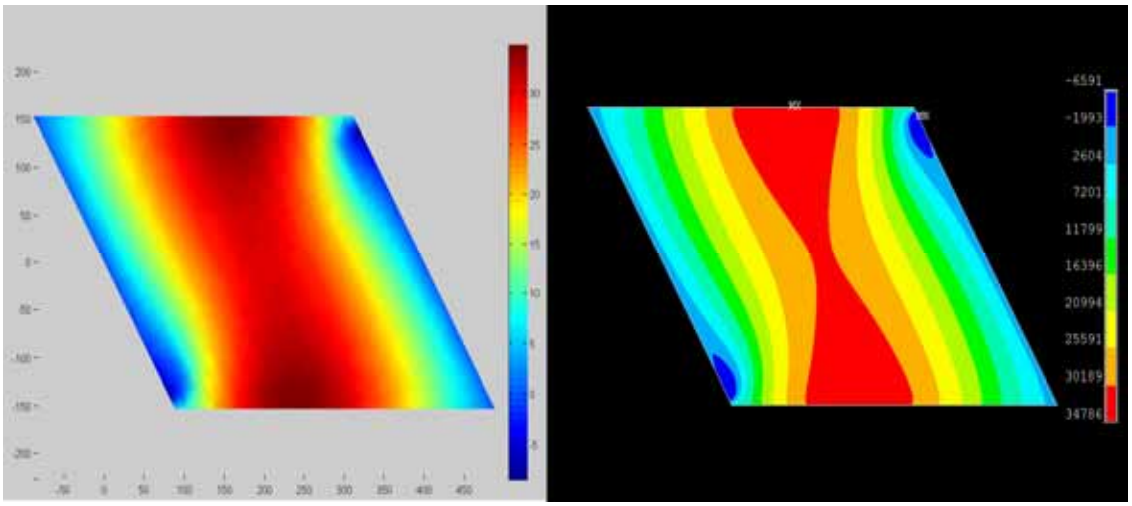

Figure 2.37 – Moment contour plots with all dead loads applied for Carmel Bridge #5191
Left: SlabRate **Right**: ANSYS model

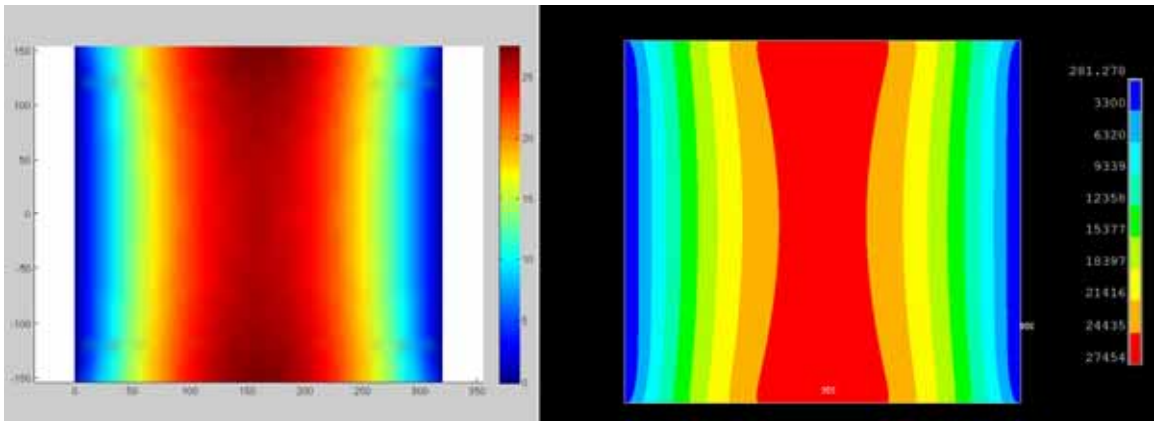

Figure 2.38 – Moment contour plots with all dead loads applied for Levant Bridge #5253
Left: SlabRate **Right**: ANSYS model

2.2.4.3.2. Live Load Comparison

The live load moments were then compared. The results for both ANSYS and SlabRate are shown in Table 2.7 – Table 2.9. The location of the truck is considered to be the top wheel of the middle axle for the HL-93 truck and the top wheel of the front axle for the HL-93 tandem loads. The truck direction is considered to be the direction that the truck is traveling. The origin of the bridges is taken as the geometric center of the bridge. The wheel that provided the maximum moment was centered over a corner node to ensure that SlabRate provided the maximum moment. This was necessary because the 8-noded elements used by SlabRate capture a linear variation in moment over the element area, so maximum moments always occur at a corner node.

Table 2.7 - Max moment due to live load for ANSYS and SlabRate for Brewer Bridge #5638

Truck Type	Location (cm)	Truck Direction	ANSYS Model (kN-m/m)	SlabRate (kN-m/m)	Percent Difference (%)
HL – 93 – Truck	(0,0)	Left	27.69	27.36	1.16
HL – 93 – Truck	(-442.13,341.53)	Left	26.48	26.13	1.31
HL – 93 – Tandem	(116.75,15.83)	Right	28.93	28.51	1.44

Table 2.8 - Max moment due to live load for ANSYS and SlabRate for Carmel Bridge #5191

Truck Type	Location (cm)	Truck Direction	ANSYS Model (kN-m/m)	SlabRate (kN-m/m)	Percent Difference (%)
HL – 93 – Truck	(-17.6,155.4)	Right	53.73	53.04	1.28
HL – 93 – Truck	(292.10,233.17)	Right	60.39	59.77	1.04
HL – 93 – Tandem	(406.95,66.29)	Right	42.77	41.93	1.97

Table 2.9 - Max moment due to live load for ANSYS and SlabRate for Levant Bridge #5253

Truck Type	Location (cm)	Truck Direction	ANSYS Model (kN-m/m)	SlabRate (kN-m/m)	Percent Difference (%)
HL – 93 – Truck	(0,223.5)	Right	53.60	53.24	0.66
HL – 93 – Truck	(310.8,111.8)	Right	52.05	51.58	0.91
HL – 93 – Tandem	(58.0,167.6)	Right	61.99	61.62	0.59

2.2.4.3.3. Discussion of Results

The results using SlabRate and ANSYS for both dead loads and live loads compare very well to each other. The maximum dead load moment percent differences range from 0.04% to 0.86%, while the maximum live load moment percent difference ranges from 0.01% to 1.97%. The average percent differences were 0.32% and 0.76% for dead load and live load models respectively. Along with the maximum values for dead load moments being within 1% the moment, contour plots for all dead loads are also very similar. This shows that the predicted moment values over the entire bridge are similar for both ANSYS and SlabRate at each point along the bridge. The live load moment contour plots from ANSYS and SlabRate which are not shown here also provide very similar shapes and magnitudes over the entire bridge. With the ANSYS models providing

very similar results to SlabRate, it shows that SlabRate's finite element code is working correctly based on the assumptions that were made while creating SlabRate (pinned supports, linearly elastic, and small deformations).

2.2.4.4. Creation of Abaqus Models

After the finite element program SlabRate was verified given the assumptions that were made in SlabRate (pinned supports, linearly elastic, and small deformations) using ANSYS. The assumptions made by SlabRate then have to be checked. The assumption of linear elasticity is conservative when computing moments, and these structures do experience small deformations and strains. However, the supports may not be truly pinned, and the slab may lift off part of one or both supports under live loading. This is particularly true for skewed bridges. To assess the significance of slab lift-off, parallel models of identical bridges were created in Abaqus (Abaqus 2009) that had compression-only supports i.e. allows support lift off.

Abaqus software was used instead of ANSYS software because there were features in Abaqus that facilitated straightforward modeling of the compression-only support, whereas this phenomenon proved to be more difficult to model in ANSYS. All of the Abaqus models use an S8R element, which is an 8-node doubly curved thick shell element with reduced integration. The S8R element is also a shear flexible element that uses quadratic shape functions, and is very similar to the element used by SlabRate.

2.2.4.4.1. Pinned Supported Models Created and Compared to ANSYS Models

Initially, models for Brewer Bridge #5637, Carmel Bridge #5191 and Levant Bridge #5253, were created in Abaqus with pinned supports to verify the solutions that

Abaqus provided. The results from each of the models are shown below in Table 2.10 – Table 2.12. Each of the models used an element edge length of 5.08 cm. Only live loads were compared between these models. This was because these models were only created in Abaqus to verify that the numbers that were displayed were correct, and also to see if they provided the same results under same boundary conditions. Also Abaqus does not report moments directly they had to be computed from stresses given directly from Abaqus. This was done by using Equation 2.4 (Bhatti 2006).

$$M_{predict} = \frac{\sigma_{predict} h^2}{6} \qquad \text{Equation 2.4}$$

Where:

$M_{predict}$ = predicted moment from the Abaqus model

$\sigma_{predict}$ = predicted stress from the Abaqus model

h = slab thickness

Table 2.10 - Max moment due to live load for ANSYS and Abaqus for Brewer Bridge #5638

Truck Type	Location (cm)	Truck Direction	Abaqus Model (kN-m/m)	ANSYS Model (kN-m/m)	Percent Difference (%)
HL – 93 – Truck	(0,0)	Left	27.57	27.69	0.4
HL – 93 – Truck	(-442.13, 341.53)	Left	26.46	26.48	0.1
HL – 93 – Tandem	(116.75,15.83)	Right	28.89	28.93	0.2

Table 2.11 - Max moment due to live load for ANSYS and Abaqus for Carmel Bridge #5191

Truck Type	Location (cm)	Truck Direction	Abaqus Model (kN-m/m)	ANSYS Model (kN-m/m)	Percent Difference (%)
HL – 93 – Truck	(-17.6,155.4)	Right	53.88	53.73	0.3
HL – 93 – Truck	(292.10,233.17)	Right	60.34	60.39	0.1
HL – 93 – Tandem	(406.95,66.29)	Right	42.75	42.77	0.1

Table 2.12 - Max moment due to live load for ANSYS and Abaqus for Levant Bridge #5253

Truck Type	Location (cm)	Truck Direction	Abaqus Model (kN-m/m)	ANSYS Model (kN-m/m)	Percent Difference (%)
HL – 93 – Truck	(0,223.5)	Right	53.56	53.60	0.1
HL – 93 – Truck	(310.8,111.8)	Right	52.07	52.05	0.0
HL – 93 – Tandem	(58.0,167.6)	Right	62.02	61.99	0.1

With all the moments within 0.4% it shows that the Abaqus also provides essentially the same solutions as the ANSYS models. This shows that the moments are being calculated correctly along with Abaqus being used correctly, since we had checked the ANSYS models against analytical models (see section 2.2.4.2.1).

2.2.4.4.2. Creating of Support Lift-Off Models

After the Abaqus outputs were checked against the ANSYS outputs, models were created to examine the possibility of slab lift-off. To model slab lift-off, the abutments were modeled as solid concrete volumes meshed with bridge elements, and a compression-only contact between the slab and each abutment was explicitly simulated. Because of this, the Abaqus models were nonlinear. Figure 2.39 shows a model that incorporates the concrete blocks as supports for the Levant Bridge. The figure also shows

all the loading when a HL-93 truck middle axle was placed at (0,223.5) cm form the center. In order for the model to be stable, the slab had to be restrained in the *x*–*y* plane when the loads were applied in the *z*–direction to ensure that slip didn't occur.

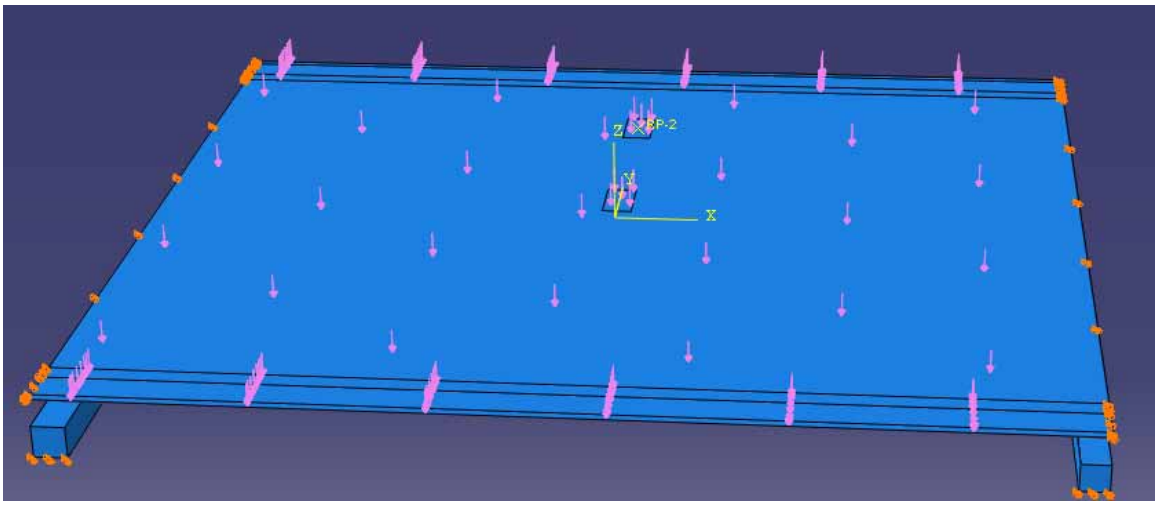

Figure 2.39 – Abaqus lift-off model for Levant Bridge #5253

Additionally, the kinematics of the slab lift-off in the Abaqus models will provide a different maximum moment due to the change in the effective span length of the bridge from the centerline-support to centerline-support span assumed by SlabRate to face-of-support to face-of-support. Figure 2.40 shows a screen shot of a deformed model illustrating how the effective span becomes the clear span as the slab bends and bears only on the inside face of the abutment. The effects of this will be discussed in more detail in section 2.2.4.5.

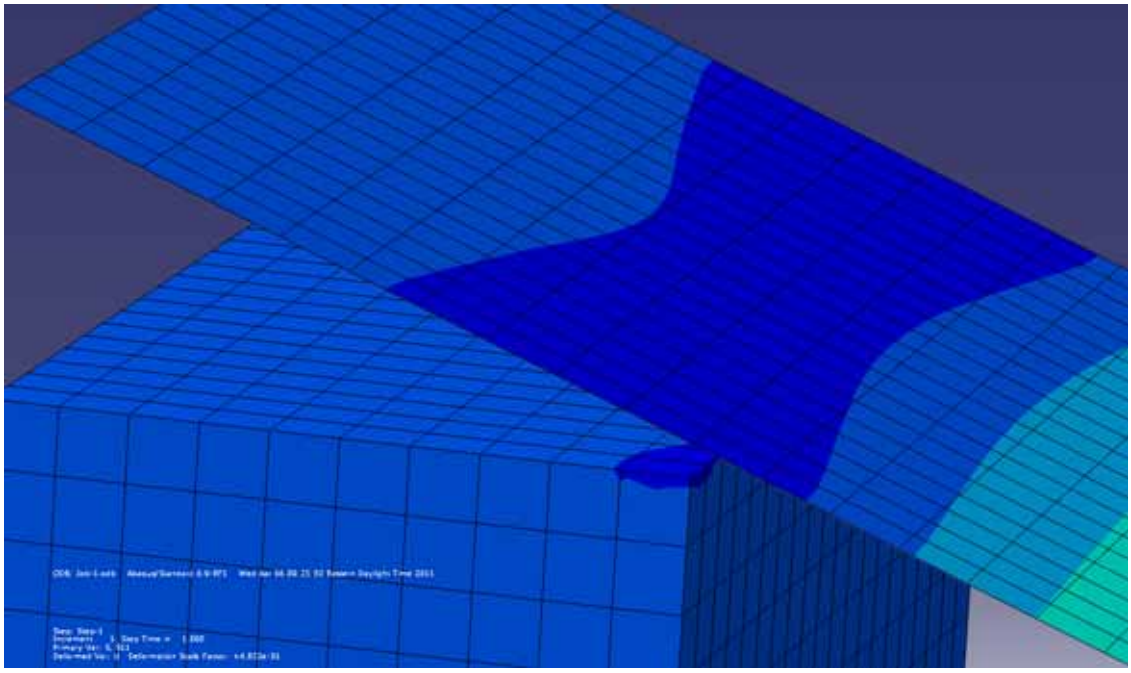

Figure 2.40 - Example of the slab lift-off from the support and the how effective length becomes the clear span

2.2.4.4.3. Convergence Study for Abaqus Models

As mentioned in section 2.2.4.1 only two bridges were modeled with compression only supports, Brewer Bridge #5638 and Levant Bridge #5253). A convergence study for the Abaqus support lift-off models was done. These convergence studies were done with all the factored loads applied, both dead and live. Brewer Bridge #5638 had an HL-93 truck with the top middle axle placed at the center of the bridge with the truck facing the left. Levant Bridge #5253 had an HL-93 truck placed (292.10, 233.17) cm from the center of the bridge with the direction of the truck facing the right. Below in Figure 2.41 and Figure 2.42 are the graphs of the results from the convergence studies. The graphs all have a vertical range of ±17.5% of the average value.

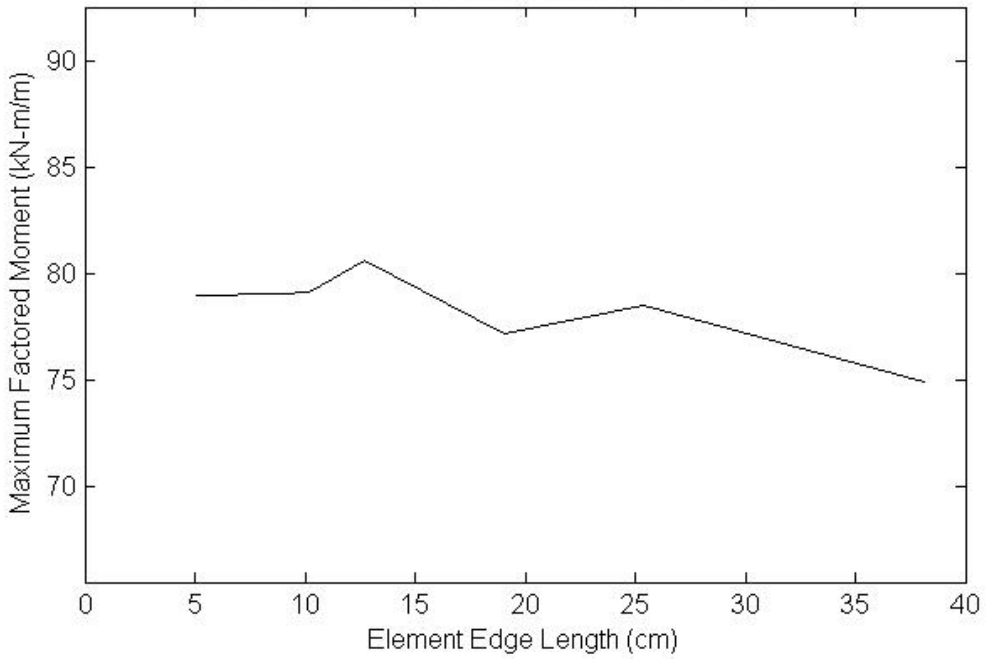

Figure 2.41 – Maximum factored moment values based on the element edge length while all loads are applied for Brewer Bridge #5638

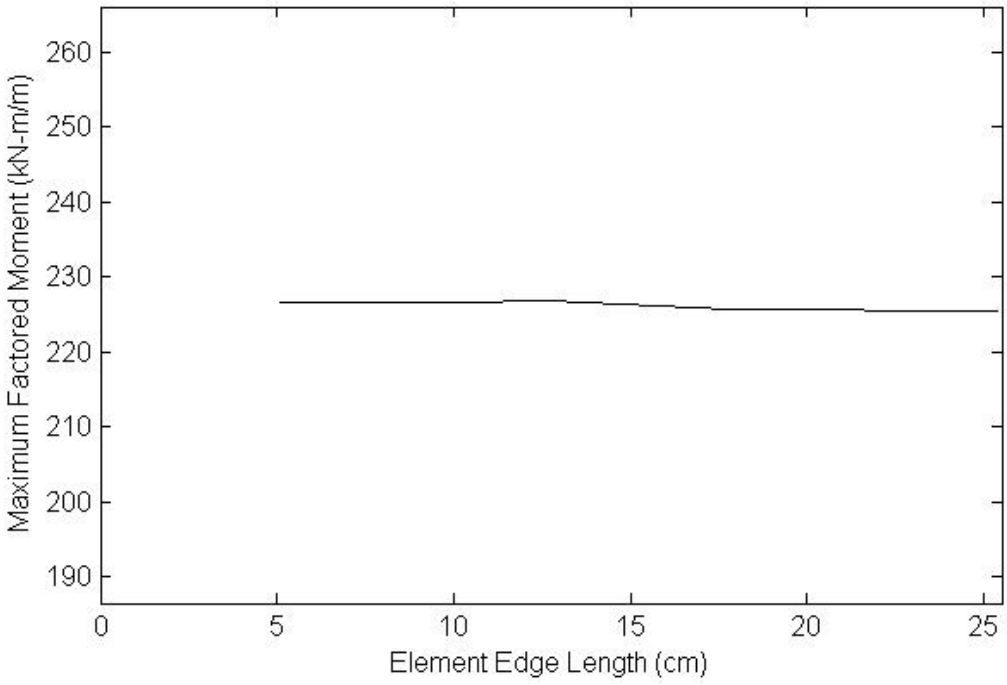

Figure 2.42 – Maximum factored moment values based on the element edge length while all loads are applied for Levant Bridge #5253

As seen from the convergence plots, Brewer Bridge has more of a variation in maximum moment when the element edge length is changed. There is an initial change of

5% going from an element edge length of 38.1 cm to 25.4 cm. The maximum moment then appears to alternate between increasing and decreasing when the element edge length is decreased. Minimal change was seen for an element edge length smaller than 10.16 cm. This shows that the moment converges to a constant value, since two other values with smaller element edge length provided moments within 0.1% of the 10.16 cm solution. The Levant Bridge seems to have already converged before an element edge length of 25.4 cm, this is determined since the maximum moments change by only 0.5% going from an element edge length of 25.4 cm to 5.08 cm.

2.2.4.4.4. Element Edge Length Recommendation

The results from the convergence studies led to the use of an 8.89 cm element length. These models led to very similar results as the 5.08 cm element length, the smallest element edge length modeled, but the run times of the models were considerably less. The total number of elements corresponding to the 8.89 cm edge length was 12920 and 9120 for the Brewer and Levant bridges, respectively.

2.2.4.5. Comparison of SlabRate and Abaqus Support Lift-Off Models

The loads applied to the Abaqus support lift-off models had to be factored due to the fact that it was a non-linear analysis. The ANSYS models, as discussed in the previous sections, used a linear analysis so the dead loads and live loads could be compared separately and the effects of both could be added using the principle of superposition. The Abaqus models had to be analyzed under all the loads, both factored dead and factored live loads, and then the models had to be analyzed under only factored dead loads. The difference between the two separate loadings is the effect of the factored

live loads. The maximum factored live load moments predicted by the Abaqus models with compression-only supports are compared to the factored live load moments produced by SlabRate in Table 2.13 and Table 2.14 for the Brewer and Levant Bridge respectively. These moments are located at the same location, the middle of a tire. The Abaqus models are expected to provided a slightly lower maximum moment, due to the change in the effective span of the bridge as explained above in section 2.2.4.4.2..

Table 2.13 - Factored max live load moment due to live load for SlabRate and Abaqus lift-off models for Brewer Bridge #5638

Truck Type	Location (cm)	Truck Direction	Abaqus Model (kN-m/m)	SlabRate (kN-m/m)	Percent Difference (%)
HL – 93 – Truck	(0,0)	Left	60.43	63.68	5.1
HL – 93 – Truck	(-442.13,341.53)	Left	56.08	60.82	8.0
HL – 93 – Tandem	(116.75,15.83)	Right	64.10	66.36	3.4

Table 2.14 – Factored max live load moment due to live load for SlabRate and Abaqus lift-off models for Levant Bridge #5253

Truck Type	Location (cm)	Truck Direction	Abaqus Model (kN-m/m)	SlabRate (kN-m/m)	Percent Difference (%)
HL – 93 – Truck	(0,223.5)	Right	118.97	123.92	4.0
HL – 93 – Truck	(310.8,111.8)	Right	111.81	120.05	6.9
HL – 93 – Tandem	(58.0,167.6)	Right	140.02	143.42	2.4

The results from the Abaqus models and SlabRate provide similar results within 8.0% of each other. The percent difference is predominantly caused by the effective span length change. The effective length of the bridge that is used in the Abaqus model (clear span) could not be used for all the loading cases above in SlabRate because as the span length changes in SlabRate the maximum moment might not occur at the location of a

node. If the maximum moment does not occur directly on a node SlabRate will underestimate the moment, since the 8-noded element linearly interpolates moments over its area. However, two of the loading cases above could be analyzed using the clear span in SlabRate without changing anything except the span length. These loading cases produced maximum moments at the center of the bridge where a line of nodes existed regardless of span length or mesh density. The results from changing the length of the bridge are shown below in Table 2.15. These results from SlabRate use the same effective span length as the Abaqus model (clear span).

Table 2.15 – Factored max live load moment due to live load for SlabRate and Abaqus lift-off models using the same effective span length

Bridge	Truck Type	Location (cm)	Truck Direction	Abaqus Model (kN-m/m)	SlabRate (kN-m/m)	Percent Difference (%)
Brewer #5638	HL – 93 – Truck	(0,0)	Left	60.43	60.94	0.8
Levant #5253	HL – 93 – Truck	(0,223.5)	Right	118.97	118.71	0.2

These two load cases provided very similar results with both Abaqus and SlabRate, demonstrating that the major discrepancy between the Abaqus and SlabRate models is the change in effective span length.

2.3. Conclusion

The main objective of this chapter was to ensure that the SlabRate finite-element implementation was correct for evaluating simply-supported and continuous flat slab bridges. The results from the ANSYS models and the SlabRate program compare very well to each other, indicating that SlabRate provides accurate solutions given the modeling assumptions and limitation inherent in the program (i.e. pinned supports, linear

elasticity, and small deformations). Further, the moment contour plots generated by ANSYS and SlabRate are very similar, showing that SlabRate is providing the correct moments in places other than where the maximum moment occurs.

The results from the Abaqus models that account for slab lift-off also compare well to the SlabRate program, with SlabRate giving conservative results in all cases when centerline span lengths were assumed.

CHAPTER 3. LOAD RATING OF EXISTING FLAT-SLAB CONCRETE BRIDGES

3.1. Introduction

In this chapter twenty existing flat slab concrete bridges will be load rated using both the conventional strip width method (AASHTO 2008) and the SlabRate finite element software described in Chapter 2. The conventional strip width method is currently being used by MaineDoT for load rating procedures. The results from both will then be presented and compared to each other to show the benefits of using finite element analysis in load rating existing bridges.

3.2. Bridge Information

Twenty sets of bridge plans were provided by the MaineDoT to be load rated. These bridges were all constructed between 1939 and 1959 (except Milo Bridge #2931 which had its deck replaced in 1994). The following section describes the characteristics of each of the bridges.

3.2.1. Bridge Characteristics

The characteristics of each of the twenty bridges that were load-rated using the conventional strip width method and the finite element program SlabRate are summarized in Table 3.1 and Table 3.2. All the bridges were assumed to have an elastic modulus of 19640 MPa, along with a Poisson's ratio of 0.19 and a unit weight of concrete equal to 2400 kg/m^3.

Dimensions were verified by bridge visits conducted during July and August of 2010 and May 2011. The dimensions that were verified included slab thickness, curb

width, curb height (both total height and heights above wearing surface), rail dimensions, striped lane offset from curb, number of lanes, span length, span width and skew angle. These measurements were taken to verify that the bridge plans represented the actual structure. If there was a difference between a measured dimension and a dimension taken from the plans, the measured value was used in the rating.

In some cases, wearing surface thickness could be field verified from the field visits in which case γ_{DW} was set to 1.25 instead of 1.50 per Table 6A.4.2.2-1 in AASHTO's *Manual for Bridge Evaluation* (AASHTO 2008). The six bridges for which the wearing surface was field verified were Argyle Township Bridge #3427, Bradford Bridge #3430, Carmel Bridge #5191, Levant Bridge #5253, Milford Bridge #2070 and Milo Bridge #2931. The wearing surface thicknesses of the other fourteen bridges could not be field verified, so the thicknesses in the plans were assumed to be correct and γ_{DW} was set to 1.50.

During the bridge visits, striped lane offset from the curb was measured. While analyzing bridges using SlabRate, wheel lines were placed no closer than 60.1 cm from the face of the curb, or at the striped lane edge.

The values for concrete compressive strength (f'_c) and yield strength of the reinforcing steel (f_y) are given for each of the bridges and are shown in Table 3.1 and Table 3.2. These values were assumed according to Tables 6A.5.2.1-1 and 6A.5.2.2-1 of AASHTO's *Manual for Bridge Evaluation* (AASHTO 2008) for f'_c and f_y respectively. These assumptions are based on the year the bridge was constructed. Albion Bridge #2529 and Milo Bridge #2931 had the value for f_y called out directly in the plans so those values were used instead of the values provided by AASHTO.

All rail weights were modeled as constant distributed loads in the analysis. The maximum moments for each bridge caused by the actual field-measured rails were determined from measured dimensions and calculated weights assuming point loads where the posts are located. From these maximum moments, a constant distributed load was calculated that produced the same maximum moment expected based on the actual post locations. The constant distributed load was used in the analysis since it was easier to apply in the finite element program SlabRate.

Both Albion Bridge #2529 and Levant Bridge #5253 were two span structures. Neither of these bridges were continuous bridges, and therefore were modeled as a single span bridges with the larger of the two spans used in the analysis. The larger of the two spans were used since each span had the same thickness and reinforcing, and as thus the longest span would control since the dead and live load moments would be greater.

All condition factors were taken from the MaineDoT bridge inspections (MaineDoT 2008). All of the bridge inspections were performed by the MaineDoT between January 2008 and December 2009. Hermon Bridge #2205 was determined to have a condition factor (φ_c) equal to 0.95 (AASHTO 2008) i.e. structural condition of the bridge found to be fair. All the other bridges had a φ_c of 1.0 (AASHTO 2008), i.e. structural condition of the bridges found to be either good or satisfactory.

Table 3.1 - Summary of bridge characteristics

Bridge	Albion #2529	Argyle #3427	Bradford #3430	Brewer #5638	Carmel #5191	Carmel #5632	Chester #5907	Exeter #5838	Greenfield #5605	Hermon #2205
Length (m)	6.33	6.66	7.16	7.04	10.16	6.69	11.31	7.59	6.66	5.79
Width (m)	7.32	8.43	7.62	11.43	7.77	8.38	8.84	9.14	7.77	9.14
Skew Angle	43.87	0	0	45	30	30	0	10.25	20	0
Slab Thickness (m)	0.381	0.406	0.419	0.349	0.559	0.343	0.610	0.470	0.343	0.445
Wearing Surface Thickness (m)	0.013	0.076	0.076	0.051	0.102	0.076	0.102	0.522	0.330	0.127
f'_c (MPa)	17.24	17.24	17.24	17.24	17.24	17.24	20.68	20.68	17.24	17.24
f_y (MPa)	248.2	227.5	227.5	275.8	227.5	275.8	275.8	275.8	257.8	227.5
Moment Resistance (kN-m/m)	178.7	288.7	240.3	314.7	468.0	286.9	904.0	481.6	277.7	285.8
Rail Weight (kN / m) Top/ Bottom	1.236 1.392	2.222 2.222	1.582 1.582	1.889 1.889	1.959 1.959	5.039 5.039	4.343 4.343	0.327 0.327	2.358 2.358	0.192 0.192
Top Curb Width/ Height (m)	0.457 0.432	0.330 0.343	0.457 0.305	1.829 0.308	0.305 0.330	0.330 0.330	0.457 0.254	0.305 0.775	0.521 0.305	0.229 0.457
Bottom Curb Width/ Height (m)	0.457 0.432	0.330 0.343	0.457 0.305	1.067 0.290	0.305 0.330	0.330 0.330	0.457 0.305	0.305 0.521	0.521 0.305	0.229 0.457

Table 3.2 – Summary of bridge characteristics

Bridge	Levant #5253	Liberty #3493	Linneus #5311	Linneus #5773	Milford #2070	Milo #2931	Monroe #5538	Newcastle #5608	Palmyra #5699	Sherman #2899
Length (m)	8.12	7.85	6.62	7.54	8.34	7.47	8.77	8.15	6.57	9.21
Width (m)	7.82	7.62	8.33	9.14	9.25	11.58	8.41	8.99	9.14	10.29
Skew Angle	0	15	30	25	15	0	7.75	6	0	16.5
Slab Thickness (m)	0.470	0.457	0.394	0.356	0.419	0.457	0.432	0.394	0.330	0.533
Wearing Surface Thickness (m)	0.102	0.203	0.203	0.178	0.114	0.102	0.152	0.102	0.072	0.102
f'_c (kPa)	17.24	17.24	17.24	20.68	17.24	20.68	17.24	17.24	17.24	17.24
f_y (MPa)	227.5	227.5	227.5	275.8	275.8	413.7	275.8	275.8	275.8	227.5
Moment Resistance (kN-m/m)	307.1	291.5	249.4	329.8	451.9	642.5	502.6	404.0	264.5	409.7
Rail Weight (kN / m) Top/ Bottom	0.898 0.898	6.807 6.807	0.965 0.965	0.288 0.288	1.187 1.187	2.632 4.028	1.273 1.273	2.246 2.246	0.232 0.236	2.729 2.379
Top Curb Width/ Height (m)	0.305 0.559	0.330 0.381	0.508 0.279	0.305 0.305	0.305 0.359	0.279 2.235	0.546 0.356	0.521 0.254	0.254 0.318	1.829 0.305
Bottom Curb Width/ Height (m)	0.305 0.559	0.330 0.381	0.508 0.279	0.305 0.305	0.305 0.356	0.127 0.381	0.546 0.356	0.521 0.305	0.254 0.318	0.533 0.305

3.2.2. Photos of Bridges

Photos of each bridge are shown in Figure 3.1– Figure 3.23. These photos show the real rails that were used to create the equivalent distributed loads. These photos also show the conditions of the roadways, curbs and rails. The dates of the bridge visits are also provided in the caption of each bridge photo.

Figure 3.1 – Photo of Albion Bridge #2529 from bridge visit in August 2010

Figure 3.2 – Photo of the rail on Albion Bridge #2529 from bridge visit in August 2010

Figure 3.3 - Photo of Argyle Bridge #3827 rails from bridge visit conducted July 2010

Figure 3.4 - Photo of Bradford Bridge #3430 rail from bridge visit conducted July 2010

Figure 3.5 - Photo of Brewer Bridge #5638 from bridge visit conducted in July 2010

Figure 3.6 - Photo of Carmel Bridge #5191 rail from bridge visit conducted in July 2010

Figure 3.7 – Photo of Carmel Bridge #5632 from bridge visit conducted in May 2011

Figure 3.8 – Photo of Chester Bridge #5907 from bridge visit conducted May 2011

Figure 3.9 – Photo of Exeter Bridge #5838 from bridge visit conducted in May 2011

Figure 3.10 – Photo of Greenfield TWP Bridge #5605 from bridge visit conducted in May 2011

Figure 3.11 - Photo of Hermon bridge rail from bridge visit conducted August 2010

Figure 3.12 - Photo of Levant Bridge #5253 from bridge visit conducted in July 2010

Figure 3.13 - Photo of Levant Bridge #5253 rail from bridge visit conducted in July 2010

Figure 3.14- Photo of Liberty Bridge #3493 from bridge visit conducted in May 2011

Figure 3.15 – Photo of Linneus Bridge #5311 from bridge visit conducted in May 2011

Figure 3.16 – Photo of Linneus Bridge #5733 from bridge visit conducted in May 2011

Figure 3.17 - Photo of Milford Bridge #2070 rail from bridge visit conducted July 2010

Figure 3.18 - Photo of Milo Bridge #2931 top rail from bridge visit conducted August 2010

Figure 3.19 - Photo of Milo Bridge #2931 bottom rail from bridge visit conducted August 2010

Figure 3.20 – Photo of Monroe Bridge #5538 from bridge visit conducted in May 2011

Figure 3.21 – Photo of Newcastle Bridge #5608 from bridge visit conducted in May 2011

Figure 3.22 - Photo of Palmyra Bridge #5699 rail from bridge visit conducted in August 2010

Figure 3.23 – Photo of Sherman Bridge #5311 from bridge visit conducted in May 2011

3.3. Truck Information

The trucks used in the analysis were the design trucks (HL-93 truck and tandem loads with lane load) for both inventory and operating levels, AASHTO legal trucks (Type 3, Type 3S2 and Type 3-3), specialized hauling vehicles (SU4, SU5, SU6 and SU7) and MaineDoT rating trucks (C1, C2, C3, C4, C5, C6, C7, C8, C9). The design, legal and specialized hauling trucks can be seen in Appendix C6A and Appendix D6A of AASHTO's *Manual for Bridge Evaluation* (2008). The MaineDoT trucks were provided directly from the MaineDoT and are provided in APPENDIX A: Figure A.1 – Figure A.9. Each bridge was analyzed for each truck even if the rating factors for the bridge exceeded one for HL-93 and/or legal trucks to provide as much information as possible regarding rating factors and live load moments for each bridge.

3.4. Load Ratings

The following sections describe the minimum load rating factors along with the maximum live load moment that caused the minimum load rating factors. These load ratings will be for each of the bridges that were discussed in section 3.2 and for all the trucks discussed in section 3.3. First the conventional strip width method results will be presented, followed by the results from SlabRate.

3.4.1. Conventional Strip Width Method

The current AASHTO *Manual for Bridge Evaluation* (AASHTO 2008) uses the equivalent strip width method for calculating live load effects in slab bridges, and provides guidelines to load rate existing bridges according to the equivalent strip width method. These load rating guidelines are what the MaineDoT currently follows for load rating bridges. The general load rating equation is still used for the finite element model. However, the finite element model is used to determine slab bending moments within the bridge instead of the conventional strip width method. The general load rating equations used with both the finite element results and the conventional strip width method are shown below in Equation 3.1 – Equation 3.3 (AASHTO 2008, Equation 6A.4.2.1 -1, 6A.4.2.1 -2, 6A.4.2.1 -3 respectively):

$$RF = \frac{C - (\gamma_{DC})(DC) - (\gamma_{DW})(DW) - (\gamma_P)(P)}{(\gamma_{LL})(LL + IM)} \qquad \text{Equation 3.1}$$

For Strength Limit States:

$$C = R_n \varphi_c \varphi_s \varphi \qquad \text{Equation 3.2}$$

And the following lower limit applies:

$$\varphi_c \varphi_s \geq 0.85 \qquad \text{Equation 3.3}$$

Where:

RF = rating factor

C = capacity

DC = dead load effect due to structural components and attachments

DW = dead load effect due to wearing surface and utilities

P = permanent loads other than dead loads

LL = live load effect

IM = dynamic load effect (impact)

γ_{DC} = LRFD load factor for structural components and attachments

γ_{DW} = LRFD load factor for wearing surface and utilities

γ_{P} = LRFD load factor for permanent loads other than dead loads

γ_{LL} = evaluation live load factor

φ_c = condition factor

φ_s = system factor

φ = LRFD resistance factor

R_n = nominal member resistance

To determine the equivalent strip width, section 4.6.2.3 of the 2010 AASHTO *LRFD Bridge Design Specifications* (AASHTO 2010) is used. The maximum moments for a wheel line are then determined for the bridge by modeling the bridge has a beam, either continuous or single span depending on the bridge, and that moment is then distributed over the equivalent strip width to get a moment per unit width. The equivalent strip is taken as the minimum of the equivalent strip width for one lane loaded or for

multiple lanes of loading. The equations to determine the strip width are shown below in Equation 3.4 and Equation 3.5 (AASHTO 2010, Equations 4.6.2.3-1 and 4.6.2.3-1 respectively):

For one lane of loading:

$$E = 250 + 0.42\sqrt{L_1 W_1} \qquad \text{Equation 3.4}$$

For multiple lanes of loading:

$$E = 2100 + 0.12\sqrt{L_1 W_1} \le \frac{W}{N_L} \qquad \text{Equation 3.5}$$

Where:

E = equivalent width (mm)

L_1 = modified span length taken equal to the lesser of the actual span or 18000 (mm)

W_1 = modified edge-to-edge width of bridge taken to be equal to the lesser of the actual width or 18000 for multilane loading, or 9000 for single-lane loading (mm)

W = physical edge to edge width of bridge (mm)

N_L = number of design lane as specified in Article 3.6.1.1.1

For skewed bridges, the longitudinal force effects may be reduced by the factor *r* given in Equation 3.6 (AASHTO 2010, Equation 4.6.2.3 -3)*:*

$$r = 1.05 - 0.25\tan\theta \le 1.00 \qquad \text{Equation 3.6}$$

Where:

θ = skew angle (degrees)

3.4.1.1. Load Rating Factors

Table 3.3 – Table 3.6 are the load rating factors based on the conventional strip width method for the twenty bridges that were provided by the MaineDoT. Load rating factors were calculated for every truck specified in section 3.3. APPENDIX B: Table B.1 provides additional data from the load rating calculations. This data includes the equivalent strip width (E), the dead load moments do to structural components and attachments (M_{DC}) and wearing surface and utilities (M_{DW}).

Table 3.3 – Rating factors for the conventional strip width for Albion Bridge #2529, Argyle Bridge #3427, Bradford Bridge #3430, Brewer Bridge #5638 and Carmel Bridge #5191

Live Load Truck	Albion Bridge #2529	Argyle Bridge #3827	Bradford Bridge #3430	Brewer Bridge #5638	Carmel Bridge #5191
Design Truck - Lane - Inventory	0.365	0.799	0.469	0.721	0.354
Design Tandem - Lane - Inventory	0.293	0.637	0.372	0.573	0.325
Design Truck - Lane - Operating	0.473	1.036	0.608	0.935	0.459
Design Tandem - Lane - Operating	0.380	0.825	0.482	0.743	0.421
AASHTO Type 3 Truck	0.471	1.026	0.603	0.929	0.515
AASHTO Type 3S2 Truck	0.516	1.126	0.651	1.006	0.537
AASHTO Type 3-3	0.572	1.246	0.733	1.128	0.634
AASHTO-notional	0.408	0.873	0.497	0.771	0.380
AASHTO-SU4	0.454	0.987	0.576	0.889	0.486
AASHTO-SU5	0.430	0.929	0.536	0.828	0.462
AASHTO-SU6	0.408	0.873	0.500	0.775	0.418
AASHTO-SU7	0.408	0.873	0.497	0.771	0.396
MaineDoT C1	0.403	0.872	0.507	0.783	0.446
MaineDoT C2	0.403	0.872	0.507	0.783	0.388
MaineDoT C3	0.403	0.872	0.507	0.783	0.414
MaineDoT C4	0.434	0.918	0.521	0.811	0.432
MaineDoT C5	0.392	0.857	0.506	0.779	0.438
MaineDoT C6	0.300	0.650	0.379	0.586	0.326
MaineDoT C7	0.375	0.799	0.462	0.714	0.395
MaineDoT C8	0.574	1.232	0.716	1.111	0.621
MaineDoT C9	0.369	0.813	0.483	0.744	0.372

Table 3.4 – Rating factors for the conventional strip width for Carmel Bridge #5632, Chester Bridge #5907, Exeter Bridge #5838, Greenfield Bridge #5605 and Hermon Bridge #2205

Live Load Truck	Carmel Bridge #5632	Chester Bridge #5907	Exeter Bridge #5838	Greenfield Bridge #5605	Hermon Bridge #2205
Design Truck - Lane - Inventory	0.741	1.090	0.818	0.587	0.347
Design Tandem - Lane - Inventory	0.593	1.052	0.660	0.470	0.285
Design Truck - Lane - Operating	0.960	1.413	1.060	0.760	0.450
Design Tandem - Lane - Operating	0.769	1.364	0.856	0.609	0.369
AASHTO Type 3 Truck	0.957	1.624	1.078	0.758	0.454
AASHTO Type 3S2 Truck	1.049	1.733	1.137	0.831	0.497
AASHTO Type 3-3	1.162	1.977	1.309	0.920	0.551
AASHTO-notional	0.812	1.195	0.862	0.644	0.408
AASHTO-SU4	0.918	1.554	1.025	0.727	0.441
AASHTO-SU5	0.862	1.464	0.948	0.683	0.424
AASHTO-SU6	0.812	1.336	0.878	0.644	0.408
AASHTO-SU7	0.812	1.263	0.862	0.644	0.408
MaineDoT C1	0.811	1.454	0.900	0.643	0.394
MaineDoT C2	0.811	1.224	0.878	0.643	0.394
MaineDoT C3	0.811	1.285	0.900	0.643	0.394
MaineDoT C4	0.858	1.330	0.910	0.680	0.440
MaineDoT C5	0.801	1.356	0.908	0.634	0.377
MaineDoT C6	0.604	1.041	0.677	0.479	0.290
MaineDoT C7	0.746	1.281	0.815	0.592	0.360
MaineDoT C8	1.155	2.020	1.273	0.915	0.565
MaineDoT C9	0.755	1.152	0.845	0.598	0.347

Table 3.5 – Rating factors for the conventional strip width for Levant Bridge #5253, Liberty Bridge #5638, Linneus Bridge #5311, Linneus Bridge #5773 and Milford Bridge #2070

Live Load Truck	Levant Bridge #5253	Liberty Bridge #5638	Linneus Bridge #5311	Linneus Bridge #5773	Milford Bridge #2070
Design Truck - Lane - Inventory	0.464	0.326	0.502	0.679	0.906
Design Tandem - Lane - Inventory	0.385	0.268	0.403	0.547	0.767
Design Truck - Lane - Operating	0.602	0.423	0.651	0.880	1.175
Design Tandem - Lane - Operating	0.499	0.347	0.523	0.710	0.994
AASHTO Type 3 Truck	0.632	0.438	0.649	0.893	1.265
AASHTO Type 3S2 Truck	0.657	0.459	0.712	0.946	1.301
AASHTO Type 3-3	0.767	0.532	0.789	1.084	1.537
AASHTO-notional	0.492	0.345	0.553	0.717	0.960
AASHTO-SU4	0.600	0.417	0.623	0.851	1.194
AASHTO-SU5	0.551	0.384	0.586	0.788	1.094
AASHTO-SU6	0.508	0.354	0.553	0.730	1.005
AASHTO-SU7	0.495	0.346	0.553	0.717	0.974
MaineDoT C1	0.514	0.365	0.551	0.747	1.045
MaineDoT C2	0.485	0.350	0.551	0.730	0.974
MaineDoT C3	0.514	0.365	0.551	0.747	1.045
MaineDoT C4	0.510	0.364	0.584	0.755	1.025
MaineDoT C5	0.517	0.369	0.543	0.751	1.047
MaineDoT C6	0.382	0.272	0.410	0.562	0.759
MaineDoT C7	0.464	0.331	0.508	0.679	0.938
MaineDoT C8	0.725	0.512	0.784	1.052	1.465
MaineDoT C9	0.467	0.338	0.511	0.702	0.938

Table 3.6 – Rating factors for the conventional strip width for Milo Bridge #2931, Monroe Bridge #5538, Newcastle Bridge #5608, Palmyra Bridge #5699 and Sherman Bridge #2899

Live Load Truck	Milo Bridge #2931	Monroe Bridge #5538	Newcastle Bridge #5608	Palmyra Bridge #5699	Sherman Bridge #2899
Design Truck - Lane - Inventory	1.975	0.849	0.814	0.815	0.283
Design Tandem - Lane - Inventory	1.575	0.736	0.683	0.654	0.250
Design Truck - Lane - Operating	2.560	1.101	1.055	1.056	0.366
Design Tandem - Lane - Operating	2.042	0.955	0.855	0.848	0.324
AASHTO Type 3 Truck	2.567	1.221	1.123	1.053	0.408
AASHTO Type 3S2 Truck	2.717	1.235	1.164	1.155	0.418
AASHTO Type 3-3	3.117	1.483	1.364	1.279	0.506
AASHTO-notional	2.070	0.902	0.864	0.898	0.301
AASHTO-SU4	2.441	1.133	1.066	1.011	0.380
AASHTO-SU5	2.257	1.047	0.977	0.952	0.355
AASHTO-SU6	2.097	0.959	0.899	0.898	0.324
AASHTO-SU7	2.070	0.923	0.873	0.898	0.310
MaineDoT C1	2.143	1.004	0.932	0.896	0.341
MaineDoT C2	2.103	0.918	0.880	0.896	0.306
MaineDoT C3	2.143	1.004	0.932	0.896	0.333
MaineDoT C4	2.173	0.976	0.920	0.961	0.327
MaineDoT C5	2.153	1.002	0.935	0.881	0.339
MaineDoT C6	1.606	0.737	0.691	0.667	0.249
MaineDoT C7	1.943	0.898	0.840	0.824	0.304
MaineDoT C8	3.027	1.408	1.316	1.268	0.477
MaineDoT C9	2.042	0.884	0.844	0.829	0.295

3.4.1.2. Max Live Load Moments

Table 3.7 – Table 3.10 are the maximum live load moments based on the conventional strip width method for the twenty bridges that were provided by the MaineDoT. These live load moments include a dynamic impact factor of 33% and also include lane load effects for vehicles where a lane load was also included.

Table 3.7 – Maximum live load moments (kN-m/m) for the conventional strip width for Albion Bridge #2529, Argyle Bridge #3427, Bradford Bridge #3430, Brewer Bridge #5638 and Carmel Bridge #5191

Live Load Truck	Albion Bridge #2529	Argyle Bridge #3827	Bradford Bridge #3430	Brewer Bridge #5638	Carmel Bridge #5191
Design Truck - Lane - Inventory	144.14	120.44	132.08	152.32	152.32
Design Tandem - Lane - Inventory	179.61	151.18	166.61	191.68	191.68
Design Truck - Lane - Operating	144.14	120.44	132.08	152.32	152.32
Design Tandem - Lane - Operating	179.61	151.18	166.61	191.68	191.68
AASHTO Type 3 Truck	108.81	91.18	99.81	115.01	115.01
AASHTO Type 3S2 Truck	99.21	83.13	92.51	106.21	106.21
AASHTO Type 3-3	89.61	75.09	82.20	94.72	94.72
AASHTO-notional	141.14	120.60	136.43	155.79	155.79
AASHTO-SU4	128.35	106.69	117.63	135.22	135.22
AASHTO-SU5	133.94	113.37	126.50	145.10	145.10
AASHTO-SU6	141.14	120.60	135.51	155.15	155.15
AASHTO-SU7	141.14	120.60	136.43	155.79	155.79
MaineDoT C1	142.81	120.71	133.62	153.45	153.45
MaineDoT C2	142.81	120.71	133.62	153.45	153.45
MaineDoT C3	142.81	120.71	133.62	153.45	153.45
MaineDoT C4	132.76	114.68	130.04	148.12	148.12
MaineDoT C5	146.82	122.80	133.98	154.25	154.25
MaineDoT C6	192.05	161.91	178.65	205.17	205.17
MaineDoT C7	153.58	131.69	146.67	168.25	168.25
MaineDoT C8	100.33	85.42	94.56	108.19	108.19
MaineDoT C9	155.98	129.50	140.31	161.49	161.49

Table 3.8 – Maximum live load moments (kN-m/m) for the conventional strip width for Carmel Bridge #5632, Chester Bridge #5907, Exeter Bridge #5838, Greenfield Bridge #5605 and Hermon Bridge #2205

Live Load Truck	Carmel Bridge #5632	Chester Bridge #5907	Exeter Bridge #5838	Greenfield Bridge #5605	Hermon Bridge #2205
Design Truck - Lane - Inventory	134.26	259.89	139.59	127.77	104.18
Design Tandem - Lane - Inventory	167.62	269.21	172.80	159.44	127.03
Design Truck - Lane - Operating	134.26	259.89	139.59	127.77	104.18
Design Tandem - Lane - Operating	167.62	269.21	172.80	159.44	127.03
AASHTO Type 3 Truck	101.06	169.57	102.89	96.17	77.53
AASHTO Type 3S2 Truck	92.12	158.89	97.55	87.67	70.69
AASHTO Type 3-3	83.23	139.32	84.74	79.18	63.84
AASHTO-notional	134.02	259.24	144.79	127.35	96.86
AASHTO-SU4	118.50	199.37	121.84	112.76	89.69
AASHTO-SU5	126.24	211.60	131.76	120.01	93.26
AASHTO-SU6	134.02	231.97	142.21	127.35	96.86
AASHTO-SU7	134.02	245.27	144.79	127.35	96.86
MaineDoT C1	134.11	213.03	138.74	127.53	100.45
MaineDoT C2	134.11	253.19	142.25	127.53	100.45
MaineDoT C3	134.11	241.23	138.74	127.53	100.45
MaineDoT C4	126.86	232.91	137.14	120.55	89.97
MaineDoT C5	135.80	228.42	137.49	129.31	105.03
MaineDoT C6	180.06	297.72	184.29	171.30	136.25
MaineDoT C7	145.77	241.89	153.11	138.56	109.80
MaineDoT C8	94.17	153.37	98.08	89.63	69.95
MaineDoT C9	144.08	268.85	147.64	137.18	113.95

Table 3.9 – Maximum live load moments (kN-m/m) for the conventional strip width for Levant Bridge #5253, Liberty Bridge #5638, Linneus Bridge #5311, Linneus Bridge #5773 and Milford Bridge #2070

Live Load Truck	Levant Bridge #5253	Liberty Bridge #5638	Linneus Bridge #5311	Linneus Bridge #5773	Milford Bridge #2070
Design Truck - Lane - Inventory	155.11	153.94	133.11	148.11	164.84
Design Tandem - Lane - Inventory	187.04	187.80	165.94	183.73	194.75
Design Truck - Lane - Operating	155.11	153.94	133.11	148.11	164.84
Design Tandem - Lane - Operating	187.04	187.80	165.94	183.73	194.75
AASHTO Type 3 Truck	110.82	111.47	100.13	109.52	114.84
AASHTO Type 3S2 Truck	106.53	106.45	91.28	103.38	111.67
AASHTO Type 3-3	91.26	91.81	82.47	90.17	94.46
AASHTO-notional	160.08	159.20	132.33	153.33	170.14
AASHTO-SU4	131.32	131.89	117.34	129.22	136.81
AASHTO-SU5	142.91	143.14	124.82	139.63	149.38
AASHTO-SU6	155.01	155.20	132.33	150.66	162.51
AASHTO-SU7	159.09	158.80	132.33	153.33	167.67
MaineDoT C1	153.31	150.44	132.69	147.19	156.38
MaineDoT C2	162.42	157.11	132.69	150.75	167.70
MaineDoT C3	153.31	150.44	132.69	147.19	156.38
MaineDoT C4	154.60	151.02	125.17	145.68	159.37
MaineDoT C5	152.29	149.10	134.60	146.57	156.11
MaineDoT C6	206.14	201.77	178.28	195.81	215.22
MaineDoT C7	169.88	166.23	144.08	162.05	174.27
MaineDoT C8	108.72	107.25	93.37	104.58	111.55
MaineDoT C9	168.52	162.58	143.01	156.76	174.25

Table 3.10 – Maximum live load moments (kN-m/m) for the conventional strip width for Milo Bridge #2931, Monroe Bridge #5538, Newcastle Bridge #5608, Palmyra Bridge #5699 and Sherman Bridge #2899

Live Load Truck	Milo Bridge #2931	Monroe Bridge #5538	Newcastle Bridge #5608	Palmyra Bridge #5699	Sherman Bridge #2899
Design Truck - Lane - Inventory	130.09	178.26	153.04	117.87	189.90
Design Tandem - Lane - Inventory	163.10	205.65	187.73	146.73	214.77
Design Truck - Lane - Operating	130.09	178.26	157.48	117.73	189.90
Design Tandem - Lane - Operating	163.10	205.65	187.73	146.73	214.77
AASHTO Type 3 Truck	97.28	120.55	110.98	88.60	127.80
AASHTO Type 3S2 Truck	91.92	119.26	107.16	80.79	124.86
AASHTO Type 3-3	80.11	99.28	91.41	72.97	103.07
AASHTO-notional	135.76	183.53	162.27	116.89	195.10
AASHTO-SU4	115.11	146.21	131.58	103.86	154.44
AASHTO-SU5	124.50	158.13	143.50	110.31	165.07
AASHTO-SU6	133.96	172.68	156.04	116.89	181.18
AASHTO-SU7	135.76	179.40	160.63	116.89	189.32
MaineDoT C1	131.11	164.90	150.39	117.24	171.88
MaineDoT C2	133.57	180.46	159.42	117.24	191.45
MaineDoT C3	131.11	164.90	150.39	117.24	176.15
MaineDoT C4	129.29	169.70	152.40	109.33	179.22
MaineDoT C5	130.47	165.30	149.95	119.18	173.12
MaineDoT C6	174.91	224.68	203.11	157.55	235.53
MaineDoT C7	144.58	184.38	166.90	127.45	192.79
MaineDoT C8	92.81	117.61	106.58	82.82	123.13
MaineDoT C9	137.57	187.27	166.19	126.69	198.97

3.4.2. FE-Based Load Ratings

The finite element-based load rating uses the program SlabRate that was described in Chapter 2. The rating factors are calculated using the same equations as the conventional strip width method, Equation 3.1 – Equation 3.3, but the dead and live load moments are computed by SlabRate using 2-D plate finite element analysis.

3.4.2.1. Load Ratings Factors

Table 3.11 – Table 3.14 are the load rating factors provided by SlabRate based on finite element analysis for the twenty bridges that were provided by the MaineDoT. APPENDIX C: Table C.1 – Table C.20 provides additional information that was calculated using SlabRate, which is used in the determination of the minimum rating factors. This information includes the number of lanes loaded, and the dead load moments due to structural components and attachments (M_{DC}) and wearing surface and utilities (M_{DW}). Also the tables present the location where the minimum rating factor occurs measured, the location is defined in the global coordinate system defined in SlabRate (see section 2.2.2).

Table 3.11 – Rating factors for the finite element analysis for Albion Bridge #2529, Argyle Bridge #3427, Bradford Bridge #3430, Brewer Bridge #5638 and Carmel Bridge #5191

Live Load Truck	Albion Bridge #2529	Argyle Bridge #3827	Bradford Bridge #3430	Brewer Bridge #5638	Carmel Bridge #5191
Design Truck - Lane - Inventory	1.100	0.979	0.567	2.804	0.934
Design Tandem - Lane - Inventory	0.992	0.804	0.451	2.714	0.832
Design Truck - Lane - Operating	1.427	1.269	0.735	3.635	1.210
Design Tandem - Lane - Operating	1.286	1.043	0.585	3.518	1.078
AASHTO Type 3 Truck	1.536	1.288	0.734	4.232	1.352
AASHTO Type 3S2 Truck	1.686	1.413	0.797	4.623	1.407
AASHTO Type 3-3	1.870	1.579	0.894	5.166	1.661
AASHTO-notional	1.455	1.100	0.603	4.046	1.004
AASHTO-SU4	1.580	1.240	0.708	4.367	1.281
AASHTO-SU5	1.528	1.166	0.660	4.226	1.208
AASHTO-SU6	1.465	1.100	0.616	4.134	1.093
AASHTO-SU7	1.452	1.100	0.604	4.088	1.034
MaineDoT C1	1.397	1.116	0.624	3.772	1.159
MaineDoT C2	1.453	1.103	0.624	3.983	1.019
MaineDoT C3	1.453	1.104	0.624	4.034	1.086
MaineDoT C4	1.430	1.161	0.648	3.825	1.102
MaineDoT C5	1.248	1.071	0.617	3.336	1.121
MaineDoT C6	1.052	0.816	0.469	2.953	0.841
MaineDoT C7	1.187	1.073	0.564	3.158	1.042
MaineDoT C8	1.703	1.533	0.879	4.464	1.571
MaineDoT C9	1.063	0.986	0.580	2.690	0.979

Table 3.12 – Rating factors for the finite element analysis for Carmel Bridge #5632, Chester Bridge #5907, Exeter Bridge #5838, Greenfield Bridge #5605 and Hermon Bridge #2205

Live Load Truck	Carmel Bridge #5632	Chester Bridge #5907	Exeter Bridge #5838	Greenfield Bridge #5605	Hermon Bridge #2205
Design Truck - Lane - Inventory	1.522	1.375	1.200	0.996	0.461
Design Tandem - Lane - Inventory	1.321	1.286	0.950	0.813	0.399
Design Truck - Lane - Operating	1.972	1.783	1.555	1.291	0.597
Design Tandem - Lane - Operating	1.522	1.668	1.232	1.053	0.518
AASHTO Type 3 Truck	2.107	2.048	1.542	1.299	0.633
AASHTO Type 3S2 Truck	2.278	2.155	1.659	1.418	0.688
AASHTO Type 3-3	2.553	2.480	1.864	1.577	0.764
AASHTO-notional	1.857	1.465	1.279	1.131	0.571
AASHTO-SU4	2.099	1.942	1.496	1.278	0.614
AASHTO-SU5	1.991	1.832	1.409	1.213	0.593
AASHTO-SU6	1.896	1.663	1.297	1.140	0.572
AASHTO-SU7	1.866	1.550	1.282	1.131	0.572
MaineDoT C1	1.887	1.799	1.355	1.142	0.573
MaineDoT C2	1.888	1.493	1.282	1.140	0.559
MaineDoT C3	1.886	1.586	1.338	1.140	0.556
MaineDoT C4	1.949	1.657	1.340	1.184	0.603
MaineDoT C5	1.753	1.685	1.286	1.080	0.515
MaineDoT C6	1.375	1.291	0.933	0.849	0.404
MaineDoT C7	1.637	1.585	1.181	1.015	0.493
MaineDoT C8	2.397	2.505	1.816	1.553	0.755
MaineDoT C9	1.494	1.453	1.225	0.999	0.455

Table 3.13 – Rating factors for the finite element analysis for Levant Bridge #5253, Liberty Bridge #5638, Linneus Bridge #5311, Linneus Bridge #5773 and Milford Bridge #2070

Live Load Truck	Levant Bridge #5253	Liberty Bridge #5638	Linneus Bridge #5311	Linneus Bridge #5773	Milford Bridge #2070
Design Truck - Lane - Inventory	0.571	0.546	1.184	1.285	1.260
Design Tandem - Lane - Inventory	0.456	0.416	1.057	1.062	1.038
Design Truck - Lane - Operating	0.740	0.708	1.535	1.666	1.634
Design Tandem - Lane - Operating	0.591	0.539	1.370	1.376	1.346
AASHTO Type 3 Truck	0.751	0.682	1.658	1.724	1.706
AASHTO Type 3S2 Truck	0.757	0.733	1.817	1.859	1.777
AASHTO Type 3-3	0.913	0.828	2.049	2.094	2.072
AASHTO-notional	0.582	0.534	1.497	1.413	1.324
AASHTO-SU4	0.723	0.658	1.662	1.683	1.649
AASHTO-SU5	0.663	0.607	1.582	1.572	1.515
AASHTO-SU6	0.606	0.554	1.513	1.451	1.388
AASHTO-SU7	0.582	0.534	1.498	1.420	1.331
MaineDoT C1	0.629	0.572	1.499	1.480	1.440
MaineDoT C2	0.595	0.551	1.494	1.446	1.351
MaineDoT C3	0.628	0.571	1.495	1.477	1.438
MaineDoT C4	0.640	0.592	1.531	1.494	1.425
MaineDoT C5	0.635	0.581	1.354	1.420	1.427
MaineDoT C6	0.473	0.433	1.088	1.106	1.073
MaineDoT C7	0.566	0.533	1.306	1.320	1.282
MaineDoT C8	0.898	0.833	1.853	1.974	1.964
MaineDoT C9	0.588	0.564	1.162	1.286	1.285

Table 3.14 – Rating factors for the finite element analysis for Milo Bridge #2931, Monroe Bridge #5538, Newcastle Bridge #5608, Palmyra Bridge #5699 and Sherman Bridge #2899

Live Load Truck	Milo Bridge #2931	Monroe Bridge #5538	Newcastle Bridge #5608	Palmyra Bridge #5699	Sherman Bridge #2899
Design Truck - Lane - Inventory	2.361	1.144	1.089	0.941	0.520
Design Tandem - Lane - Inventory	1.909	0.980	0.911	0.769	0.435
Design Truck - Lane - Operating	3.061	1.483	1.411	1.219	0.675
Design Tandem - Lane - Operating	2.475	1.271	1.181	0.996	0.564
AASHTO Type 3 Truck	3.092	1.613	1.483	1.237	0.723
AASHTO Type 3S2 Truck	3.307	1.639	1.544	1.357	0.740
AASHTO Type 3-3	3.781	1.958	1.808	1.509	0.879
AASHTO-notional	2.556	1.212	1.157	1.070	0.538
AASHTO-SU4	2.975	1.515	1.421	1.198	0.681
AASHTO-SU5	2.801	1.402	1.299	1.132	0.632
AASHTO-SU6	2.578	1.286	1.204	1.069	0.576
AASHTO-SU7	2.560	1.230	1.171	1.073	0.547
MaineDoT C1	2.644	1.351	1.253	1.074	0.605
MaineDoT C2	2.571	1.227	1.163	1.069	0.548
MaineDoT C3	2.644	1.329	1.250	1.069	0.594
MaineDoT C4	2.690	1.295	1.223	1.121	0.588
MaineDoT C5	2.575	1.321	1.226	1.031	0.593
MaineDoT C6	1.961	0.988	0.928	0.790	0.443
MaineDoT C7	2.351	1.189	1.105	0.976	0.542
MaineDoT C8	3.580	1.830	1.698	1.480	0.850
MaineDoT C9	2.410	1.172	1.112	0.948	0.545

3.4.2.2. Max Live Load Moments

Table 3.15 – Table 3.18 are the maximum live load moments provided by SlabRate based on finite element analysis for the twenty bridges that were provided by the MaineDoT. These live load moments include a dynamic impact factor of 33% and also include lane load effects for vehicles where a lane load was also included.

Table 3.15 – Maximum live load moments (kN-m/m) for the finite element analysis for Albion Bridge #2529, Argyle Bridge #3427, Bradford Bridge #3430, Brewer Bridge #5638 and Carmel Bridge #5191

Live Load Truck	Albion Bridge #2529	Argyle Bridge #3827	Bradford Bridge #3430	Brewer Bridge #5638	Carmel Bridge #5191
Design Truck - Lane - Inventory	65.55	100.81	111.84	51.38	139.54
Design Tandem - Lane - Inventory	69.22	119.71	136.22	52.64	156.92
Design Truck - Lane - Operating	65.55	100.81	111.84	51.38	139.54
Design Tandem - Lane - Operating	69.22	119.71	136.22	52.64	156.92
AASHTO Type 3 Truck	45.04	72.67	81.43	32.82	93.67
AASHTO Type 3S2 Truck	41.02	66.28	77.31	30.30	90.01
AASHTO Type 3-3	37.51	59.31	66.90	27.17	76.38
AASHTO-notional	53.49	95.81	111.49	38.95	141.87
AASHTO-SU4	49.58	84.93	97.88	36.08	111.41
AASHTO-SU5	50.94	90.36	105.04	37.29	117.97
AASHTO-SU6	53.13	95.77	109.27	38.14	130.62
AASHTO-SU7	53.61	95.76	111.43	38.54	137.99
MaineDoT C1	69.83	94.36	107.66	42.44	122.97
MaineDoT C2	51.67	95.53	107.71	39.57	139.80
MaineDoT C3	51.70	95.42	107.72	39.07	131.41
MaineDoT C4	55.18	91.75	108.95	42.62	129.26
MaineDoT C5	63.21	98.35	112.30	47.24	127.14
MaineDoT C6	75.01	129.06	147.84	53.36	169.45
MaineDoT C7	66.49	104.56	122.80	49.91	138.19
MaineDoT C8	46.34	69.48	80.41	35.30	93.41
MaineDoT C9	74.21	109.42	119.57	58.58	145.48

Table 3.16 – Maximum live load moments (kN-m/m) for the finite element analysis for Carmel Bridge #5632, Chester Bridge #5907, Exeter Bridge #5838, Greenfield Bridge #5605 and Hermon Bridge #2205

Live Load Truck	Carmel Bridge #5632	Chester Bridge #5907	Exeter Bridge #5838	Greenfield Bridge #5605	Hermon Bridge #2205
Design Truck - Lane - Inventory	74.97	206.40	107.97	89.18	88.35
Design Tandem - Lane - Inventory	86.98	217.28	134.10	109.23	102.00
Design Truck - Lane - Operating	74.97	206.40	107.97	89.18	88.35
Design Tandem - Lane - Operating	86.98	217.28	134.10	109.23	102.00
AASHTO Type 3 Truck	53.03	134.75	80.34	66.44	62.55
AASHTO Type 3S2 Truck	49.05	126.10	73.28	60.86	57.55
AASHTO Type 3-3	43.77	113.07	66.45	54.72	51.80
AASHTO-notional	67.67	208.71	108.97	82.50	78.02
AASHTO-SU4	59.52	159.83	93.19	75.99	72.60
AASHTO-SU5	62.68	166.87	97.01	80.07	75.15
AASHTO-SU6	63.10	183.79	105.39	81.80	77.85
AASHTO-SU7	64.09	197.26	108.72	82.50	77.90
MaineDoT C1	63.40	169.91	102.86	81.92	77.72
MaineDoT C2	63.70	204.75	106.69	81.92	79.61
MaineDoT C3	63.41	192.71	102.22	81.92	80.10
MaineDoT C4	64.46	184.54	102.03	82.00	73.87
MaineDoT C5	71.72	184.27	108.34	89.86	86.42
MaineDoT C6	90.73	236.80	137.66	114.41	110.22
MaineDoT C7	76.21	195.87	115.77	95.58	90.36
MaineDoT C8	52.51	123.94	75.94	62.52	59.03
MaineDoT C9	83.49	217.09	115.91	97.20	97.84

Table 3.17 – Maximum live load moments (kN-m/m) for the finite element analysis for Levant Bridge #5253, Liberty Bridge #5638, Linneus Bridge #5311, Linneus Bridge #5773 and Milford Bridge #2070

Live Load Truck	Levant Bridge #5253	Liberty Bridge #5638	Linneus Bridge #5311	Linneus Bridge #5773	Milford Bridge #2070
Design Truck - Lane - Inventory	130.79	111.29	74.98	91.67	126.49
Design Tandem - Lane - Inventory	154.53	133.30	80.21	107.62	147.82
Design Truck - Lane - Operating	130.79	111.29	74.98	91.67	126.49
Design Tandem - Lane - Operating	154.53	133.30	80.21	107.62	147.82
AASHTO Type 3 Truck	91.26	79.01	52.05	66.26	87.45
AASHTO Type 3S2 Truck	90.09	73.47	47.49	59.75	85.53
AASHTO Type 3-3	75.11	65.05	42.90	54.55	72.01
AASHTO-notional	132.46	113.51	61.94	88.43	126.74
AASHTO-SU4	110.38	92.13	58.43	75.70	101.81
AASHTO-SU5	116.24	99.71	61.39	79.49	110.79
AASHTO-SU6	127.29	109.36	61.30	86.12	120.93
AASHTO-SU7	132.43	113.35	61.90	88.01	126.07
MaineDoT C1	122.51	105.96	64.79	84.46	116.55
MaineDoT C2	129.56	109.94	62.10	86.41	126.54
MaineDoT C3	122.74	106.05	62.02	84.61	116.70
MaineDoT C4	120.42	102.37	63.15	86.25	119.44
MaineDoT C5	121.40	104.26	71.69	90.51	119.67
MaineDoT C6	168.83	139.99	89.28	116.50	159.10
MaineDoT C7	140.99	125.58	74.04	97.58	133.31
MaineDoT C8	90.90	81.07	52.40	65.12	86.97
MaineDoT C9	138.78	119.70	83.55	100.17	135.71

Table 3.18 – Maximum live load moments (kN-m/m) for the finite element analysis for Milo Bridge #2931, Monroe Bridge #5538, Newcastle Bridge #5608, Palmyra Bridge #5699 and Sherman Bridge #2899

Live Load Truck	Milo Bridge #2931	Monroe Bridge #5538	Newcastle Bridge #5608	Palmyra Bridge #5699	Sherman Bridge #2899
Design Truck - Lane - Inventory	101.00	140.32	123.67	101.82	136.35
Design Tandem - Lane - Inventory	124.90	163.74	142.68	122.66	163.05
Design Truck - Lane - Operating	101.00	140.32	123.67	101.82	136.35
Design Tandem - Lane - Operating	124.90	163.74	142.68	122.66	163.05
AASHTO Type 3 Truck	74.99	96.74	85.18	74.09	95.47
AASHTO Type 3S2 Truck	70.12	94.89	81.83	67.55	93.22
AASHTO Type 3-3	61.69	79.68	71.61	60.75	78.47
AASHTO-notional	100.90	144.29	122.89	97.86	144.29
AASHTO-SU4	87.67	115.48	100.06	87.48	114.08
AASHTO-SU5	93.11	124.77	109.40	92.56	122.88
AASHTO-SU6	100.07	136.01	118.10	98.01	134.78
AASHTO-SU7	100.79	139.62	118.18	97.61	141.90
MaineDoT C1	97.54	129.45	113.44	95.97	128.29
MaineDoT C2	100.34	142.55	122.21	96.47	141.68
MaineDoT C3	97.55	131.66	113.74	96.44	130.69
MaineDoT C4	96.47	135.59	117.17	94.22	131.97
MaineDoT C5	101.31	132.93	120.06	101.64	130.86
MaineDoT C6	132.99	177.64	153.18	132.67	175.16
MaineDoT C7	110.94	147.13	128.66	107.29	143.21
MaineDoT C8	73.29	95.93	84.40	71.38	96.15
MaineDoT C9	110.84	153.27	132.41	110.55	149.91

3.5. Comparison / Discussion

The results show that the FEA model SlabRate increases the rating factors compared to the conventional strip width method by an average of 24.14% for non-skewed bridges, 48.12% for 15° skew bridges, 146.65% for 30° skew bridges and 299.75% for 45° skew bridges for all of the trucks. Similar increases were generally observed for the HL-93 design loadings, AASHTO legal loads, specialized hauling vehicles, and the MaineDoT rating trucks. These results indicate that finite element analysis is less conservative than the equivalent strip width method that is conventionally used in load rating.

Per the results of the SlabRate analyses, thirteen bridges that would have had an operating rating factor less than one and were at risk for posting based on the conventional strip width method had rating factors greater than one based on finite-element analysis. These bridges are Albion Bridge #2529, Argyle Township Bridge #3827, Brewer Bridge #5638, Carmel Bridge #5191, Carmel Bridge #5632, Exeter Bridge #5838, Greenfield Township Bridge #5605, Linneus Bridge #5311, Linneus Bridge #5773, Milford Bridge #2070, Monroe Bridge #5538, Newcastle Bridge #5608 and Palmyra Bridge #5699. Two bridges, Chester Bridge #5907 and Milo Bridge #2931 had rating factors greater than one using the conventional strip width method.

However, one issue that had not been sufficiently addressed at the time these load ratings were done is the effect of skew angle. The SlabRate analyses considers only longitudinal bending moments, and as skew angle increases, the transverse and torsional bending moments become more significant, which may lead to lower rating factors. Menassa et al. (2007) studied the effect of skew angle on slab analysis, concluding that

the AASHTO provisions for predicting longitudinal bending moments can be very conservative for skew angles over 20 degrees, which is consistent with the results of this chapter. However, as discussed by Théoret et al. (2011), large skew angles can cause large transverse moments as well as shear forces that may govern capacity, and simplified code provisions must account for these transverse moments and shear forces. Denton and Burgoyne (1996) examined the flexural assessment of reinforced concrete slabs with skewed reinforcement, proposing refined methods where skew is rigorously taken into account when determining bending strength.

The effect of skew angle is probably most pronounced for the Albion Bridge #2529, Brewer Bridge #5638, Carmel Bridge #5191, Carmel Bridge #5632, Linneus Bridge #5311, and Linneus Bridge #5773, which had skew angles greater than 20 degrees. Additional research was done to assess the significance of skew angle and develop modified FE-based slab load rating procedures to better account for slab skew angle. This is discussed in greater detail in Chapter 5, but no values were modified in this chapter due to the conclusions in Chapter 5.

CHAPTER 4. FIELD LOAD TESTING

The purpose of the live load testing was to gain experience with the BDI STS-WiFi bridge load test instrumentation system, and to provide data for comparison with finite element predictions of slab response. The MaineDoT provided personnel for traffic control along with the test trucks used to load the bridge. The Bridge Diagnostics Inc. (BDI) wireless structural testing system (STS-WiFi) was used for recording strain data during the tests. This chapter includes a description of the BDI STS-WiFi system, the test bridge characteristics, the instrumentation plan, and the test truck information. The test data and comparisons of test data to finite element modeling are also reported and discussed.

4.1. BDI STS-WiFi System

The BDI STS-WiFi System is a wireless system that is used in non-destructive live load testing of existing bridges. The system was used due to its ease of installation compared with traditional wired systems and gauges, as well as the ability to re-use gauges in future tests. The following sections describe the equipment used in the BDI STS-WiFi system.

4.1.1. BDI STS-WiFi Intelligent Strain Transducers

The BDI STS – WiFi system incorporated the use of BDI's ST350 Intelligent Strain Transducers (gauges). The gauges use a full Wheatstone bring circuit, with four active 350 ohm foil gauges with a 4-wire hookup allowing for more sensitive strain readings to be captured by the system, providing accuracy of $\pm 2\mu\varepsilon$ (Bridge Diagnostics Inc. 2010). The gauges have a built in environmental protective cover. Each gauge

measures 111 mm x 32 mm x 13 mm and weighs approximately 85 g. These transducers have an effective gauge length of 76.2 mm. Each individual gauge contains a memory chip with its identification number so the BDI software automatically identifies each gauge and applies the correct calibration factor to each gauge. The gauges can also be attached to extensions. When testing concrete structures, the use of the extensions will allow the effective gauge length to increase from 76.2 mm to 609.6 mm in intervals of 76.2 mm. Each gauge has a cable that is between 4.57 m to 7.62 m long to attach to the STS-WiFi Nodes. Figure 4.1 shows two gauges attached to Bradford Bridge #3430 before the test was run. One gauge has an extension and one does not. The identification number is visible on each gauge.

Figure 4.1 – BDI ST350 Intelligent Strain Transducers attached to Bradford Bridge #3430 for live load test

4.1.2. BDI STS-WiFi Nodes and Base Station

The STS-WiFi Mobile Base Station is a rechargeable battery powered wireless relay station. It transmits the data from the nodes to the computer running the BDI data acquisition software. Up to four gauges can be attached to a single STS WiFi node, The nodes and mobile base station are powered by rechargeable batteries and use broadband wireless technology to communicate between the nodes and the mobile base station. Each node also has its own identification number so the software can recognize which nodes are synchronized to the base station. A photo of an STS-WiFi Node is shown in Figure 4.2.

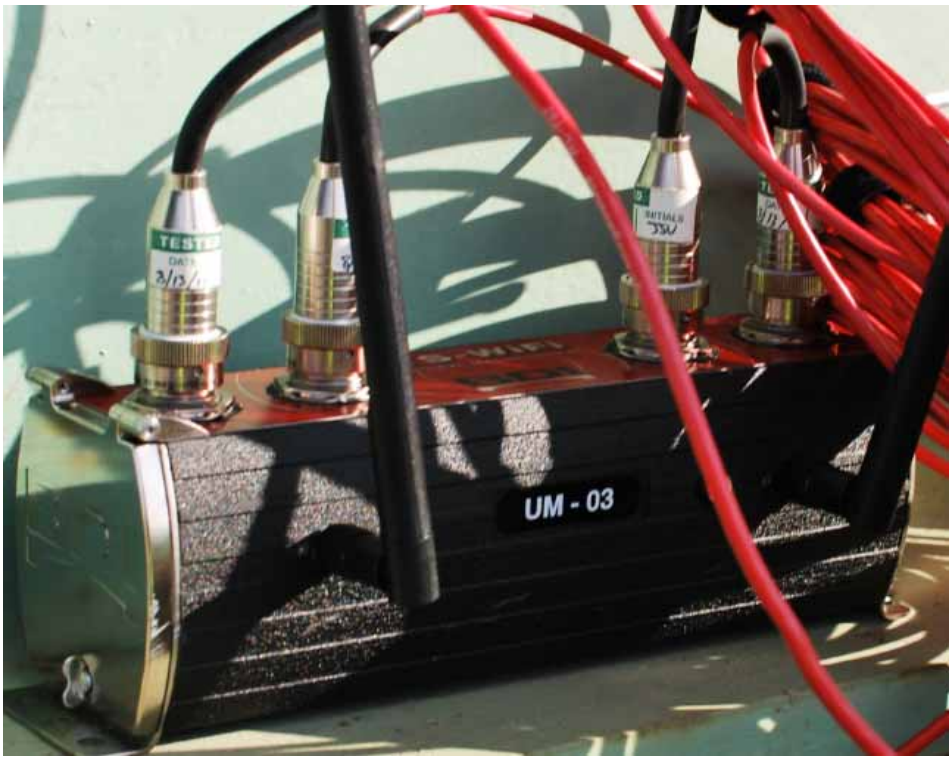

Figure 4.2 – Photo of the STS-WiFi Node, with gauges plugged into each of the four ports

4.2. Test Set-Up

This section addresses the testing plan for the live load tests of Bradford Bridge #3430. This will include the bridge characteristics, the instrumentation plan for the bridge and the test truck information used in the live load test.

4.2.1. Bridge Information

The Bradford Bridge #3430 was chosen for the live load test because this constant thickness concrete slab bridge has no skew and is near the University of Maine. At the time of the bridge test the effects of large skews had not been definitively quantified, making a non-skewed bridge preferred for testing. Additionally, the bridge had a load rating of less than one, which makes the load effect of a heavy truck more pronounced than on a bridge with a rating factor exceeding one.

4.2.1.1. Bridge Characteristics

The characteristics of Bradford Bridge #3430 are shown in Table 4.1. The concrete slab was assumed to have a compressive strength $f_c^{'}$ of 17.24 MPa, an elastic modulus of 19640 MPa, a Poisson's ratio of 0.19 and a unit weight of 2400 kg/m^3. The plans for the bridge were provided by the MaineDoT. The length is the considered to be the distance between the centerline of each support.

The plans provided by the MaineDoT did not include the clear distance to the reinforcing or the area of steel in the transverse direction. A value of 51 mm was assumed for the clear distance to the reinforcing. Review of the plans of similar structures from the same era indicated clear distances of 25 mm to 51 mm. The area of steel in the transverse direction was assumed by using a similar procedure. The transverse reinforcing of similar bridges that were built around the same time were examined and it was found that two bridges had similar properties (year of construction, non-skewed and span length) to that of the Bradford Bridge. These structures had #5 bars transversely spaced at 0.24 m, which was assumed to be the transverse reinforcement for the Bradford Bridge #3430. The longitudinal moment resistance, transverse moment resistance, and longitudinal cracking moment, are also summarized in Table 4.1. The moment resistances were computed according to AASHTO provisions (2010), and these values do not include the strength reduction factor ϕ . The cracking moment was computed assuming a composite section consisting of uncracked concrete and steel and a modular ratio n = 10.18. The tensile rupture strength of the concrete taken to be 2310 kPa based on AASHTO (2010) and the assumed value for $f_c^{'}$ of 17.24 MPa.

Table 4.1 – Bridge characteristics of Bradford Bridge #3430

Length (m)	Width (m)	Slab Thickness (m)	Area of Steel – Longit. (cm2/m)	Area of Steel – Transv. (cm2/m)	Moment Resistance (Mn) – Longit. (kN-m/m)	Moment Resistance (Mn) – Transv.(kN-m/m)	Cracking Moment – Longit. (kN-m/m)	Cracking Moment – Transv. (kN-m/m)
7.16	7.62	0.419	31.92	8.20	240.3	70.81	77.6	71.2

Bradford Bridge #3430 was one of the bridges that were load rated using both the conventional strip width and the FEA methods in Chapter 3. The final load ratings for the bridge are summarized in Table 4.2. These load ratings provided are the minimum values for each of the load rating transient loads: design loads, legal loads and the Maine Department of Transportation (MaineDoT) loads. The design transient loads include the HL-93 Truck and HL-93 Tandem trucks, which include the design lane load, as specified in the AASHTO Bridge Design Specifications (AASHTO 2010). These design trucks were analyzed under both inventory and operating levels. The legal transient loads included the AASHTO Legal loads and the specialized hauling vehicles, as specified in AASHTO Bridge Design Specifications (AASHTO 2010). The MaineDoT transient loads included MaineDoT trucks C1 – C9, these axle spacing and weights for these trucks are given in APPENDIX A: Figure A.1 – Figure A.9.

Table 4.2 – Load ratings for Bradford Bridge #3430

	Strip Width Method	FEA Method
Design Load Rating HL-93 Operating Rating	0.482	0.585
AASHTO Legal Load Rating	0.497	0.603
MaineDoT Load Rating	0.379	0.469

4.2.1.2. Instrumentation Plan

Twenty two gauges were placed on the bridge for the live load test. The locations of the gauges are shown in Figure 4.3 and Figure 4.4 for the gauges on the top and bottom of the bridge respectively. The wide range of gauge locations was chosen to provide a complete picture of the response of the structure and provide redundant measurements. Table 4.3 summarizes gauge locations and which gauges used extensions during the tests. The *x* and *y* locations are measured from the centerline of the support on the downstream right side of the bridge (bottom left of Figure 4.3 and Figure 4.4). Gauges were not placed on the top side of the interior part of the bridge (everywhere other than the curbs and rails) because this would have necessitated removal of the wearing surface in order to place the gauge directly to the top of the slab. The gauges that were placed on the top of the bridge are located on either the top of the inner curb or the top of the bottom railing as shown in Figure 4.5. The top gauges that have y-locations of 0.23 m and 7.39 m are placed on the top of the bottom rail like gauge B3058 in Figure 4.5. The gauges with y-locations of 0.38 m and 7.24 m are located on the top of the inner side of the curb like gauge B3071 in Figure 4.5. Even though extensions are recommended when testing reinforced concrete we could not use them for every gauge as our system only included six extensions. However, the most critical gauges located at the bottom of the slab at mid-span (10, 12, 14, 16 and 18) all had extensions.

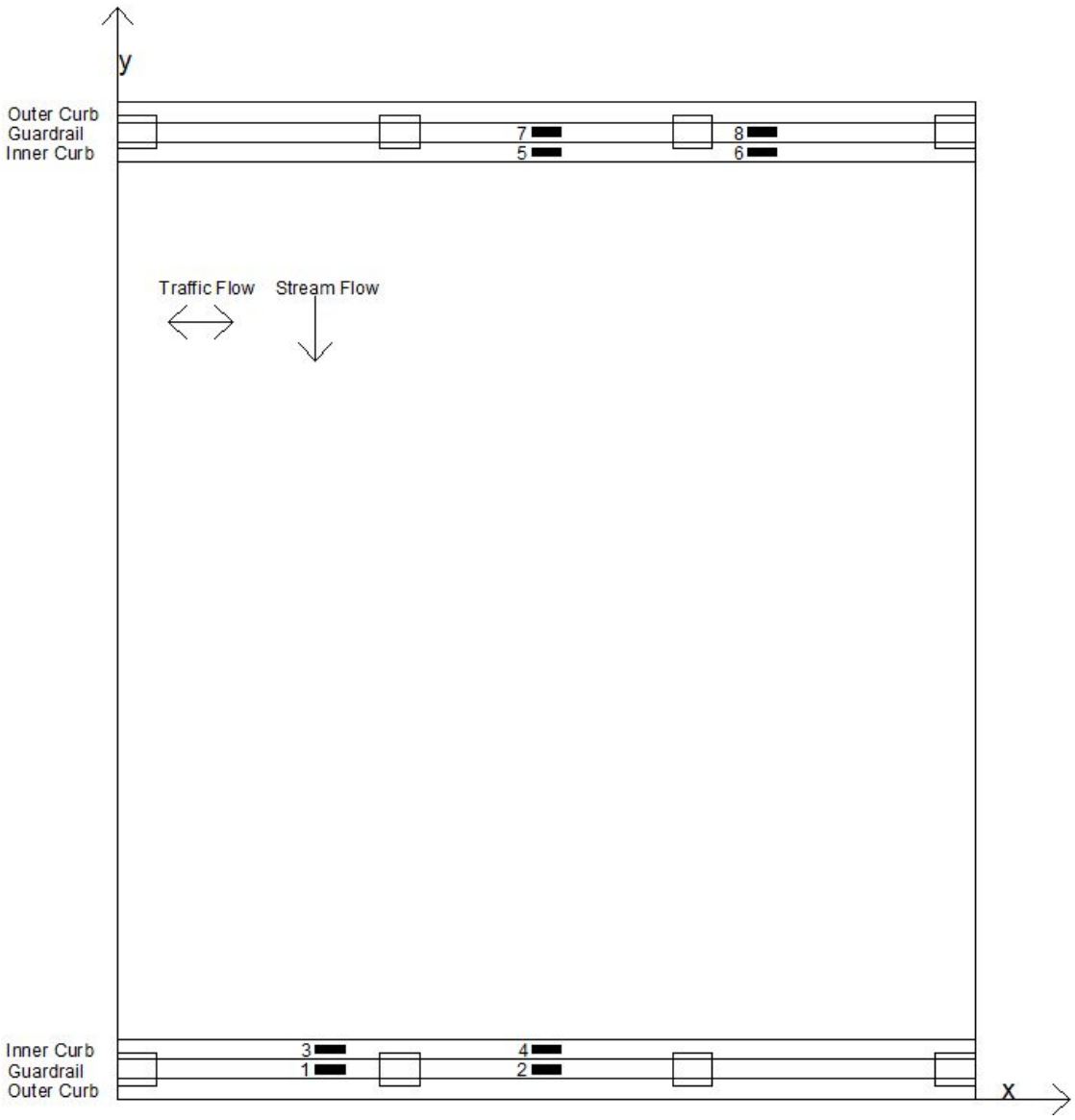

Figure 4.3 – Schematic of gauges located on the top of the bridge

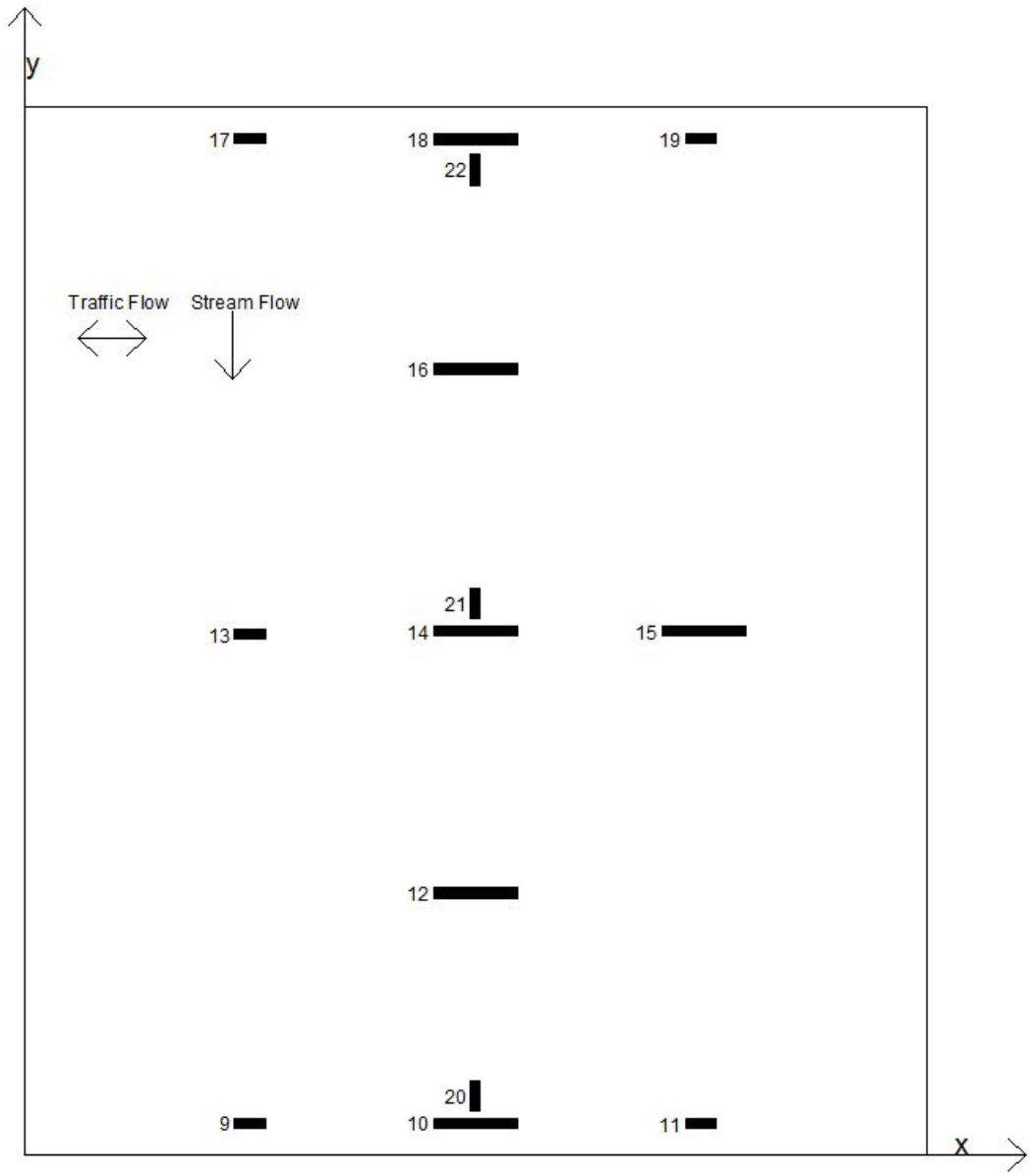

Figure 4.4 – Schematic of gauges located on the bottom of the bridge (longer gauges indicates an extension)

Table 4.3 – Location of each of the 22 gauges used in the live load test of Bradford Bridge #3430

Figure Reference Number	BDI Gauge Number	x – Location (m)	y – Location (m)	Top or Bottom	Gauge Direction	Extension?
1	B3058	1.96	0.23	Top	Longitudinal	No
2	B3065	3.58	0.23	Top	Longitudinal	No
3	B3071	1.96	0.38	Top	Longitudinal	No
4	B3055	3.58	0.38	Top	Longitudinal	No
5	B3056	3.58	7.24	Top	Longitudinal	No
6	B3069	5.23	7.24	Top	Longitudinal	No
7	B3066	3.58	7.39	Top	Longitudinal	No
8	B3061	5.23	7.39	Top	Longitudinal	No
9	B3072	1.96	0.23	Bottom	Longitudinal	No
10	B3070	3.58	0.23	Bottom	Longitudinal	Yes
11	B3068	5.23	0.23	Bottom	Longitudinal	No
12	B3076	3.58	1.91	Bottom	Longitudinal	Yes
13	B7073	1.96	3.81	Bottom	Longitudinal	No
14	B3062	3.58	3.81	Bottom	Longitudinal	Yes
15	B3060	5.23	3.81	Bottom	Longitudinal	Yes
16	B3064	3.58	5.71	Bottom	Longitudinal	Yes
17	B3063	1.96	7.39	Bottom	Longitudinal	No
18	B3059	3.58	7.39	Bottom	Longitudinal	Yes
19	B3075	5.23	7.39	Bottom	Longitudinal	No
20	B3057	3.58	0.32	Bottom	Transverse	No
21	B3074	3.58	3.9	Bottom	Transverse	No
22	B3067	3.58	7.28	Bottom	Transverse	No

Figure 4.5 – Top gauge placements on the top of curb and top of the bottom rail

4.2.2. Truck Information

The Bradford Bridge live load test was conducted with two trucks provided by the MaineDoT. The total weight of each individual truck was measured. The length of one tire revolution was determined for each truck, so the longitudinal position of the truck could be determined throughout the test. This was done by measuring the distance that truck moves for nine full tire revolutions. Both of the trucks traveled 29.96 m. Therefore one tire revolution covered a distance of 3.33 m. Figure 4.6 and Figure 4.7 show the distances between each of the axles and individual wheels for MaineDoT trucks #1 and #2 respectively. The measured width of each wheel was 228.6 mm.

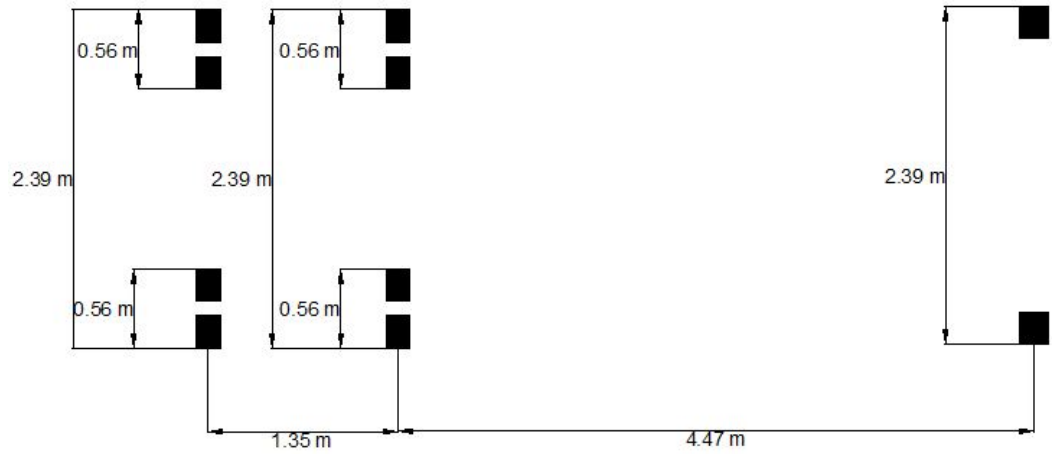

Figure 4.6 – Wheel spacing for MaineDoT Truck #1

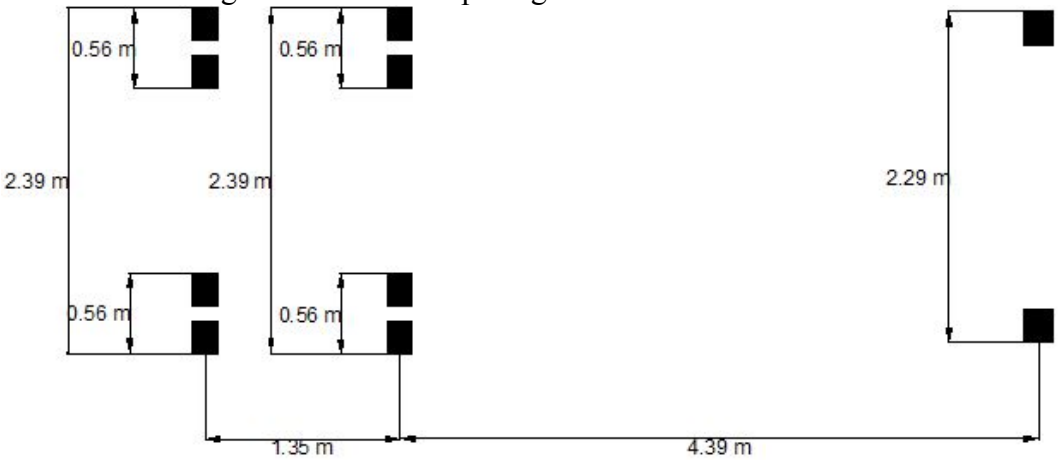

Figure 4.7 – Wheel spacing for MaineDoT Truck #2

The weights of each individual axle were not recorded, but were estimated by averaging five separate MaineDoT trucks that were used during previous live load testing done by the AEWC Center. The truck axle weights and total truck weights for each of the trucks that have been used previously are shown in Table 4.4 – Table 4.7. Table 4.4 is the average of two separate trucks while Table 4.5 - Table 4.7 are only one truck.

Table 4.4 – Axle positions and weights for the average of two MaineDoT Trucks used in first Neal Bridge live load test

Axle Position (mm from front axle)	Weight of Each Axle (kN)	Percentage of Total Weight (kN)
0	75.84	26%
4521.2	112.32	37%
5918.2	108.31	37%
Total Weight	296.47	

Table 4.5 – Axle positions and weights for the MaineDoT Truck used in second Neal Bridge live load test (2011)

Axle Position (mm from front axle)	Weight of Each Axle (kN)	Percentage of Total Weight (kN)
0	63.61	26%
4826.0	88.96	37%
6197.6	88.96	37%
Total Weight	241.54	

Table 4.6 – Axle positions and weights for the MaineDoT Truck used in Fairfield Bridge live load test

Axle Position (mm from front axle)	Weight of Each Axle (kN)	Percentage of Total Weight (kN)
0	65.90	21%
4521.2	122.20	40%
5994.4	120.30	39%
Total Weight	308.40	

Table 4.7 – Axle positions and weights for the MaineDoT Truck used in Coplin Plantation live load test

Axle Position (mm from front axle)	Weight of Each Axle (kN)	Percentage of Total Weight (kN)
0	57.50	20%
4394.2	114.10	40%
5753.1	113.90	40%
Total Weight	285.50	

As can be seen in Table 4.4 – Table 4.7 all the trucks have relatively the same distribution of weights. The front axle is between 20-26% of the total truck weight while the back axles are all between 37-40%. Since all these trucks have the same relative

distribution, the average of the axle distributions were used to determine the axle weights for the trucks used in the Bradford live load test as given in Table 4.8 and Table 4.9.

Table 4.8 – Axle positions and weights for the MaineDoT Truck #1 used in Bradford Bridge live load test

Axle Position (mm from front axle)	Axle Weight (kN)	Percentage of Total Weight
0	58.03	23%
4470.4	95.88	38%
5816.6	98.40	39%
Total Weight	252.30	

Table 4.9- Axle positions and weights for the MaineDoT Truck #2 used in Bradford Bridge live load test

Axle Position (mm from front axle)	Axle Weight (kN)	Percentage of Total Weight
0	59.54	23%
4394.2	98.38	38%
5740.4	100.97	39%
Total Weight	258.89	

4.2.2.1. Individual Wheel Weights and Sizes

When creating the finite element models to compare to the test data the individual wheel weights and the size of the contact area had to be determined. It was assumed that each tire in each axle shared the weight equally. Therefore to determine the weights on each individual tire the axle weight had to be divided by the number of wheels on that axle.

The contact area of each tire also needed to be determined for the Abaqus models so the tire contact area in the models was similar to the size of the actual tire contact area. It was assumed the inflation pressure of each tire was 620.5 kPa and that the tire contact pressure was uniform. The widths of the tires were measured during the test and each tire was 228.6 mm wide. The contact length of the tire was calculated by Equation 4.1. The

contact length for each axle's tires for MaineDoT truck #1 and #2 are shown in Table 4.10 and Table 4.11 respectively.

$$L = \frac{P_{tire}}{620.5\text{kPa} \times 0.2286\text{m}} \qquad \text{Equation 4.1}$$

Where;

L = contact length of the tire

P_{tire} = weight in each individual tire

Table 4.10 – Contact length for MaineDoT Truck #1 used in Bradford Bridge #3430 live load test

Axle Position (mm from front axle)	Weight to Each Tire (kN)	Contact Length (m)
0	29.02	0.205
4470.4	23.97	0.169
5816.6	24.60	0.173

Table 4.11 – Contact length for MaineDoT Truck #2 used in Bradford Bridge #3430 live load test

Axle Position (mm from front axle)	Weight to Each Tire (kN)	Contact Length (m)
0	29.77	0.210
4394.2	24.60	0.173
5740.4	25.24	0.178

4.3. Live Load Test

The live load test of Bradford Bridge #3430 was conducted on October 21st, 2011 using the MaineDoT three axle dump trucks described above. The MaineDoT also provided flaggers for the test so the traffic on the bridge could be stopped during the test.

4.3.1. Test Truck Positions

Seven different tests were run during the live load test of the Bradford Bridge. Four different transverse truck positions were used during the test. Tests 1 and 2 used the same transverse truck position, tests 3 and 4 used the same transverse truck position and

tests 5 and 6 used the same transverse truck positions. These truck positions were run twice to ensure the results were consistent and repeatable.

The truck position for tests 1 and 2 are shown in Figure 4.8. The outside of the front tire was placed 0.61 m away from the inside face of the downstream side of the inner curb. Figure 4.9 shows the truck position for test 3 and 4. This truck position was the opposite of test 1 and 2, as it was the outside of the front tire placed 0.61 m away from the inside face of the upstream side curb. Both of the tests used truck #2 provided by the MaineDoT because it was the larger of the two trucks. These positions were used because it was as close as it could be placed to the edge of the bridge according to AASHTO's *Manual for Bridge Evaluation* (AASHTO 2008). Also, since with the striped lane width on the Bradford Bridge was only 2.74 m, and the truck was 2.29 m wide, only one truck pass was run for each lane. Test 1-4 were run to maximize the strains in the gauges located on the outside edges of the bridge.

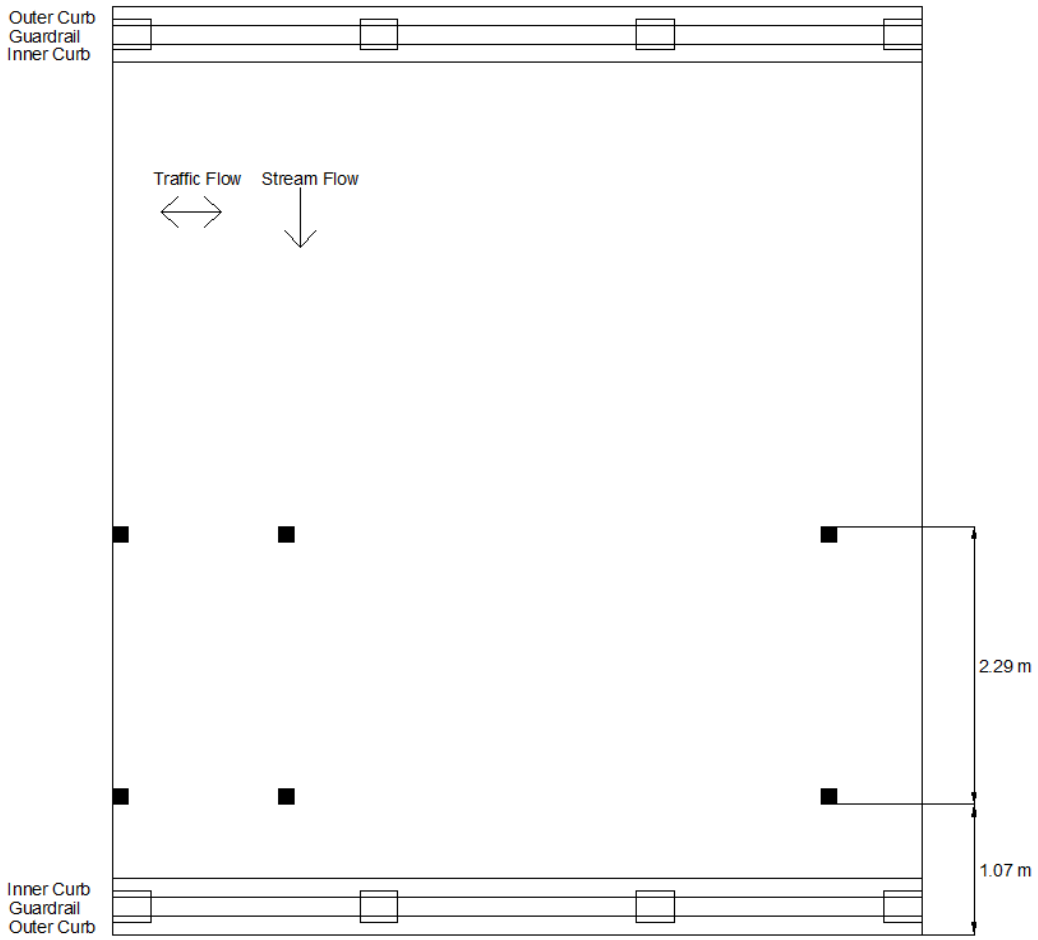

Figure 4.8 – Position of truck during live load tests 1 and 2

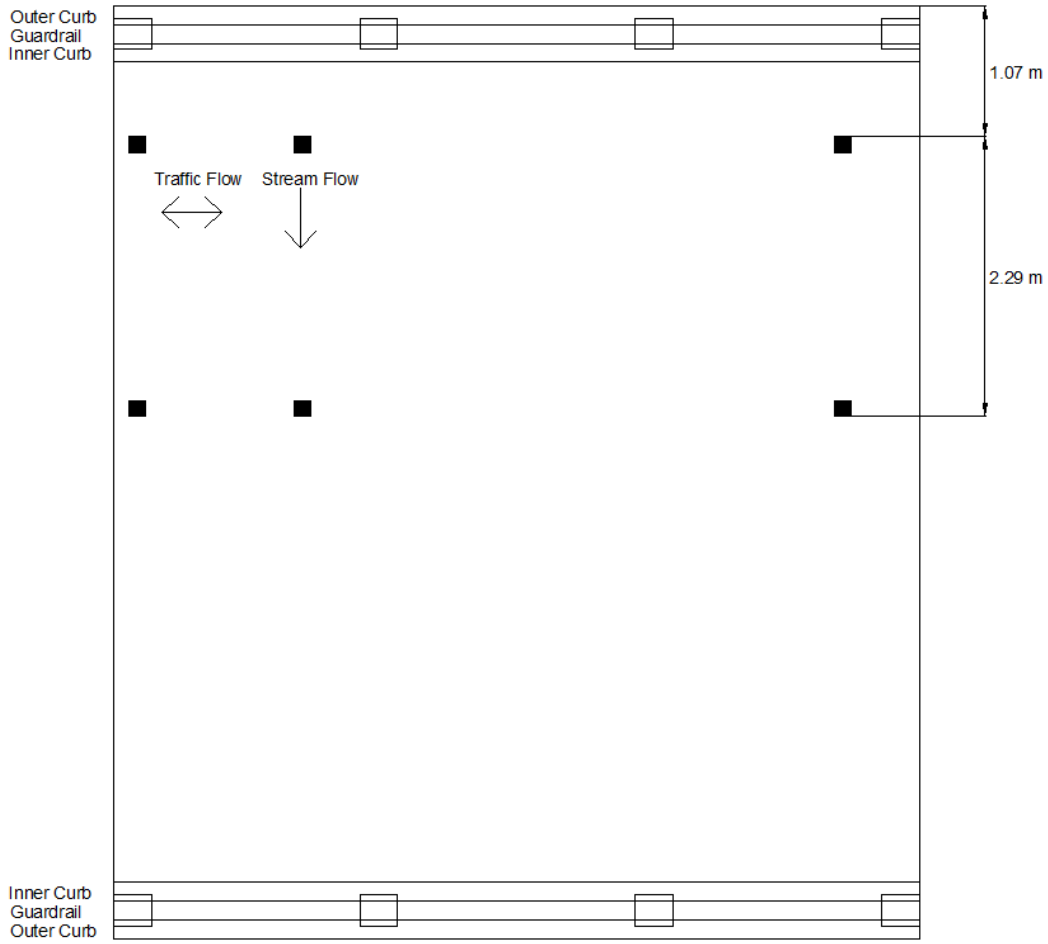

Figure 4.9 – Position of truck during live load tests 3 and 4

Figure 4.10 shows the transverse truck placement for tests 5 and 6. These tests were conducted with both the trucks on the bridge, truck # 2 placed on the upstream side and truck # 1 on the downstream side. Truck #2 was placed 0.61 m away from the upstream inner curb just like in test 3 and 4. With truck #1 placed 1.22 m away from truck #2, the closest distance to place trucks according to AASHTO's *Manual for Bridge Evaluation* (AASHTO 2008), that left the outside of truck #1's tires 0.31 m from the inner face of the downstream curb. The reason the test was not done the other way (truck #2 placed 0.61 m from the downstream face of the inner curb and truck #1 placed 1.22 m away from the inner tires) was that it only shifted the trucks by 0.31 m, which was not expected to significantly affect strains.

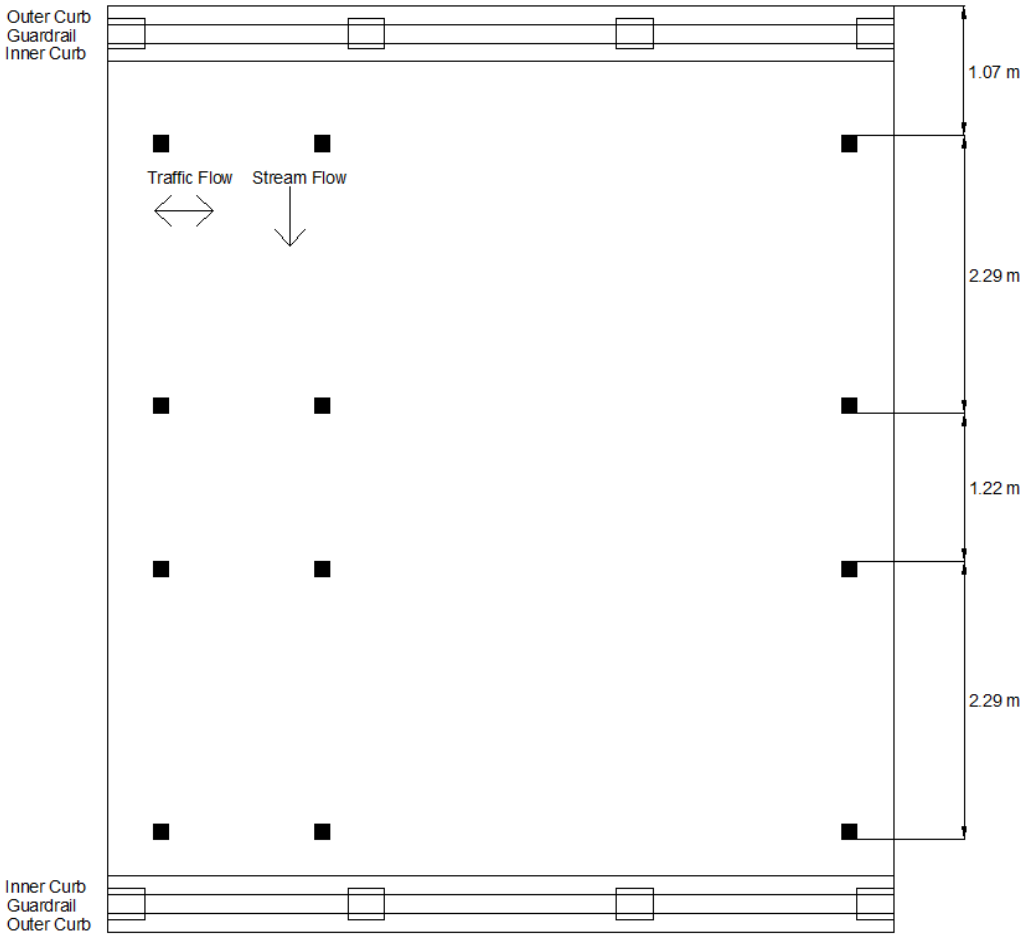

Figure 4.10 – Position of truck during live load tests 5 and 6

Figure 4.11 shows the placement of the truck during test #7. The centerline of the truck was positioned over the transverse centerline of the bridge. Truck #2 was used in this test like the other test that only used one truck because it was heavier then truck #1. This test was run to maximize the strains over the transverse centerline of the bridge when only one truck was placed on the bridge.

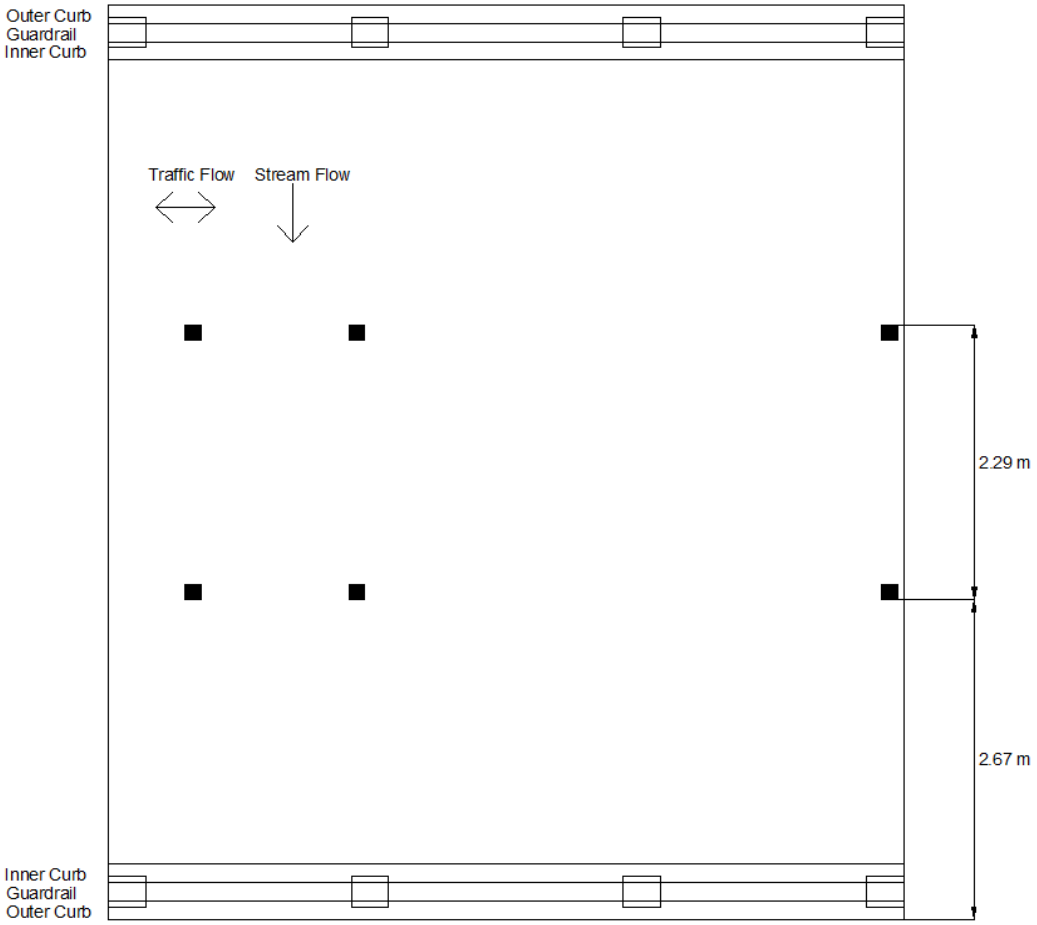

Figure 4.11 – Position of truck #2 during live load test 7

4.3.2. Resulting Strains for Each Live Load Test

From each of the seven tests the resulting strains in the twenty two gauges were recorded. The resulting strains from each live load test can be seen in APPENDIX D: Figure D.1 – Figure D.49. Figure 4.12 – Figure 4.18 are plots of strains vs. truck position during the live load test that produces the maximum strain for each individual gauge for only one truck of loading, live load tests 1 – 4 and 7. Figure 4.19 – Figure 4.25 are plots of strain vs. truck position for the tests that caused the maximum strain in each individual gauge when two trucks were used in the live load test, test 5 and 6. The position of the front axle is measured from the centerline of the support where the truck started moving.

The maximum value of strain in each gauge for both one and two truck loading cases will be compared to the Abaqus finite element model that is presented in the following sections.

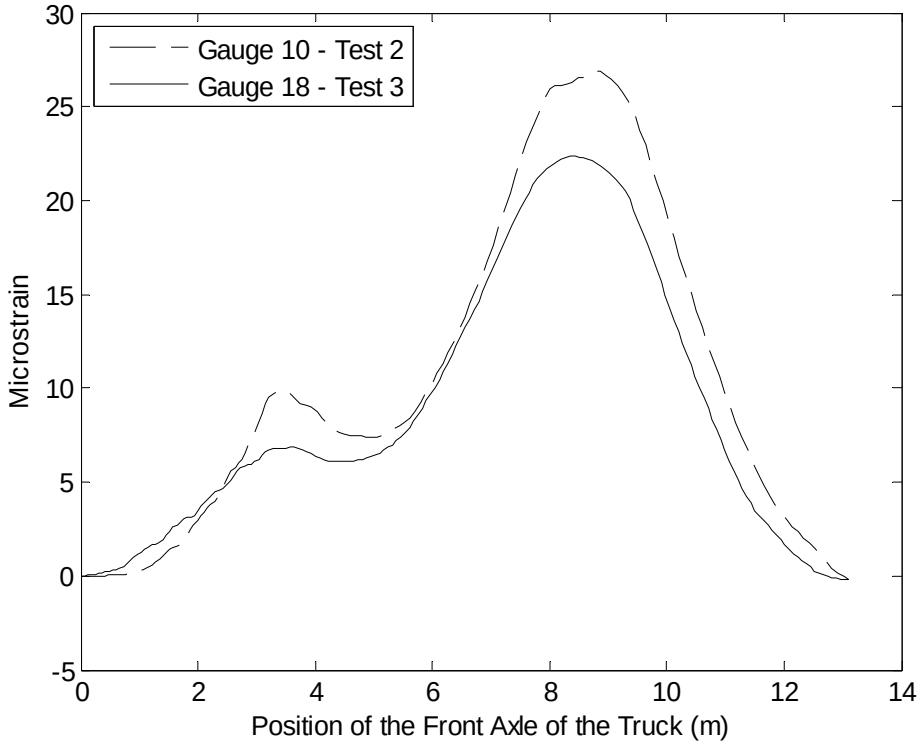

Figure 4.12 – Worst one-truck loading case for gauges located under the curb at centerline span

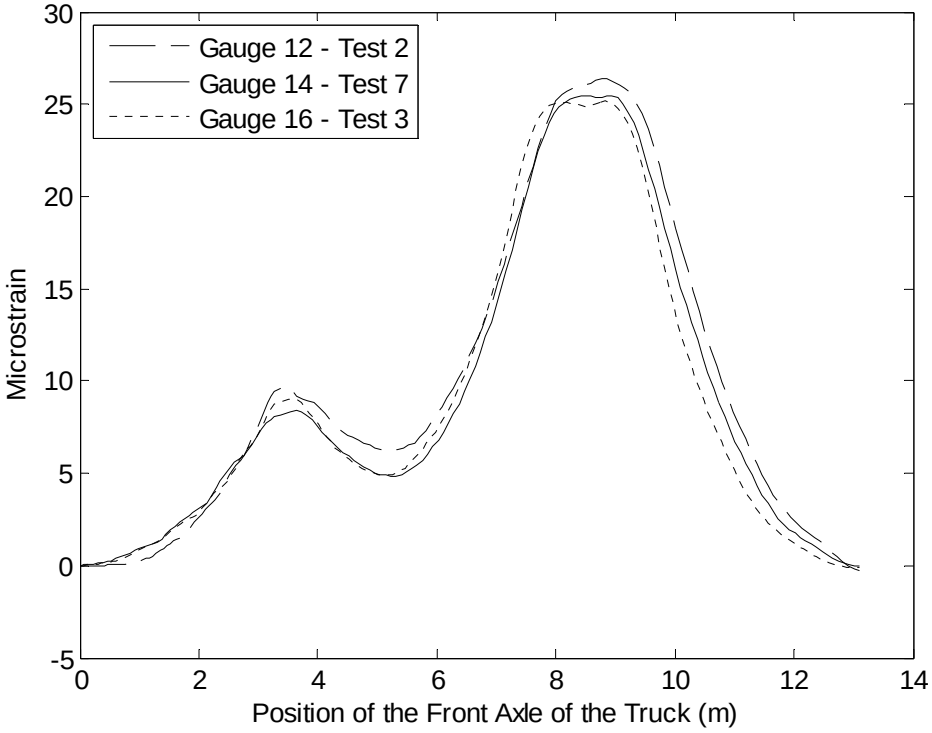

Figure 4.13 – Worst one-truck loading case for bottom gauges located at centerline span away from the curbs

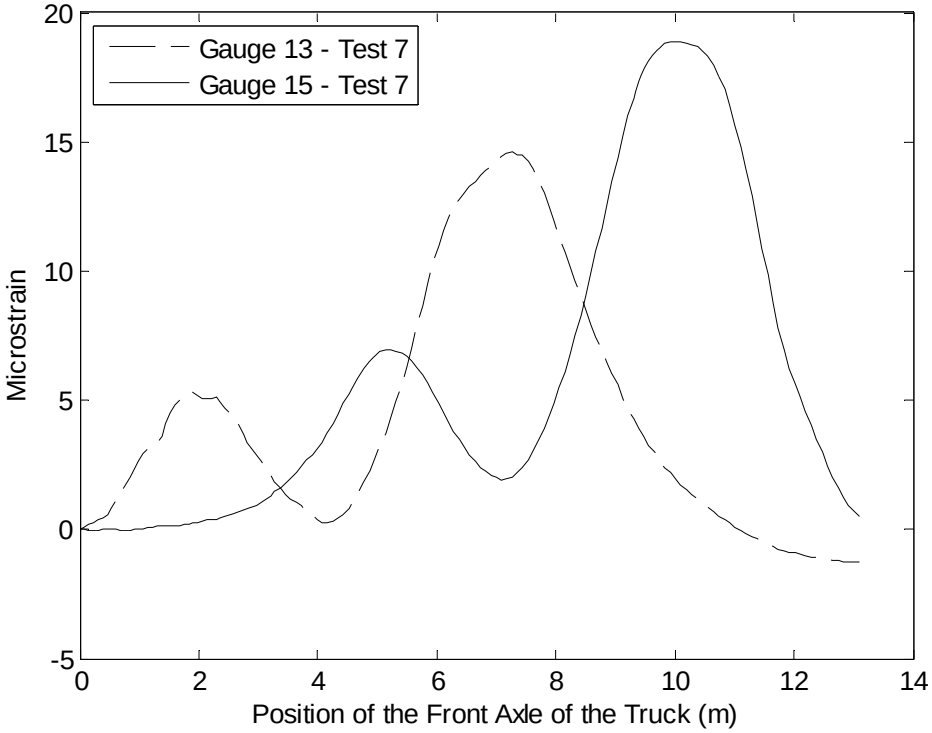

Figure 4.14 – Worst one-truck loading case for bottom gauges located at the transverse centerline at the quarter spans

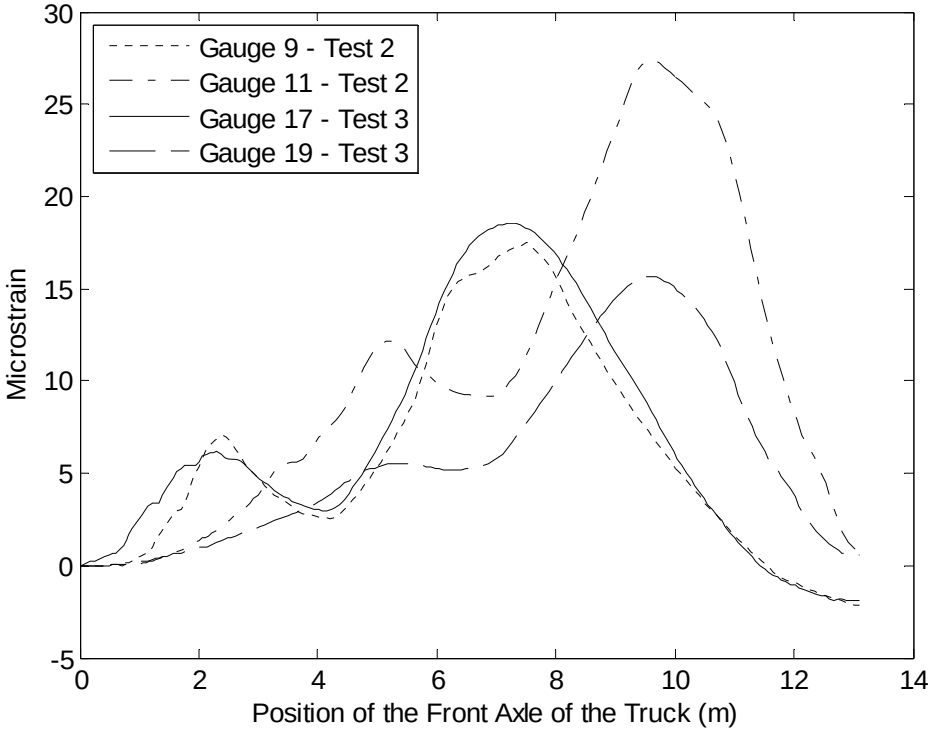

Figure 4.15 – Worst one-truck loading case for bottom gauges located under the curbs at the quarter spans

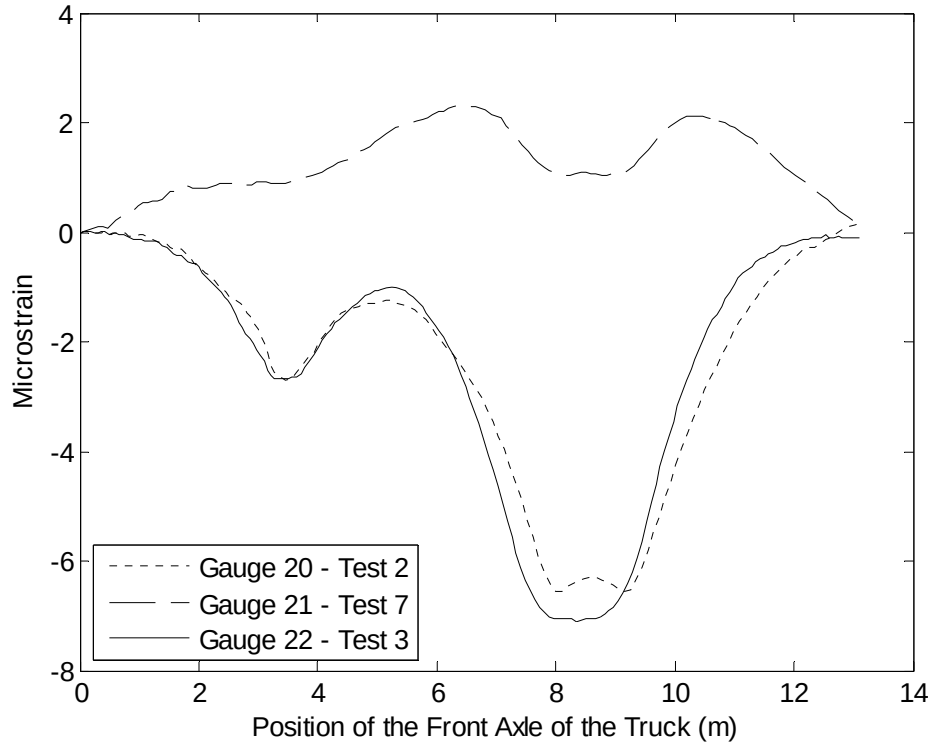

Figure 4.16 – Worst one-truck loading case for transverse gauges located at centerline span

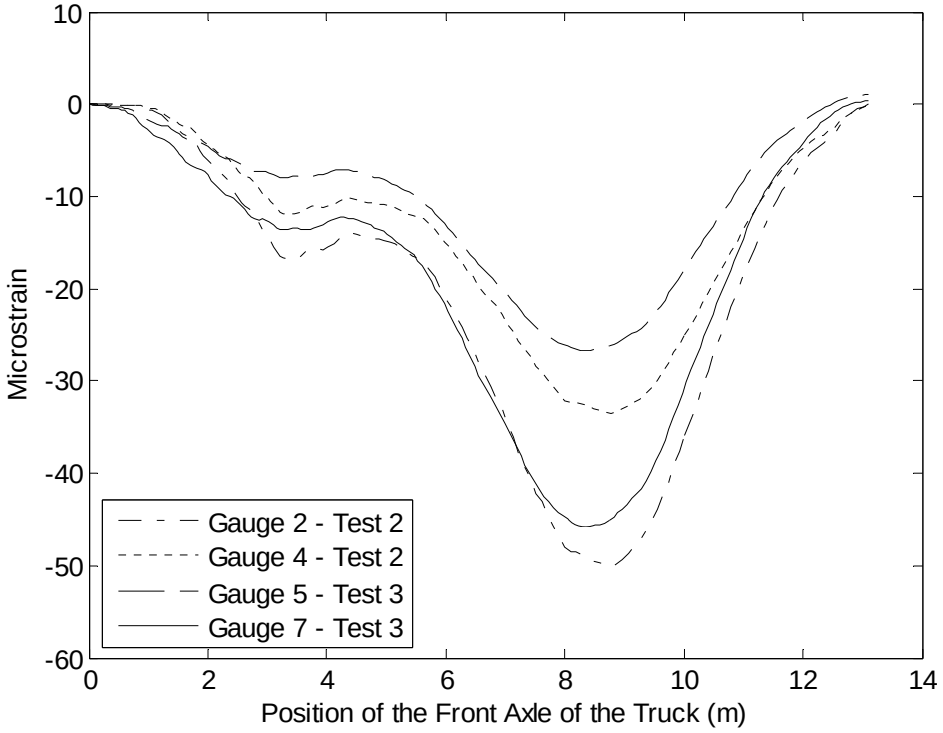

Figure 4.17 – Worst one-truck loading case for top gauges located at centerline span

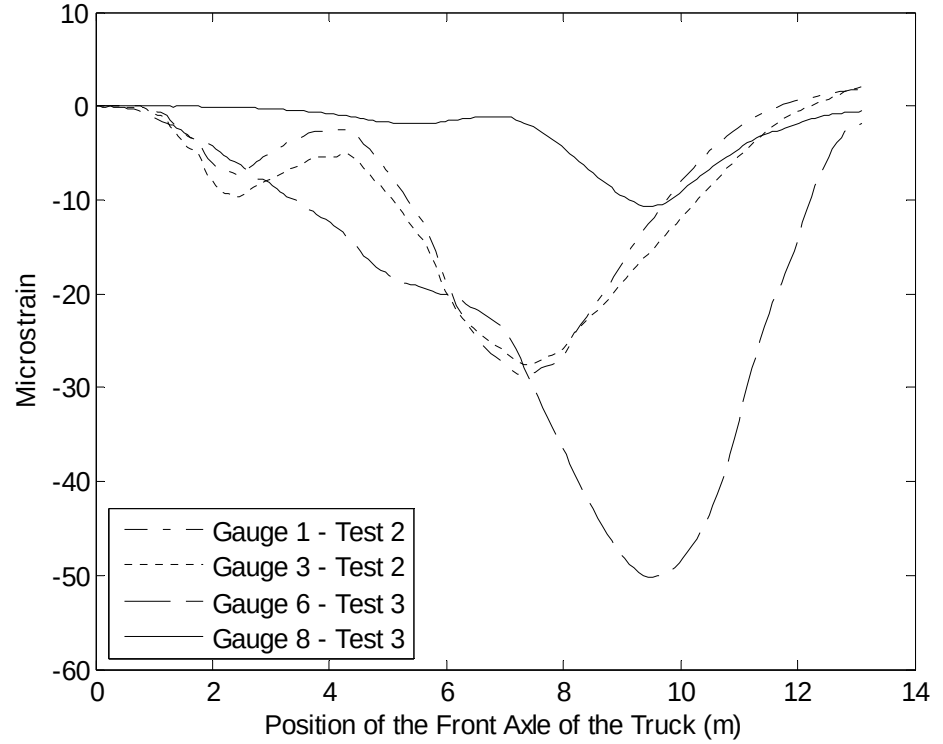

Figure 4.18 – Worst one-truck loading case for the top gauges located at the quarter spans

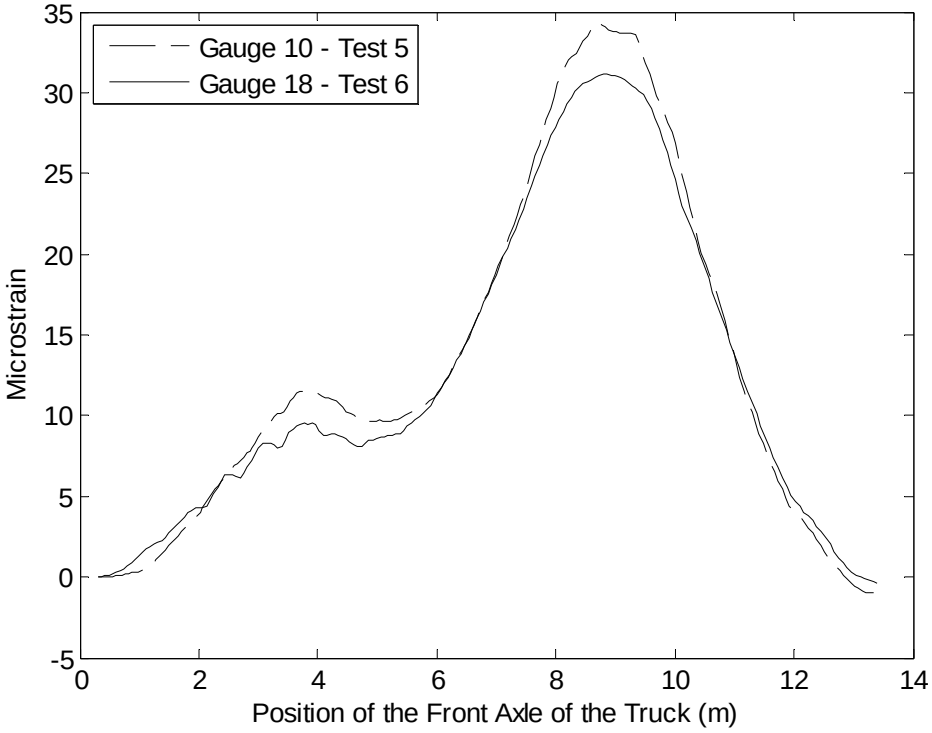

Figure 4.19 – Worst two-truck loading case for gauges located under the curb at centerline span

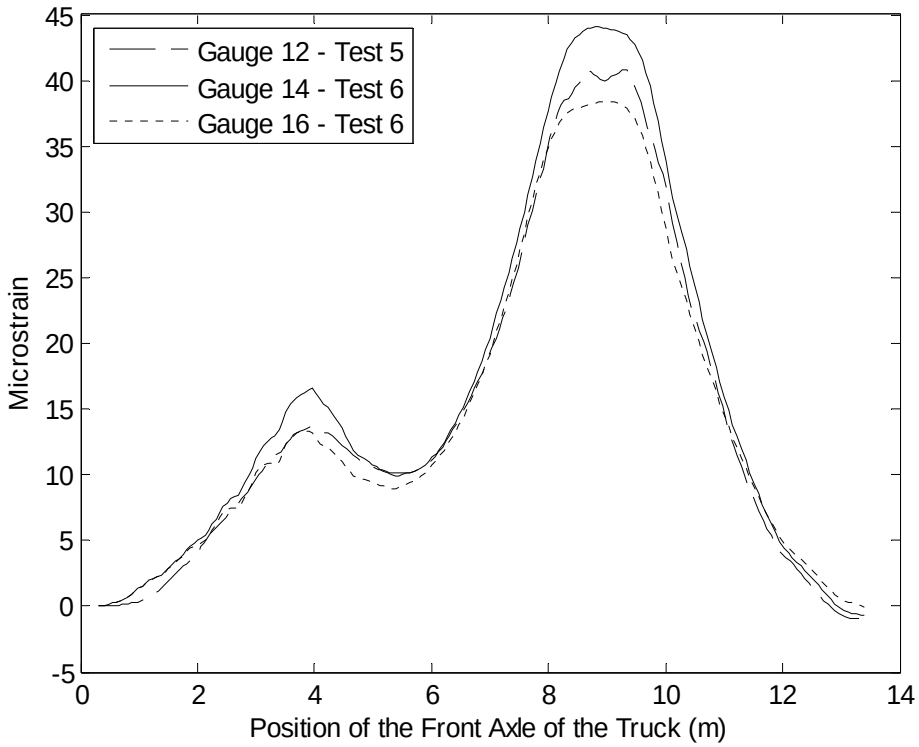

Figure 4.20 – Worst two-truck loading case for bottom gauges located at centerline span away from the curbs

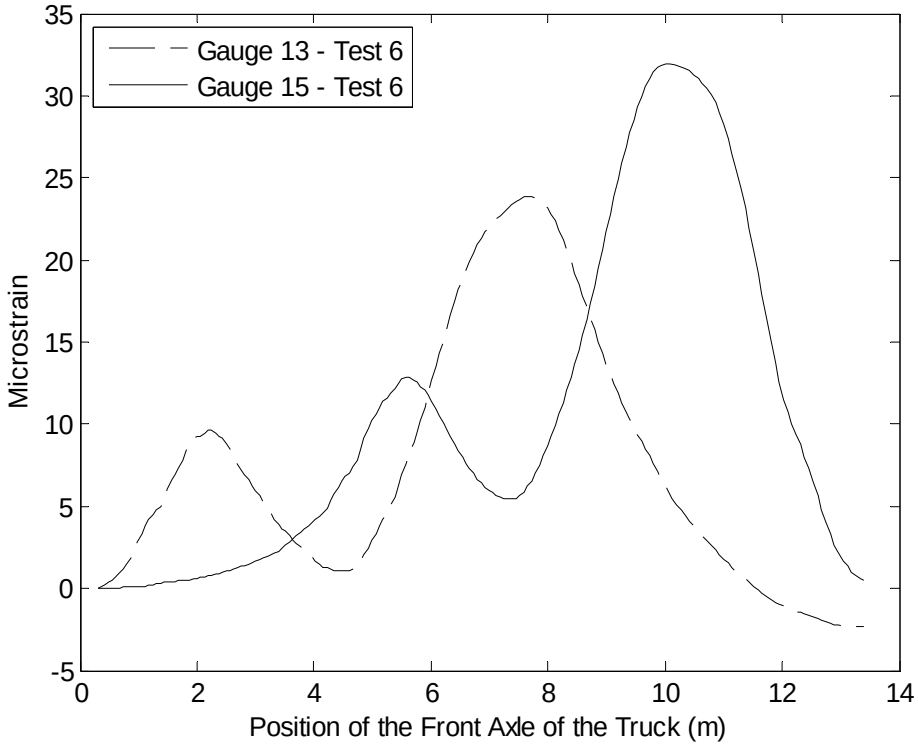

Figure 4.21 – Worst two-truck loading case for bottom gauges located at the transverse centerline at the quarter spans

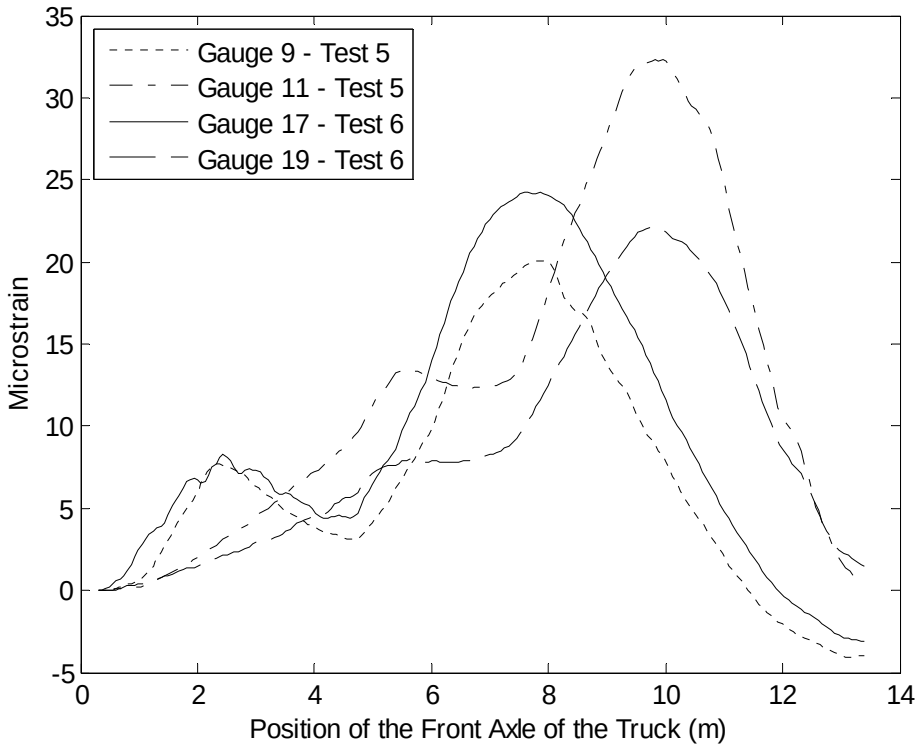

Figure 4.22 – Worst two-truck loading case for bottom gauges located under the curbs at the quarter spans

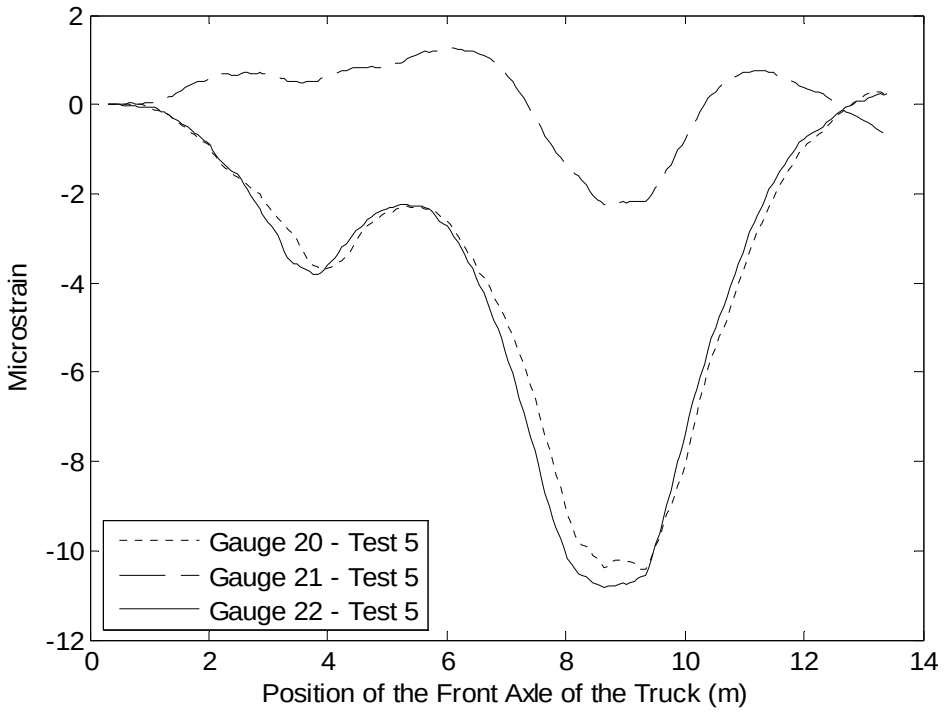

Figure 4.23 – Worst two-truck loading case for transverse gauges located at centerline span

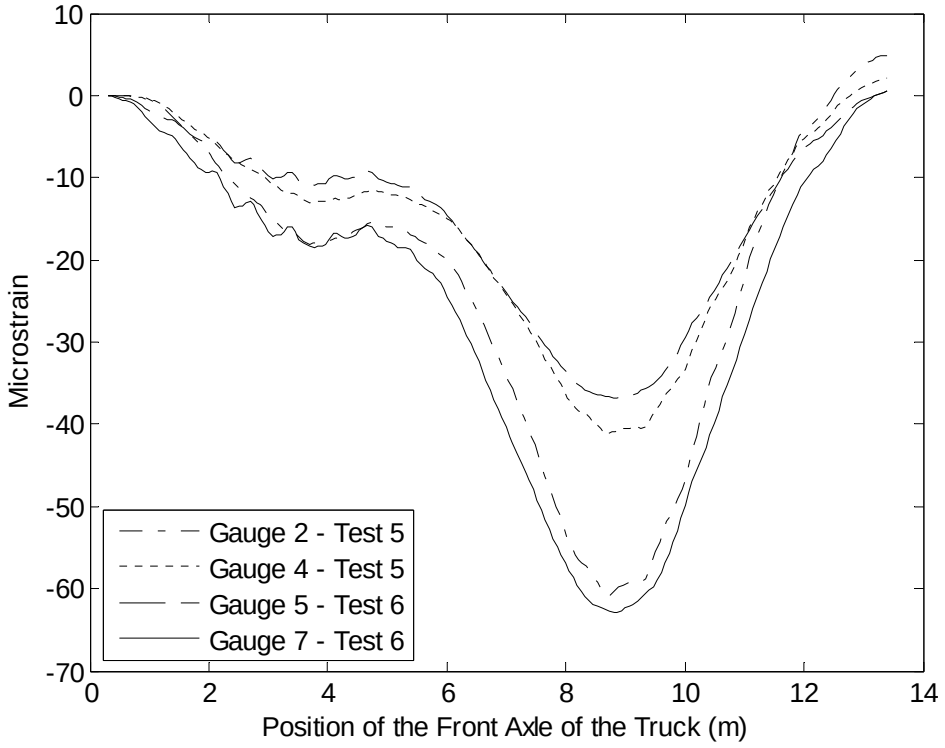

Figure 4.24 – Worst two-truck loading case for top gauges located at centerline span

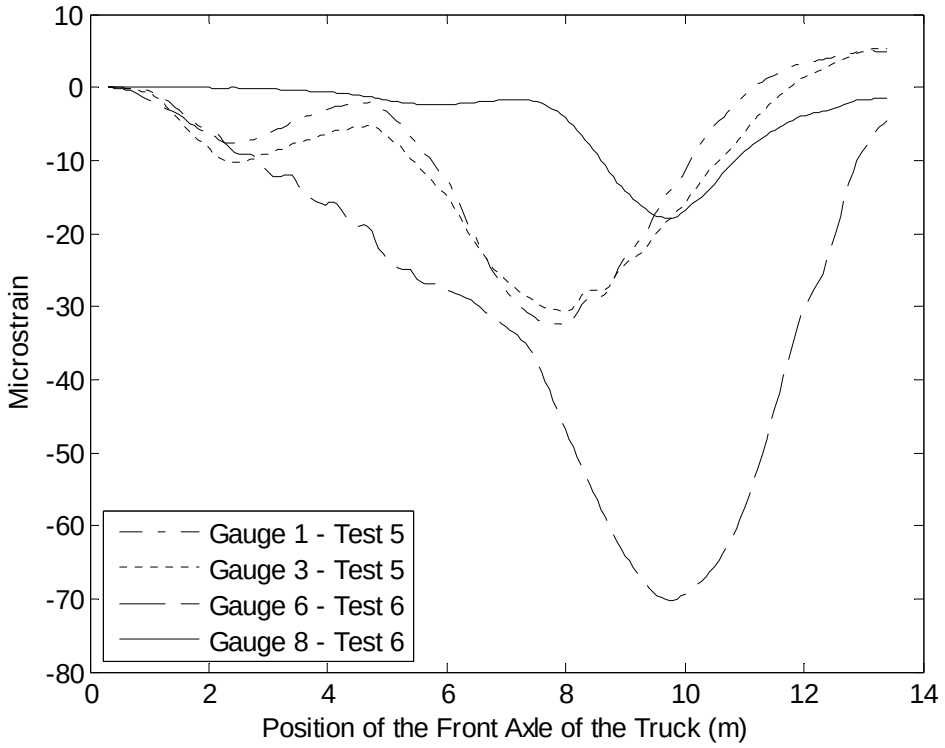

Figure 4.25 – Worst one-truck loading case for the top gauges located at the quarter spans

4.3.3. Discussion of Live Load Test Results

As can be seen in all the plots the results are consistent for similar gauges. All peaks of gauges located in similar positions are relatively the same, sometimes with the only major difference being where the peaks occur. These differences in the location of the peaks are caused by the longitudinal position of the gauge, either the gauge being located at the quarter point close to the initial position of the truck or the opposite quarter point . The small initial peak in the data is caused by the front axle passing over the longitudinal position of the gauge while the larger peak is caused by the back axles traveling over the longitudinal position of the gauge.

The only gauges that do not provide consistent results are the top gauges located at the quarter points of the span. The results in the top gauges located at the quarter points on one side of the bridge are not similar to gauges located at the other side of the bridge.

One possible cause for this discrepancy is the attachment of the curbs and rails to the slab. Details of this attachment are not given in the existing plans.

It must be noted that the truck positions corresponding to each strain value are not exact. The truck position was measured based on revolutions of the tire. A marker was placed on the tire and every time that marker went one full cycle it was recorded with the strain data. The truck was assumed to be traveling at a constant rate between recorded wheel revolutions.

4.4. Modeling Field Live Load Tests

After the live load tests were completed the results were compared to finite element predictions developed using Abaqus. Results from both the field live load test and Abaqus were compared to assess the accuracy of the finite-element model.

4.4.1. Abaqus Model

The finite-element models used pinned boundary conditions spaced centerline-to-centerline of the actual supports, as discussed in Chapter 2. No additional stiffness was added for the curbs and rails, and the slab thickness of 0.419 m was used for the entire bridge. Each individual tire was placed on the bridge so the tires sizes and weights corresponded to those of the actual truck that was used in the live load test. Figure 4.26 shows a screen shot of an Abaqus model with the tire loads from two trucks placed on the bridge. The assumed tire inflation pressure of 620.5 kPa was applied to each wheel load areas.

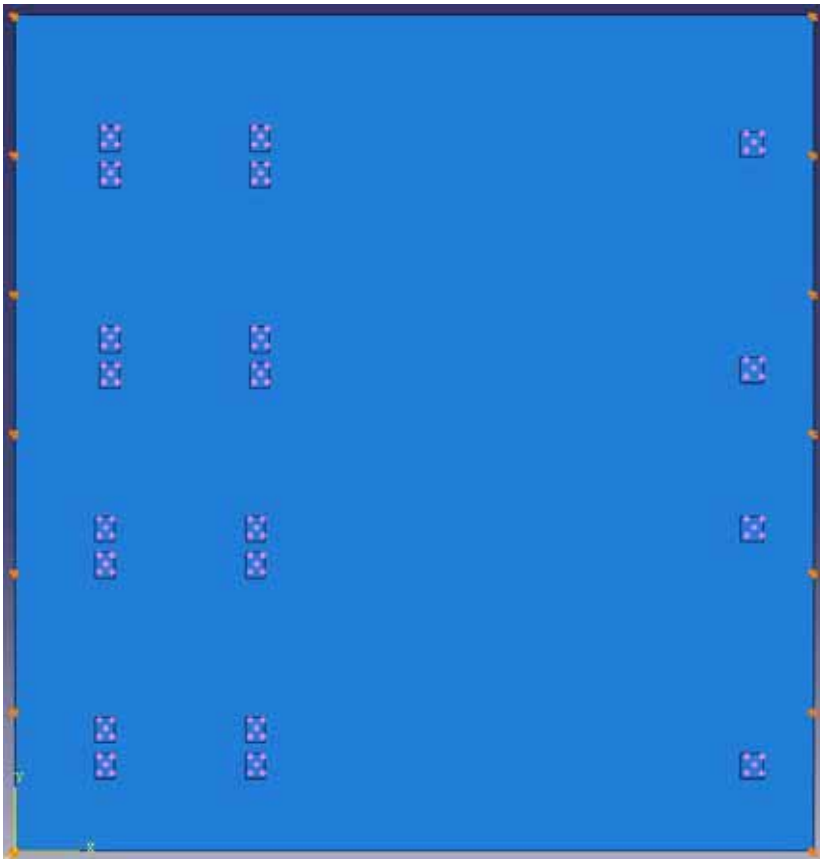

Figure 4.26 – Screen shot of the Abaqus Model with the applied wheel loads

Quadratic thick shell elements (Abaqus S8R elements) with an element edge length of 0.051 m were used in the model based on the convergence studies detailed in Chapter 2. The small element edge length resulted in the model having approximately 25,000 elements. Figure 4.27 provides a screen shot of the mesh that was generated by Abaqus using the element edge length of 0.051 m.

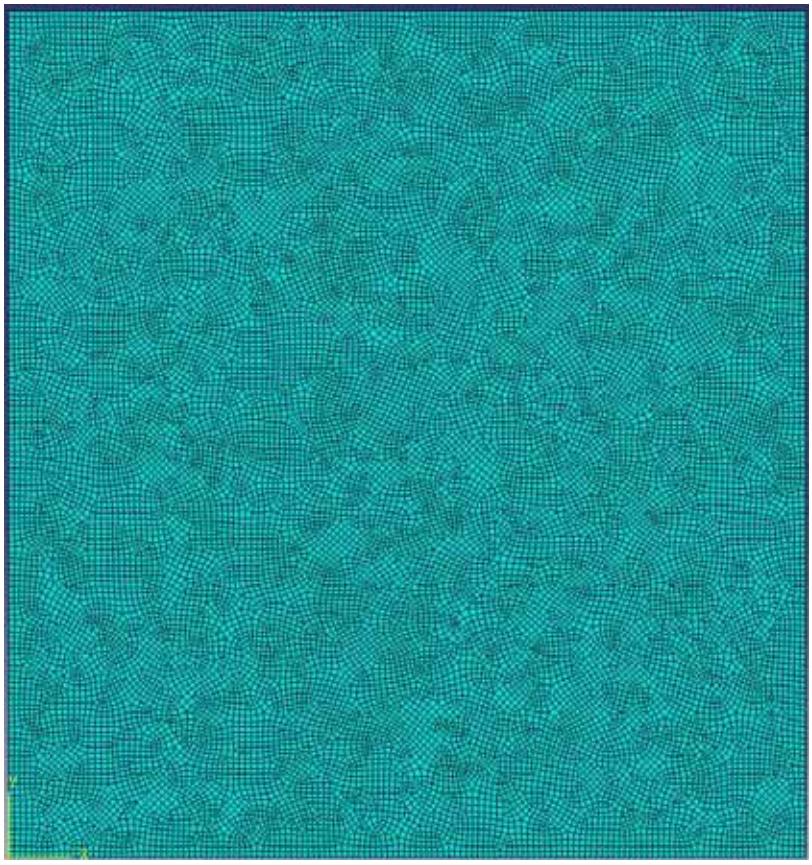

Figure 4.27 – Screen shot of the Abaqus generated mesh using element edge length of 0.051 m

The model was used to predict the moments at given locations of the bridge. Since Abaqus does not report moments directly they had to be computed from stresses given directly from Abaqus. This was done by using Equation 4.2 (Bhatti 2006).

$$M_{predict} = \frac{\sigma_{predict} h^2}{6} \qquad \text{Equation 4.2}$$

Where:

$M_{predict}$ = predicted moment from the Abaqus model

$\sigma_{predict}$ = predicted stress from the Abaqus model

h = slab thickness

4.4.2. Live Load Test Calculated Moments

To convert the measured strain from the live load test to moment it was assumed that the steel had not yielded and the section was still linear elastic. Most reinforced concrete structures behave as cracked sections under service loads. However, since gauges were not placed at the top of the slab, the neutral axis was not located from the field data and thus it was not definitively known whether the slab was cracked, uncracked or in the transition zone. Therefore the moments were determined based on both a fully cracked section and an uncracked section. The formula used to calculate the live load test moments from the resulting strains based on cracked and uncracked section properties are shown in Equation 4.3 and Equation 4.4 respectively. While calculating the section modulus (S_{cr} and S_{uncr}) for the bottom gauges located under the curbs the contributions from the curbs were not included i.e. the edge gauges had the same section properties as the interior gauges. The top gauges located on the curbs and rails also did not include the contributions from the curb except in the calculation of the depth to the neutral axis. The section modulus values shown below are for bottom gauges, top gauges located on the curb and top gauges located on the rail.

$$M_{cr} = \varepsilon E_c S_{cr} \qquad \text{Equation 4.3}$$

$$M_{uncr} = \varepsilon E_c S_{uncr} \qquad \text{Equation 4.4}$$

Where;

M_{cr} = moment based on cracked section properties

M_{uncr} = moment based on uncracked section properties

ε = strain

E_c = elastic modulus of concrete

S_{cr} = section modulus based on cracked section properties = 2.45 x 10^{-3} m^3 (bottom), 2.06 x 10^{-3} m^3 (curb) and 1.15 x 10^{-3} m^3 (rail)

S_{uncr} = section modulus based on uncracked section properties = 1.02 x 10^{-2} m^3 (bottom), 4.57 x 10^{-3} m^3 (curb) and 2.82 x 10^{-3} m^3 (rail)

Specific loadings were chosen for each gauge to model using Abaqus. These loadings corresponded with the maximum strain that was seen in each individual gauge for one and two truck loading cases. Since there were twenty two gauges this provided forty four comparisons of the live load test to the Abaqus model predictions.

After the moments were calculated from the maximum strains recorded during the live load tests, they were compared to the predicted moments provided by the Abaqus models. The predicted Abaqus moments are the maximum moments ($M_{predict}$) occurring at the location of the gauge with the truck configuration corresponding to the test number that provided the largest strain in the gauge. The longitudinal truck position is the distance from the centerline of the support to the center of the front axle on the truck. The locations of the tires were shifted by 0.127 m longitudinally at a time in order to ensure the maximum moment was accurately estimated with the Abaqus model.

Table 4.12 – Table 4.25 summarize the maximum live load test moments, based on both cracked (M_{cr}) and uncracked (M_{uncr}) section properties along with the predicted moments from the Abaqus models ($M_{predict}$). The peak moments computed from the measured strains using the cracked section properties exceeded the cracking moment of 77.6 kN-m/m at gauge 14. The predicted moment based on cracked section properties for the other gauges were less than the calculated predicted moments. Even though the other gauges did not exceed the calculated cracking moment at the other longitudinal gauges

with extensions located away from the curbs (12, 15 and 16), the results indicate that the bridge behaved as a fully cracked section. Moments back-calculated from measured strains assuming an uncracked section significantly exceed the expected moments at the locations of gauges 12 – 16. Further, it is likely that even if the load test did not produce moments in excess of M_{cr}, the cracking moment was exceeded during the service life of the bridges.

Table 4.12 – Table 4.25 also provide the maximum strain that were seen in each gauge, the test that caused the maximum strain, and the location of the truck that caused the maximum moments in both the live load test and the Abaqus models. Table 4.12 – Table 4.18 show the results when one truck was placed on the bridge and Table 4.19 – Table 4.25 show the results when two trucks were placed on the bridge. The positive strain values correspond to tensile strain while negative strain values corresponding to compressive strain. The locations of the trucks are measured from the centerline of the support to the center of the front axle.

Table 4.12 – Maximum strain, calculated moments and predicted moments for worst one-truck loading case for gauges located under the curbs at centerline span.

		Live Load Test Results				Abaqus Model Results	
Gauge Number	Live Load Test	Truck Position (m)	Maximum Strain (Micro strain)	M_{cr} (kN-m/m)	M_{uncr} (kN-m/m)	Truck Position (m)	$M_{predict}$ (kN-m/m)
10	2	8.91	26.90	50.9	213.1	8.64	54.22
18	3	8.48	22.38	42.4	177.3	8.64	54.20

Table 4.13 – Maximum strain, calculated moments and predicted moments for worst one-truck loading case for bottom gauges located at centerline span away from the curbs.

		Live Load Test Results				Abaqus Model Results	
Gauge Number	Live Load Test	Truck Position (m)	Maximum Strain (Micro strain)	M_{cr} (kN-m/m)	M_{uncr} (kN-m/m)	Truck Position (m)	$M_{predict}$ (kN-m/m)
12	2	8.91	26.42	50.0	209.2	9.02	50.62
14	7	9.00	25.46	48.2	201.6	8.89	43.80
16	3	8.96	25.15	47.6	199.2	9.02	50.62

Table 4.14 – Maximum strain, calculated moments and predicted moments for worst one-truck loading case for bottom gauges located at the transverse centerline at the quarter spans.

		Live Load Test Results				Abaqus Model Results	
Gauge Number	Live Load Test	Truck Position (m)	Maximum Strain (Micro strain)	M_{cr} (kN-m/m)	M_{uncr} (kN-m/m)	Truck Position (m)	$M_{predict}$ (kN-m/m)
13	7	7.38	14.60	27.6	115.6	7.62	36.99
15	7	10.17	18.90	35.8	149.7	9.78	36.59

Table 4.15 – Maximum strain, calculated moments and predicted moments for worst one-truck loading case for bottom gauges located under the curbs at the quarter spans.

		Live Load Test Results				Abaqus Model Results	
Gauge Number	Live Load Test	Truck Position (m)	Maximum Strain (Micro strain)	M_{cr} (kN-m/m)	M_{uncr} (kN-m/m)	Truck Position (m)	$M_{predict}$ (kN-m/m)
9	2	7.64	17.50	33.1	138.6	7.49	44.35
11	2	9.79	27.42	51.9	217.2	9.78	44.10
17	3	7.37	18.57	35.1	147.0	7.62	44.35
19	3	9.75	15.65	29.6	123.9	9.78	44.10

Table 4.16 – Maximum strain, calculated moments and predicted moments for worst one-truck loading case for transverse gauges located at centerline span.

		Live Load Test Results				Abaqus Model Results	
Gauge Number	Live Load Test	Truck Position (m)	Maximum Strain (Micro strain)	M_{cr} (kN-m/m)	M_{uncr} (kN-m/m)	Truck Position (m)	$M_{predict}$ (kN-m/m)
20	1	9.07	-7.01	4.5	51.0	8.64	1.98
21	7	6.48	2.31	1.5	16.8	8.64	15.64
22	3	8.48	-7.10	4.6	51.6	8.64	2.24

Table 4.17 - Maximum strain, calculated moments and predicted moments for worst one-truck loading case for top gauges located at centerline span.

		Live Load Test Results				Abaqus Model Results	
Gauge Number	Live Load Test	Truck Position (m)	Maximum Strain (Micro strain)	M_{cr} (kN-m/m)	M_{uncr} (kN-m/m)	Truck Position (m)	$M_{predict}$ (kN-m/m)
2	2	8.91	-50.19	44.6	109.4	8.64	54.22
4	2	8.91	-33.53	53.5	118.6	8.64	53.98
5	3	8.48	-26.70	42.6	94.5	8.64	53.98
7	3	8.48	-45.86	40.7	99.9	8.64	54.22

Table 4.18 – Maximum strain, calculated moments and predicted moments for worst one-truck loading case for the top gauges located at the quarter spans.

		Live Load Test Results				Abaqus Model Results	
Gauge Number	Live Load Test	Truck Position (m)	Maximum Strain (Micro strain)	M_{cr} (kN-m/m)	M_{uncr} (kN-m/m)	Truck Position (m)	$M_{predict}$ (kN-m/m)
1	2	7.44	-28.59	25.4	62.3	7.49	44.35
3	2	7.44	-27.48	43.8	97.2	7.49	44.44
6	3	9.67	-50.25	80.1	177.8	9.78	44.17
8	3	9.59	-10.69	9.5	23.3	9.78	44.10

Table 4.19 – Maximum strain, calculated moments and predicted moments for worst two-truck loading case for gauges located under the curbs at centerline span.

		Live Load Test Results				Abaqus Model Results	
Gauge Number	Live Load Test	Truck Position (m)	Maximum Strain (Micro strain)	M_{cr} (kN-m/m)	M_{uncr} (kN-m/m)	Truck Position (m)	$M_{predict}$ (kN-m/m)
10	5	8.54	34.35	65.0	272.1	8.76	79.12
18	6	8.70	31.17	59.0	246.9	8.64	72.26

Table 4.20 – Maximum strain, calculated moments and predicted moments for worst two-truck loading case for bottom gauges located at centerline span away from the curbs.

		Live Load Test Results				Abaqus Model Results	
Gauge Number	Live Load Test	Truck Position (m)	Maximum Strain (Micro strain)	M_{cr} (kN-m/m)	M_{uncr} (kN-m/m)	Truck Position (m)	$M_{predict}$ (kN-m/m)
12	5	9.67	40.79	77.2	323.1	8.76	76.86
14	6	8.63	44.08	83.4	349.2	8.76	75.69
16	6	8.90	38.38	72.6	304.0	8.89	73.70

Table 4.21 – Maximum strain, calculated moments and predicted moments for worst two-truck loading case for bottom gauges located at the transverse centerline at the quarter spans.

		Live Load Test Results				Abaqus Model Results	
Gauge Number	Live Load Test	Truck Position (m)	Maximum Strain (Micro strain)	M_{cr} (kN-m/m)	M_{uncr} (kN-m/m)	Truck Position (m)	$M_{predict}$ (kN-m/m)
13	6	7.47	23.88	45.2	189.1	7.75	62.10
15	6	9.85	31.93	60.4	252.9	9.78	61.20

Table 4.22 – Maximum strain, calculated moments and predicted moments for worst two-truck loading case for bottom gauges located under the curbs at the quarter spans.

		Live Load Test Results				Abaqus Model Results	
Gauge Number	Live Load Test	Truck Position (m)	Maximum Strain (Micro strain)	M_{cr} (kN-m/m)	M_{uncr} (kN-m/m)	Truck Position (m)	$M_{predict}$ (kN-m/m)
9	5	7.66	20.09	38.0	159.1	7.75	64.54
11	5	9.67	32.29	61.1	255.7	9.78	63.41
17	6	7.47	24.25	45.9	192.1	7.75	57.18
19	6	9.65	22.13	41.9	175.3	9.65	56.52

Table 4.23 – Maximum strain, calculated moments and predicted moments for worst two-truck loading case for transverse gauges located at centerline span.

		Live Load Test Results				Abaqus Model Results	
Gauge Number	Live Load Test	Truck Position (m)	Maximum Strain (Micro strain)	M_{cr} (kN-m/m)	M_{uncr} (kN-m/m)	Truck Position (m)	$M_{predict}$ (kN-m/m)
20	5	9.17	10.41	6.7	75.7	8.76	2.38
21	5	8.54	2.27	1.5	16.5	8.64	12.88
22	5	8.48	10.81	7.0	78.6	8.64	1.55

Table 4.24 – Maximum strain, calculated moments and predicted moments for worst two-truck loading case for top gauges located at centerline span.

		Live Load Test Results				Abaqus Model Results	
Gauge Number	Live Load Test	Truck Position (m)	Maximum Strain (Micro strain)	M_{cr} (kN-m/m)	M_{uncr} (kN-m/m)	Truck Position (m)	$M_{predict}$ (kN-m/m)
2	5	8.54	60.91	54.1	132.7	8.76	79.12
4	5	8.54	41.17	65.7	145.7	8.76	79.72
5	6	8.70	36.84	58.7	130.3	8.64	72.26
7	6	8.63	62.93	55.9	137.1	8.64	72.26

Table 4.25 – Maximum strain, calculated moments and predicted moments for worst two-truck loading case for the top gauges located at the quarter spans.

		Live Load Test Results				Abaqus Model Results	
Gauge Number	Live Load Test	Truck Position (m)	Maximum Strain (Micro strain)	M_{cr} (kN-m/m)	M_{uncr} (kN-m/m)	Truck Position (m)	$M_{predict}$ (kN-m/m)
1	5	7.85	32.51	28.9	70.8	7.75	64.54
3	5	7.85	30.67	48.9	108.5	7.75	65.04
6	6	9.58	70.18	112	248	9.65	56.81
8	6	9.58	17.96	16.0	39.1	9.65	56.52

One note to make about the calculation of the moments, both longitudinal and transverse, is that the strain in each of the directions is a function of both the longitudinal and transverse moment. This means that ε_x is not only a function of M_x but is also has contributions from M_y, therefore M_x and M_y cannot be directly computed from their respective strains. With the possibility of concrete cracking in the longitudinal direction but not in the transverse direction calculation the moments would not obey elastic plate theory causing non-linear behavior and load distribution (Jáuregui et al. 2007, 2010). Based on other live load testing done (Jáuregui et al. 2007, 2010) and (Amer et al. 1999), who ignore the contribution from the other direction it was assumed that our predictions of the moments based on only that respective strain provided acceptable results.

4.4.3. Comparison of the Abaqus and Live Load Test Moments

The live load test results and the Abaqus models indicate that Bradford Bridge #3430 is fully cracked in the longitudinal direction over at least the middle ½ of the span. Gauges that definitively show this are the longitudinal gauges that are located on the bottom of the interior part of the bridge (away from the curbs). These gauges include 12, 13, 14, 15 and 16. The predicted moments from the Abaqus models are close to the

moments from the live load test based on cracked section properties when both one and two trucks are applied to the bridge. All of the predicted moments in Abaqus models of those gauges except for 13 are within 9% of the actual moments from the live load test based on a fully cracked section for both one and two truck loading cases. Gauge 13 was the outlier of this group, where the Abaqus-predicted moments were 34% and 37% greater than the live load test moments based on a cracked section. This discrepancy is believed to be due to gauge 13 not having an extension attached to it, since the maximum strain seen in the gauge was much less then that seen in the symmetrically located gauge 15 under similar loading, which was theoretically subjected to the same bending moment as gauge 13. Gauge 13 likely did not span over a crack which would cause the gauge to see less strain over that given length, whereas all other gauges in this group had a gauge length of 0.61 m and most likely spanned over multiple cracks and measured the average strain over their entire length, giving more representative results.

The longitudinal gauges located at the bottom of the slab under the curbs are 9, 10, 11, 17, 18 and 19. All the Abaqus-predicted moments except for gauge 10 are between 18% and 33% higher than the live load test moments based on a cracked section when only one truck was applied to the bridge. Gauge 10 is 6% higher than the moment based on a cracked section. When two trucks are applied to the bridge similar results are seen in the Abaqus-predicted moments with all gauges except 11 and 9 being between 20% and 35% of the live load moments based on cracked section properties. Gauge 11 was 4% larger and gauge 9 was 70% larger. The fact that these gauges have higher FE-predicted moments than the test moment is likely due to the additional stiffness provided by the curbs at the slab edges. The net effect of the curb is to increase the local bending

rigidity of the slab, resulting in a lower field-measured strain. When the cracked section of the slab only is used to compute a slab moment with this strain, this moment is then artificially low.

While the bottom gauges had similar trends the top gauges did not. The top gauges located along the centerline of the bridge lead to the belief that the curb and the bottom of the rail are directly attached to the concrete slab. These gauges also provided similar moments as the bottom gauges at the same locations. But the top gauges located at the quarter points of the bridge did not provide similar moments to the gauges located under the curb at the quarter points. As mentioned in section 4.3.3 there are very inconsistent results for the top gauges and there is no way of knowing what the reinforcing is in the curb and/or if they are cast directly into slab. Therefore conclusions were not made for the gauges located on the top of the bridge at the quarter points.

The Abaqus model results for the transverse gauges provide very different results than the results of the longitudinal gauges. The Abaqus models predicted moments correlated very well with the live load test moments based on an uncracked section. The Abaqus model results of transverse gauges located along the edges are less than 50% and 5% of the moments seen during the live load test based on cracked and uncracked section analysis. The results also show that the gauges actually go into compression at these two locations when the Abaqus model predicts that the gauges should go into tension. This observation indicates that the curbs may tend to prevent rotation of the edges about the longitudinal axis of the bridge, providing partial moment fixity at the slab edges. This would explain the transverse gauges located under the curb to experience compression.

Modeling in Abaqus was done to test this theory; it was done by using the true thickness of the rails and curbs providing those regions to be stiffer than the rest of the slab.

The model that was created in Abaqus used the same type of elements, S8R along with the same element edge length, 0.051 m, that were used for all the other models. The only difference in the model was the increase of the relative stiffness of the curbs and rails. This was done by modeling the additional height of the curb and rail to the slab thickness, an additional 0.23 m and 0.51 m respectively. The additional thickness of the curb and rail can be seen in Figure 4.28. The model results agreed with the opinion that the additional stiffness of the curb causes compression at the location of the transverse gauges under the curb. Figure 4.29 shows the results of the model and how the slab underneath the curbs and rails, located at the top and the bottom of the figure, is in compression like the live load test results showed.

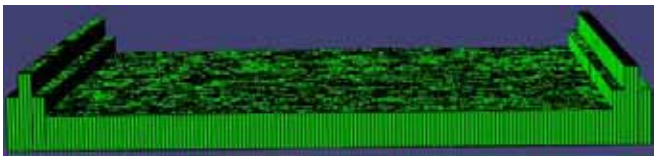

Figure 4.28 – Rendered Abaqus model that include the additional height of the rail and the curb.

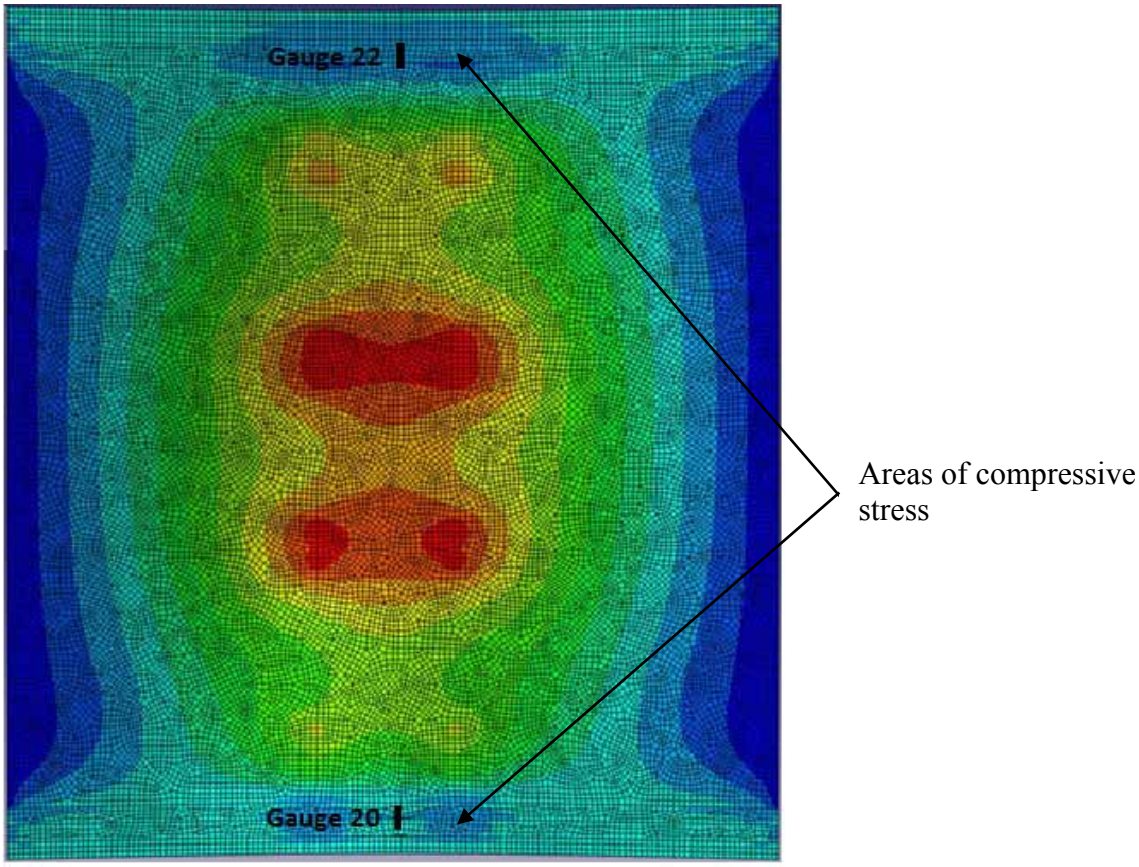

Figure 4.29 – Resulting stresses from the Abaqus Model using the true thickness of the curbs and rails

To more closely examine the model predictions for a wider range of loadings, one entire truck pass was modeled for gauges 12, 14, 15 and 16. These gauges were chosen because they are all located at the bottom of the slab, and had extensions, which made them the most reliable. These gauges were also minimally affected by the curb. Tests 5 and 6 were modeled using Abaqus because these test provided the largest strain during the live load test. These tests were modeled by starting the truck off the bridge and moving the truck forward at increments of 0.127 m when any of the axles were within 0.508 m of the location of the gauge being modeled, Increments of 0.254 m were used when the axles were further away from gauge.

Figure 4.30 – Figure 4.33 show the predicted moments in Abaqus and the live load test moments based on a cracked section analysis for the entire truck pass for gauges 12,14, 15 and 16, respectively.

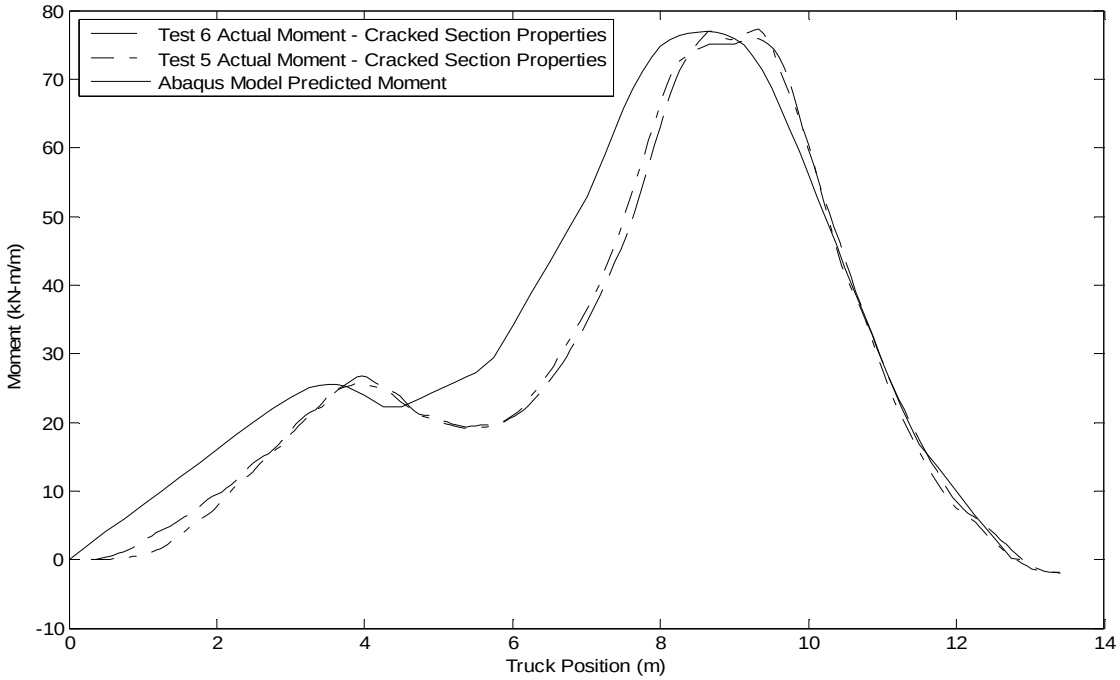

Figure 4.30 – Plot of live load moments inferred from measured strains and Abaqus predicted moments for gauge 12 for entire truck pass for live load tests 5 and 6

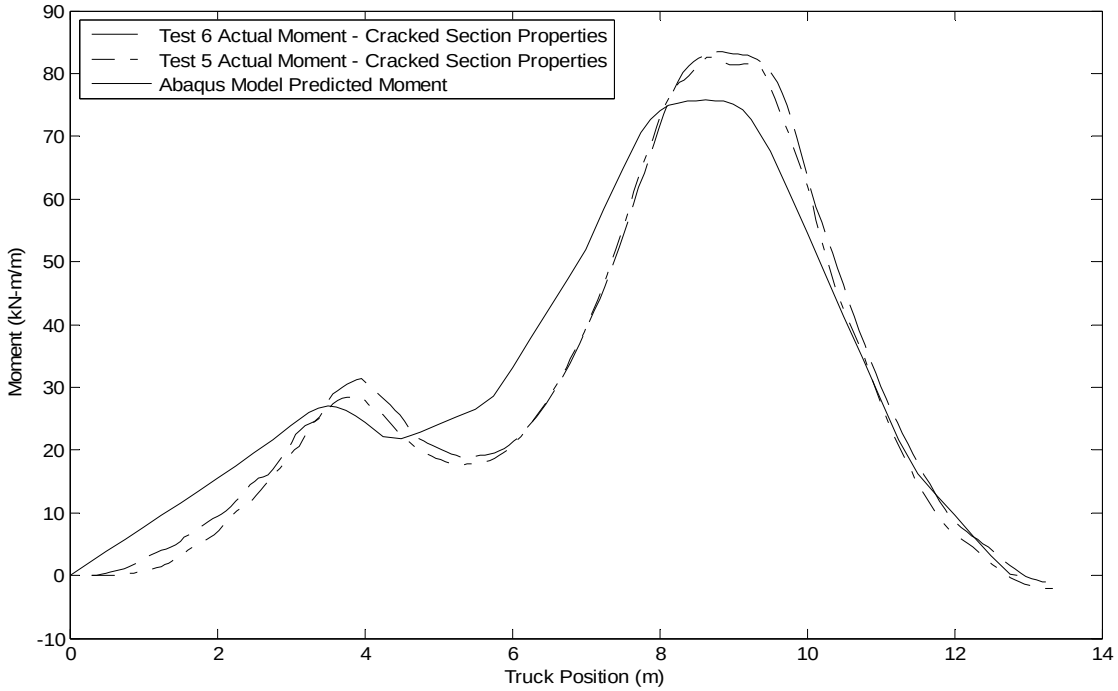

Figure 4.31 – Plot of live load moments inferred from measured strains and Abaqus predicted moments for gauge 14 for entire truck pass for live load tests 5 and 6

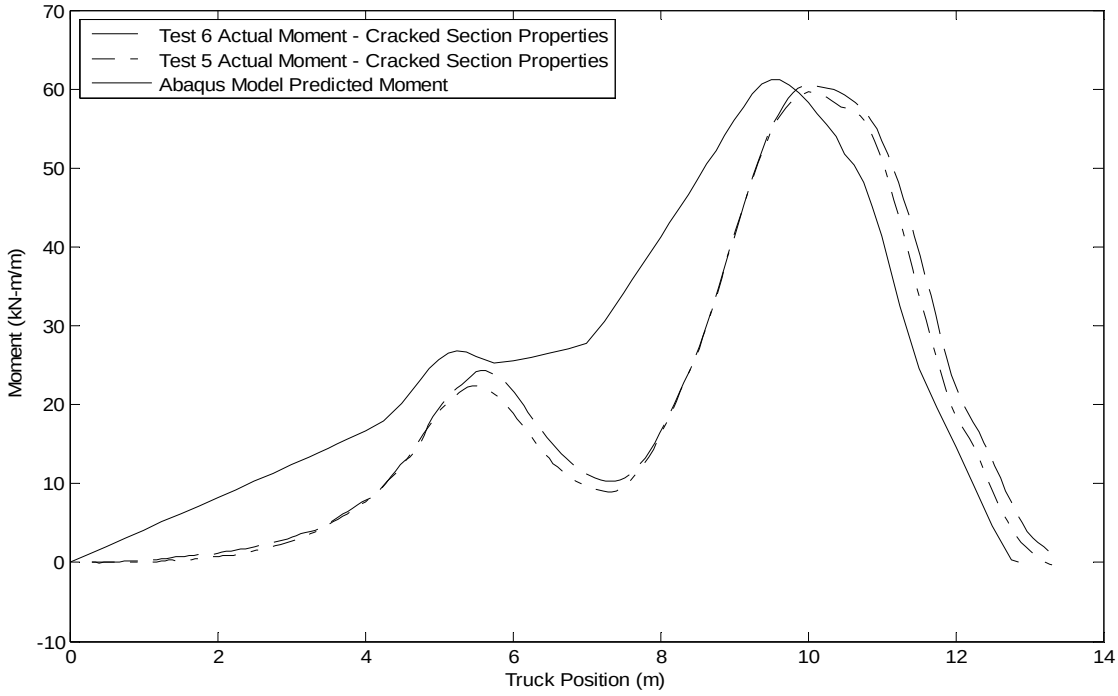

Figure 4.32 – Plot of live load moments inferred from measured strains and Abaqus predicted moments for gauge 15 for entire truck pass for live load tests 5 and 6

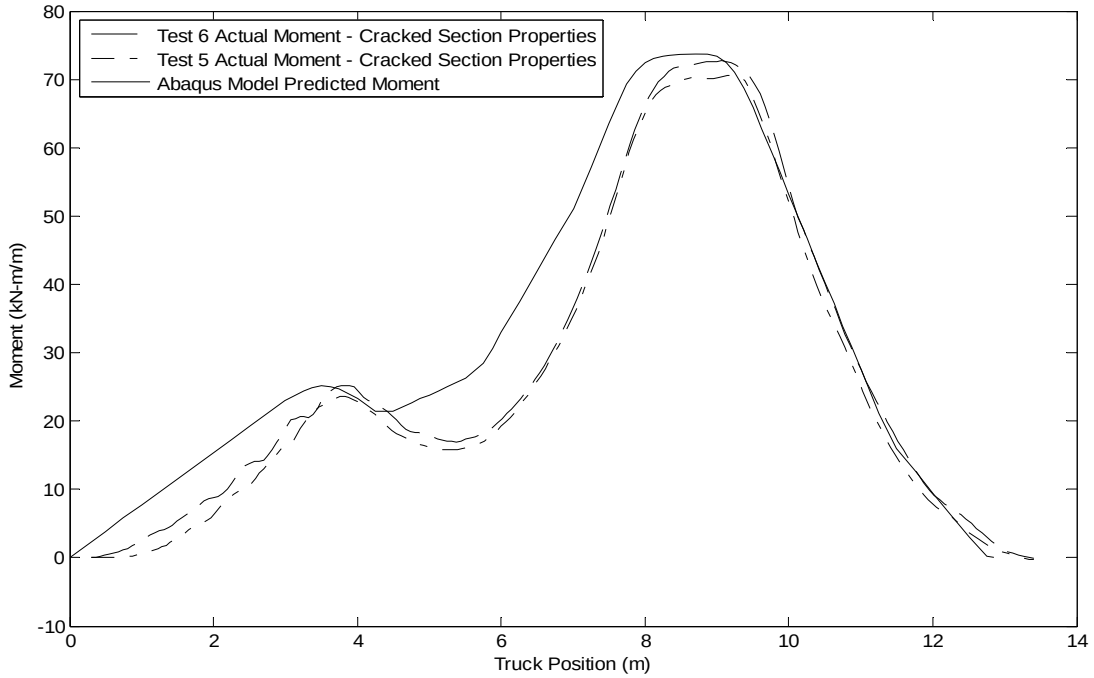

Figure 4.33 – Plot of live load moments inferred from measured strains and Abaqus predicted moments for gauge 16 for entire truck pass for live load tests 5 and 6

As can be seen in the Figure 4.30 - Figure 4.33, the Abaqus predicted moments are very similar to the live load test moments based on a cracked section for all truck positions. One Major difference is the truck position where the peaks occur. This is because the truck positions from the live load test are estimated as discussed previously in section 4.3.3. Other than the location of the peaks the data is still very similar for all truck positions. All the results from the live load test and predicted moments follow the same general pattern as each other for each individual gauge. The Abaqus model generally predicts moments that are greater than the actual live load test results, only Gauge 14 has predicting moments less than the actual live load test results. The differences between the predicted moments and live load test results could be caused by many errors that could have happened during the live load test. One error could be the two trucks might not have been exactly lined up next to each other and/ or the trucks could have drifted transversely during the test. Another possible cause is the actual

concrete elastic modulus and cracked section rigidity being higher than the assumed value. But the results still predict very similar results to each other despite these possibly sources of discrepancy.

4.5. Summary

In summary, the live load test was successful: the finite-element analysis predictions of response agreed well with the load test results at regions of high bending moment, and the BDI system proved easy to use and provided repeatable results. These results justify the use of finite-element analysis for the load rating of flat slab bridges.

Even though Abaqus was used as a finite element model in this chapter, the results of the comparison extend to the SlabRate software used to load rate the twenty flat slab bridges in Chapter 3, since the SlabRate predictions have been shown to compare well with Abaqus in Chapter 2.

CHAPTER 5. EFFECT OF SKEW ANGLE ON FE-BASED LOAD RATING

5.1. Introduction

The finite-element analysis and load ratings considered in Chapter 3 of this thesis considered only longitudinal bending moments. However, as skew angle increases, the transverse and torsional bending moments become more significant, which can lead to lower rating factors. Menassa et al. (2007) studied the effect of skew angle on slab analysis, concluding that the AASHTO provisions for predicting longitudinal bending moments can be very conservative for skew angles over 20°. However, as discussed by Théoret et al. (2011), large skew angles can cause large transverse moments as well as shear forces that can govern capacity, and simplified code provisions must account for these transverse moments and shear forces. Denton and Burgoyne (1996) examined the flexural assessment of reinforced concrete slabs with skewed reinforcement, proposing refined analysis methods where skew is rigorously taken into account when determining bending strength.

Of the slab bridges analyzed in Chapter 3, the effect of skew angle is probably most pronounced for the Albion Bridge #2529, Brewer Bridge #5638, Carmel Bridge #5191, Carmel Bridge #5632, Linneus Bridge #5311, and Linneus Bridge #5773, which have skew angles greater than 20°. The purpose of this chapter is to assess the effect of skew angle on the response of flat slab concrete bridges and determine what, if any, restrictions on skew angle should be imposed when load rating slab bridges using the finite-element methods of Chapter 3.

5.2. Modeling Skew Effects

Abaqus models were created to quantify the effect of skew angle on values of longitudinal, transverse and torsional bending moments. Ten total models were created in Abaqus. Two separate basic bridge characteristics were used (span length, width, thickness and reinforcing), and each basic bridge was modeled at five different skew angles. The two bridges whose characteristics were used in the model were Carmel Bridge #5191 and Linneus Bridge #5773. The skew angles used ranged from 0° to 40° in increments of 10° measured counterclockwise from the transverse axis. Carmel Bridge #5191 and Linneus Bridge #5773 were chosen for several reasons. First, the actual skew of these bridges is 30° and 25°, respectively, which lies between the upper and lower bounds of skew angles modeled here. Second, each of these bridges has a load rating factor below one using the conventional strip width method, and a rating factor greater than one using the finite element analysis. The final reason for choosing these two bridges is their span lengths. Carmel Bridge #5191 is 10.16 m long while Linneus Bridge #5773 is 7.54 m, and Menassa et al. (2007) show that the transverse moments are larger in longer bridges than in shorter bridges.

Both dead and live load factored moments were determined in all analyses. The dead load factor used for the all dead loads was 1.25 for Carmel Bridge #5191, which includes the weight of the slab, curbs, guardrails and wearing surface. A load factor of 1.25 was used for the wearing surface because it was one of the bridges where the thickness could be verified in the field during the bridge visit in the summer of 2010. Linneus Bridge #5773 used a dead load factor of 1.25 for the weight of the slab, curbs and guardrails. A dead load factor of 1.5 was used for the wearing surface, as the depth of

the wearing surface could not be field verifiec. The HL-93 tandem live load was used in all the models that were created, and tire loads included an impact factor (33%) along with the operating live load factor (1.35). Multiple presence factors of 1.2 for one truck loading and 1.0 for two truck loading was considered in this analysis.

5.2.1. Truck Positions

Two separate live load loading cases were used. The first loading case used one HL-93 tandem truck with the back inner most wheel centered on the center of the bridge. This configuration was used for all the different skew angles that were analyzed. Figure 5.1 and Figure 5.2 below show the placement of the HL-93 tandem on the Carmel and Linneus bridges with a skew of 40°. In both of the figures the traffic on the bridge travels from side to side. The lines along the top and bottom of the bridges are the locations and widths of the curbs on the bridge.

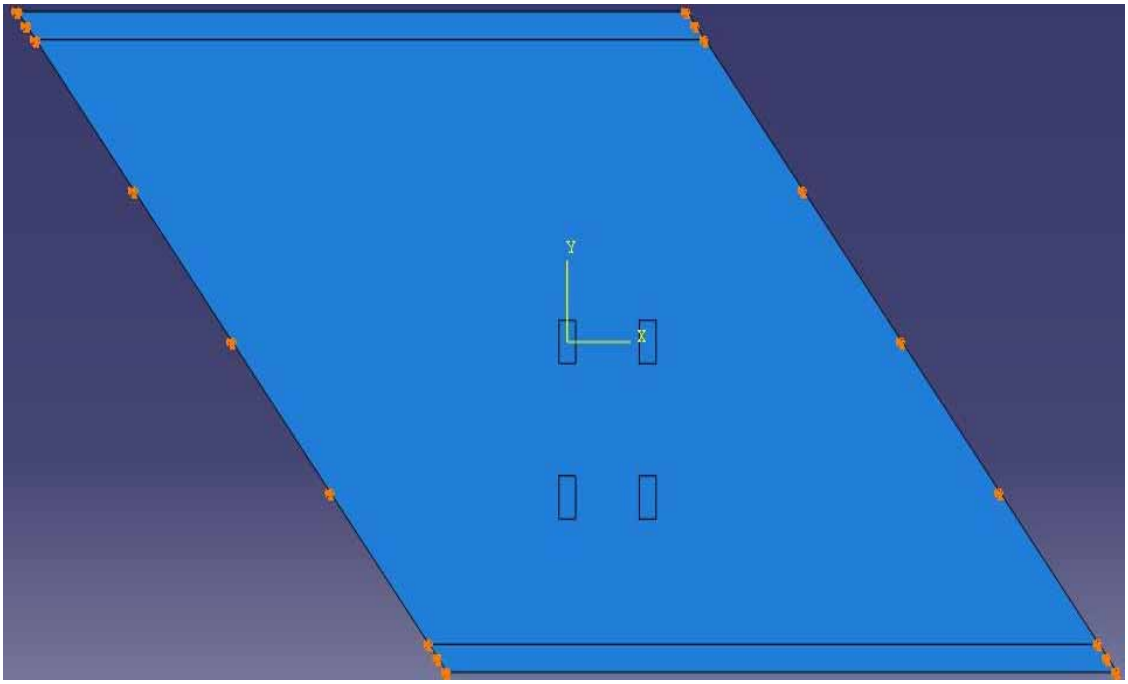

Figure 5.1 – Tire placements with one tandem applied to Carmel Bridge #5191 with 40° skew

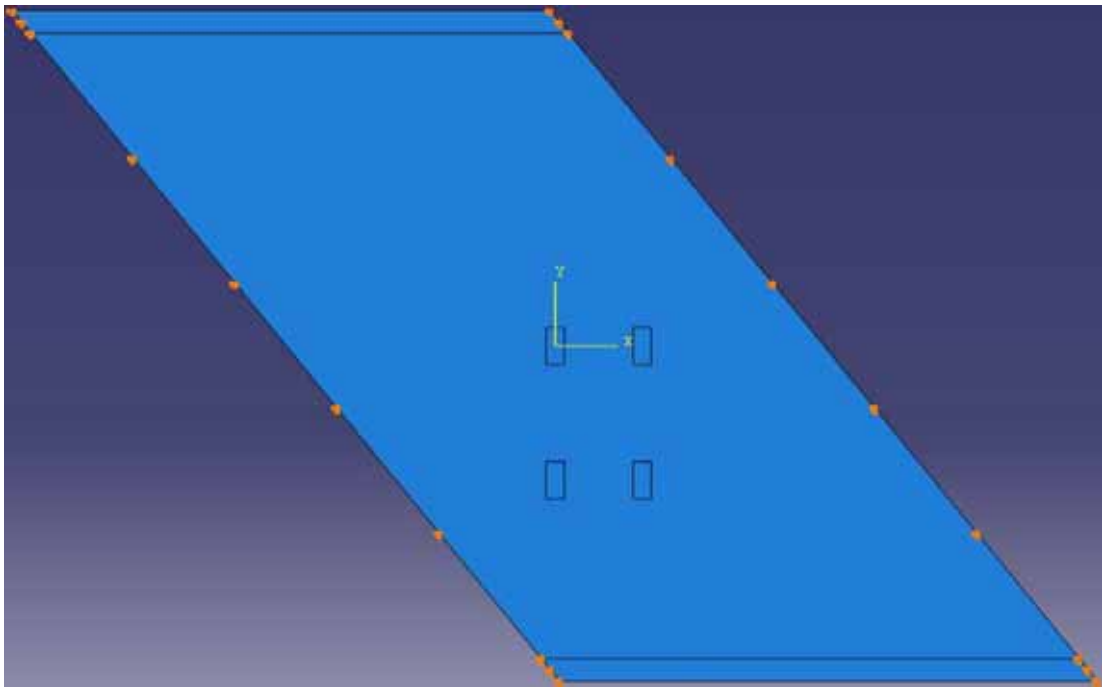

Figure 5.2 – Tire placements with one tandem applied to Linneus Bridge #5773 with 40° skew

The second loading case implemented two trucks. The bottom of the two HL-93 tandems was placed as close to the curb as possible according to AASHTO's *Manual for Bridge Evaluation* (AASHTO 2008), with the center of the bottom-most wheel placed 0.61m from the face of the curb. The back outside tire of the bottom truck was also centered at the longitudinal mid-span of the bridge. The second truck is placed as close to the bottom truck as allowed by the AASHTO *Manual for Bridge Evaluation* (AASHTO 2008), which implies a 1.22 m clear spacing between adjacent wheels of the trucks. The back inner tire of the top truck was also placed along the mid-span of the bridge to keep the tires of two trucks at the same relative position along the span of the bridge. Figure 5.3 and Figure 5.4 show the placement of the two truck loading case for both bridges with a skew angle of 40°.

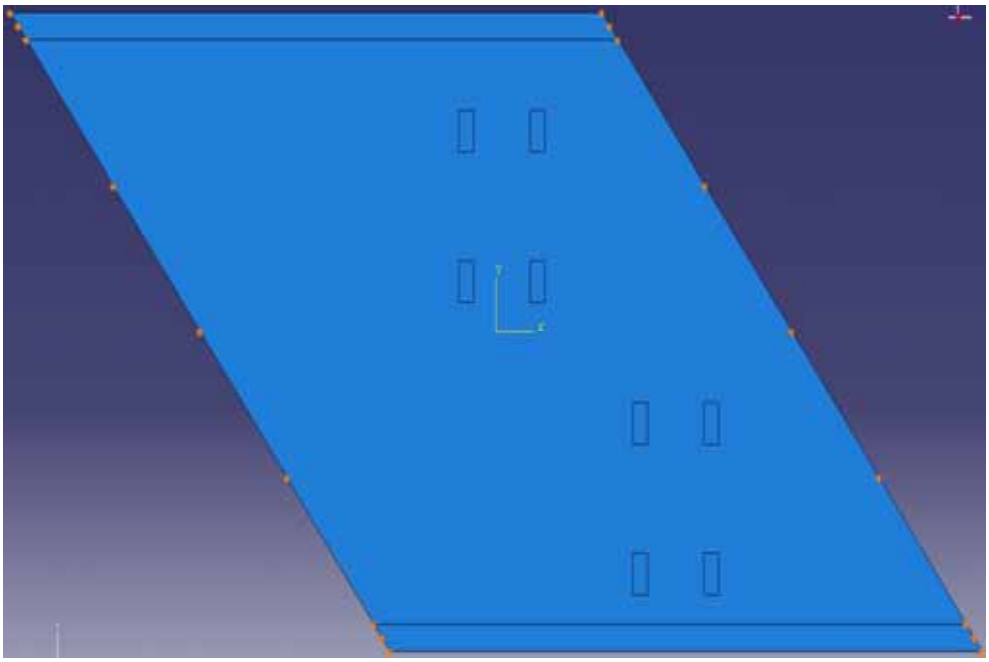

Figure 5.3 – Tire placements with two tandems applied to Carmel Bridge #5191 with 40° skew

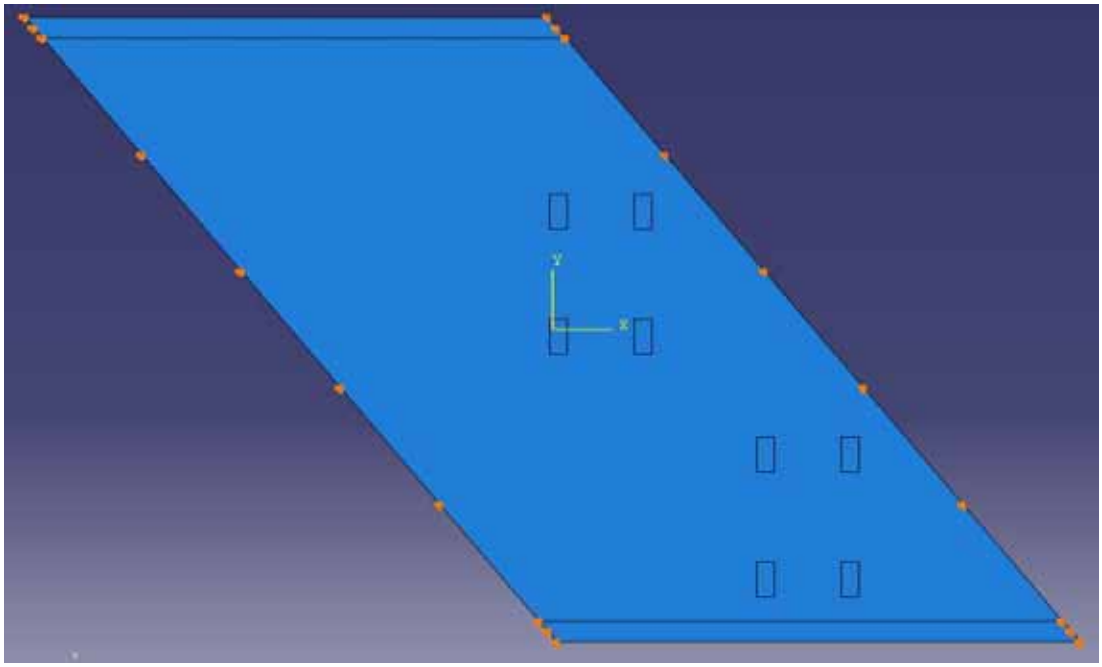

Figure 5.4 - Tire placements with two tandems applied to Linneus Bridge #5773 with 40° skew

5.2.2. Results of Abaqus Simulations

In order to capture the effects of the skew on the slab not only does the longitudinal bending moment (M_x) have to be computed but also the transverse bending moment (M_y) and torsional bending moment (M_{xy}). As stated in Section 2.2.4.4.1 bending moments cannot be directly outputted from the Abaqus models, so bending stresses were recorded and converted to bending moment by using Equation 5.1– Equation 5.3 (Bhatti, 2006).

$$M_x = \frac{\sigma_x h^2}{6}$$ Equation 5.1

$$M_y = \frac{\sigma_y h^2}{6}$$ Equation 5.2

$$M_{xy} = \frac{\tau_{xy} h^2}{6}$$ Equation 5.3

Where:

M_x = longitudinal bending moment

σ_x = longitudinal bending stress from the Abaqus model

M_y = transverse bending moment

σ_y = transverse bending stress from the Abaqus model

M_{xy} = torsional bending moment

σ_{xy} = torsional bending stress from the Abaqus model

h = slab thickness

The slab thicknesses of Carmel Bridge #5191 and Linneus Bridge #5773 are 0.56 m and 0.356 m respectively. The resulting bending moments from the models are shown below in Table 5.1 – Table 5.6. Table 5.1 and Table 5.2 show the total factored moments (both dead and live) for the one truck loading cases for both the Carmel bridge and the Linneus bridge. The results provided are the resulting moments at the center of the bridge. While the center of the bridge does not see the largest M_x, there is a greater contribution of transverse and torsional bending moments at the center of the bridge than at the location of the maximum longitudinal bending moment. Further, the location of the maximum moment varies with skew angle, and taking moments at the center of the bridge eliminates this variation.

Table 5.1 – One truck loading case resulting longitudinal, transverse and torsional bending moments (M_x , M_y and M_{xy}) at the center of Carmel Bridge #5191 for different skew angles

Skew Angle (°)	M_x (kN-m/m)	M_y (kN-m/m)	M_{xy} (kN-m/m)
0	416.9	78.2	3.5
10	402.0	81.8	48.9
20	358.1	91.3	87.0
30	292.8	105.6	110.9
40	207.9	122.0	114.2

Table 5.2 – One truck loading case resulting longitudinal, transverse and torsional bending moments (M_x , M_y and M_{xy}) at the center of Linneus Bridge #5191 for different skew angles

Skew Angle (°)	M_x (kN-m/m)	M_y (kN-m/m)	M_{xy} (kN-m/m)
0	225.5	72.0	2.8
10	217.3	74.5	26.2
20	192.9	81.6	44.3
30	156.8	90.2	52.6
40	116.9	95.2	48.7

Table 5.3 – Table 5.6 summarize the results of the two truck loading cases. Table 5.3 and Table 5.4 are the resulting bending moments at the center of the bridge for each the bridges while Table 5.5 and Table 5.6 are the results at mid-span of the bridge 0.17 m up from the bottom edge, generally the location of the maximum longitudinal bending moment. The results at two separate locations are provided to show how the center of the bridge is affected more than the edge of the bridge by the transverse and torsional bending moments even though the longitudinal bending moments are greater at the edge.

Table 5.3 – Two truck loading case resulting longitudinal, transverse and torsional bending moments (M_x, M_y and M_{xy}) at the center of Carmel Bridge #5191 for different skew angles

Skew Angle (°)	M_x (kN-m/m)	M_y (kN-m/m)	M_{xy} (kN-m/m)
0	484.34	52.13	0.44
10	458.59	56.53	59.74
20	395.69	67.97	107.20
30	305.36	83.44	135.35
40	199.00	99.32	137.09

Table 5.4 – Two truck loading case resulting longitudinal, transverse and torsional bending moments (M_x, M_y and M_{xy}) at the center of Linneus Bridge #5191 for different skew angles

Skew Angle (°)	M_x (kN-m/m)	M_y (kN-m/m)	M_{xy} (kN-m/m)
0	266.5	62.0	1.5
10	249.3	65.3	33.0
20	210.7	73.6	56.5
30	159.4	82.3	62.7
40	106.6	85.5	53.6

Table 5.5 – Two truck loading case resulting longitudinal, transverse and torsional bending moments (M_x, M_y and M_{xy}) at the edge of the slab of Carmel Bridge #5191 for different skew angles

Skew Angle (°)	M_x (kN-m/m)	M_y (kN-m/m)	M_{xy} (kN-m/m)
0	507.0	2.1	0.8
10	490.5	2.3	29.4
20	437.1	2.8	50.9
30	359.8	3.5	60.2
40	274.7	3.9	56.4

Table 5.6 – Two truck loading case resulting longitudinal, transverse and torsional bending moments (M_x, M_y and M_{xy}) at the edge of the slab of Linneus Bridge #5191 for different skew angles

Skew Angle (°)	M_x (kN-m/m)	M_y (kN-m/m)	M_{xy} (kN-m/m)
0	287.2	2.1	0.6
10	278.4	2.4	19.8
20	248.5	2.8	33.5
30	206.2	3.3	40.3
40	158.6	3.3	37.8

As can be seen in the tables, as the skew angle increases then the resulting transverse and torsional moments generally become larger. The longitudinal moments steadily decrease over all the skew angles that were tested.

5.3. Comparing Capacity to Resulting Moments

After the moments were determined from the Abaqus models they had to be compared to the flexural capacity of the bridge. This was done using the method

developed by Denton and Burgoyne (1996), who provides equations to determine the flexural capacity and the applied moments at different failure planes.

5.3.1. Flexural Capacity of the Bridge

While determining the flexural capacity for the bridges both the longitudinal and transverse reinforcement had to be considered. The transverse reinforcement was assumed to always be parallel to the skew angle of the bridge because in all 13 of the skewed bridges analyzed in Chapter 3, the transverse reinforcement was placed parallel to the skew of the bridge. Equation 5.4 – Equation 5.6 were used to determine the flexural capacity in the M_x, M_y and M_{xy} directions (Denton and Burgoyne 1996).

$$M_x^* = \sum_i \left(M_{\alpha i} \cos^2 \alpha_i \right) \quad \text{Equation 5.4}$$

$$M_y^* = \sum_i \left(M_{\alpha i} \sin^2 \alpha_i \right) \quad \text{Equation 5.5}$$

$$M_{xy}^* = -\sum_i \left(M_{\alpha i} \cos \alpha_i \sin \alpha_i \right) \quad \text{Equation 5.6}$$

Where:

α_i = angle between the ith layer of reinforcement and the longitudinal axis

$M_{\alpha i}$ = Moment of resistance of the ith layer of reinforcement about an axis perpendicular to its direction, neglecting all other layers of reinforcement.

The reduced flexural resistance of Carmel Bridge #5191 is 421.20 kN-m/m in the longitudinal direction and 95.41 kN-m/m parallel to the skew of the bridge. Linneus Bridge #5773 has a reduced flexural resistance of 296.8 kN-m/m in the longitudinal direction and 61.6 kN-m/m parallel to the skew of the bridge. Table 5.7 and Table 5.8 provide M_x^*, M_y^* and M_{xy}^* for both of the bridges at each skew angle that was modeled. Values in Table 5.7 and Table 5.8 with an asterisk indicate that the cracking moment

(M_{cr}) was used. This is because there is always a minimum resistance equal to the cracking moment in both the longitudinal and transverse direction. AASHTO's (2010) limit of reinforcement being more then $1.2M_{cr}$ was ignored (AASHTO section 5.7.3.3.2) in this analysis. By ignoring this limit it would lead to a brittle failure, because once the concrete has cracked there is not enough reinforcement to withstand the applied moments that caused the concrete to crack.

Table 5.7 –Longitudinal, transverse and torsional bending capacity (M_x^*, M_y^* and M_{xy}^*) for Carmel Bridge #5191 for different skew angles

Skew Angle (°)	M_x^* (kN-m/m)	M_y^* (kN-m/m)	M_{xy}^* (kN-m/m)
0	421.2	121.65*	0.0
10	424.1	121.65*	20.8*
20	432.3	121.65*	39.1*
30	445.0	121.65*	52.7*
40	460.6	121.65*	59.9*

Table 5.8 –Longitudinal, transverse and torsional bending capacity (M_x^*, M_y^* and M_{xy}^*) for Linneus Bridge #5773 for different skew angles

Skew Angle (°)	M_x^* (kN-m/m)	M_y^* (kN-m/m)	M_{xy}^* (kN-m/m)
0	296.8	61.6	0.0
10	298.7	59.7	10.5
20	304.0	54.4	19.8
30	312.2	54.0*	23.4*
40	322.3	54.0*	26.6*

5.3.2. Comparing Capacity to Applied Moments

Denton and Burgoyne (1996) provide not only a method to compute the directional capacities for the bridge but also a method to assess if capacity exceeds the applied loads. To assess bridge capacity, it is not sufficient to look only at the capacity vs. demand for M_x, M_y and M_{xy} individually. Different failure angles that could occur must also be considered. To illustrate, consider the case where there is no capacity in the

torsional bending direction (M_{xy}^{*} = 0kN) but the longitudinal and transverse directions are over reinforced (M_x^{*} is much greater then M_x and M_y^{*} is much greater than M_y . Even though there is no torsional bending resistance there are still contributions from the longitudinal and transverse directions at every failure angle that might provide enough torsional resistance so that the bridge reinforcement is adequate. Equation 5.7 and Equation 5.8 provide bending capacity and applied bending moments for any failure angle respectively (Denton and Burgoyne 1996).

$$M_n^{*} = M_x^{*}\cos^2(\theta) + M_y^{*}\sin^2(\theta) - 2M_{xy}^{*}\sin(\theta)\cos(\theta) \qquad \text{Equation 5.7}$$

$$M_n = M_x\cos^2(\theta) + M_y\sin^2(\theta) - 2M_{xy}\sin(\theta)\cos(\theta) \qquad \text{Equation 5.8}$$

Where;

M_n^{*} = moment capacity

M_n^{*} = applied moment

θ = angle of failure plane (with respect to the longitudinal failure plane)

Different failure planes were analyzed, ranging from -90° to 90° degrees for each of the loading cases. Figure 5.5 and Figure 5.6 show the reduced moment capacities for both Carmel Bridge #5191 and Linneus Bridge #5773 at every failure plane angle. Figure 5.7 and Figure 5.8 are the resulting factored moments at the center of the bridge under the one truck loading case for the Carmel and Linneus bridges respectively. Figure 5.9 – Figure 5.12 are the resulting factored moments for the two truck loading case. Figure 5.9 and Figure 5.10 are the resulting moments at the center of the bridge while Figure 5.11 and Figure 5.12 are the resulting moments at the edge of the bridge.

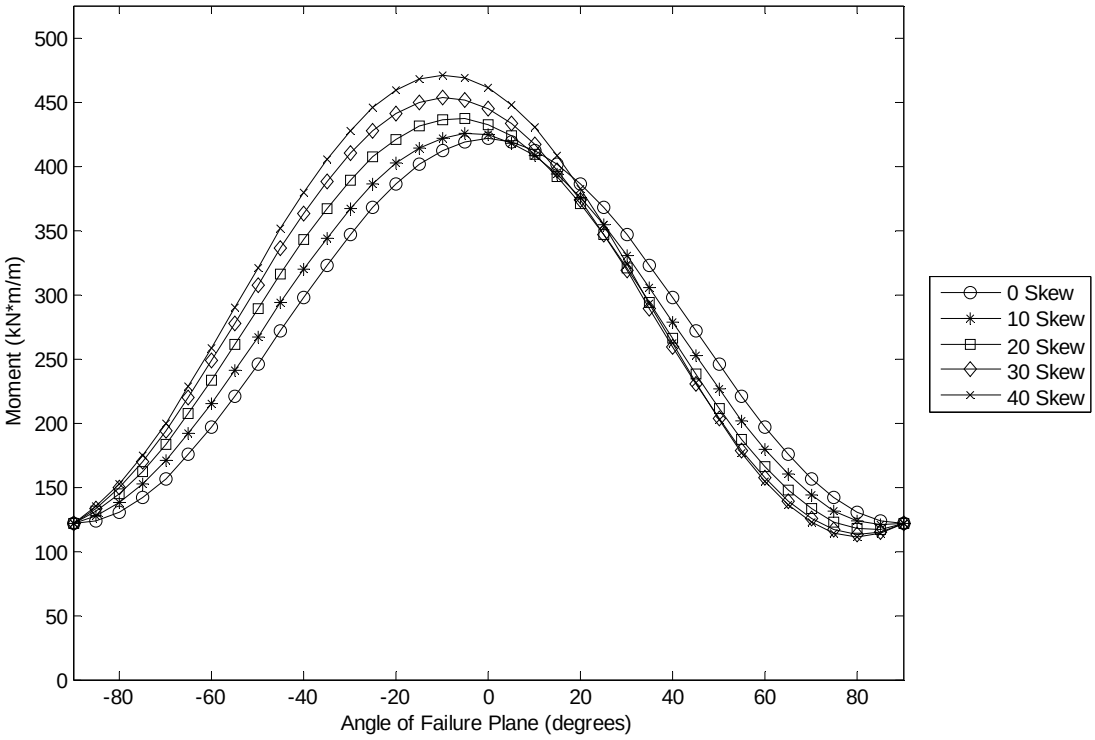

Figure 5.5 – Moment capacity of Carmel Bridge #5191 at different failure planes for different skew angles

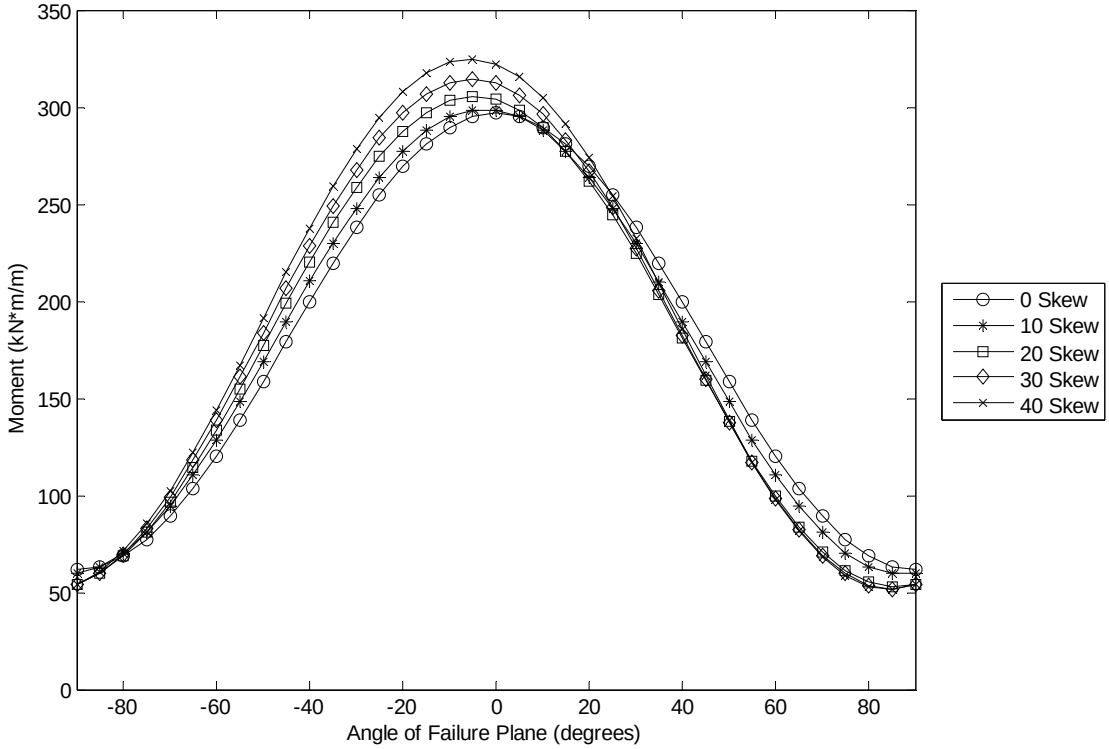

Figure 5.6 – Moment capacity of Linneus Bridge #5773 at different failure planes for different skew angles

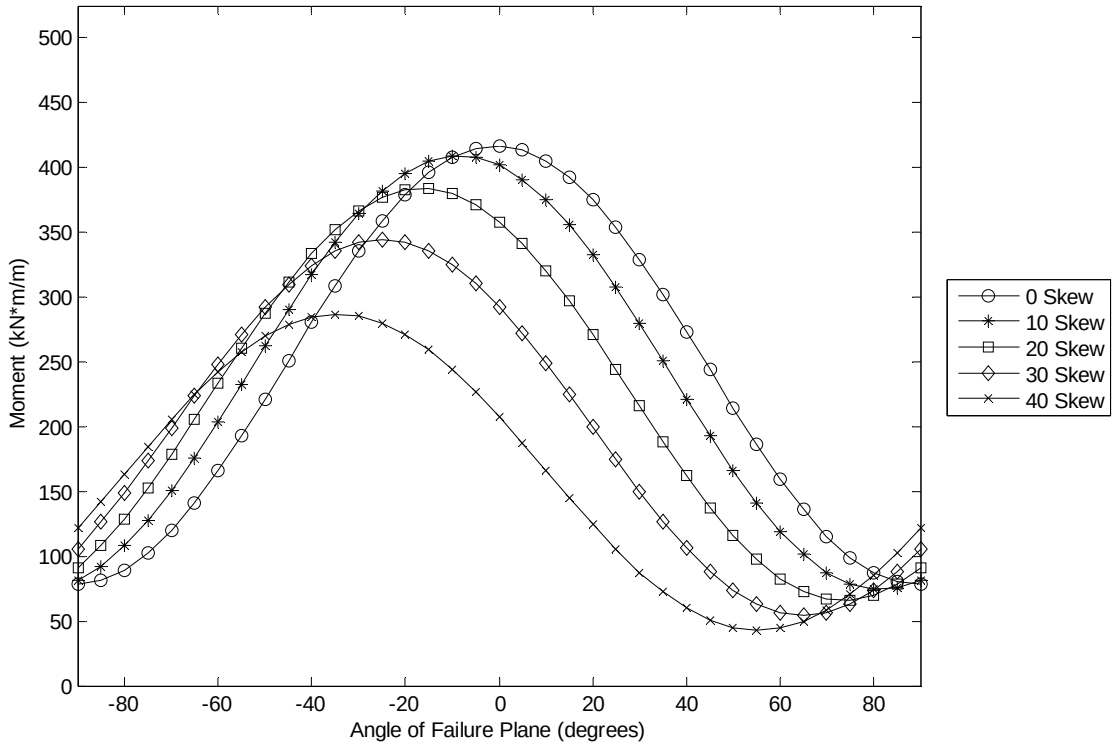

Figure 5.7 – One truck loading case resulting moment at the center of the bridge for Carmel Bridge #5191

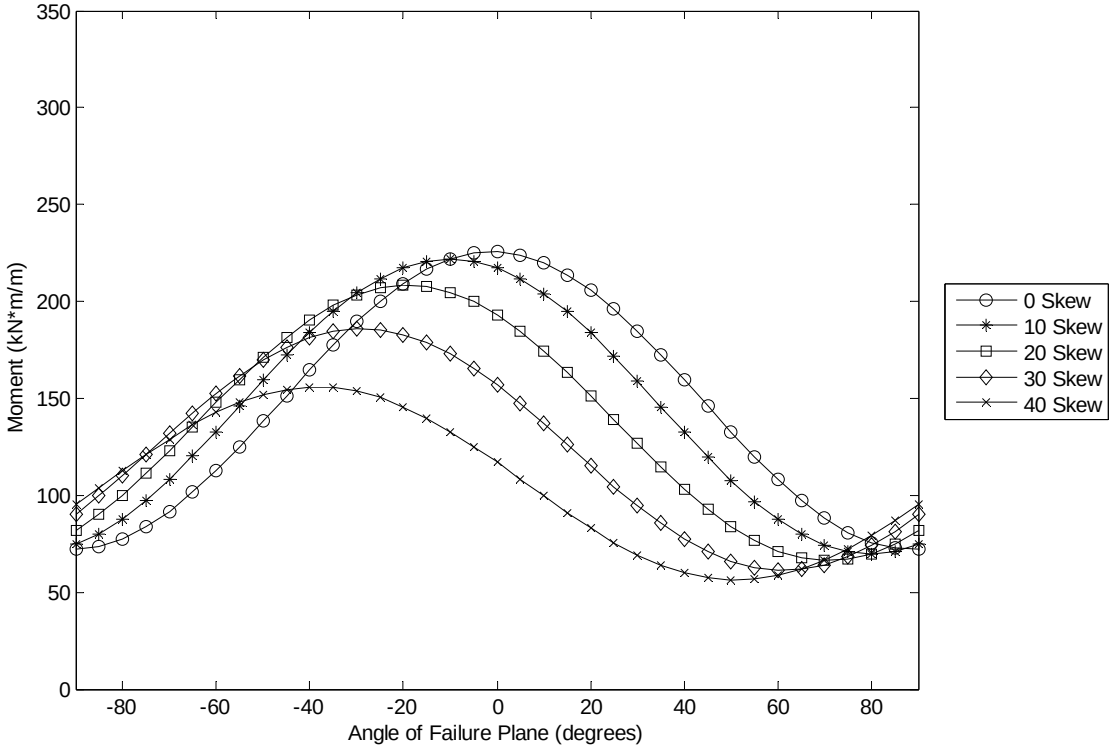

Figure 5.8 – One truck loading case resulting moment at the center of the bridge for Linneus Bridge #5773

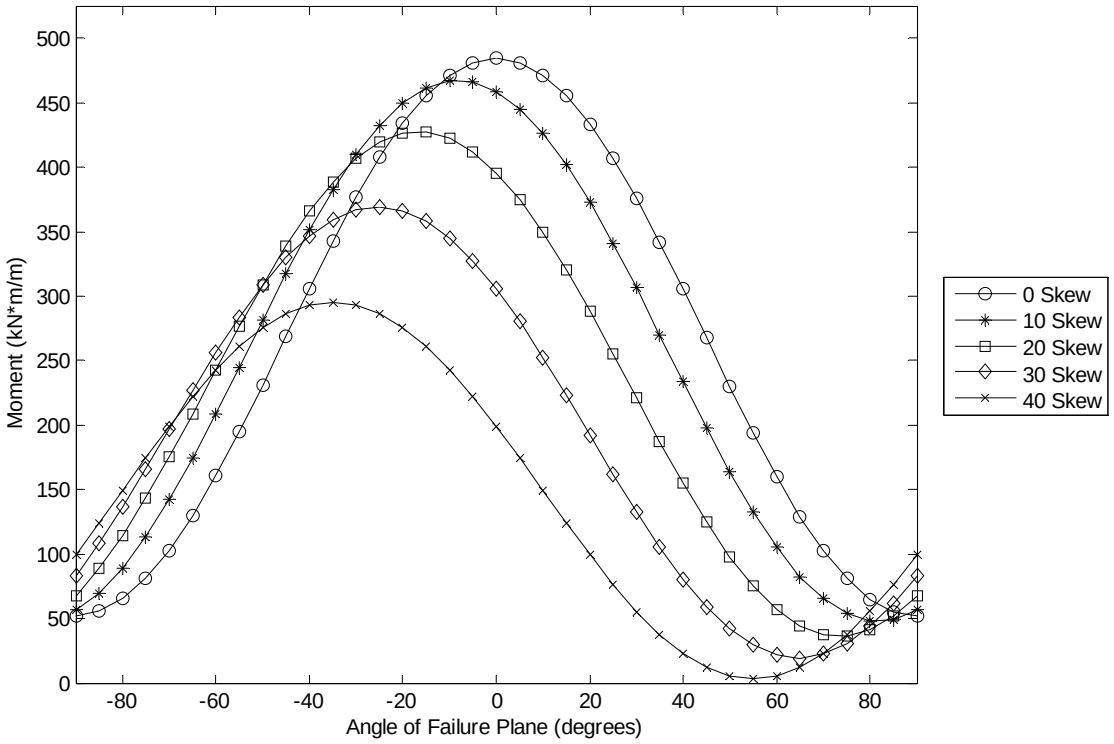

Figure 5.9 – Two truck loading case resulting moment at the center of the bridge for Carmel Bridge #5191

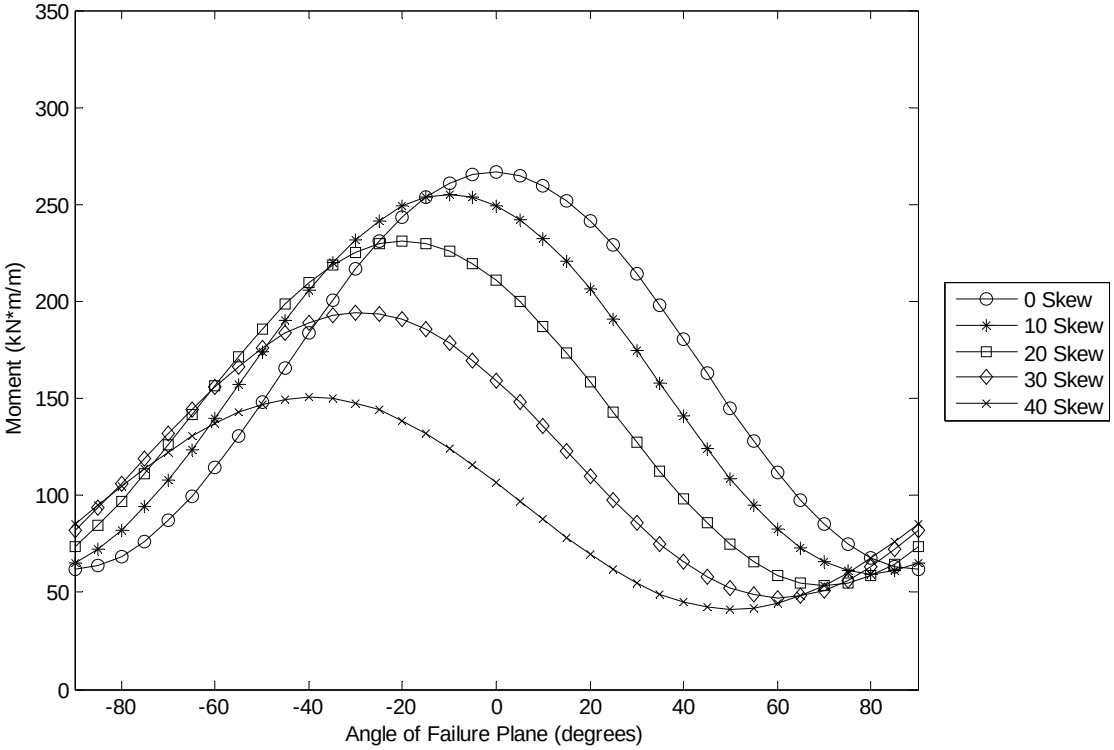

Figure 5.10 – Two truck loading case resulting moment at the center of the bridge for Linneus Bridge #5773

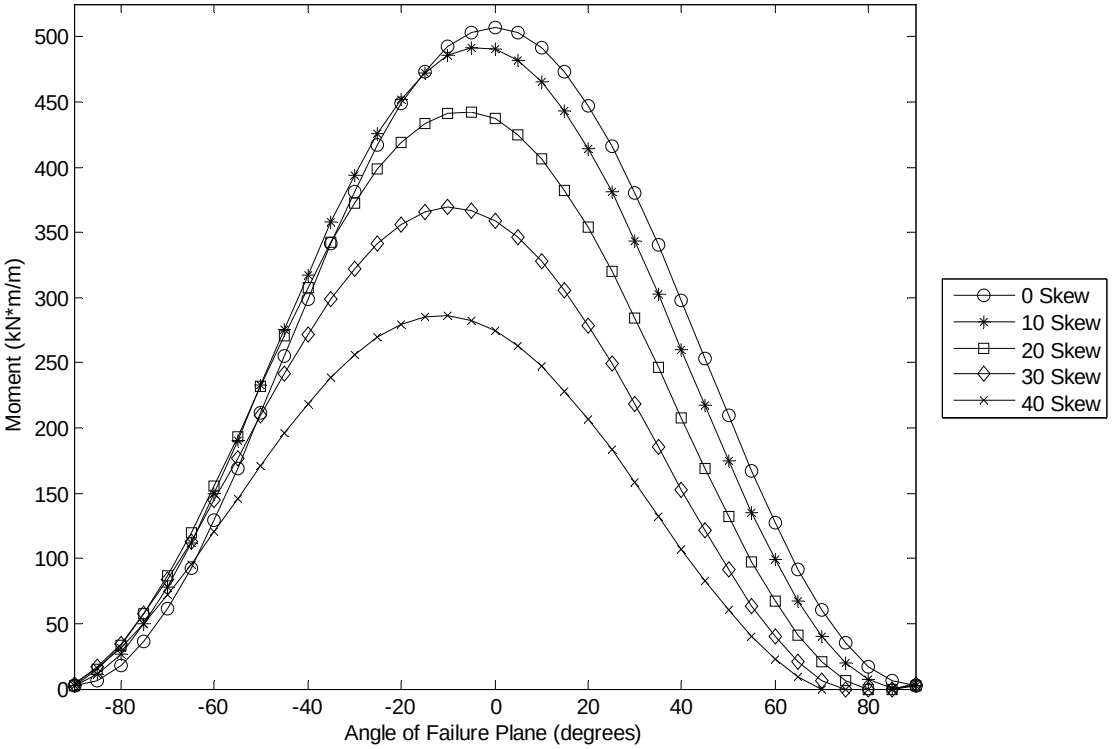

Figure 5.11 – Two truck loading case resulting moments at the edge of the bridge for Carmel Bridge #5191

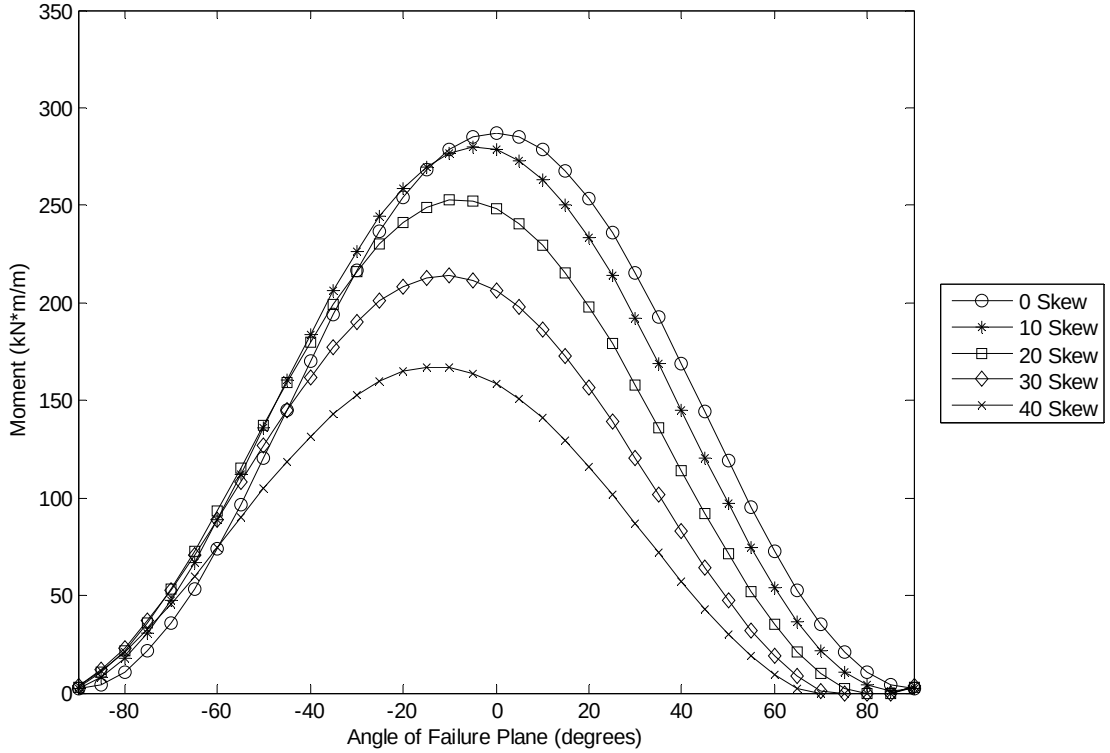

Figure 5.12 – Two truck loading case resulting moments at the edge of the bridge for Linneus Bridge #5773

Along with the plots showing moment capacity and the resulting moments for Carmel Bridge #5191 and Linneus Bridge #5773, the rating factors were also calculated at each failure plane for each bridge skew angle. This was done by determining the factored dead and factored live load separately, then using Equation 5.9 to determine the rating factor for each skew angle of the bridge at each failure angle.

$$RF = \frac{C - (\gamma_D)(M_D)}{(\gamma_L)(M_L)}$$ Equation 5.9

Where;

RF = rating factor

C = reduced moment capacity

$(\gamma_D)(M_D)$ = factored dead moment

$(\gamma_L)(M_L)$ = factored live moment

Figure 5.13 – Figure 5.18 are plots of the rating factors at each of the failure planes for each of the loading cases and bridges. Figure 5.13 and Figure 5.14 are the rating factors for Carmel Bridge #5191 and Linneus Bridge #5773 respectively under the one truck loading case. Figure 5.15 and Figure 5.16 are the rating factors at the center of the bridge under the two truck loading case while Figure 5.17 and Figure 5.18 are the rating factors at the edge of the bridge.

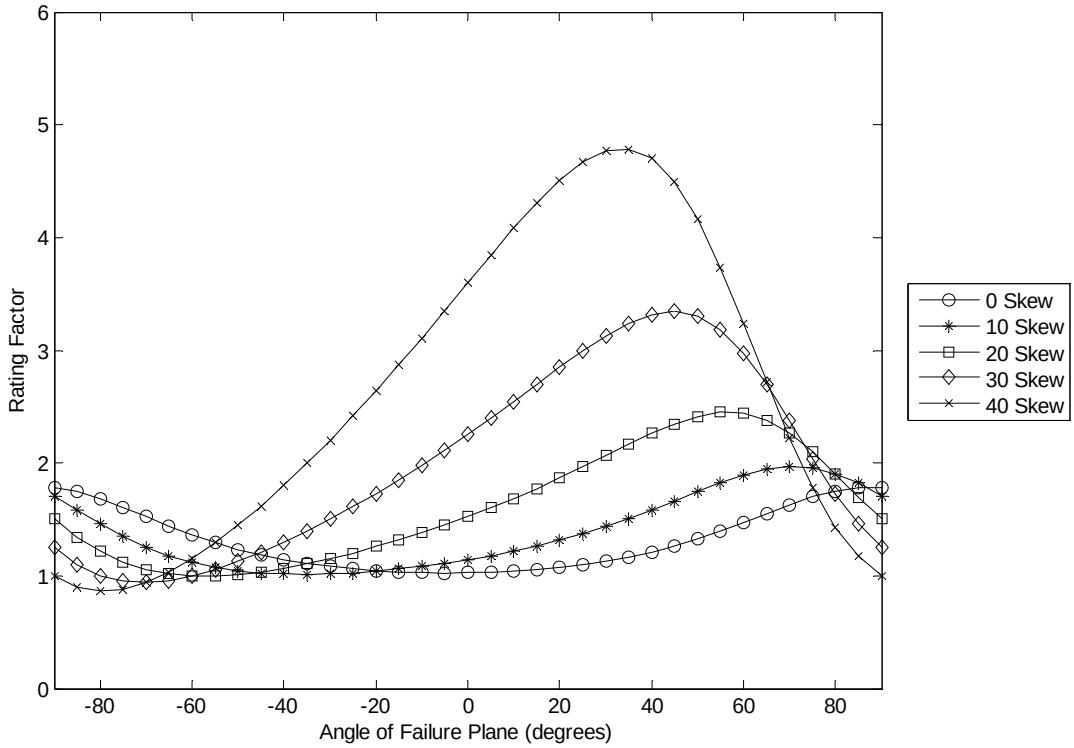

Figure 5.13 – Rating factors at the center of the bridge under the one truck loading case for Carmel Bridge #5191

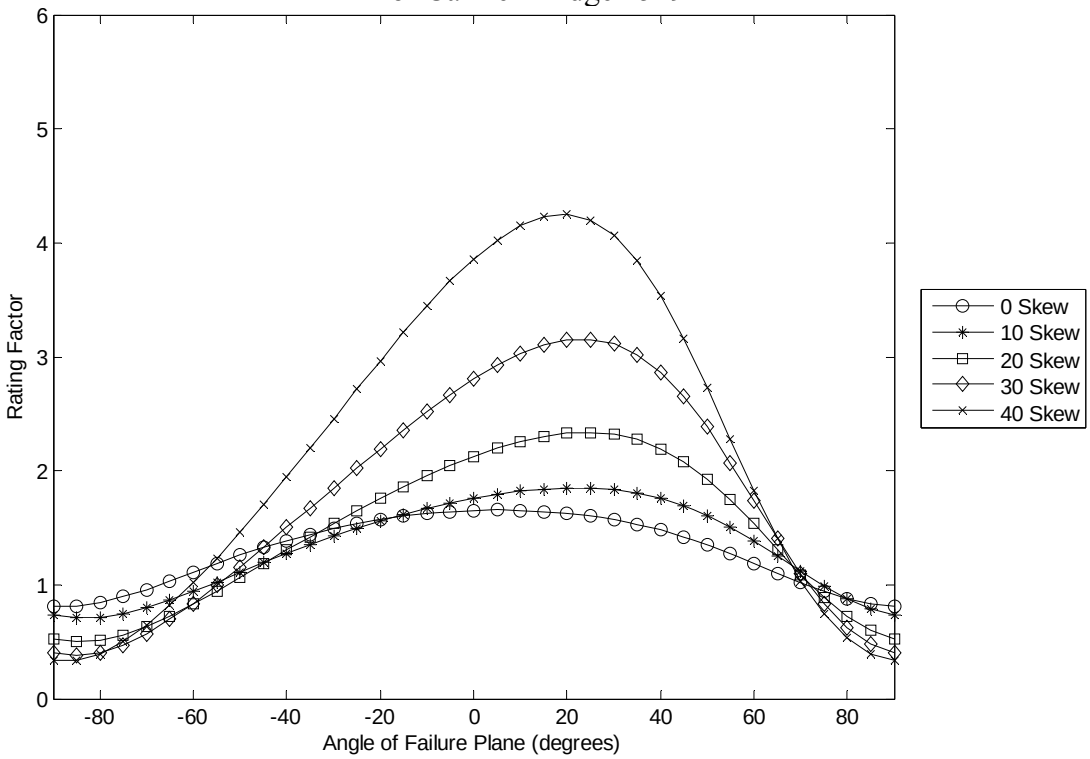

Figure 5.14 – Rating factors at the center of the bridge under the one truck loading case for Linneus Bridge #5773

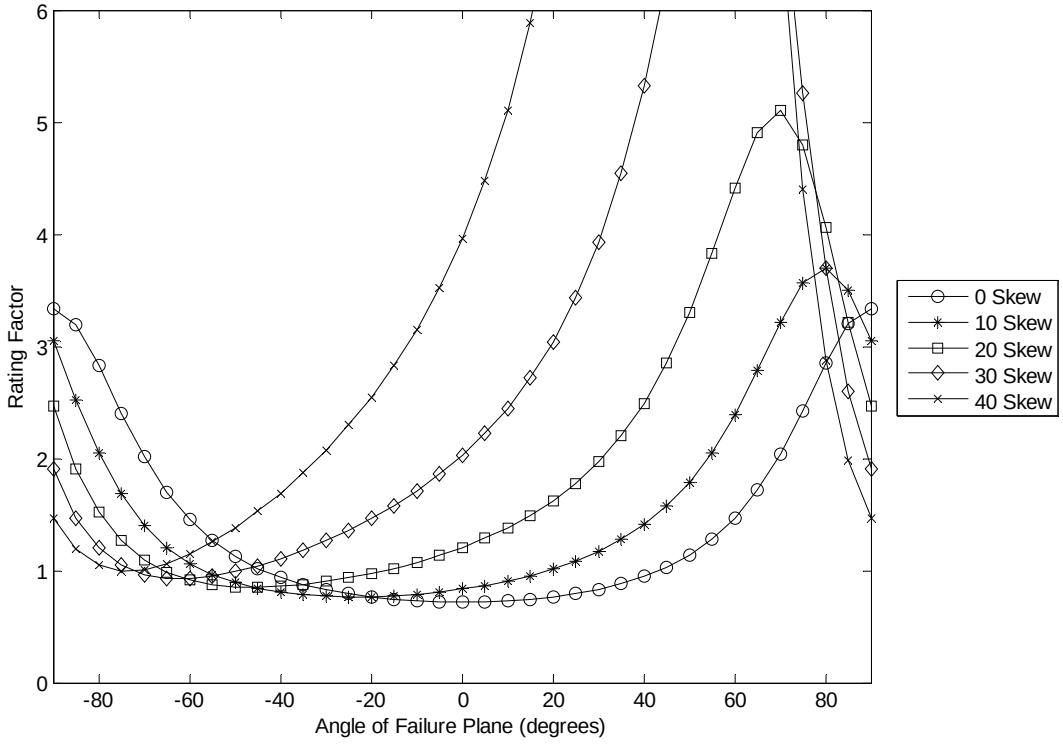

Figure 5.15 – Rating factors at the center of the bridge under the two truck loading case for Carmel Bridge #5191

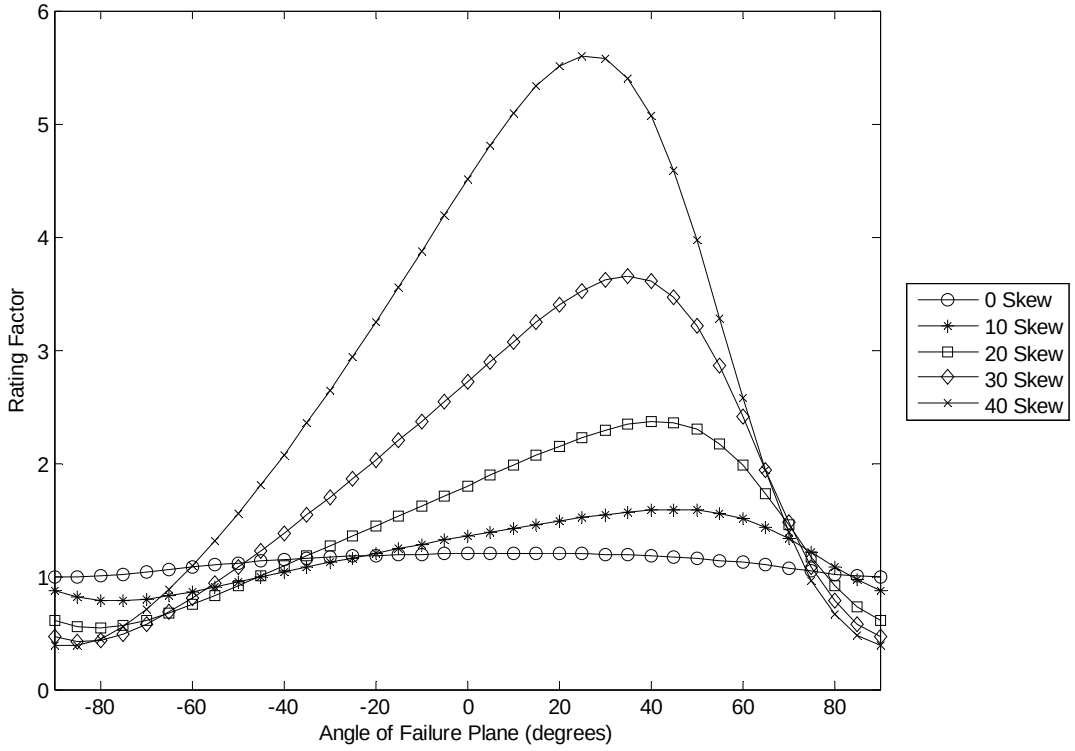

Figure 5.16 – Rating factors at the center of the bridge under the two truck loading case for Linneus Bridge #5773

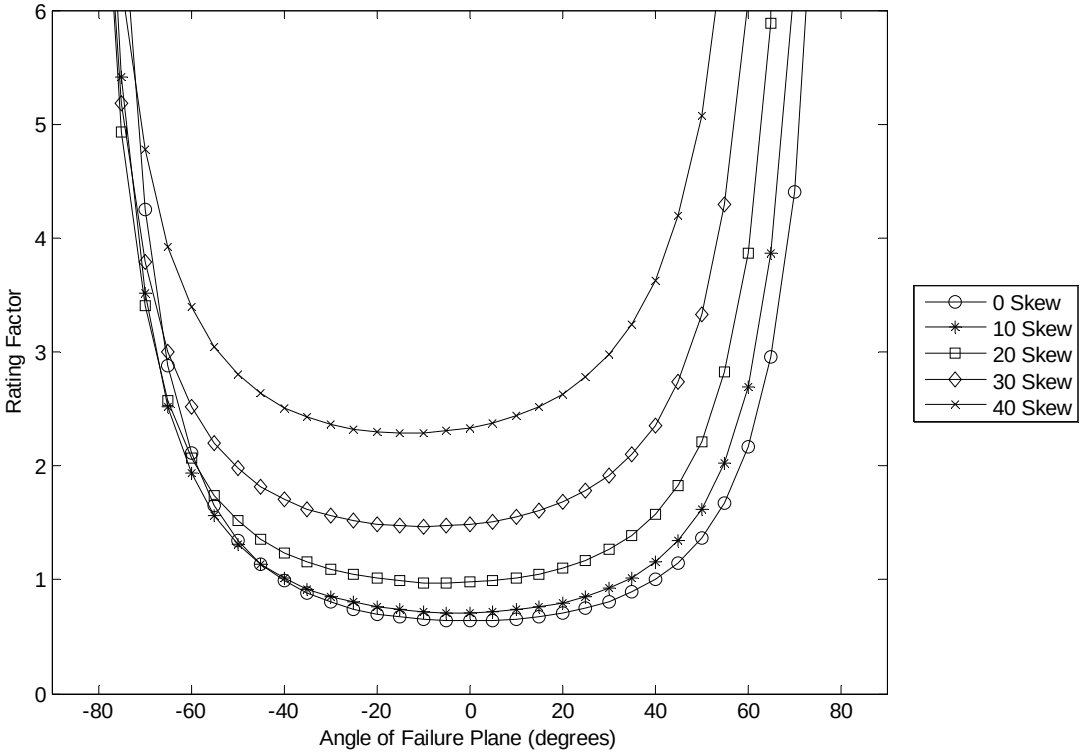

Figure 5.17 – Rating factors at the edge of the bridge under the two truck loading case for Carmel Bridge #5191

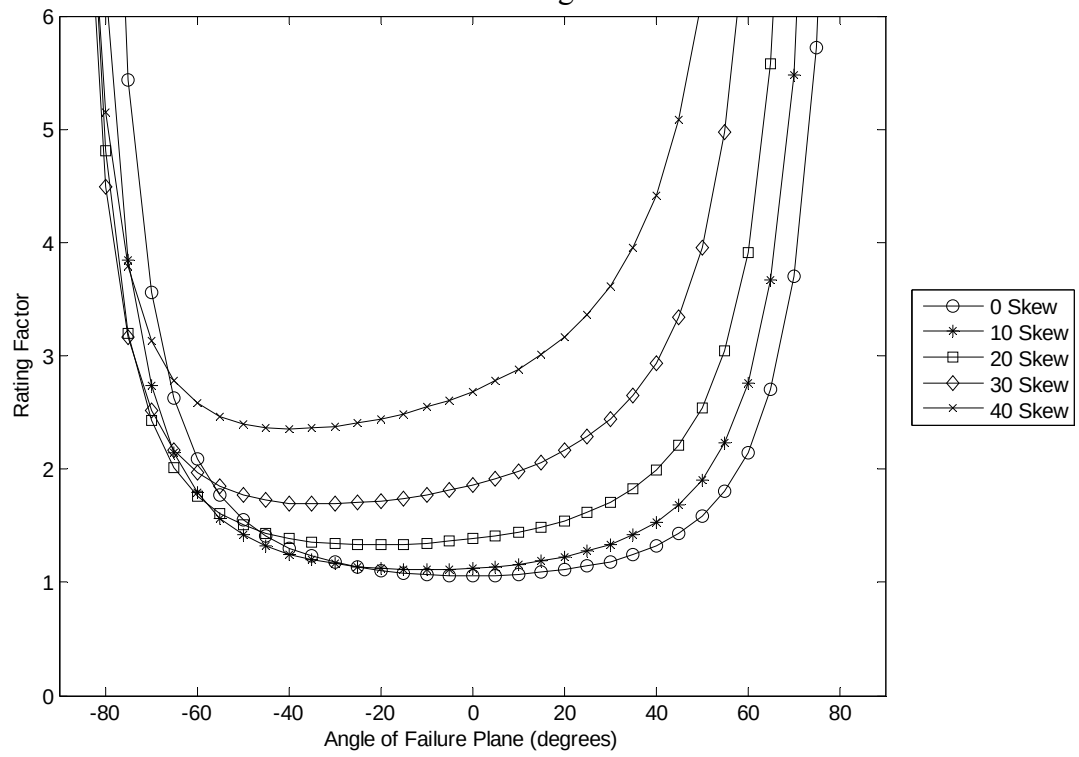

Figure 5.18 – Rating factors at the edge of the bridge under the two truck loading case for Linneus Bridge #5773

The minimum rating factors for each of the bridge skews are shown below in Table 5.9 for Carmel Bridge #5191 and Table 5.10 for Linneus Bridge #5773. Along with reporting the minimum rating factor, the failure angle at which the minimum rating factor occurs is also provided. The failure angles are reported to the nearest multiple of 5 degrees (0°, 5°, 10°, 15° etc.).

Table 5.9 – Minimum rating factors and angle of the failure plane for Carmel Bridge #5191 for each loading case

	One truck loading case (center)		Two truck loading case (center)		Two truck loading case (edge)	
	Minimum rating factor	Angle of Failure Plane (°)	Minimum rating factor	Angle of Failure Plane (°)	Minimum rating factor	Angle of Failure Plane (°)
0° Skew	1.03	-5	0.72	0	0.64	0
10° Skew	1.01	-35	0.77	-25	0.71	0
20° Skew	1.00	-55	0.85	-45	0.97	-5
30° Skew	0.94	-70	0.93	-60	1.47	-10
40° Skew	0.86	-80	1.00	-75	2.28	-15

Table 5.10 – Minimum rating factors and angle of the failure plane for Linneus Bridge #5773 for each loading case

	One truck loading case (center)		Two truck loading case (center)		Two truck loading case (edge)	
	Minimum rating factor	Angle of Failure Plane (°)	Minimum rating factor	Angle of Failure Plane (°)	Minimum rating factor	Angle of Failure Plane (°)
0° Skew	0.81	-90	0.99	-85	1.06	0
10° Skew	0.71	-85	0.78	-75	1.11	-10
20° Skew	0.50	-85	0.54	-80	1.33	-20
30° Skew	0.38	-85	0.42	-85	1.69	-35
40° Skew	0.33	-90	0.39	-85	2.36	-40

5.4. SlabRate vs. Skew Models

In order to be able to make conclusions regarding the significance of skew angle, the results of the previous section need to be compared to the rating factors that only take longitudinal bending into consideration. Table 5.11 and Table 5.12 are the resulting

rating factors for each bridge under each loading case at a failure plane of 0°, which corresponds to only the longitudinal direction.

Table 5.11 – Longitudinal rating factors for Carmel Bridge #5191 for each loading case

	One truck loading case (center)	Two truck loading case (center)	Two truck loading case (edge)
0° Skew	1.03	0.72	0.64
10° Skew	1.14	0.84	0.71
20° Skew	1.52	1.20	0.98
30° Skew	2.25	2.03	1.49
40° Skew	3.60	3.96	2.33

Table 5.12 – Longitudinal rating factors for Linneus Bridge #5773 for each loading case

	One truck loading case (center)	Two truck loading case (center)	Two truck loading case (edge)
0° Skew	1.65	1.20	1.06
10° Skew	1.76	1.36	1.13
20° Skew	2.12	1.80	1.38
30° Skew	2.80	2.72	1.86
40° Skew	3.86	4.51	2.69

When comparing the results from Table 5.9 and Table 5.10 to Table 5.11 and Table 5.12, there is a significant different between the rating factors that only consider the longitudinal direction compared to the minimum rating factors that the bridge does see. The 0° skew for the Carmel bridge is the only case were the minimum rating factor is the longitudinal rating factor. The minimum rating factors in Table 5.9 and Table 5.10 that account for the full range of failure planes decrease as the skew angle of the bridge increases while the longitudinal rating factor (Table 5.11 and Table 5.12) increase.

5.5. Conclusion

Before final conclusions could be made for the slab bridges the transverse reinforcement was examined in more detail. The transverse reinforcement of all the other bridges that were analyzed in Chapter 3 was determined, and it was found that all of the

bridges' transverse reinforcement was between 20–30% of the longitudinal reinforcement. Since all the bridges were built between 1939 and 1959 (except Milo Bridge #2931 which had its deck replaced in 1994), the amount of transverse reinforcement existing in those bridges was compared with current AASHTO standards (AASHTO 2010).

The current AASHTO design requirement for transverse reinforcement in reinforced concrete slab bridges is provided as a percentage of the longitudinal reinforcement. Equation 5.10 provides the percentage of the longitudinal reinforcement that is required for the transverse reinforcement (AASHTO 2010 Section 5.14.4.1).

$$\frac{1750}{L} \leq 50\% \qquad \text{Equation 5.10}$$

Where;

L = Span Length (mm)

With bridge spans of 10.16 m and 7.54 m for Carmel Bridge #5191 and Linneus Bridge #5773 respectively, the minimum transverse reinforcement should be between 17% and 23% of the longitudinal reinforcement. The transverse reinforcement is actually 23% and 21% of the longitudinal reinforcement. Even though Linneus Bridge #5773 does not meet AASHTO's current standards it is still very close. By using Equation 5.10 it was found that all the other bridges analyzed in Chapter 3 have sufficient transverse reinforcement according to AASHTO's design specifications (AASHTO 2010). Since all of the bridges have adequate (or very close to adequate) transverse reinforcement according to AASHTO, it is reasonable to assume that most flat slab bridges in Maine follow the same transverse reinforcement pattern as all the bridges analyzed in Chapter 3.

The analysis in this chapter provides inconclusive results in determining a maximum skew angle for which it is sufficient to consider only longitudinal bending moments when load rating a slab bridge. The analysis in this chapter indicates that the bridges have inadequate transverse reinforcement, when in actuality bridges with large skews do not indicate significant distress due to transverse bending. However, one aspect of the structure not taken into account is its inherent ductility, which allows locally high moments to be dispersed over a larger area so then the bridge can carry the load. Using an elastic analysis as done here instead of an inelastic analysis, which would be needed to take into account the ductility, will result in the strength of the bridge being under-estimated (Middleton 2008). Further, neglecting the stiffness contribution from the curbs and rails could also be providing conservative results in terms of transverse moments. As shown in section 4.5 the curbs act like stiff beams along the edge of the slab, which might reduce transverse and torsional moments. In order to better quantify the effects of these possible areas of conservatism a live load test of a bridge with a significant skew should be performed. A large number of gauges with extensions should be placed in both the transverse and longitudinal directions, which would lead to being able to quantify the true moments that occur in the bridge.

Even though the analyses of this chapter are inconclusive, it is believed that that the SlabRate analysis of Chapter 3 is valid up to skew angles of at least 20°. In addition to these bridges not exhibiting distress due to transverse or torsional bending, the increase in rating factors beyond the conventional strip width method when using SlabRate for a 20° skew is approximately around 75%, whereas the increase in rating factor is on average 150% and 300% for bridges with 30° skew and 45°skew respectively. Building

on this conclusion, the load rating results of Albion Bridge #2529, Brewer Bridge #5638, Carmel Bridge #5191, Carmel Bridge #5632, Linneus Bridge #5311, and Linneus Bridge #5773, which have skew angles greater than 20 degrees, should be examined in more detail with a combination of field load testing and finite-element analyses that take into account the additional capacity provided by curbs, railing, etc. Nonlinear finite-element analyses that capture slab ductility and load redistribution may also be useful.

CHAPTER 6. CONCLUSION AND RECOMMENDATIONS

6.1. Conclusions

The verification done in Chapter 2 shows that SlabRate's finite element implementation is correct for evaluating simply-supported and continuous flat slab bridges. Results developed from comparing the ANSYS models to SlabRate (section 2.2.4.3) shows that SlabRate provides accurate solutions given the modeling assumptions and limitations inherent in the program (i.e. pinned supports, linear elasticity, and small deformations). The modeling showed that SlabRate's peak moments due to live and dead loads provide results within 1.97% and 0.86% of ANSYS's results due to the same loadings. Along with the maximum moments comparing very well, very similar distributions and magnitudes of moments over the entire bridge were seen due to both live and dead loads. The live load testing outlined in Chapter 4 also provided results that agree well with the finite-element analysis predictions at regions of high bending moment. Even though SlabRate was not used directly in Chapter 4, the results from the finite element model that was used have been shown to compare well with SlabRate.

The assumptions and limitations inherent in SlabRate (i.e. pinned supports, linear elasticity, and small deformations) were also found to be verified. The assumption of linear elasticity provides conservative results when computing moments, and these structures do experience small deformations and strains. The assumption of pinned supports was also verified with the modeling done using Abaqus (section 2.2.4.5), with the results of peak moments due to factored live loads provided by SlabRate being within 8% of those provided by the Abaqus models. The majority of this error is caused by a

change in effective span length captured by Abaqus' explicit modeling of the actual support width and loss of contact between the slab and support; the SlabRate analysis took the span length as abutment centerline to abutment centerline. Due to this difference in span length, SlabRate always provided conservative results. When the same effective span length was used with both software packages, they predicted results were within 1% of each other.

Load rating factors computed by SlabRate were higher than those predicted using AASHTO's conventional strip width method. These larger load rating factors could prevent bridges from being weight restricted or closed. SlabRate increased rating factors by an average of 24.1% for non-skewed bridges, 48.1% for 15° skew bridges, 146.6% for 30° skew bridges and 299.7% for 45° skew bridges for all of the trucks configurations discussed in section 3.3.

When comparing the finite element models to the results from the live load test of the Bradford Bridge it was found that the predicted moments for the critical strain gauges with extensions corresponded very well with the resulting moments based on a cracked section. The resulting peak moment based on the cracked sections properties were within 9% of peak moments predicted by the finite element model. These results were not only seen for peak moments but also for all truck positions all along the bridge (shown in section 4.4.3). It was also found during the live load tests that the BDI system was easily set up and removed. All the twenty two gauges were set up on the bridge and removed the day of the live load test. It was also determined that when placing strain gauges on concrete, extensions should be used. The gauges with extensions provided more

consistent results during the tests along with providing results more in-line with the finite element models in comparison to the gauges without the extensions.

Based on the analyses in Chapter 5 it was concluded that SlabRate can be reliably used to load rate flat slab bridges having skews of 20° or less. This maximum skew angle recommendation is based in part on other research done on the same topic as discussed in section 5.5.

Considering only bridges with 20° skew or less, seven out of fourteen bridges would have rating factors above one using SlabRate while below one using the conventional strip width method. These bridges are Argyle Township Bridge #3827, Exeter Bridge #5838, Greenfield Township Bridge #5605, Milford Bridge #2070, Monroe Bridge #5538, Newcastle Bridge #5608 and Palmyra Bridge #5699. Two bridges, Chester Bridge #5907 and Milo Bridge #2931 had rating factors greater than one using the conventional strip width method along with SlabRate.

6.2. Recommendations

One recommendation for future work is to live load test a bridge with intermediate skew (between 20° and 30°) and a bridge with a significant skew (greater than 30°). The instrumentation on these bridges should include many gauges placed both longitudinally and transversely with gauge extensions. The reason for the gauge extensions is that the bridges are made of concrete and with the gauge extensions it would be able to average the strain over larger distance to ensure that more accurate strain data is collected. This is evident in the analysis of Chapter 4, where the gauges with extensions provided more consistent data that was more in line with finite-element model predictions. Gauges should also be placed longitudinally and transversely to correctly

capture the effect that the skew has on the moments in both directions. To do this with the current BDI system that was used in Chapter 4, more extensions should be purchased, as six extensions would not be sufficient since both longitudinal and transverse strains need to be predicted with accuracy. Also for these live load tests, gauges should be placed on the top of the slab, which will allow the direct measurement of neutral axis location and the more accurate prediction of bending moments from the strain data.

If the live load test show that the transverse bending moments are significant in comparison to the longitudinal bending moments, this should be investigated further analytically. This could lead to the amount of transverse reinforcement having to be increased for skewed bridges as current AASHTO standards only require a percentage of the longitudinal reinforcement (AASHTO 2010). This percentage is only based on span length, while this might be valid for non-skewed bridges it may be unconservative for bridges with larger skews. The results from the live load test could also show that a nonlinear finite-element analysis may be needed to analyze the transverse direction. This may be needed if the results of the live load test are much less then the predicted moments based on the linear finite-element models. This is because the linear model cannot account for the inherent ductility in the structure which would allow locally high moments to disperse over a larger area so then the bridge can still carry the load.

Even after the refined analysis is used to analyze the flat-slab concrete bridges, many of these bridges will still be deemed inadequate. To ensure these bridges can stay open, a cost-effective, non-proprietary retrofit strategy should be developed. This will allow for these bridges to stay open without having to completely replace the bridge. Expectations of this retrofitting system would be to increasing the service life of each

bridge by 10 - 20 years. This would then allow the state of Maine be able to replace these bridges over a longer time frame, so then the funding for bridge construction would not have to increase per year while still providing safe and reliable bridges.

REFERENCES

AASHTO (2009). *Manual for Bridge Evaluation*. American Association of Highway and Transportation Officials, Washington, D.C.

AASHTO (2010). *LRFD Bridge Design Specifications*. American Association of Highway and Transportation Officials, Washington, D.C.

Abaqus/CAE Version 6.9 (2009). http://www.simulia.com/products/abaqus_fea.html (accessed 2/15/2)

ANSYS Version 12.0.1(2009). http://www.ansys.com/Products/ (accessed 12/1/2010)

Amer, A., M. Arockiasamy, and M. Shahawy. (1999). "Load Distribution of Existing Solid Slab Bridges Based on Field Tests." *Journal of Bridge Engineering* 4.3: 189.

Bhatti, A. (2006). *Advanced Topics in Finite Element Analysis of Structures*. John Wiley & Sons, New York, NY.

Denton, S.R. and Burgoyne, C.J. (1996). "The Assessment of Reinforced Concrete Slabs." *The Structural Engineer,* 74(9): 147-152.

Jáuregui, D.V., Licon-Lozano, A. and Kulkarni, K. (2007). "Improved Load Rating of Reinforced Concrete Slab Bridges." Report No. NM05STR-02, New Mexico Dept. of Transportation, Albuquerque, NM.

Jáuregui, David V., Alicia Licon-Lozano, and Kundan Kulkarni. (2010). "Higher Level Evaluation of a Reinforced Concrete Slab Bridge." *Journal of Bridge Engineering* 15.2

MaineDoT (2003), *Bridge Design Guide*. Maine Department of Transportation, Augusta, ME.

MaineDoT (2007), *Keeping Our Bridges Safe.* Maine Department of Transportation, Augusta, ME.

MaineDoT (2008), http://www.maine.gov/mdot/publicbridges/ (accessed 6/2010)

MathWorks (2009). http://www.mathworks.com/products/ (accessed 9/28/2009).

Menassa, C., Mabsout, M., Tarhini, K. and Frederick, G. (2007). “Influence of Skew Angle on Reinforced Concrete Slab Bridges.” *Journal of Bridge Engineering*, 12(2): 205-214.

Middleton, C. R. (2008). "Generalised Collapse Analysis of Concrete Bridges." *Magazine of Concrete Research* 60.8: 575-85.

Saraf, Vijay K. (1998)."Evaluation of Existing RC Slab Bridges." *Journal of Performance of Constructed Facilities* 12.1: 20.

Théoret, P., Massicotte, B. and Conciatori, D. (2011). Analysis and Design of Straight and Skewed Slab Bridges. Journal of Bridge Engineering (in press, doi:10.1061/(ASCE)BE.1943-5592.0000249).

Timoshenko, S.P. and Woinowsky-Krieger, S. (1959). *Theory of Plates and Shells*. McGraw-Hill Book Company, New York, NY.

APPENDIX A: MAINEDOT RATING TRUCKS

Figure A.1 – Figure A.9 are the truck configuration that were provided by the MaineDoT.

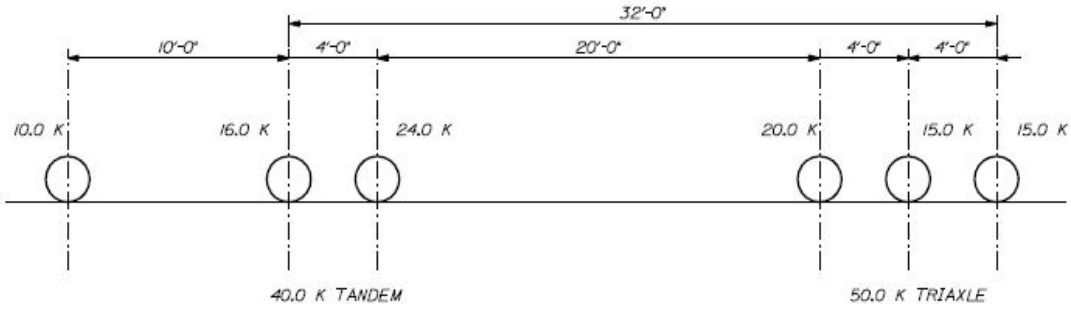

Figure A.1 – MaineDoT truck C1

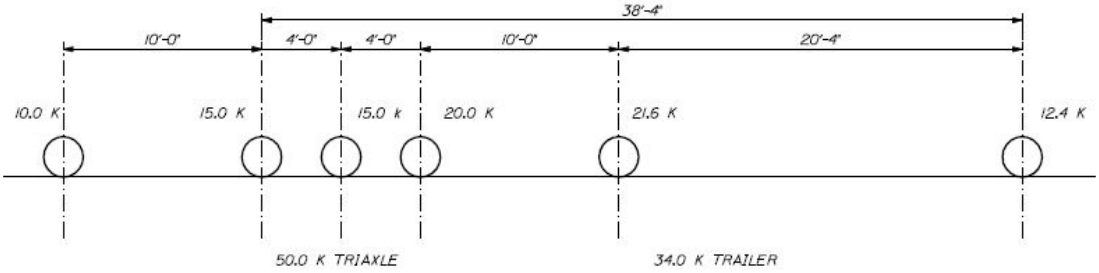

Figure A.2 – MaineDoT truck C2

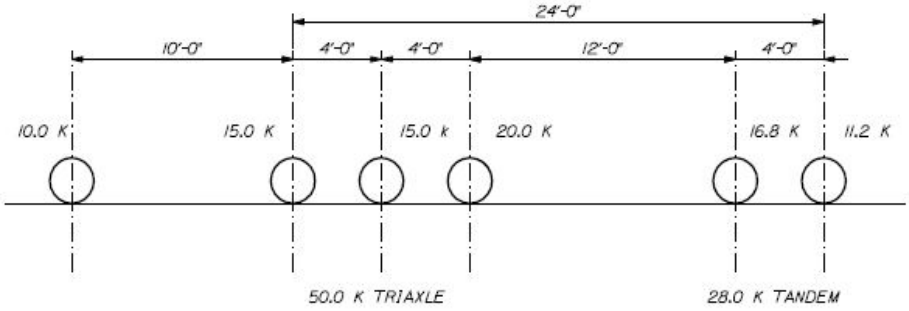

Figure A.3 – MaineDoT truck C3

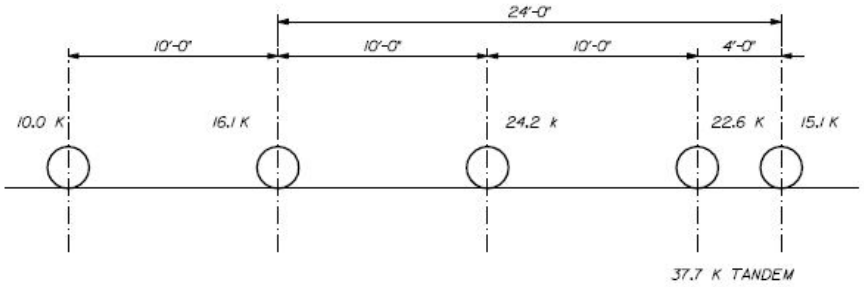

Figure A.4 – MaineDoT truck C4

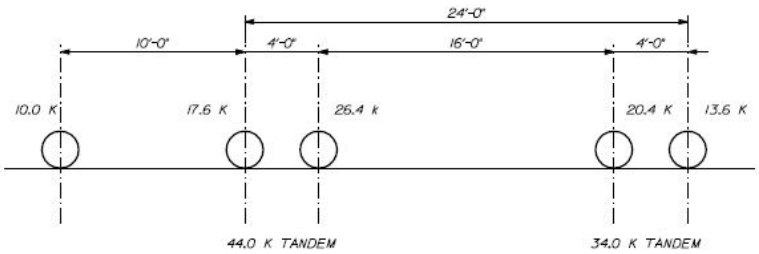

Figure A.5 – MaineDoT truck C5

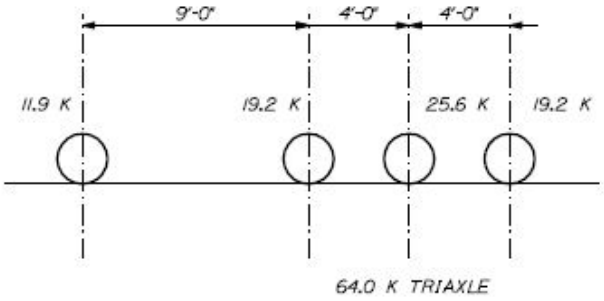

Figure A.6 – MaineDoT truck C6

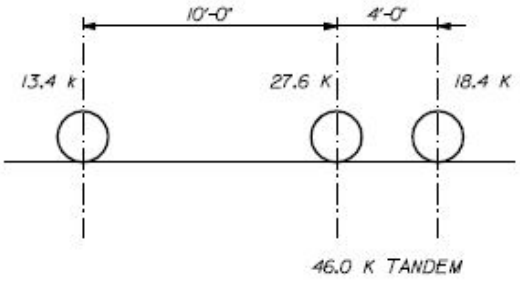

Figure A.7 – MaineDoT truck C7

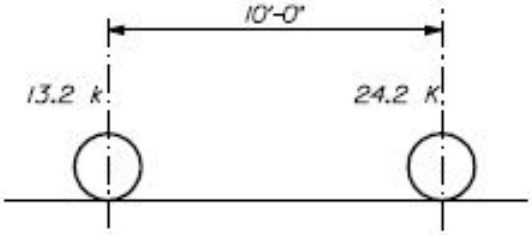

Figure A.8 – MaineDoT truck C8

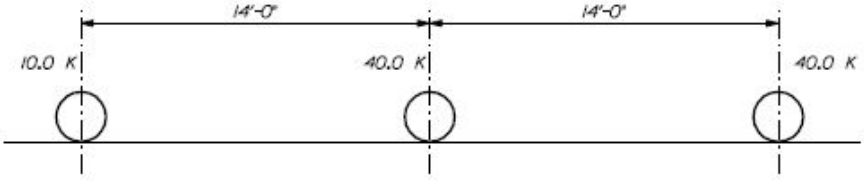

Figure A.9 – MaineDoT truck C9

APPENDIX B: ADDITIONAL CONVENTIONAL STRIP WIDTH RATING INFORMATION

Table B.1 provides additional information that was used during the load rating of each of the twenty bridges using the conventional strip width method. This information includes the equivalent strip width (E) the dead load moment due to structural components (M_{DC}) and the dead load moment due to wearing surface (M_{DW}).

Table B.1 – Equivalent strip width and dead load moments used in the calculating the rating factors using the conventional strip width method

	E (m)	M_{DC} (kN-m/m)	M_{DW} (kN-m/m)
Albion Bridge #2529	2.39	53.15	1.44
Argyle Bridge #3427	3.03	60.38	12.76
Bradford Bridge #3430	3.02	71.52	14.74
Brewer Bridge #5638	2.57	64.19	7.12
Carmel Bridge #5191	2.90	184.27	29.65
Carmel Bridge #5632	2.75	55.30	10.04
Chester Bridge #5907	3.33	275.38	35.72
Exeter Bridge #5838	3.13	87.61	82.78
Greenfield Bridge #5605	2.87	55.57	34.56
Hermon Bridge #2205	3.01	46.35	52.19
Levant Bridge #5253	3.09	101.35	18.92
Liberty Bridge #3493	3.01	102.62	34.38
Linneus Bridge #5311	2.74	56.54	24.50
Linneus Bridge #5773	2.92	63.35	27.77
Milford Bridge #2070	3.19	92.81	23.39
Milo Bridge #2931	3.25	88.64	15.99
Monroe Bridge #5538	3.16	111.18	32.22
Newcastle Bridge #5608	3.16	87.51	19.88
Palmyra Bridge #5699	3.06	44.44	9.68
Sherman Bridge #2899	3.22	150.67	24.36

APPENDIX C: ADDITIONAL FEA LOAD RATING INFORMATION

Table C.1 - Table C.20 provides additional information that was used in the load rating of each of the twenty bridges using SlabRate. The location on the bridge where the minimum rating factor occurs for each truck is presented, the locations are measured from the geometric center of the bridge. Along with the location of the minimum rating factor the number of lanes loaded that caused the minimum rating factor is presented. The dead load moments are also presented, these moments include the dead load moment due to structural components (M_{DC}) and the dead load moment due to the wearing surface (M_{DW}).

Table C.1 – Location of rating factors, dead load moments and number of trucks causing the minimum rating factors for each truck configuration for Albion Bridge #2529

Albion Bridge #2529	Location of minimum rating factor (m)		Number of trucks	M_{DC} (kN-m/m)	M_{DW} (kN-m/m)
	x	*y*			
Design Truck - Lane - Inventory	0.75	2.59	1	26.96	0.54
Design Tandem - Lane - Inventory	0.79	3.55	1	31.77	0.59
Design Truck - Lane - Operating	0.75	2.59	1	26.96	0.54
Design Tandem - Lane - Operating	0.79	3.55	1	31.77	0.59
AASHTO Type 3 Truck	0.56	2.80	1	28.33	0.55
AASHTO Type 3S2 Truck	0.56	2.80	1	28.33	0.55
AASHTO Type 3-3	0.75	2.59	1	26.96	0.54
AASHTO-notional	0.56	2.80	1	28.33	0.55
AASHTO-SU4	0.66	2.69	1	27.67	0.54
AASHTO-SU5	0.56	2.80	1	28.33	0.55
AASHTO-SU6	0.56	2.80	1	28.33	0.55
AASHTO-SU7	0.56	2.80	1	28.33	0.55
MaineDoT C1	0.29	2.59	1	26.98	0.51
MaineDoT C2	0.79	3.55	1	31.77	0.59
MaineDoT C3	0.79	3.55	1	31.77	0.59
MaineDoT C4	0.75	2.59	1	26.96	0.54
MaineDoT C5	0.29	2.59	1	26.98	0.51
MaineDoT C6	0.75	2.59	1	26.96	0.54
MaineDoT C7	0.75	2.59	1	26.96	0.54
MaineDoT C8	0.75	2.59	1	26.96	0.54
MaineDoT C9	0.75	2.59	1	26.96	0.54

Table C.2 – Location of rating factors, dead load moments and number of trucks causing the minimum rating factors for each truck configuration for Argyle Bridge #3427

Argyle Bridge #3427	Location of minimum rating factor (m)		Number of trucks	M_{DC} (kN-m/m)	M_{DW} (kN-m/m)
	x	*y*			
Design Truck - Lane - Inventory	3.33	-1.23	2	58.25	11.50
Design Tandem - Lane - Inventory	3.33	-2.97	2	61.64	11.43
Design Truck - Lane - Operating	3.33	-1.23	2	58.25	11.50
Design Tandem - Lane - Operating	3.33	-2.97	2	61.64	11.43
AASHTO Type 3 Truck	3.33	-2.97	2	61.64	11.43
AASHTO Type 3S2 Truck	3.33	-2.97	2	61.64	11.43
AASHTO Type 3-3	3.33	-2.97	2	61.64	11.43
AASHTO-notional	3.33	-2.97	2	61.64	11.43
AASHTO-SU4	3.33	-2.97	2	61.64	11.43
AASHTO-SU5	3.33	-2.97	2	61.64	11.43
AASHTO-SU6	3.33	-2.97	2	61.64	11.43
AASHTO-SU7	3.33	-2.97	2	61.64	11.43
MaineDoT C1	3.33	-2.97	2	61.64	11.43
MaineDoT C2	3.33	-2.97	2	61.64	11.43
MaineDoT C3	3.33	-2.97	2	61.64	11.43
MaineDoT C4	3.81	-2.97	2	60.40	11.19
MaineDoT C5	3.33	-2.97	2	61.64	11.43
MaineDoT C6	3.33	-2.97	2	61.64	11.43
MaineDoT C7	3.33	-2.97	2	61.64	11.43
MaineDoT C8	3.81	-2.97	2	60.40	11.19
MaineDoT C9	3.33	-1.23	2	58.25	11.50

Table C.3 – Location of rating factors, dead load moments and number of trucks causing the minimum rating factors for each truck configuration for Bradford Bridge #3430

Bradford Bridge #3430	Location of minimum rating factor (m)		Number of trucks	M_{DC} (kN-m/m)	M_{DW} (kN-m/m)
	x	*y*			
Design Truck - Lane - Inventory	3.58	-2.75	2.00	71.65	12.60
Design Tandem - Lane - Inventory	3.58	-3.58	2.00	74.26	12.63
Design Truck - Lane - Operating	3.58	-2.75	2.00	71.65	12.60
Design Tandem - Lane - Operating	3.58	-3.58	2.00	74.26	12.63
AASHTO Type 3 Truck	3.58	-3.58	2.00	74.26	12.63
AASHTO Type 3S2 Truck	3.58	-2.75	2.00	71.65	12.60
AASHTO Type 3-3	3.58	-3.58	2.00	74.26	12.63
AASHTO-notional	3.58	-3.58	2.00	74.26	12.63
AASHTO-SU4	3.58	-2.75	2.00	71.65	12.60
AASHTO-SU5	3.58	-2.75	2.00	71.65	12.60
AASHTO-SU6	3.58	-3.58	2.00	74.26	12.63
AASHTO-SU7	3.58	-3.58	2.00	74.26	12.63
MaineDoT C1	3.58	-3.58	2.00	74.26	12.63
MaineDoT C2	3.58	-3.58	2.00	74.26	12.63
MaineDoT C3	3.58	-3.58	2.00	74.26	12.63
MaineDoT C4	3.07	-2.75	2.00	70.21	12.34
MaineDoT C5	3.58	-2.75	2.00	71.65	12.60
MaineDoT C6	3.58	-2.75	2.00	71.65	12.60
MaineDoT C7	3.58	-2.75	2.00	71.65	12.60
MaineDoT C8	3.07	-2.75	2.00	70.21	12.34
MaineDoT C9	3.58	-2.75	2.00	71.65	12.60

Table C.4 – Location of rating factors, dead load moments and number of trucks causing the minimum rating factors for each truck configuration for Brewer Bridge #5638

Brewer Bridge #5638	Location of minimum rating factor (m)		Number of trucks	M_{DC} (kN-m/m)	M_{DW} (kN-m/m)
	x	*y*			
Design Truck - Lane - Inventory	-0.16	3.69	1	22.72	1.78
Design Tandem - Lane - Inventory	-0.67	3.69	1	24.56	1.66
Design Truck - Lane - Operating	-0.16	3.69	1	22.72	1.78
Design Tandem - Lane - Operating	-0.67	3.69	1	24.56	1.66
AASHTO Type 3 Truck	-0.67	3.69	1	24.56	1.66
AASHTO Type 3S2 Truck	-0.16	3.69	1	22.72	1.78
AASHTO Type 3-3	-0.16	3.69	1	22.72	1.78
AASHTO-notional	-0.16	3.69	1	22.72	1.78
AASHTO-SU4	-0.16	3.69	1	22.72	1.78
AASHTO-SU5	-0.16	3.69	1	22.72	1.78
AASHTO-SU6	-0.16	3.69	1	22.72	1.78
AASHTO-SU7	-0.16	3.69	1	22.72	1.78
MaineDoT C1	0.34	3.69	1	19.50	1.80
MaineDoT C2	-0.16	3.69	1	22.72	1.78
MaineDoT C3	-0.16	3.69	1	22.72	1.78
MaineDoT C4	2.52	1.01	2	15.46	2.01
MaineDoT C5	-0.16	3.69	1	22.72	1.78
MaineDoT C6	-0.16	3.69	1	22.72	1.78
MaineDoT C7	-0.16	3.69	1	22.72	1.78
MaineDoT C8	-0.16	3.69	1	22.72	1.78
MaineDoT C9	-0.16	3.69	1	22.72	1.78

Table C.5 – Location of rating factors, dead load moments and number of trucks causing the minimum rating factors for each truck configuration for Carmel Bridge #5191

Carmel Bridge #5191	Location of minimum rating factor (m)		Number of trucks	M_{DC} (kN-m/m)	M_{DW} (kN-m/m)
	x	*y*			
Design Truck - Lane - Inventory	4.39	3.72	2	135.64	18.97
Design Tandem - Lane - Inventory	3.66	3.72	2	135.45	18.82
Design Truck - Lane - Operating	4.39	3.72	2	135.64	18.97
Design Tandem - Lane - Operating	3.66	3.72	2	135.45	18.82
AASHTO Type 3 Truck	4.39	3.72	2	135.64	18.97
AASHTO Type 3S2 Truck	4.39	3.72	2	135.64	18.97
AASHTO Type 3-3	3.66	3.72	2	135.45	18.82
AASHTO-notional	4.39	3.72	2	135.64	18.97
AASHTO-SU4	3.66	3.72	2	135.45	18.82
AASHTO-SU5	4.39	3.72	2	135.64	18.97
AASHTO-SU6	3.66	3.72	2	135.45	18.82
AASHTO-SU7	3.66	3.72	2	135.45	18.82
MaineDoT C1	4.39	3.72	2	135.64	18.97
MaineDoT C2	4.39	3.72	2	135.64	18.97
MaineDoT C3	3.66	3.72	2	135.45	18.82
MaineDoT C4	4.39	3.72	2	135.64	18.97
MaineDoT C5	4.39	3.72	2	135.64	18.97
MaineDoT C6	4.39	3.72	2	135.64	18.97
MaineDoT C7	3.89	3.32	2	133.97	18.77
MaineDoT C8	4.17	2.85	2	130.61	18.51
MaineDoT C9	4.39	3.72	2	135.64	18.97

Table C.6 – Location of rating factors, dead load moments and number of trucks causing the minimum rating factors for each truck configuration for Carmel Bridge #5632

Carmel Bridge #5632	Location of minimum rating factor (m)		Number of trucks	M_{DC} (kN-m/m)	M_{DW} (kN-m/m)
	x	*y*			
Design Truck - Lane - Inventory	1.71	-2.85	1	39.64	6.04
Design Tandem - Lane - Inventory	2.18	-2.85	2	38.40	6.08
Design Truck - Lane - Operating	1.71	-2.85	1	39.64	6.04
Design Tandem - Lane - Operating	2.18	-2.85	2	38.40	6.08
AASHTO Type 3 Truck	2.18	-2.85	2	38.40	6.08
AASHTO Type 3S2 Truck	2.18	-2.85	2	38.40	6.08
AASHTO Type 3-3	2.18	-2.85	2	38.40	6.08
AASHTO-notional	2.18	-2.85	2	38.40	6.08
AASHTO-SU4	2.11	-2.97	2	39.32	6.12
AASHTO-SU5	1.71	-2.85	2	39.64	6.04
AASHTO-SU6	1.98	-4.03	2	45.76	6.43
AASHTO-SU7	1.98	-4.03	2	45.76	6.43
MaineDoT C1	1.98	-4.03	2	45.76	6.43
MaineDoT C2	1.98	-4.03	2	45.76	6.43
MaineDoT C3	1.98	-4.03	2	45.76	6.43
MaineDoT C4	1.23	-2.85	1	38.95	5.71
MaineDoT C5	2.18	-2.85	2	38.40	6.08
MaineDoT C6	1.71	-2.85	2	39.64	6.04
MaineDoT C7	4.99	2.85	1	39.64	6.04
MaineDoT C8	1.23	-2.85	1	38.95	5.71
MaineDoT C9	1.71	-2.85	1	39.64	6.04

Table C.7 – Location of rating factors, dead load moments and number of trucks causing the minimum rating factors for each truck configuration for Chester Bridge #5907

Chester Bridge #5907	Location of minimum rating factor (m)		Number of trucks	M_{DC} (kN-m/m)	M_{DW} (kN-m/m)
	x	*y*			
Design Truck - Lane - Inventory	5.66	3.20	2	280.33	30.94
Design Tandem - Lane - Inventory	5.66	4.12	2	286.22	31.10
Design Truck - Lane - Operating	5.66	3.20	2	280.33	30.94
Design Tandem - Lane - Operating	5.66	4.12	2	286.22	31.10
AASHTO Type 3 Truck	5.66	3.20	2	280.33	30.94
AASHTO Type 3S2 Truck	5.66	4.12	2	286.22	31.10
AASHTO Type 3-3	4.86	3.20	2	274.67	30.31
AASHTO-notional	5.66	4.12	2	286.22	31.10
AASHTO-SU4	5.66	3.20	2	280.33	30.94
AASHTO-SU5	5.66	4.12	2	286.22	31.10
AASHTO-SU6	5.66	4.12	2	286.22	31.10
AASHTO-SU7	5.66	4.12	2	286.22	31.10
MaineDoT C1	5.66	4.12	2	286.22	31.10
MaineDoT C2	5.66	4.12	2	286.22	31.10
MaineDoT C3	5.66	4.12	2	286.22	31.10
MaineDoT C4	5.66	4.12	2	286.22	31.10
MaineDoT C5	5.66	3.20	2	280.33	30.94
MaineDoT C6	5.66	4.12	2	286.22	31.10
MaineDoT C7	5.66	3.20	2	280.33	30.94
MaineDoT C8	5.66	3.20	2	280.33	30.94
MaineDoT C9	4.86	3.20	2	274.67	30.31

Table C.8 – Location of rating factors, dead load moments and number of trucks causing the minimum rating factors for each truck configuration for Exeter Bridge #5838

Exeter Bridge #5838	Location of minimum rating factor (m)		Number of trucks	M_{DC} (kN-m/m)	M_{DW} (kN-m/m)
	x	*y*			
Design Truck - Lane - Inventory	4.11	-1.31	2	79.12	72.42
Design Tandem - Lane - Inventory	3.57	-1.31	2	80.63	73.64
Design Truck - Lane - Operating	4.11	-1.31	2	79.12	72.42
Design Tandem - Lane - Operating	3.57	-1.31	2	80.63	73.64
AASHTO Type 3 Truck	3.57	-1.31	2	80.63	73.64
AASHTO Type 3S2 Truck	3.25	-3.05	2	83.83	73.79
AASHTO Type 3-3	3.57	-1.31	2	80.63	73.64
AASHTO-notional	3.57	-1.31	2	80.63	73.64
AASHTO-SU4	3.57	-1.31	2	80.63	73.64
AASHTO-SU5	3.25	-3.05	2	83.83	73.79
AASHTO-SU6	3.25	-3.05	2	83.83	73.79
AASHTO-SU7	3.57	-1.31	2	80.63	73.64
MaineDoT C1	3.57	-1.31	2	80.63	73.64
MaineDoT C2	3.25	-3.05	2	83.83	73.79
MaineDoT C3	3.25	-3.05	2	83.83	73.79
MaineDoT C4	3.25	-3.05	2	83.83	73.79
MaineDoT C5	3.57	-1.31	2	80.63	73.64
MaineDoT C6	3.25	-3.05	2	83.83	73.79
MaineDoT C7	3.25	-3.05	2	83.83	73.79
MaineDoT C8	3.79	-3.05	2	82.93	73.26
MaineDoT C9	4.11	-1.31	2	79.12	72.42

Table C.9 – Location of rating factors, dead load moments and number of trucks causing the minimum rating factors for each truck configuration for Greenfield Bridge #5605

Greenfield Bridge #5605	Location of minimum rating factor (m)		Number of trucks	M_{DC} (kN-m/m)	M_{DW} (kN-m/m)
	x	*y*			
Design Truck - Lane - Inventory	2.33	2.76	2	46.34	24.70
Design Tandem - Lane - Inventory	2.81	2.76	2	46.07	24.96
Design Truck - Lane - Operating	2.33	2.76	2	46.34	24.70
Design Tandem - Lane - Operating	2.81	2.76	2	46.07	24.96
AASHTO Type 3 Truck	2.81	2.76	2	46.07	24.96
AASHTO Type 3S2 Truck	2.81	2.76	2	46.07	24.96
AASHTO Type 3-3	2.81	2.76	2	46.07	24.96
AASHTO-notional	4.23	-3.76	2	50.65	25.20
AASHTO-SU4	2.81	2.76	2	46.07	24.96
AASHTO-SU5	2.33	2.76	2	46.34	24.70
AASHTO-SU6	4.23	-3.76	2	50.65	25.20
AASHTO-SU7	4.23	-3.76	2	50.65	25.20
MaineDoT C1	4.23	-3.76	2	50.65	25.20
MaineDoT C2	4.23	-3.76	2	50.65	25.20
MaineDoT C3	4.23	-3.76	2	50.65	25.20
MaineDoT C4	2.33	2.76	2	46.34	24.70
MaineDoT C5	2.81	2.76	2	46.07	24.96
MaineDoT C6	2.33	2.76	2	46.34	24.70
MaineDoT C7	4.34	-2.76	2	46.49	24.70
MaineDoT C8	2.81	2.76	2	46.07	24.96
MaineDoT C9	2.33	2.76	2	46.34	24.70

Table C.10 – Location of rating factors, dead load moments and number of trucks causing the minimum rating factors for each truck configuration for Hermon Bridge #2205

Hermon Bridge #2205	Location of minimum rating factor (m)		Number of trucks	M_{DC} (kN-m/m)	M_{DW} (kN-m/m)
	x	*y*			
Design Truck - Lane - Inventory	2.90	-1.08	2	44.82	48.15
Design Tandem - Lane - Inventory	2.90	-1.08	2	44.82	48.15
Design Truck - Lane - Operating	2.90	-1.08	2	44.82	48.15
Design Tandem - Lane - Operating	2.90	-1.08	2	44.82	48.15
AASHTO Type 3 Truck	2.90	-1.08	2	44.82	48.15
AASHTO Type 3S2 Truck	2.90	-1.08	2	44.82	48.15
AASHTO Type 3-3	2.90	-1.08	2	44.82	48.15
AASHTO-notional	2.90	-1.08	2	44.82	48.15
AASHTO-SU4	2.90	-1.08	2	44.82	48.15
AASHTO-SU5	2.90	-1.08	2	44.82	48.15
AASHTO-SU6	2.90	-1.08	2	44.82	48.15
AASHTO-SU7	2.90	-1.08	2	44.82	48.15
MaineDoT C1	2.90	-1.08	2	44.82	48.15
MaineDoT C2	2.90	-1.08	2	44.82	48.15
MaineDoT C3	2.90	-1.08	2	44.82	48.15
MaineDoT C4	2.90	-1.08	2	44.82	48.15
MaineDoT C5	2.90	-1.08	2	44.82	48.15
MaineDoT C6	2.90	-1.08	2	44.82	48.15
MaineDoT C7	2.90	-1.08	2	44.82	48.15
MaineDoT C8	2.90	-1.08	2	44.82	48.15
MaineDoT C9	2.90	-1.08	2	44.82	48.15

Table C.11 – Location of rating factors, dead load moments and number of trucks causing the minimum rating factors for each truck configuration for Levant Bridge #5253

Levant Bridge #5253	Location of minimum rating factor (m)		Number of trucks	M_{DC} (kN-m/m)	M_{DW} (kN-m/m)
	x	*y*			
Design Truck - Lane - Inventory	3.48	2.75	2	101.17	15.44
Design Tandem - Lane - Inventory	4.06	3.63	2	106.63	15.80
Design Truck - Lane - Operating	3.48	2.75	2	101.17	15.44
Design Tandem - Lane - Operating	4.06	3.63	2	106.63	15.80
AASHTO Type 3 Truck	4.06	3.63	2	106.63	15.80
AASHTO Type 3S2 Truck	4.06	2.75	2	103.25	15.77
AASHTO Type 3-3	4.06	3.63	2	106.63	15.80
AASHTO-notional	4.06	3.63	2	106.63	15.80
AASHTO-SU4	4.06	2.75	2	103.25	15.77
AASHTO-SU5	4.06	3.63	2	106.63	15.80
AASHTO-SU6	4.06	3.63	2	106.63	15.80
AASHTO-SU7	4.06	3.63	2	106.63	15.80
MaineDoT C1	4.06	3.63	2	106.63	15.80
MaineDoT C2	4.06	3.63	2	106.63	15.80
MaineDoT C3	4.06	3.63	2	106.63	15.80
MaineDoT C4	4.06	3.63	2	106.63	15.80
MaineDoT C5	4.06	3.63	2	106.63	15.80
MaineDoT C6	4.06	2.75	2	103.25	15.77
MaineDoT C7	4.06	2.75	2	103.25	15.77
MaineDoT C8	4.64	2.75	2	101.17	15.44
MaineDoT C9	3.48	2.75	2	101.17	15.44

Table C.12 – Location of rating factors, dead load moments and number of trucks causing the minimum rating factors for each truck configuration for Liberty Bridge #3493

Liberty Bridge #3493	Location of minimum rating factor (m)		Number of trucks	M_{DC} (kN-m/m)	M_{DW} (kN-m/m)
	x	*y*			
Design Truck - Lane - Inventory	4.60	-2.50	2	94.75	28.53
Design Tandem - Lane - Inventory	4.35	-3.65	2	101.46	29.21
Design Truck - Lane - Operating	4.60	-2.50	2	94.75	28.53
Design Tandem - Lane - Operating	4.35	-3.65	2	101.46	29.21
AASHTO Type 3 Truck	4.35	-3.65	2	101.46	29.21
AASHTO Type 3S2 Truck	4.35	-3.65	2	101.46	29.21
AASHTO Type 3-3	4.35	-3.65	2	101.46	29.21
AASHTO-notional	4.35	-3.65	2	101.46	29.21
AASHTO-SU4	4.35	-3.65	2	101.46	29.21
AASHTO-SU5	4.35	-3.65	2	101.46	29.21
AASHTO-SU6	4.35	-3.65	2	101.46	29.21
AASHTO-SU7	4.35	-3.65	2	101.46	29.21
MaineDoT C1	4.35	-3.65	2	101.46	29.21
MaineDoT C2	4.35	-3.65	2	101.46	29.21
MaineDoT C3	4.35	-3.65	2	101.46	29.21
MaineDoT C4	4.35	-3.65	2	101.46	29.21
MaineDoT C5	4.35	-3.65	2	101.46	29.21
MaineDoT C6	4.35	-3.65	2	101.46	29.21
MaineDoT C7	4.57	-2.39	2	94.23	28.51
MaineDoT C8	4.01	-2.39	2	93.47	28.49
MaineDoT C9	4.01	-2.39	2	93.47	28.49

Table C.13 – Location of rating factors, dead load moments and number of trucks causing the minimum rating factors for each truck configuration for Linneus Bridge #5311

Linneus Bridge #5311	Location of minimum rating factor (m)		Number of trucks	M_{DC} (kN-m/m)	M_{DW} (kN-m/m)
	x	*y*			
Design Truck - Lane - Inventory	4.96	2.85	1	38.68	13.92
Design Tandem - Lane - Inventory	5.17	4.04	1	43.71	14.38
Design Truck - Lane - Operating	4.96	2.85	1	38.68	13.92
Design Tandem - Lane - Operating	5.17	4.04	1	43.71	14.38
AASHTO Type 3 Truck	4.96	2.85	1	38.68	13.92
AASHTO Type 3S2 Truck	4.96	2.85	1	38.68	13.92
AASHTO Type 3-3	5.43	2.85	1	37.45	13.06
AASHTO-notional	5.17	4.04	1	43.71	14.38
AASHTO-SU4	4.96	2.85	1	38.68	13.92
AASHTO-SU5	4.96	2.85	1	38.68	13.92
AASHTO-SU6	5.17	4.04	1	43.71	14.38
AASHTO-SU7	5.17	4.04	1	43.71	14.38
MaineDoT C1	4.96	2.85	1	38.68	13.92
MaineDoT C2	5.17	4.04	1	43.71	14.38
MaineDoT C3	5.17	4.04	1	43.71	14.38
MaineDoT C4	5.04	2.98	1	39.20	13.91
MaineDoT C5	4.96	2.85	1	38.68	13.92
MaineDoT C6	4.96	2.85	1	38.68	13.92
MaineDoT C7	5.04	2.98	1	39.20	13.91
MaineDoT C8	4.96	2.85	1	38.68	13.92
MaineDoT C9	4.96	2.85	1	38.68	13.92

Table C.14 – Location of rating factors, dead load moments and number of trucks causing the minimum rating factors for each truck configuration for Linneus Bridge #5773

Linneus Bridge #5773	Location of minimum rating factor (m)		Number of trucks	M_{DC} (kN-m/m)	M_{DW} (kN-m/m)
	x	*y*			
Design Truck - Lane - Inventory	5.36	3.41	1	4.97	1.96
Design Tandem - Lane - Inventory	5.29	4.42	2	5.36	2.05
Design Truck - Lane - Operating	5.36	3.41	1	4.97	1.96
Design Tandem - Lane - Operating	5.29	4.42	2	5.36	2.05
AASHTO Type 3 Truck	4.82	3.41	2	4.97	1.99
AASHTO Type 3S2 Truck	5.29	4.42	2	5.36	2.05
AASHTO Type 3-3	4.82	3.41	2	4.97	1.99
AASHTO-notional	5.29	4.42	2	5.36	2.05
AASHTO-SU4	4.95	3.69	2	5.09	2.01
AASHTO-SU5	5.29	4.42	2	5.36	2.05
AASHTO-SU6	5.29	4.42	2	5.36	2.05
AASHTO-SU7	5.29	4.42	2	5.36	2.05
MaineDoT C1	5.29	4.42	2	5.36	2.05
MaineDoT C2	5.29	4.42	2	5.36	2.05
MaineDoT C3	5.29	4.42	2	5.36	2.05
MaineDoT C4	5.36	3.41	2	4.97	1.96
MaineDoT C5	4.82	3.41	2	4.97	1.99
MaineDoT C6	5.36	3.41	2	4.97	1.96
MaineDoT C7	5.36	3.41	2	4.97	1.96
MaineDoT C8	4.82	3.41	2	4.97	1.99
MaineDoT C9	5.36	3.41	1	4.97	1.96

Table C.15 – Location of rating factors, dead load moments and number of trucks causing the minimum rating factors for each truck configuration for Milford Bridge #2070

Milford Bridge #2070	Location of minimum rating factor (m)		Number of trucks	M_{DC} (kN-m/m)	M_{DW} (kN-m/m)
	x	*y*			
Design Truck - Lane - Inventory	4.38	-3.66	2	83.20	18.97
Design Tandem - Lane - Inventory	4.77	4.45	2	90.44	20.04
Design Truck - Lane - Operating	4.38	-3.66	2	83.20	18.97
Design Tandem - Lane - Operating	4.77	4.45	2	90.44	20.04
AASHTO Type 3 Truck	3.57	-4.45	2	90.44	20.04
AASHTO Type 3S2 Truck	5.15	3.66	2	86.90	19.60
AASHTO Type 3-3	3.57	-4.45	2	90.44	20.04
AASHTO-notional	4.77	4.45	2	90.44	20.04
AASHTO-SU4	3.57	-4.45	2	90.44	20.04
AASHTO-SU5	3.57	-4.45	2	90.44	20.04
AASHTO-SU6	3.57	-4.45	2	90.44	20.04
AASHTO-SU7	3.57	-4.45	2	90.44	20.04
MaineDoT C1	3.57	-4.45	2	90.44	20.04
MaineDoT C2	3.19	-3.66	2	86.90	19.60
MaineDoT C3	3.57	-4.45	2	90.44	20.04
MaineDoT C4	4.60	3.81	2	87.67	19.79
MaineDoT C5	3.79	-3.66	2	86.99	19.73
MaineDoT C6	3.57	-4.45	2	90.44	20.04
MaineDoT C7	3.19	-3.66	2	86.90	19.60
MaineDoT C8	4.56	3.66	2	86.99	19.73
MaineDoT C9	4.38	-3.66	2	83.20	18.97

Table C.16 – Location of rating factors, dead load moments and number of trucks causing the minimum rating factors for each truck configuration for Milo Bridge #2931

Milo Bridge #2931	Location of minimum rating factor (m)		Number of trucks	M_{DC} (kN-m/m)	M_{DW} (kN-m/m)
	x	*y*			
Design Truck - Lane - Inventory	3.74	-2.26	2	83.09	13.72
Design Tandem - Lane - Inventory	3.74	-2.26	2	83.09	13.72
Design Truck - Lane - Operating	3.74	-2.26	2	83.09	13.72
Design Tandem - Lane - Operating	3.74	-2.26	2	83.09	13.72
AASHTO Type 3 Truck	3.74	-2.26	2	83.09	13.72
AASHTO Type 3S2 Truck	3.74	-2.26	2	83.09	13.72
AASHTO Type 3-3	3.21	-2.26	2	81.35	13.45
AASHTO-notional	3.74	-4.09	2	86.61	13.91
AASHTO-SU4	3.74	-2.26	2	83.09	13.72
AASHTO-SU5	3.74	-2.26	2	83.09	13.72
AASHTO-SU6	3.74	-4.09	2	86.61	13.91
AASHTO-SU7	3.74	-4.09	2	86.61	13.91
MaineDoT C1	3.74	-4.09	2	86.61	13.91
MaineDoT C2	3.74	-4.09	2	86.61	13.91
MaineDoT C3	3.74	-4.09	2	86.61	13.91
MaineDoT C4	3.21	-4.09	2	84.85	13.63
MaineDoT C5	3.74	-2.26	2	83.09	13.72
MaineDoT C6	3.74	-2.26	2	83.09	13.72
MaineDoT C7	3.74	-2.26	2	83.09	13.72
MaineDoT C8	3.21	-2.26	2	81.35	13.45
MaineDoT C9	4.81	-2.26	2	76.16	12.63

Table C.17 – Location of rating factors, dead load moments and number of trucks causing the minimum rating factors for each truck configuration for Monroe Bridge #5538

Monroe Bridge #5538	Location of minimum rating factor (m)		Number of trucks	M_{DC} (kN-m/m)	M_{DW} (kN-m/m)
	x	*y*			
Design Truck - Lane - Inventory	4.53	3.05	2	109.93	22.66
Design Tandem - Lane - Inventory	4.53	3.05	2	109.93	22.66
Design Truck - Lane - Operating	4.53	3.05	2	109.93	22.66
Design Tandem - Lane - Operating	4.53	3.05	2	109.93	22.66
AASHTO Type 3 Truck	4.53	3.05	2	109.93	22.66
AASHTO Type 3S2 Truck	3.98	3.05	2	110.63	22.75
AASHTO Type 3-3	4.53	3.05	2	109.93	22.66
AASHTO-notional	3.98	3.05	2	110.63	22.75
AASHTO-SU4	3.98	3.05	2	110.63	22.75
AASHTO-SU5	3.98	3.05	2	110.63	22.75
AASHTO-SU6	3.98	3.05	2	110.63	22.75
AASHTO-SU7	4.40	-4.07	2	114.49	22.86
MaineDoT C1	3.98	3.05	2	110.63	22.75
MaineDoT C2	3.98	3.05	2	110.63	22.75
MaineDoT C3	4.81	-3.05	2	110.63	22.75
MaineDoT C4	4.53	3.05	2	109.93	22.66
MaineDoT C5	4.53	3.05	2	109.93	22.66
MaineDoT C6	4.53	3.05	2	109.93	22.66
MaineDoT C7	4.81	-3.05	2	110.63	22.75
MaineDoT C8	4.53	3.05	2	109.93	22.66
MaineDoT C9	5.07	3.05	2	105.68	21.83

Table C.18 – Location of rating factors, dead load moments and number of trucks causing the minimum rating factors for each truck configuration for Newcastle Bridge #5608

Newcastle Bridge #5608	Location of minimum rating factor (m)		Number of trucks	M_{DC} (kN-m/m)	M_{DW} (kN-m/m)
	x	*y*			
Design Truck - Lane - Inventory	3.59	-0.88	2	81.84	17.14
Design Tandem - Lane - Inventory	4.41	-3.06	2	88.16	17.28
Design Truck - Lane - Operating	3.59	-0.88	2	81.84	17.14
Design Tandem - Lane - Operating	4.41	-3.06	2	88.16	17.28
AASHTO Type 3 Truck	4.41	-3.06	2	88.16	17.28
AASHTO Type 3S2 Truck	4.41	-3.06	2	88.16	17.28
AASHTO Type 3-3	4.18	-0.88	2	83.54	17.45
AASHTO-notional	4.41	-3.06	2	88.16	17.28
AASHTO-SU4	4.41	-3.06	2	88.16	17.28
AASHTO-SU5	4.41	-3.06	2	88.16	17.28
AASHTO-SU6	4.41	-3.06	2	88.16	17.28
AASHTO-SU7	4.54	-4.37	2	93.04	17.30
MaineDoT C1	4.41	-3.06	2	88.16	17.28
MaineDoT C2	4.41	-3.06	2	88.16	17.28
MaineDoT C3	4.41	-3.06	2	88.16	17.28
MaineDoT C4	3.82	-3.06	2	86.91	17.09
MaineDoT C5	3.59	-0.88	2	81.84	17.14
MaineDoT C6	4.41	-3.06	2	88.16	17.28
MaineDoT C7	4.41	-3.06	2	88.16	17.28
MaineDoT C8	3.82	-3.06	2	86.91	17.09
MaineDoT C9	3.59	-0.88	2	81.84	17.14

Table C.19 – Location of rating factors, dead load moments and number of trucks causing the minimum rating factors for each truck configuration for Palmyra Bridge #5699

Palmyra Bridge #5699	Location of minimum rating factor (m)		Number of trucks	M_{DC} (kN-m/m)	M_{DW} (kN-m/m)
	x	*y*			
Design Truck - Lane - Inventory	3.29	-3.65	2	46.29	8.42
Design Tandem - Lane - Inventory	3.29	-4.42	2	48.30	8.51
Design Truck - Lane - Operating	3.29	-3.65	2	46.29	8.42
Design Tandem - Lane - Operating	3.29	-4.42	2	48.30	8.51
AASHTO Type 3 Truck	3.29	-4.42	2	48.30	8.51
AASHTO Type 3S2 Truck	3.29	-4.42	2	48.30	8.51
AASHTO Type 3-3	3.29	-4.42	2	48.30	8.51
AASHTO-notional	3.29	-3.65	2	46.29	8.42
AASHTO-SU4	3.29	-3.65	2	46.29	8.42
AASHTO-SU5	3.29	-3.65	2	46.29	8.42
AASHTO-SU6	3.29	-3.65	2	46.29	8.42
AASHTO-SU7	3.29	-3.65	2	46.29	8.42
MaineDoT C1	3.29	-4.42	2	48.30	8.51
MaineDoT C2	3.29	-4.42	2	48.30	8.51
MaineDoT C3	3.29	-4.42	2	48.30	8.51
MaineDoT C4	2.82	-3.65	2	45.35	8.24
MaineDoT C5	3.29	-3.65	2	46.29	8.42
MaineDoT C6	3.29	-3.65	2	46.29	8.42
MaineDoT C7	3.29	-3.65	2	46.29	8.42
MaineDoT C8	3.76	-3.65	2	45.35	8.24
MaineDoT C9	3.29	-3.65	2	46.29	8.42

Table C.20 – Location of rating factors, dead load moments and number of trucks causing the minimum rating factors for each truck configuration for Sherman Bridge #2899

Sherman Bridge #2899	Location of minimum rating factor (m)		Number of trucks	M_{DC} (kN-m/m)	M_{DW} (kN-m/m)
	x	*y*			
Design Truck - Lane - Inventory	3.79	-4.99	2	143.07	43.77
Design Tandem - Lane - Inventory	3.79	-4.99	2	143.07	43.77
Design Truck - Lane - Operating	3.79	-4.99	2	143.07	43.77
Design Tandem - Lane - Operating	3.79	-4.99	2	143.07	43.77
AASHTO Type 3 Truck	3.79	-4.99	2	143.07	43.77
AASHTO Type 3S2 Truck	3.79	-4.99	2	143.07	43.77
AASHTO Type 3-3	3.79	-4.99	2	143.07	43.77
AASHTO-notional	3.79	-4.99	2	143.07	43.77
AASHTO-SU4	3.79	-4.99	2	143.07	43.77
AASHTO-SU5	3.79	-4.99	2	143.07	43.77
AASHTO-SU6	3.79	-4.99	2	143.07	43.77
AASHTO-SU7	3.79	-4.99	2	143.07	43.77
MaineDoT C1	3.79	-4.99	2	143.07	43.77
MaineDoT C2	3.79	-4.99	2	143.07	43.77
MaineDoT C3	3.79	-4.99	2	143.07	43.77
MaineDoT C4	3.79	-4.99	2	143.07	43.77
MaineDoT C5	3.79	-4.99	2	143.07	43.77
MaineDoT C6	3.79	-4.99	2	143.07	43.77
MaineDoT C7	3.79	-4.99	2	143.07	43.77
MaineDoT C8	4.02	-4.23	2	138.84	42.90
MaineDoT C9	4.02	-4.23	2	138.84	42.90

APPENDIX D: RESULTING STRAINS FROM EACH LIVE LOAD TEST

Figure D.1 –Figure D.49 are the results strains from each gauge from each of the live load tests conducted on Bradford Bridge #3430.

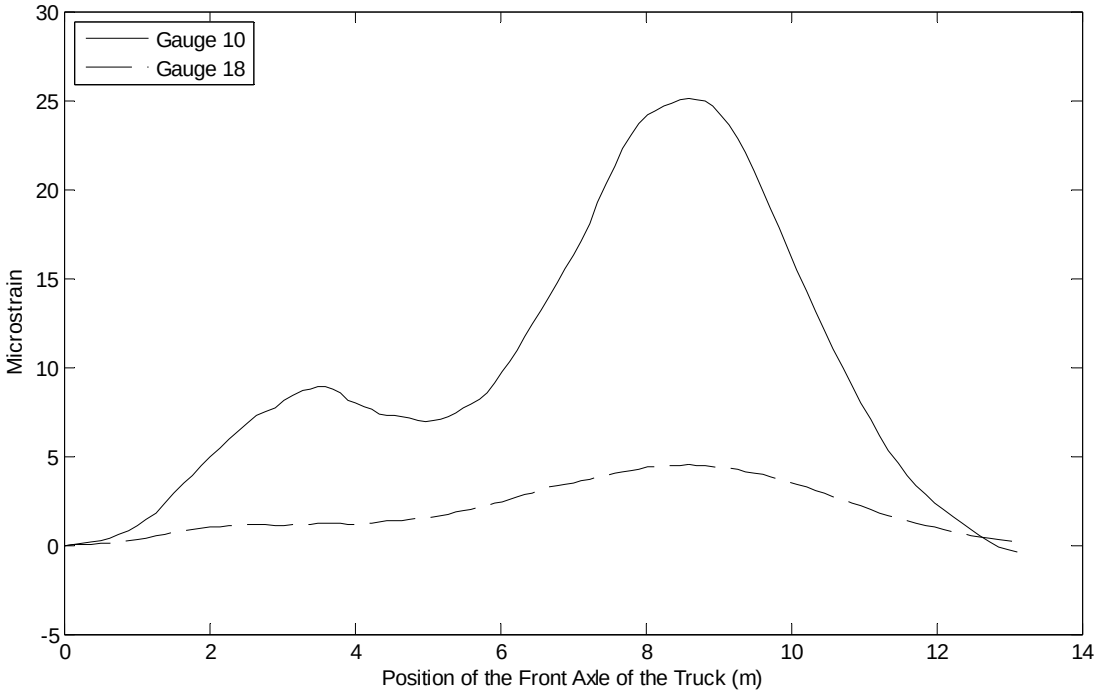

Figure D.1 – Resulting strains for gauges located under the curb along the centerline span during test 1

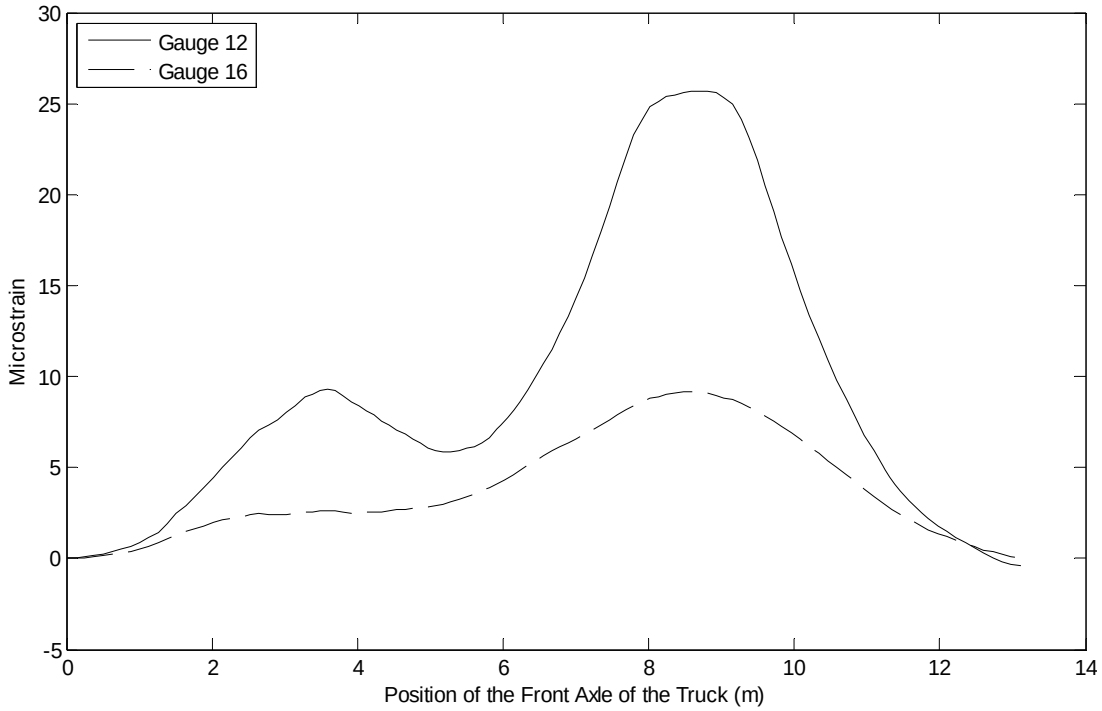

Figure D.2 – Resulting strains for gauges located at the transverse quarter points along the centerline span for test 1

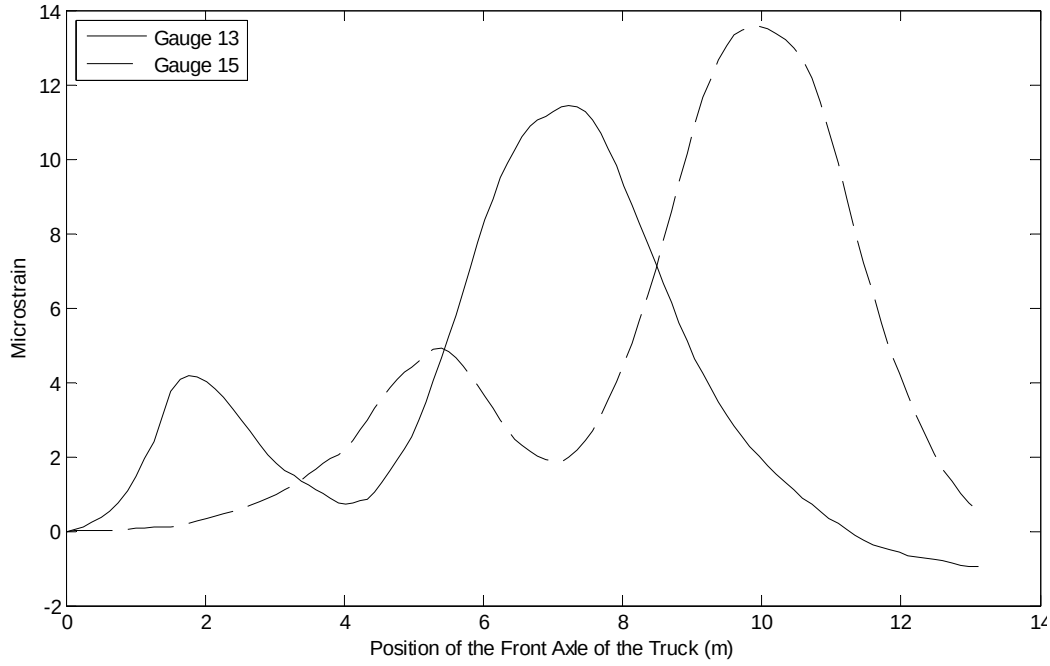

Figure D.3 – Resulting strains for bottom gauges located at the transverse centerline along the quarter span for test 1

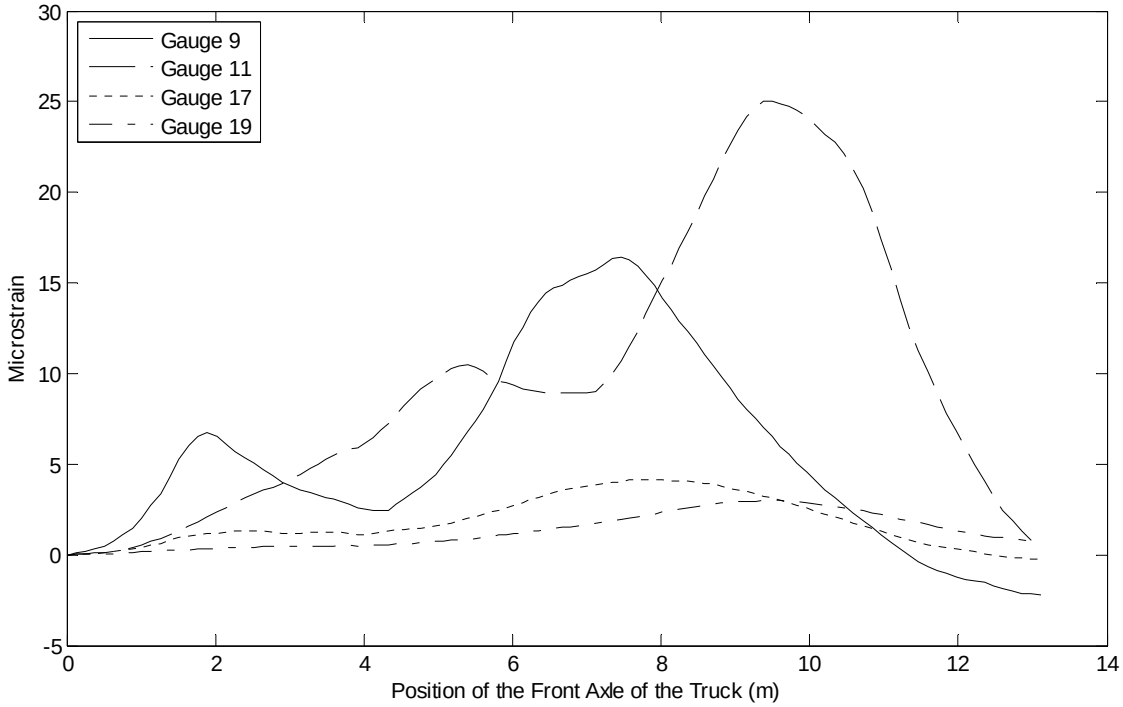

Figure D.4 – Resulting strains for the gauges located under the curbs along the quarter span for test 1

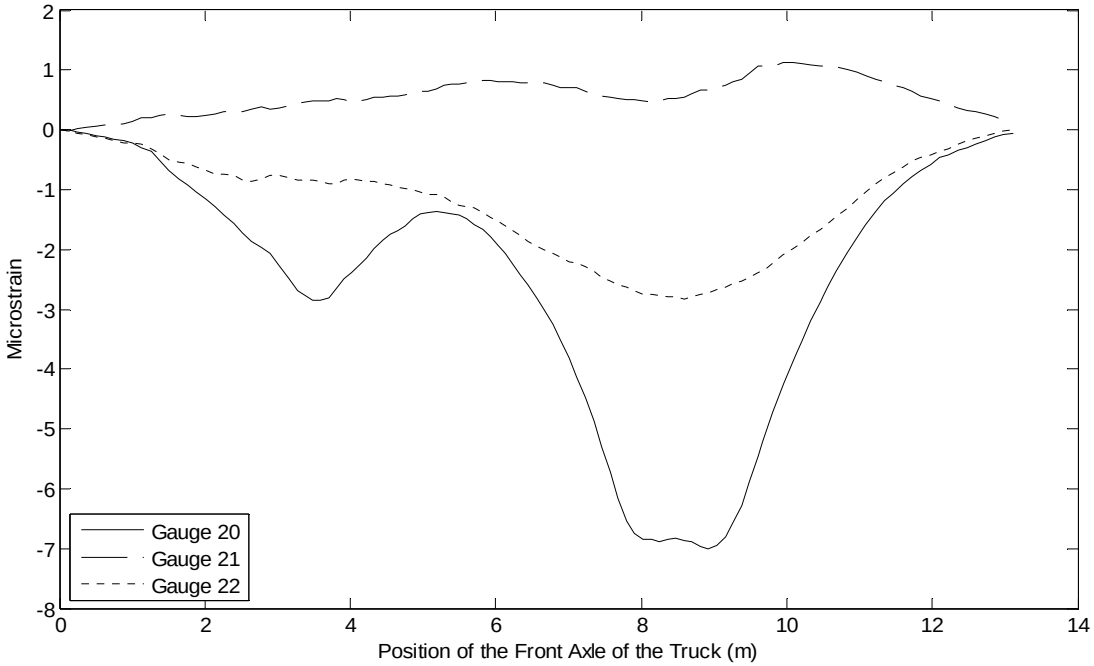

Figure D.5 – Resulting strains for the transverse gauges located along the centerline span for test 1

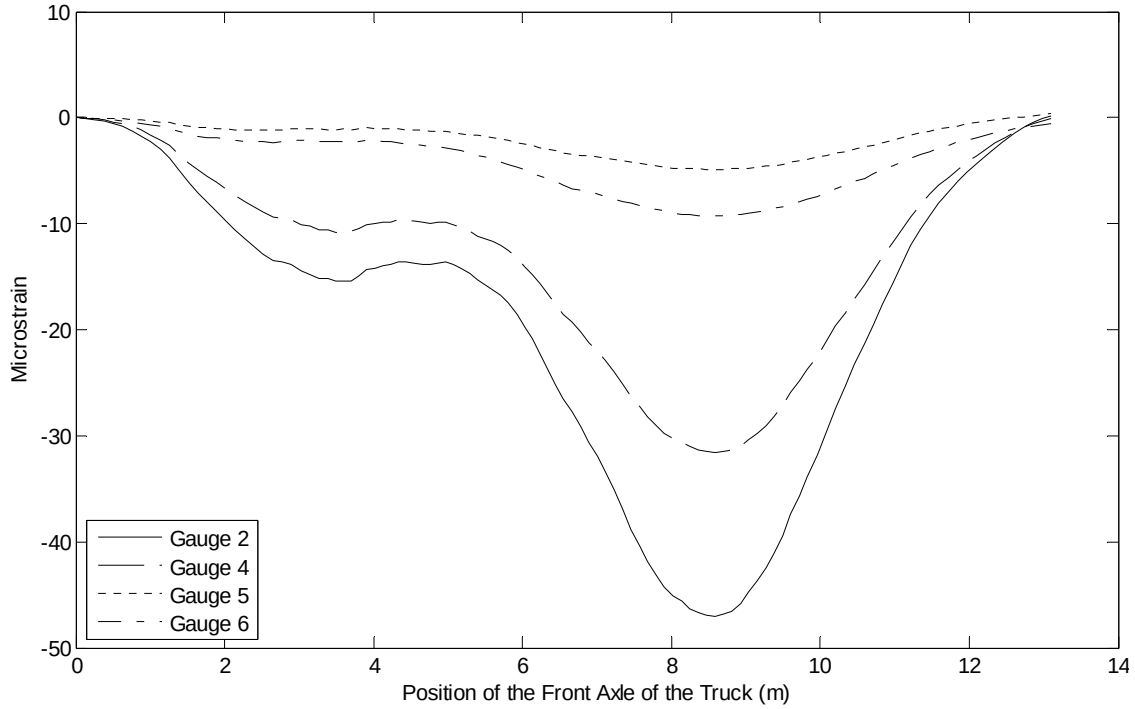

Figure D.6 – Resulting strains for the top gauges located at the centerline span for test 1

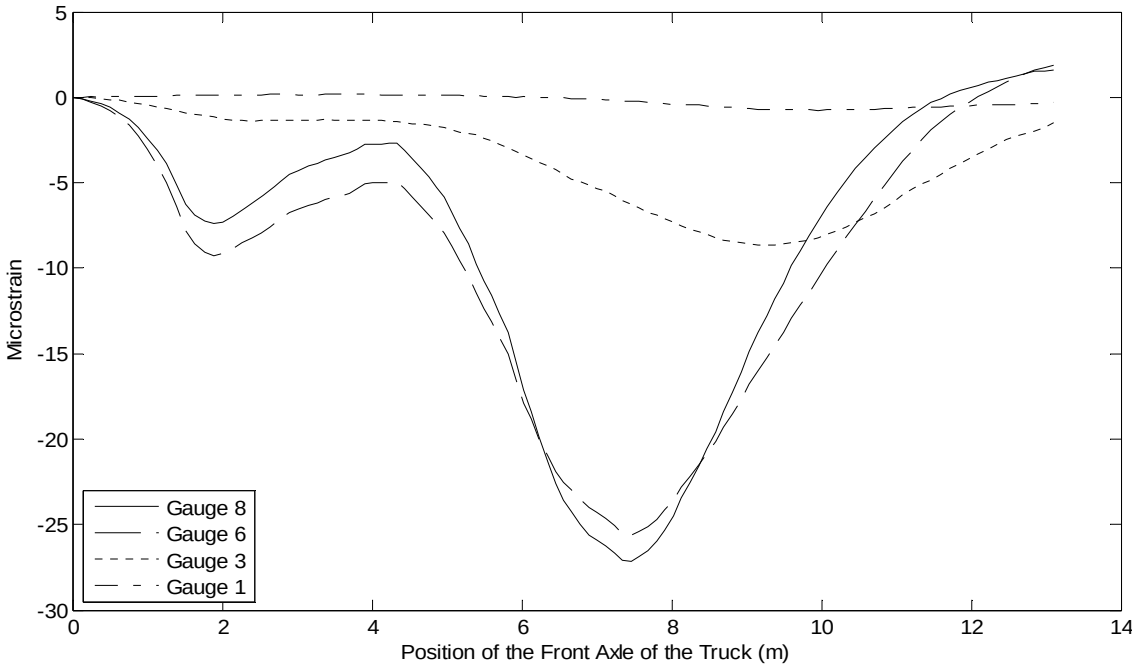

Figure D.7 – Resulting strains for the top gauges located along the quarter span for test 1

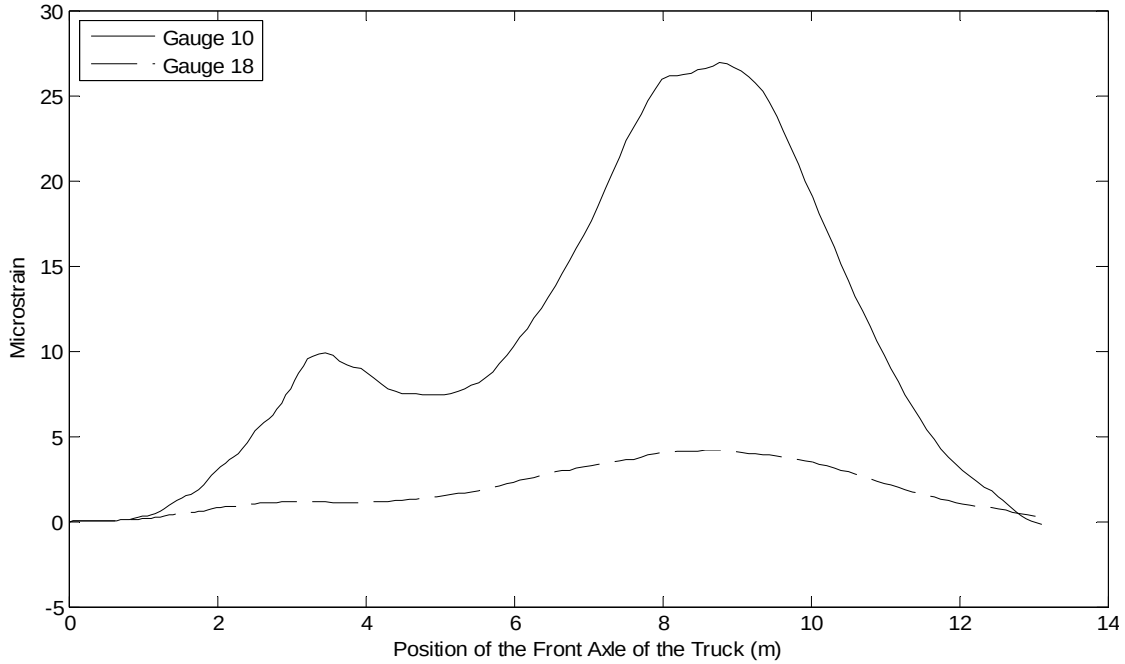

Figure D.8 – Resulting strains for gauges located under the curb along the centerline span during test 2

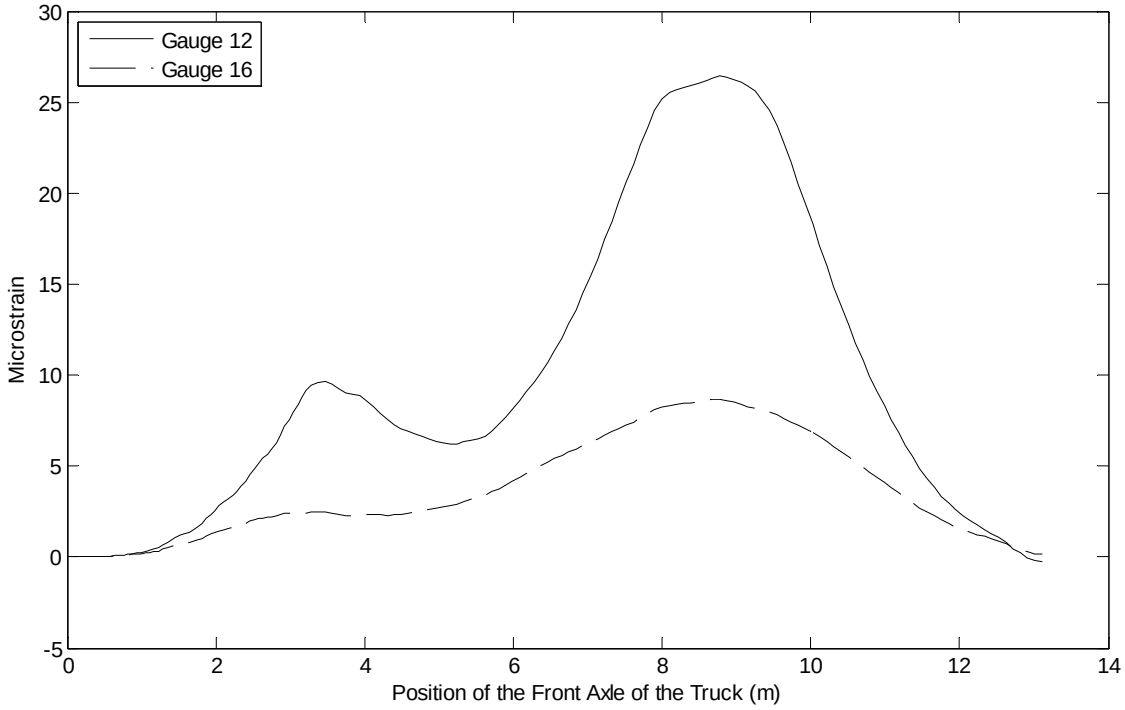

Figure D.9 – Resulting strains for gauges located at the transverse quarter point along the centerline span for test 2

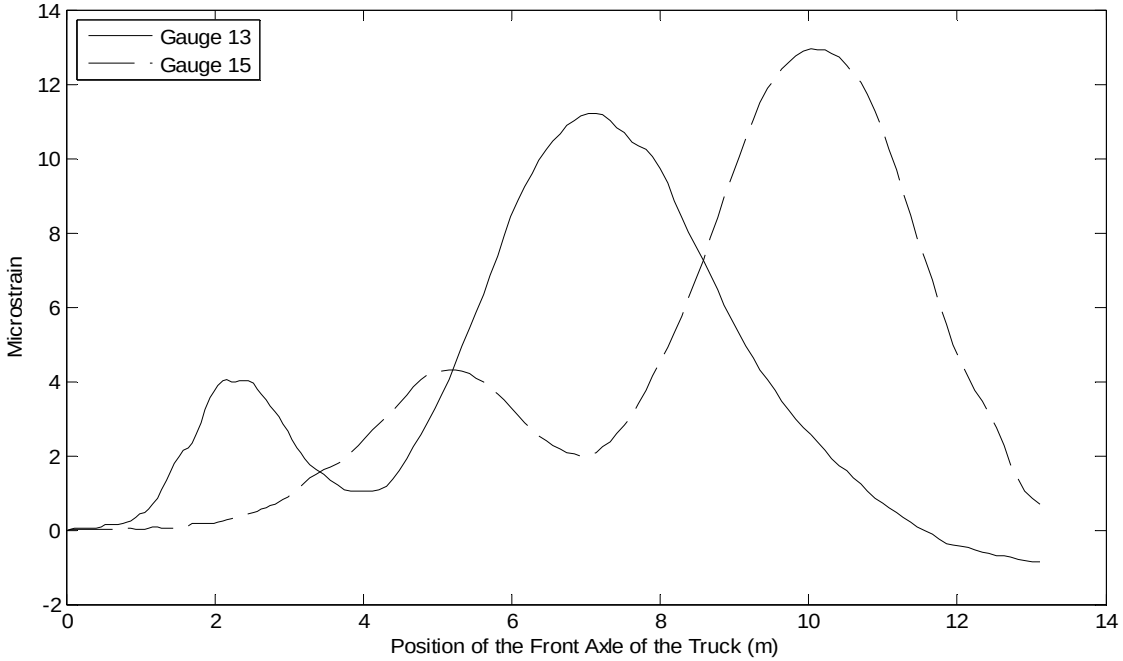

Figure D.10 – Resulting strains for bottom gauges located at the transverse centerline along the quarter span for test 2

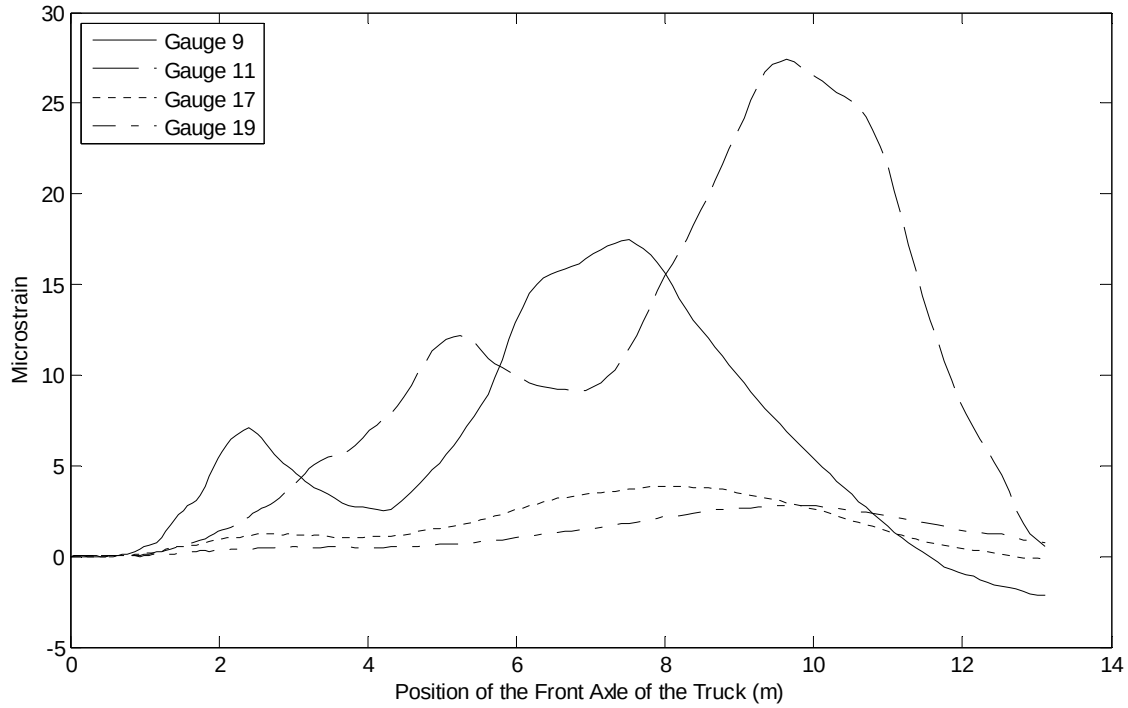

Figure D.11 – Resulting strains for the gauges located under the curbs along the quarter span for test 2

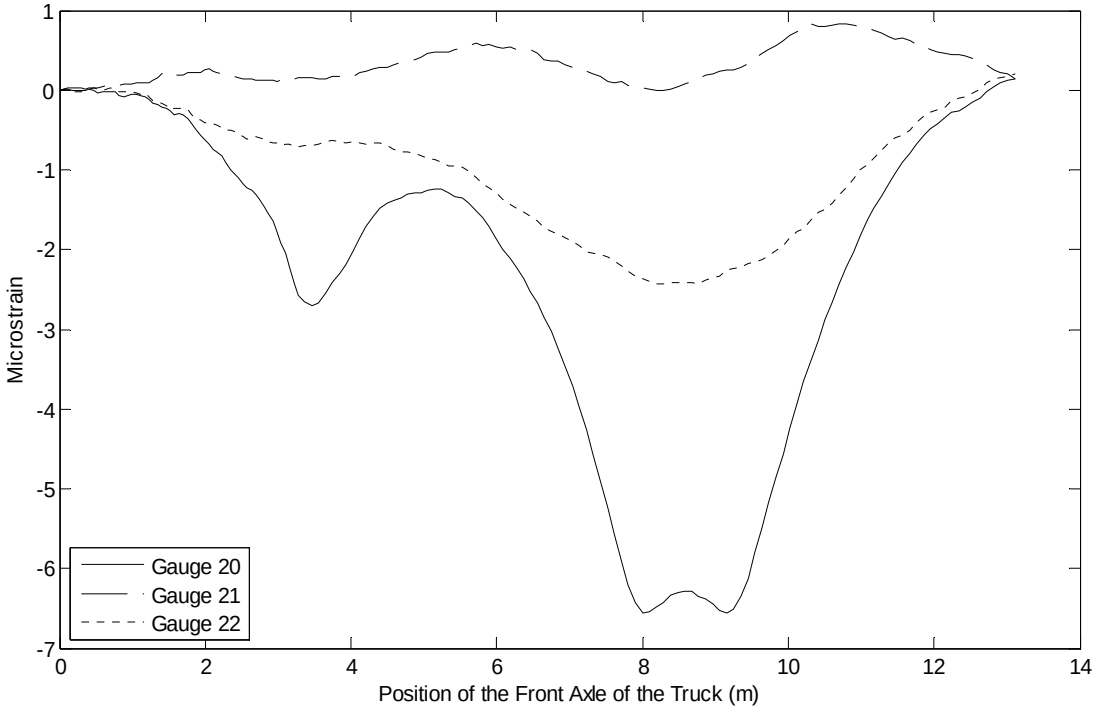

Figure D.12 – Resulting strains for the transverse gauges located along the centerline span for test 2

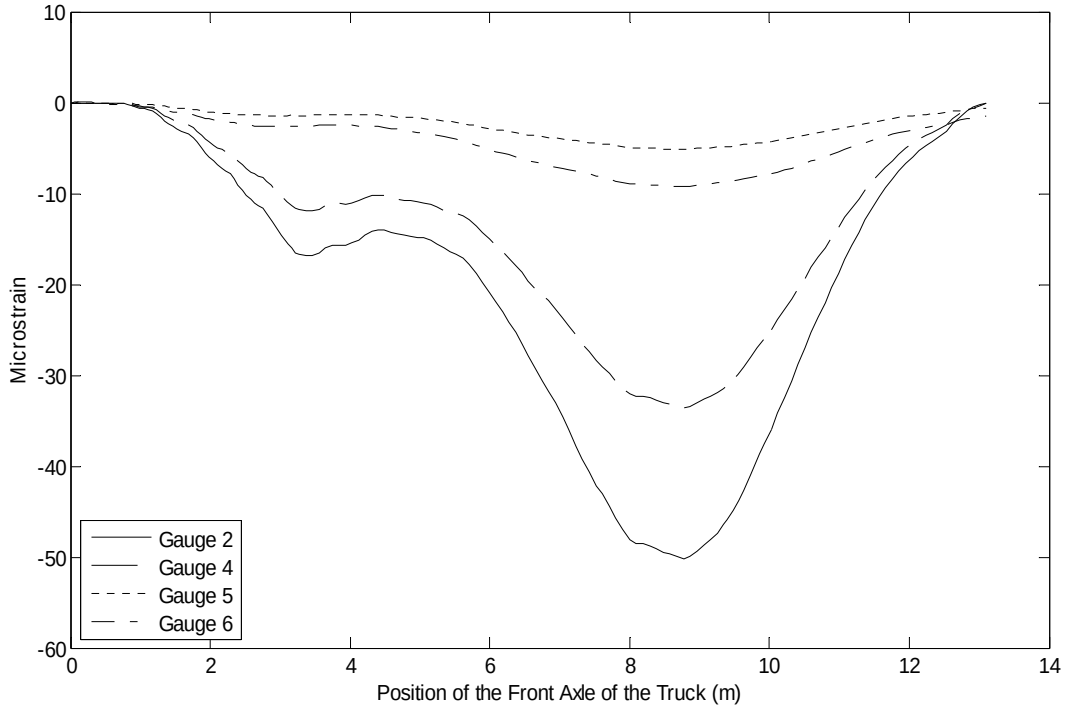

Figure D.13 – Resulting strains for the top gauges located at the centerline span for test 2

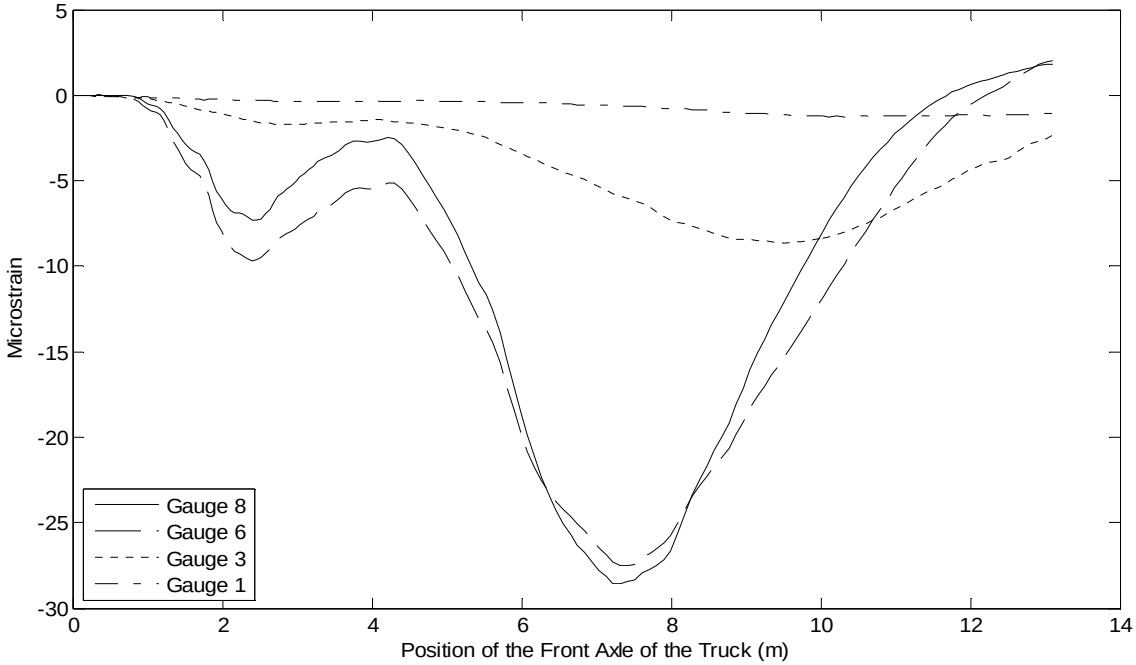

Figure D.14 – Resulting strains for the top gauges located along the quarter span for test 2

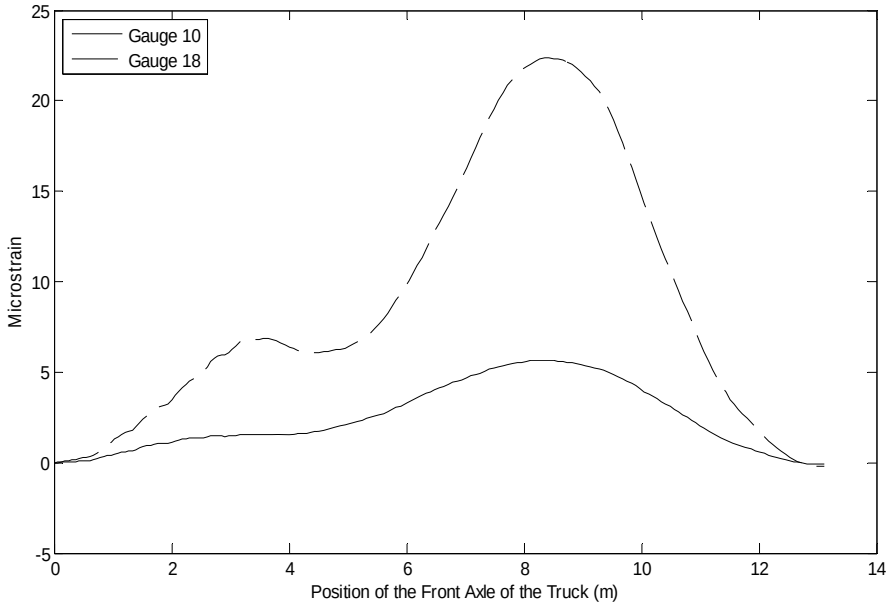

Figure D.15 – Resulting strains for gauges located under the curb along the centerline span during test 3

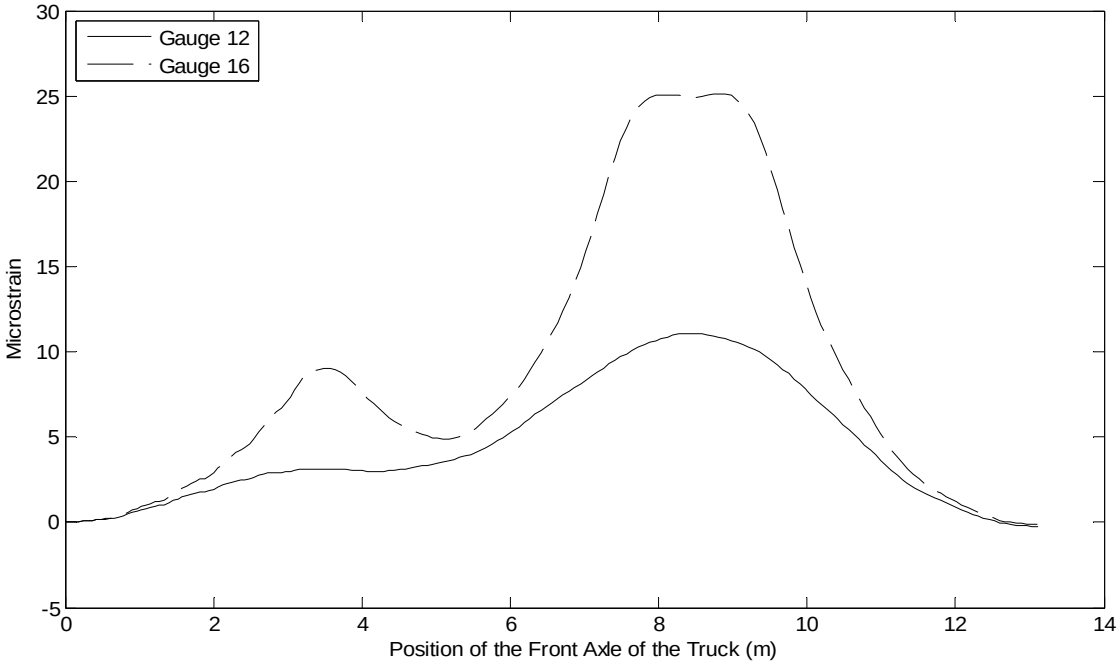

Figure D.16 – Resulting strains for gauges located at the transverse quarter points along the centerline span for test 3

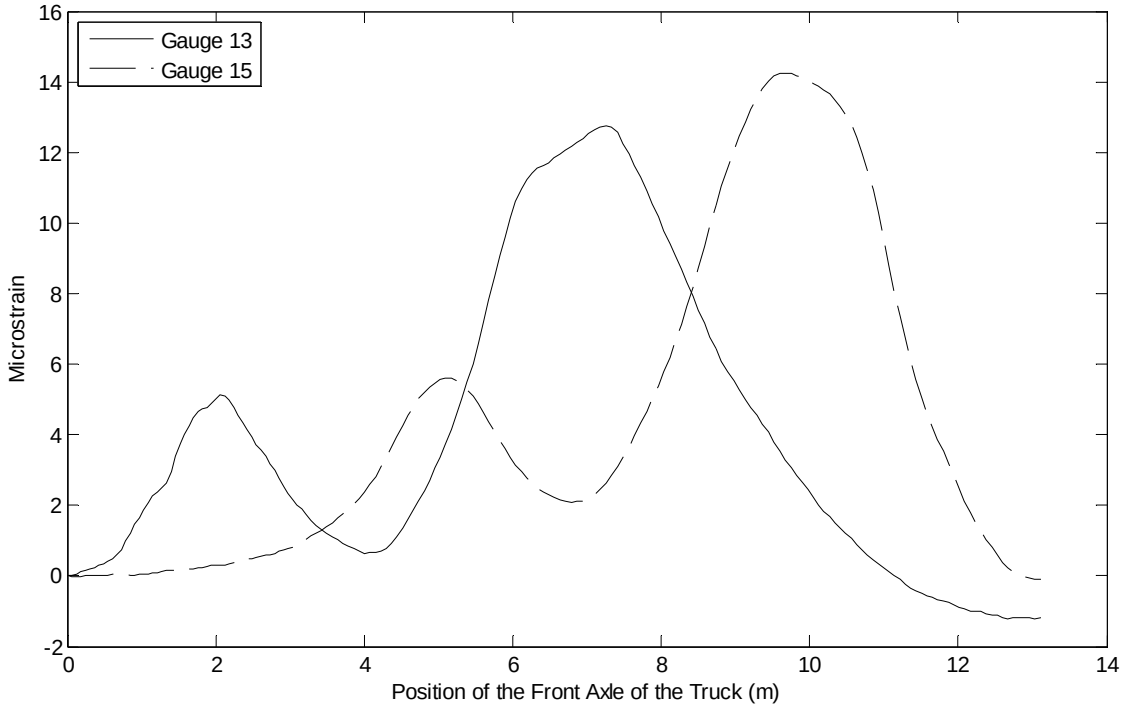

Figure D.17 – Resulting strains for bottom gauges located at the transverse centerline along the quarter span for test 3

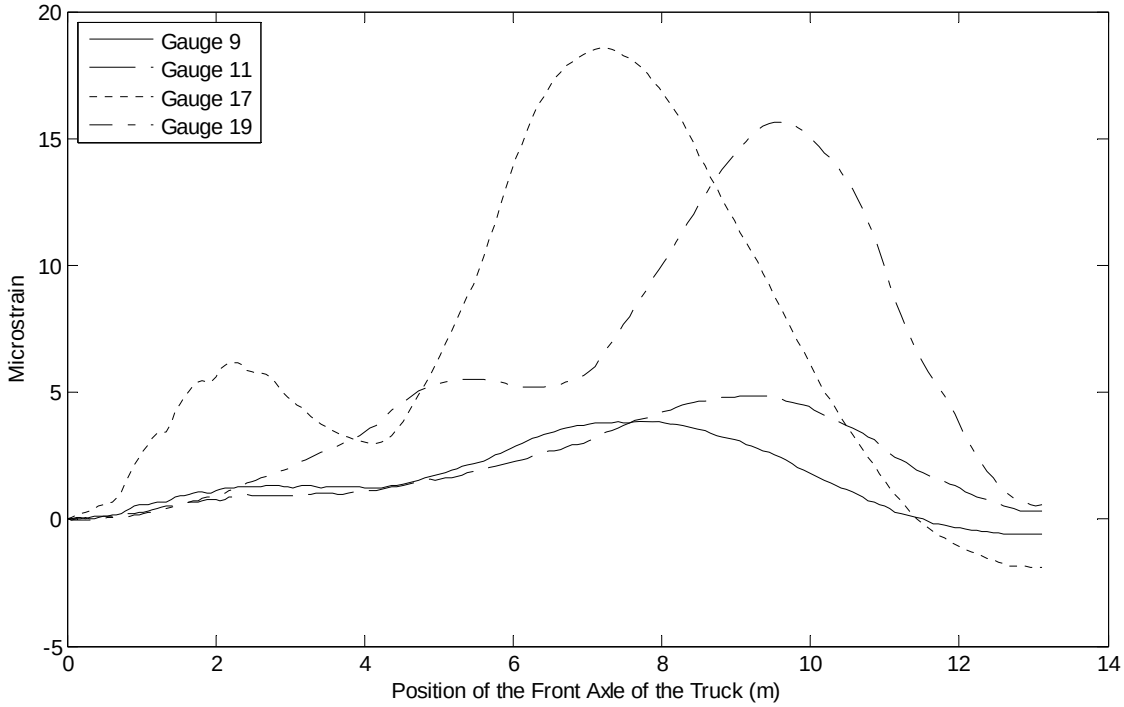

Figure D.18 – Resulting strains for the gauges located under the curbs along the quarter span for test 3

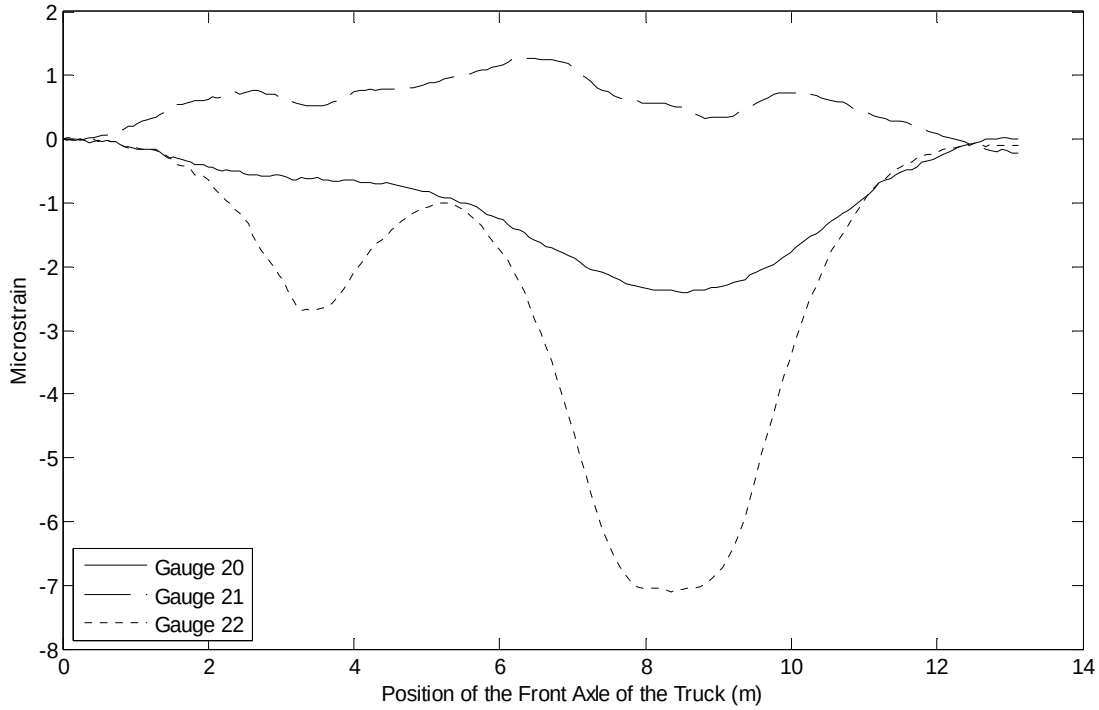

Figure D.19 – Resulting strains for the transverse gauges located along the centerline span for test 3

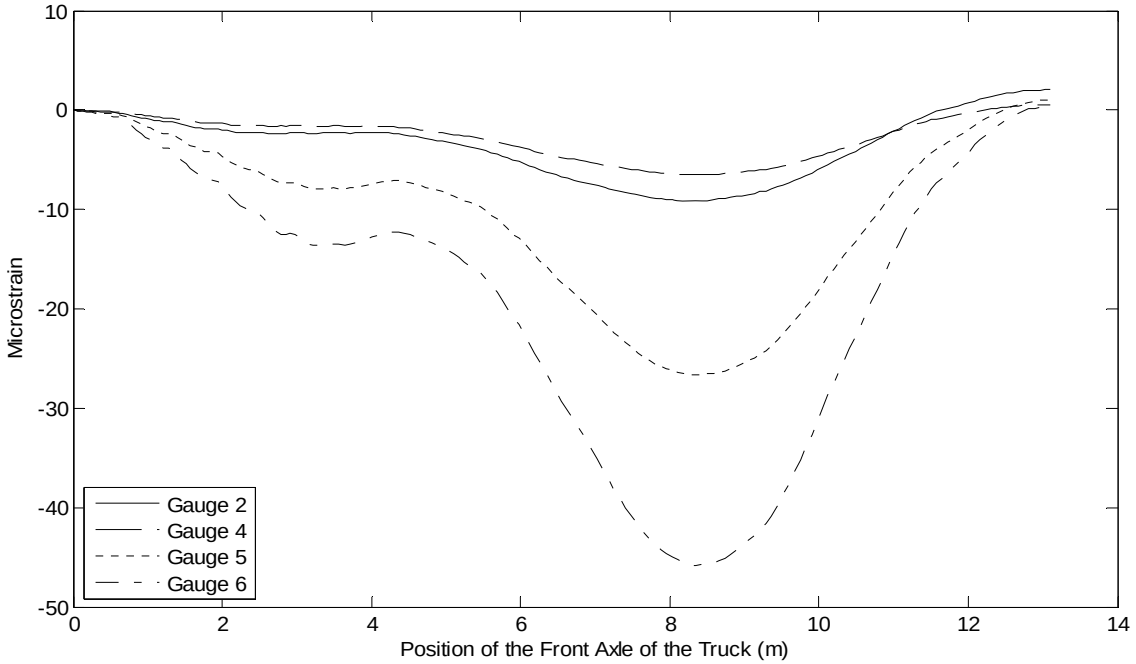

Figure D.20 – Resulting strains for the top gauges located at the centerline span for test 3

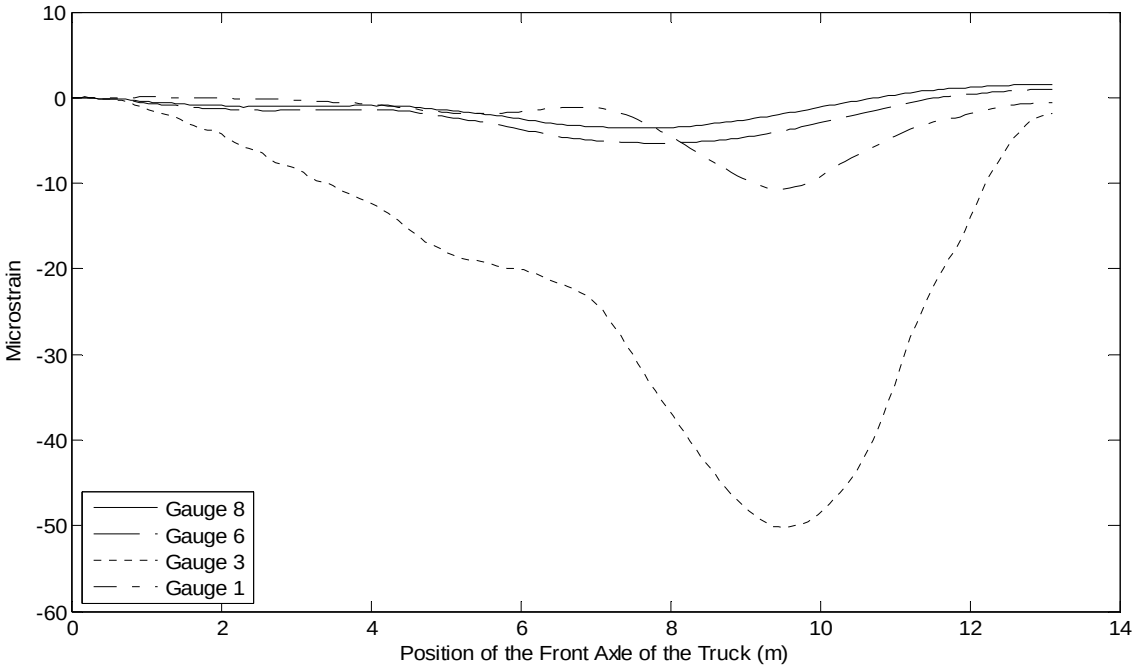

Figure D.21 – Resulting strains for the top gauges located along the quarter span for test 3

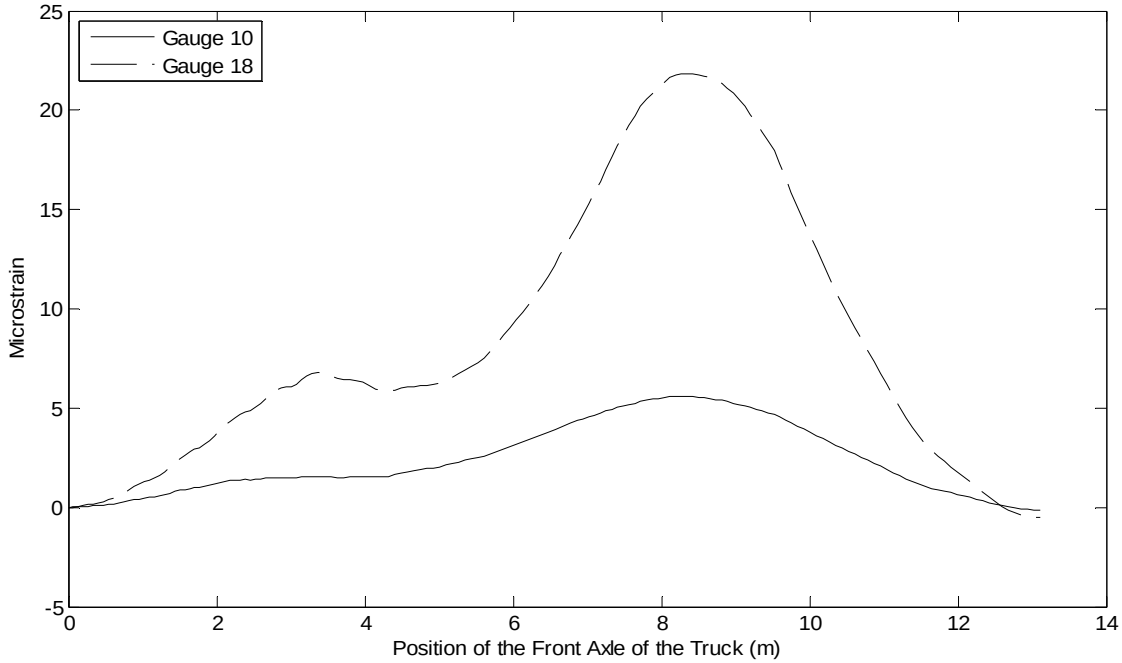

Figure D.22 – Resulting strains for gauges located under the curb along the centerline span during test 4

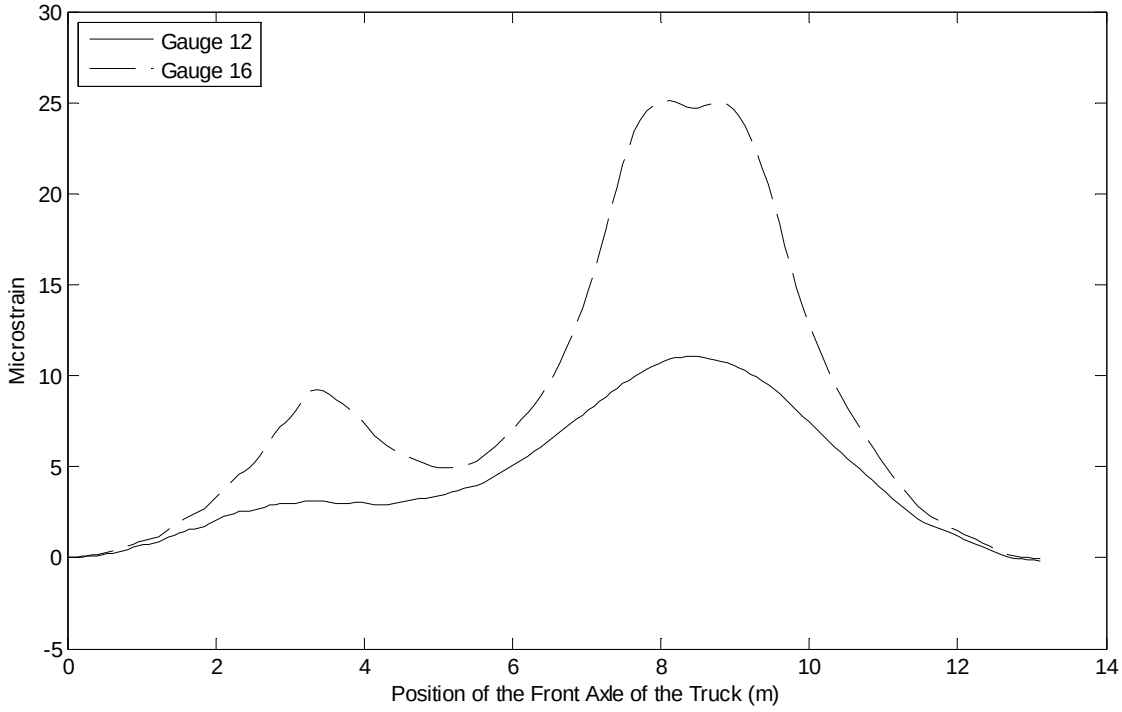

Figure D.23 – Resulting strains for gauges located at the transverse quarter points along the centerline span for test 4

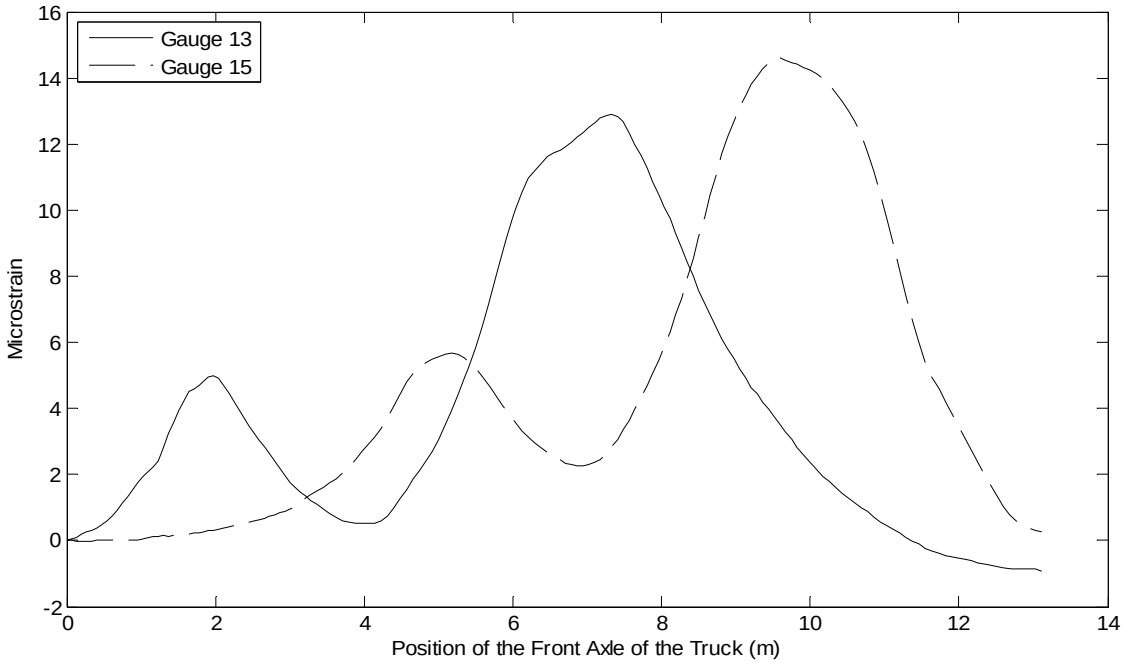

Figure D.24 – Resulting strains for bottom gauges located at the transverse centerline along the quarter span for test 4

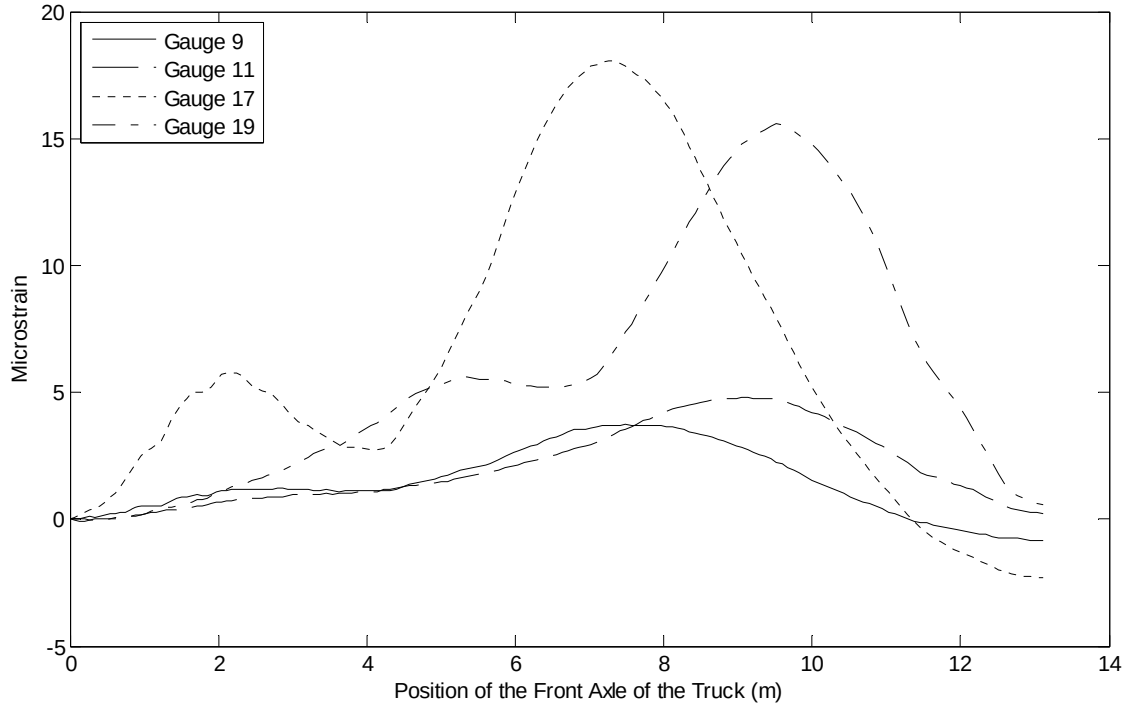

Figure D.25 – Resulting strains for the gauges located under the curbs along the quarter span for test 4

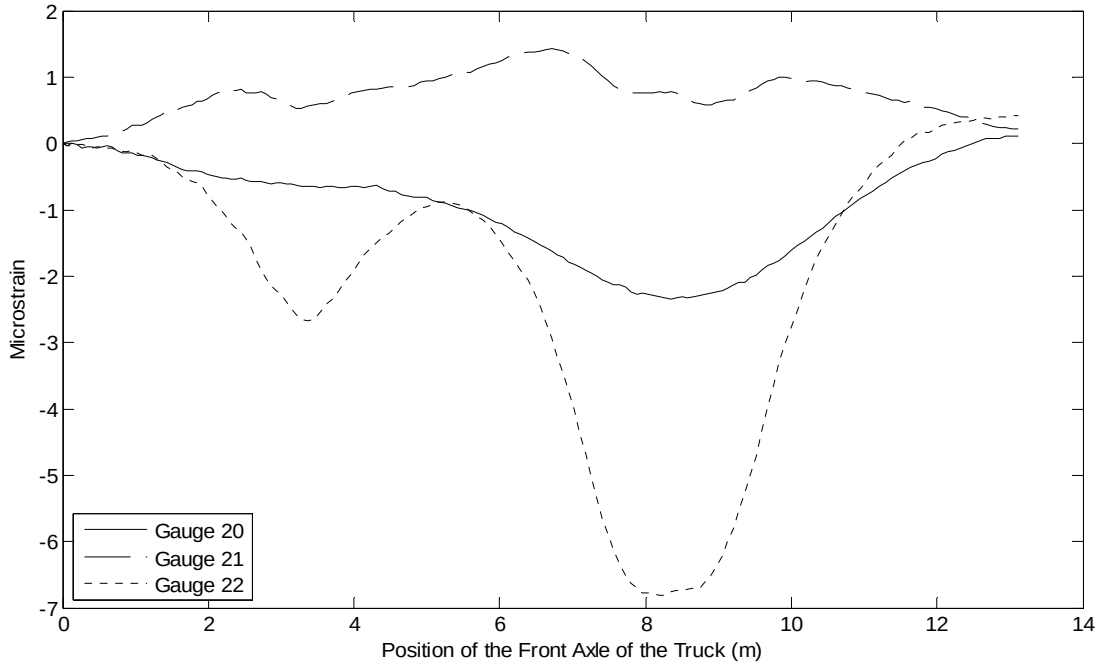

Figure D.26 – Resulting strains for the transverse gauges located along the centerline span for test 4

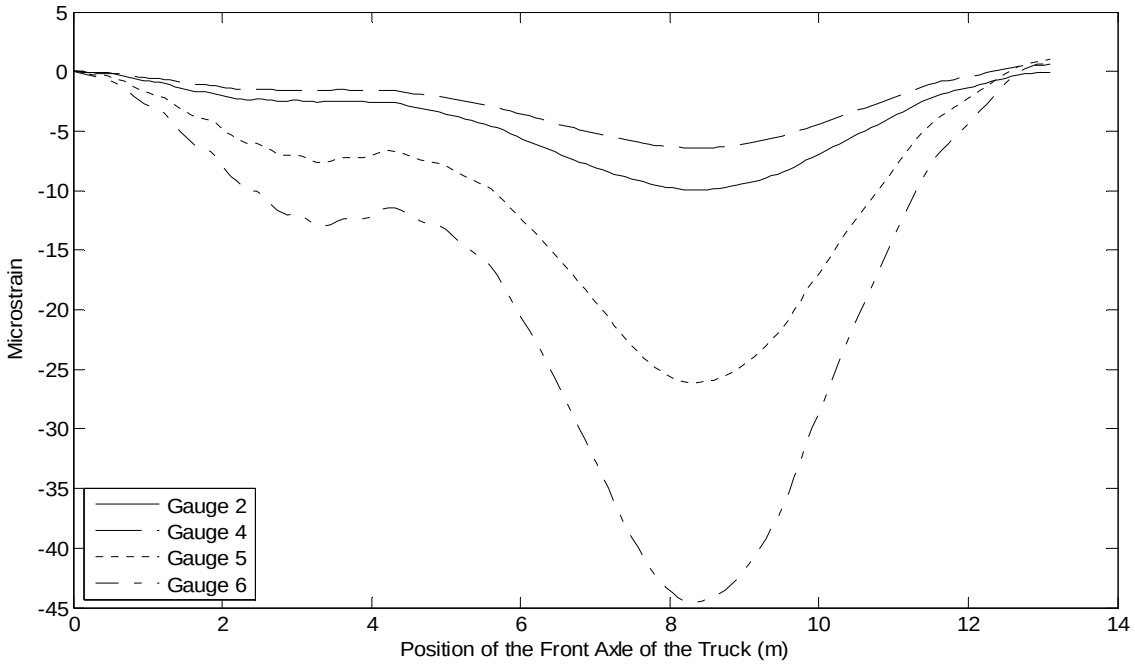

Figure D.27 – Resulting strains for the top gauges located at the centerline span for test 4

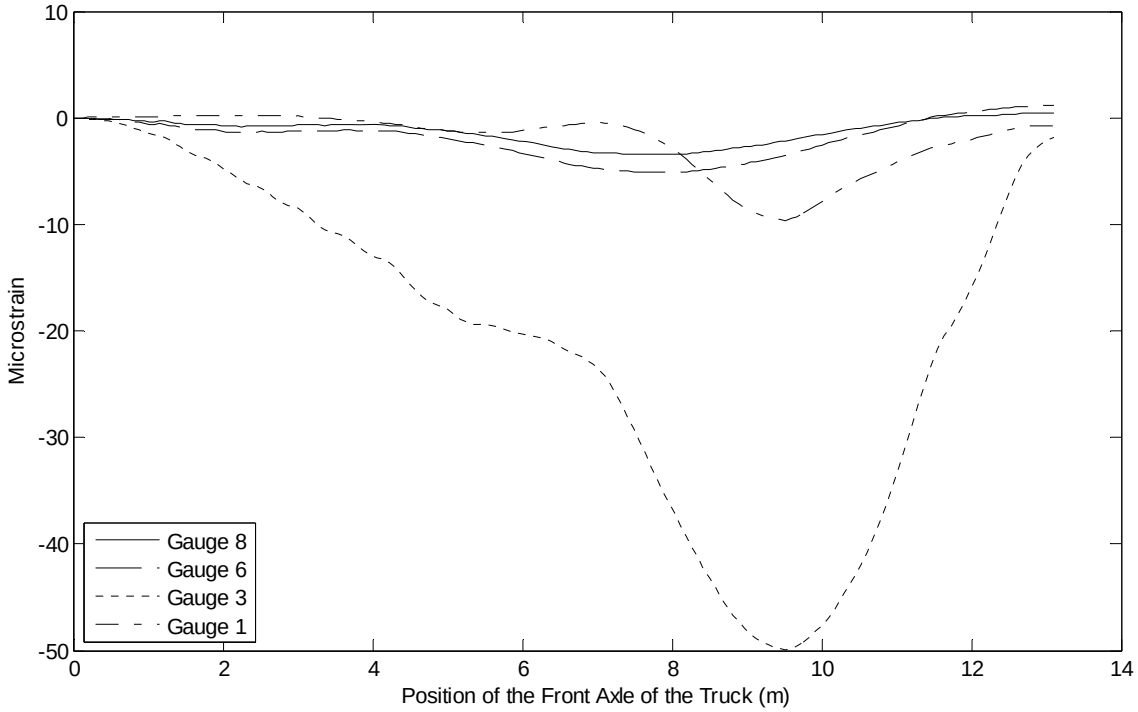

Figure D.28 – Resulting strains for the top gauges located along the quarter span for test 4

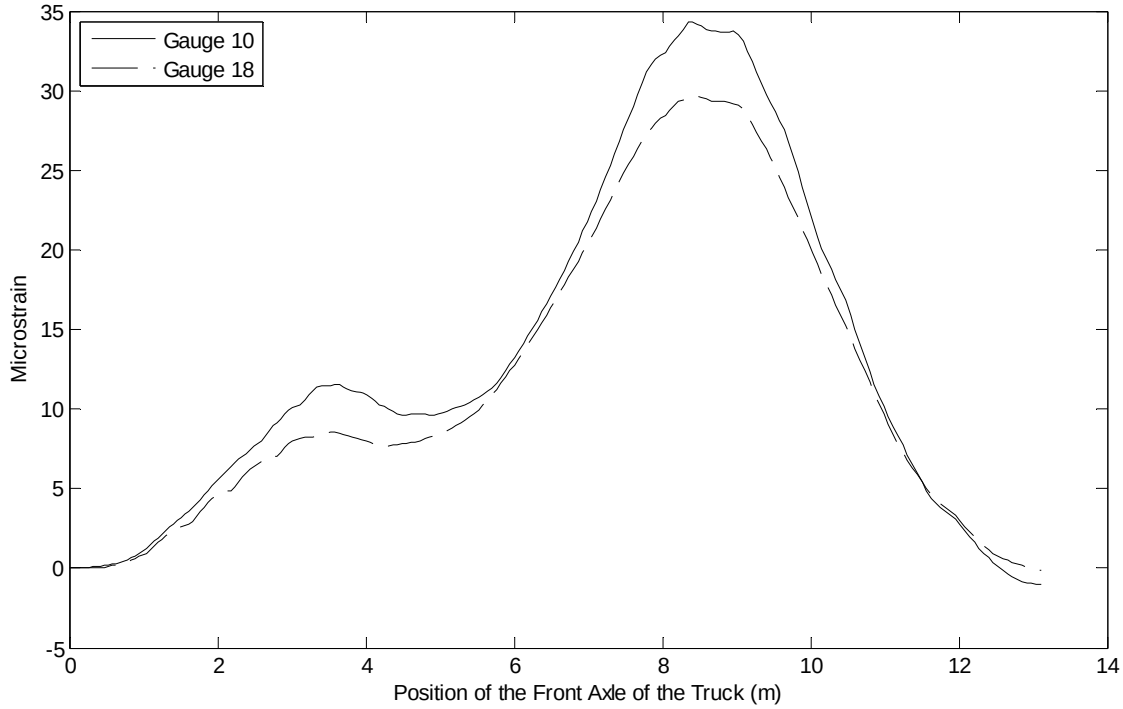

Figure D.29 – Resulting strains for gauges located under the curb along the centerline span during test 5

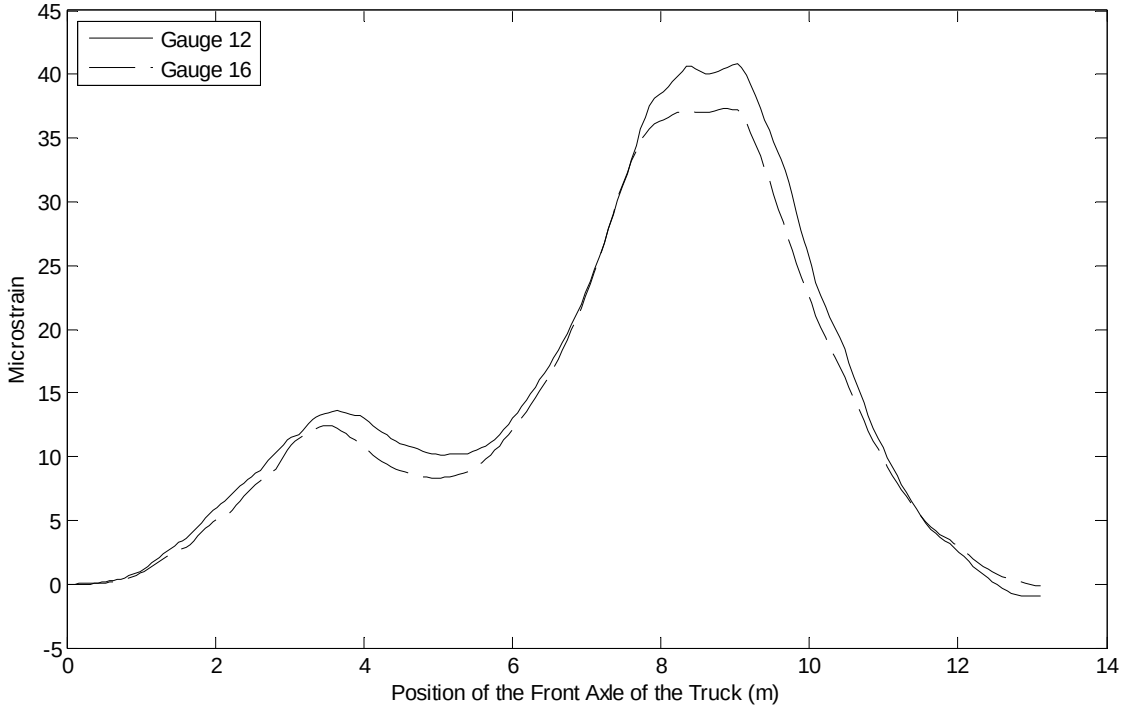

Figure D.30 – – Resulting strains for gauges located at the transverse quarter points along the centerline span for test 5

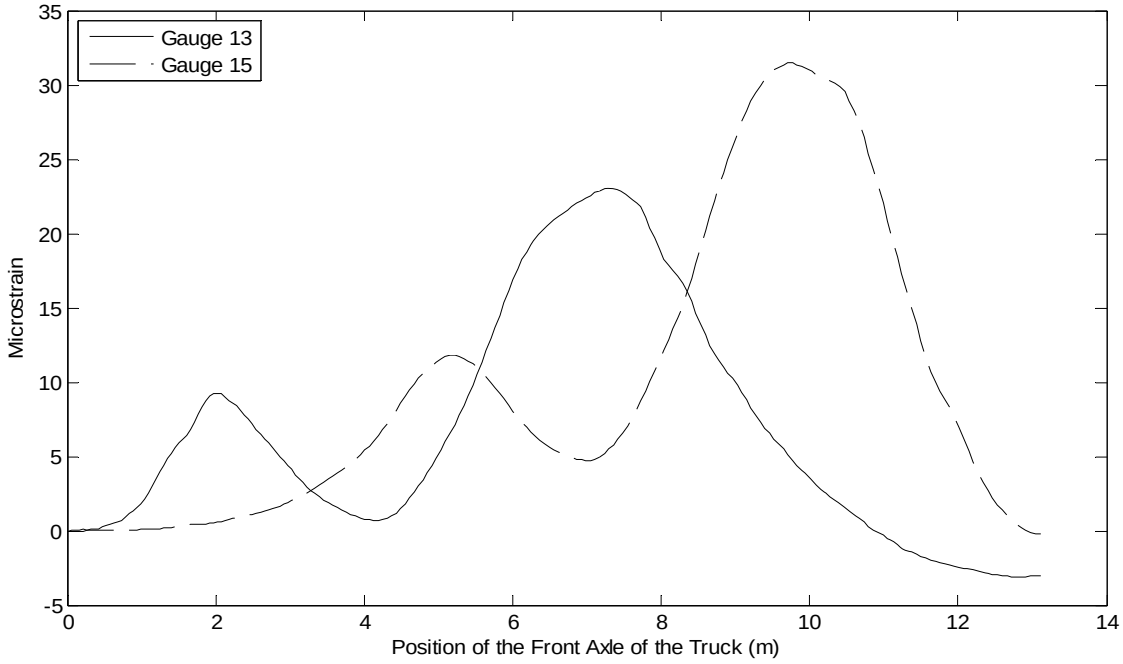

Figure D.31 – Resulting strains for bottom gauges located at the transverse centerline along the quarter span for test 5

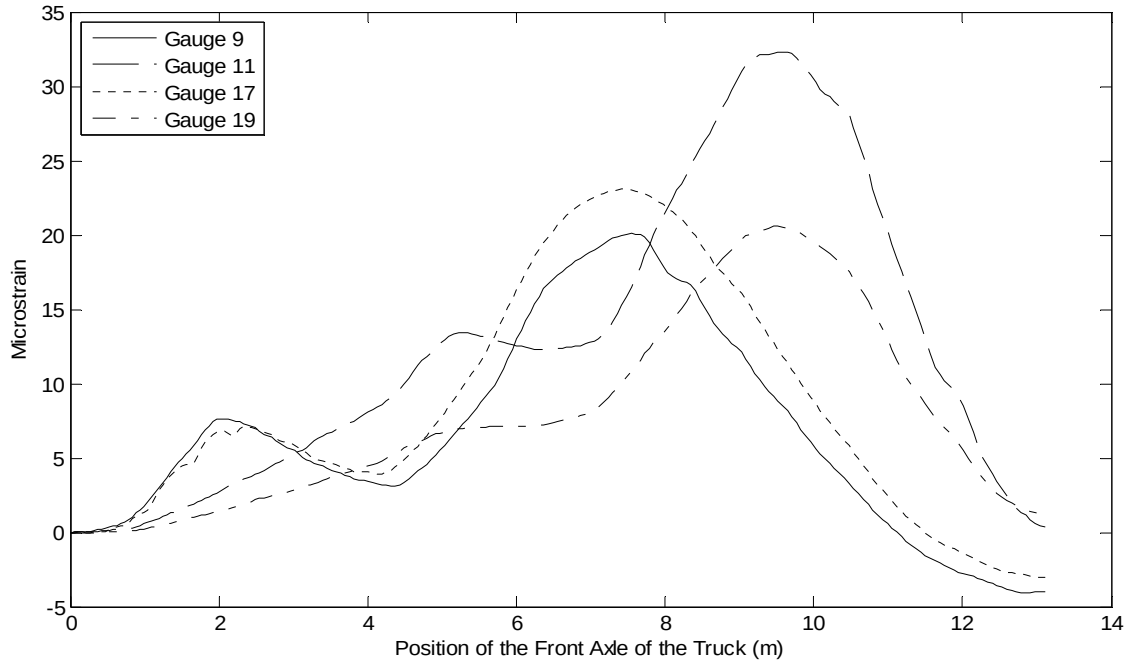

Figure D.32 – Resulting strains for the gauges located under the curbs along the quarter span for test 5

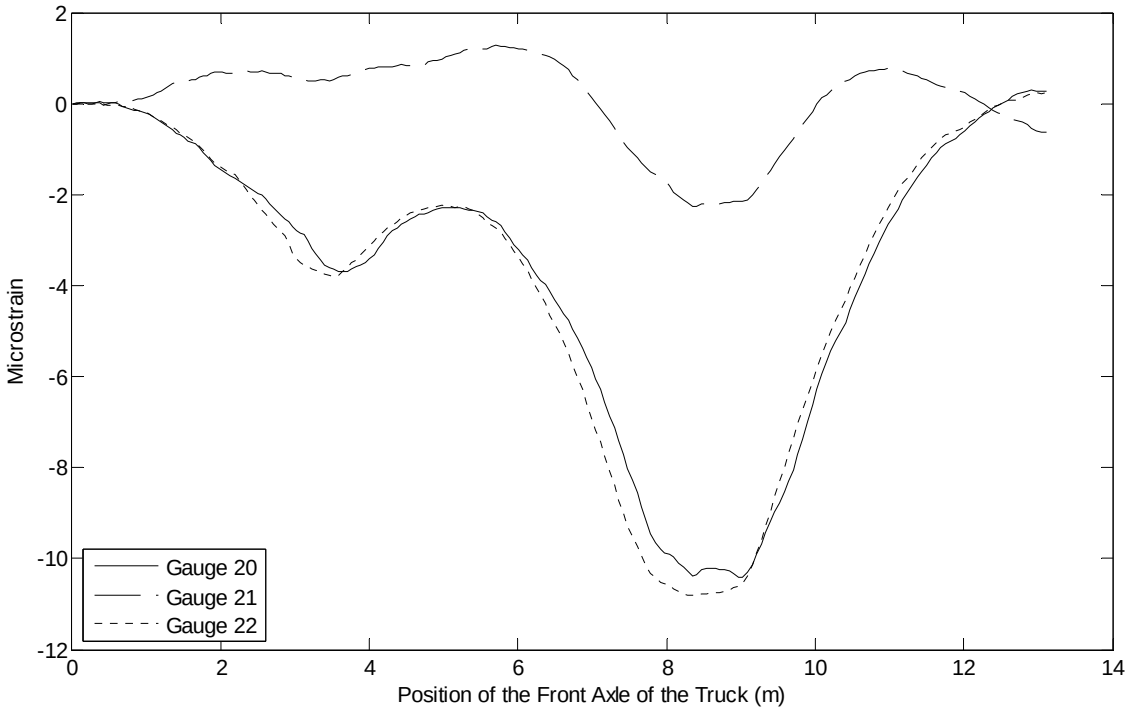

Figure D.33 – Resulting strains for the transverse gauges located along the centerline span for test 5

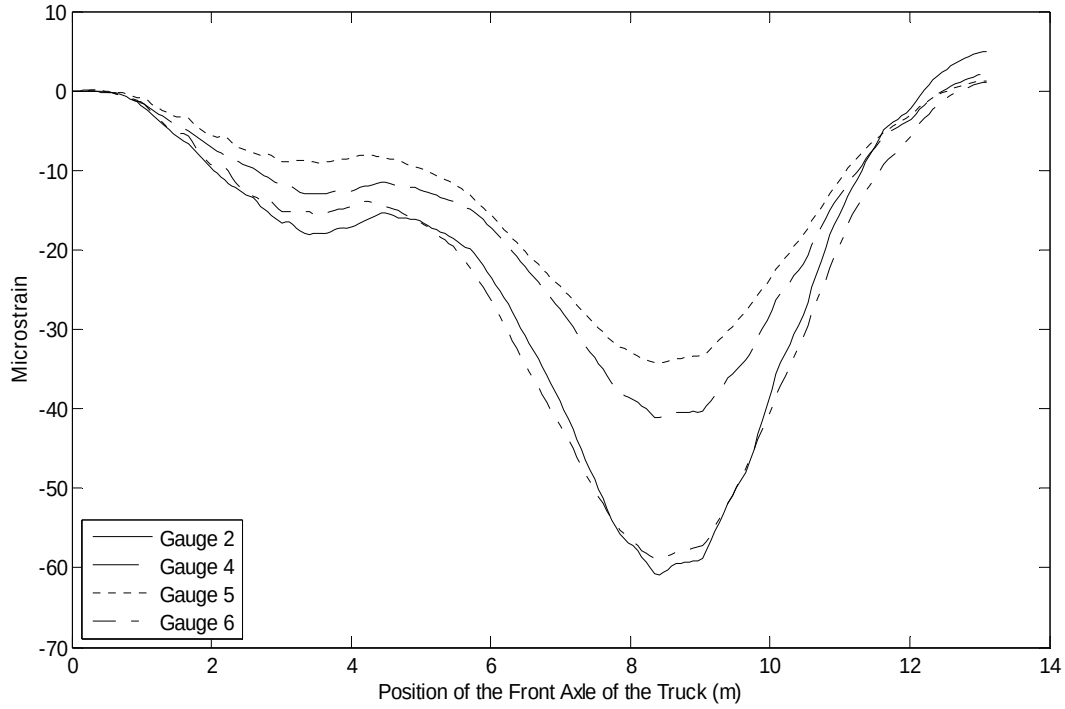

Figure D.34 – Resulting strains for the top gauges located at the centerline span for test 5

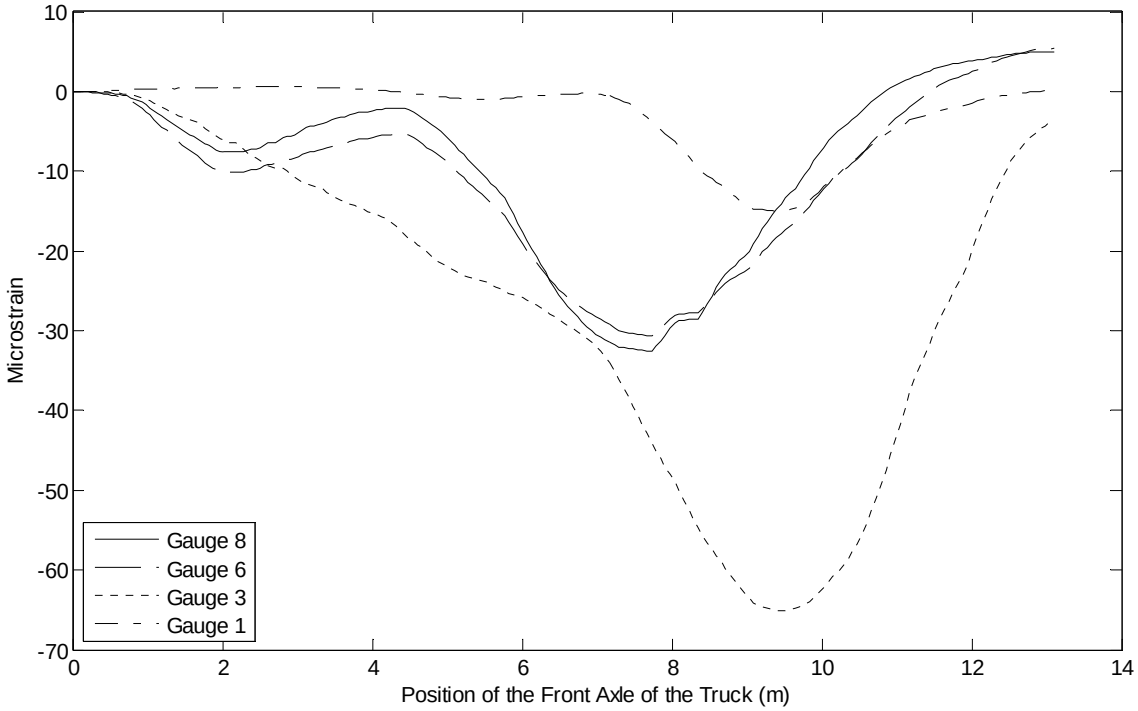

Figure D.35 – Resulting strains for the top gauges located along the quarter span for test 5

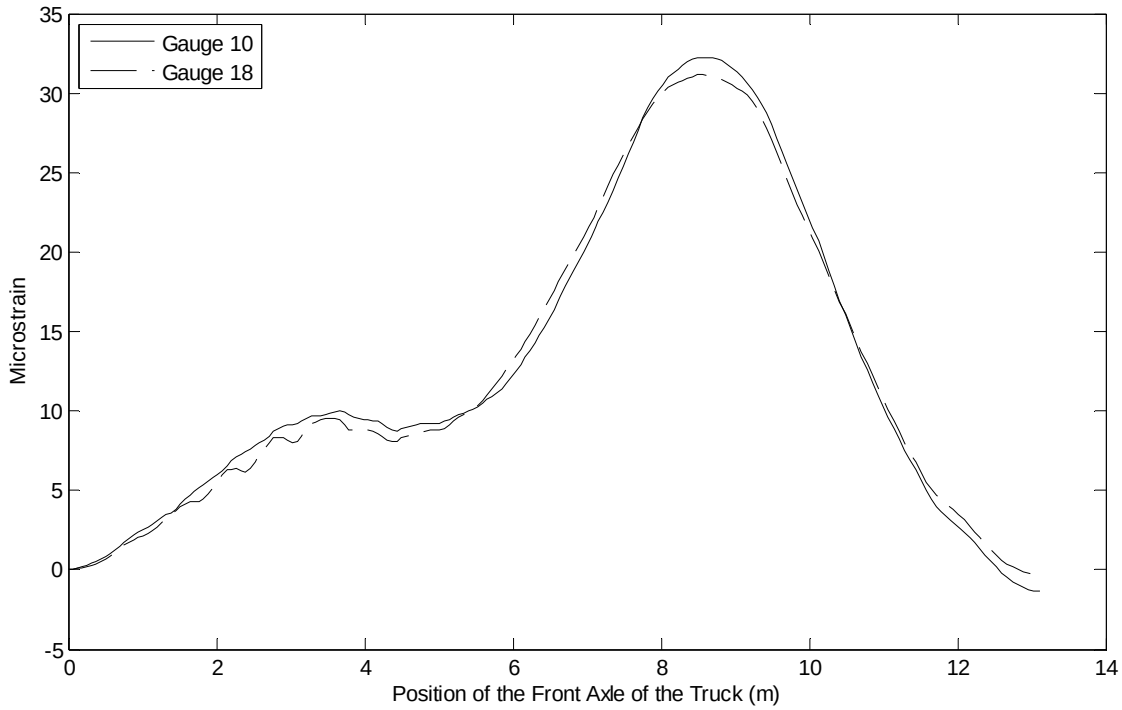

Figure D.36 – Resulting strains for gauges located under the curb along the centerline span during test 6

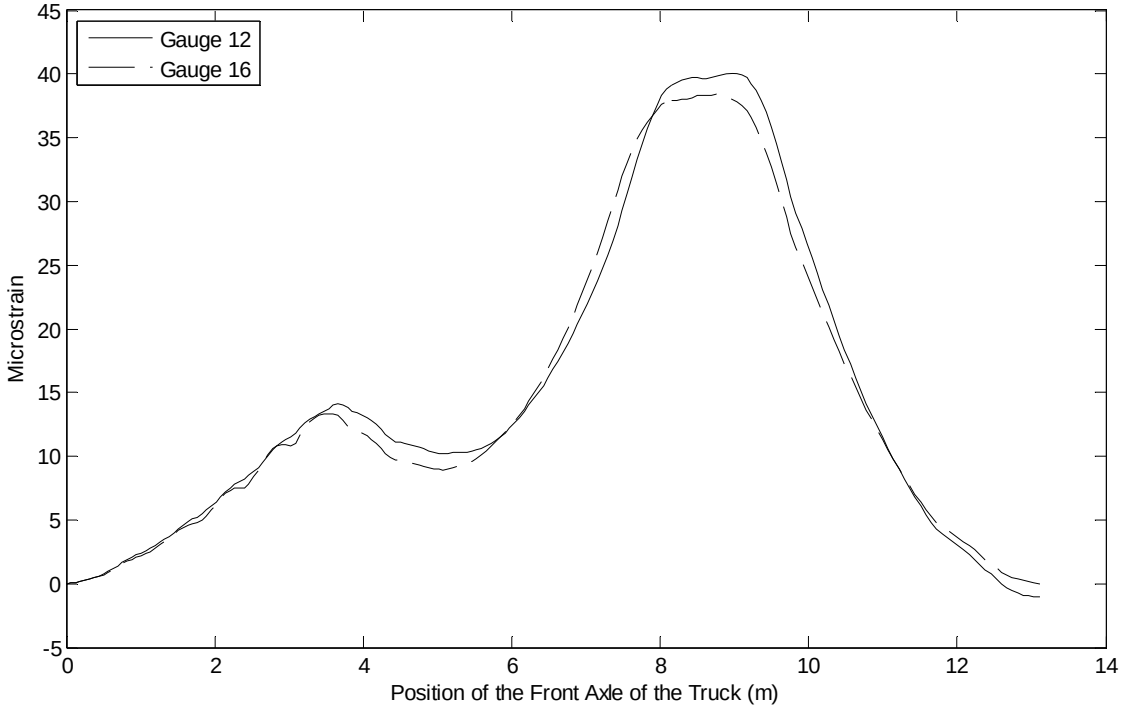

Figure D.37 – Resulting strains for gauges located at the transverse quarter points along the centerline span for test 6

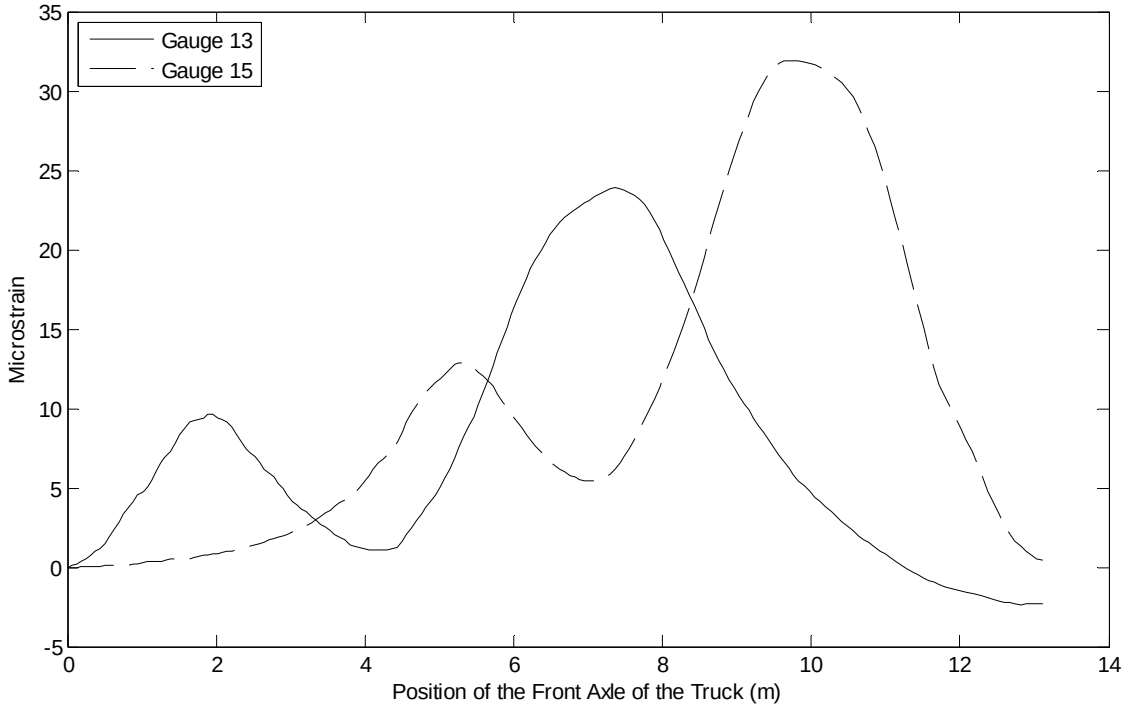

Figure D.38 – Resulting strains for bottom gauges located at the transverse centerline along the quarter span for test 6

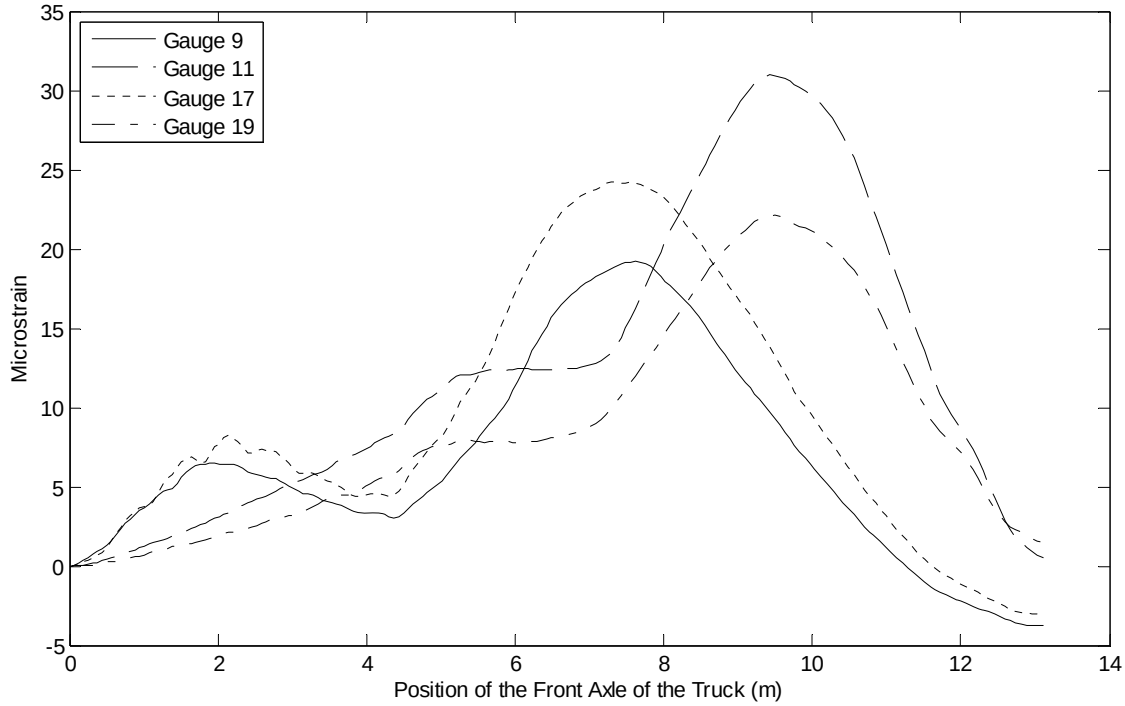

Figure D.39 – Resulting strains for the gauges located under the curbs along the quarter span for test 6

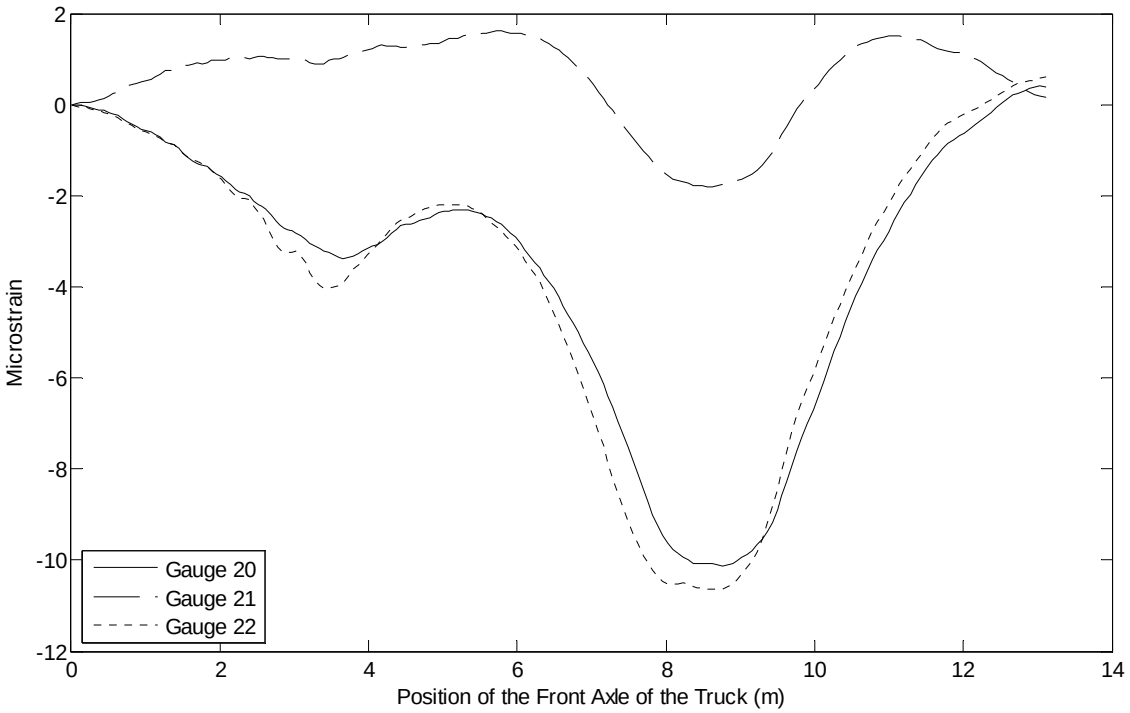

Figure D.40 – Resulting strains for the transverse gauges located along the centerline span for test 6

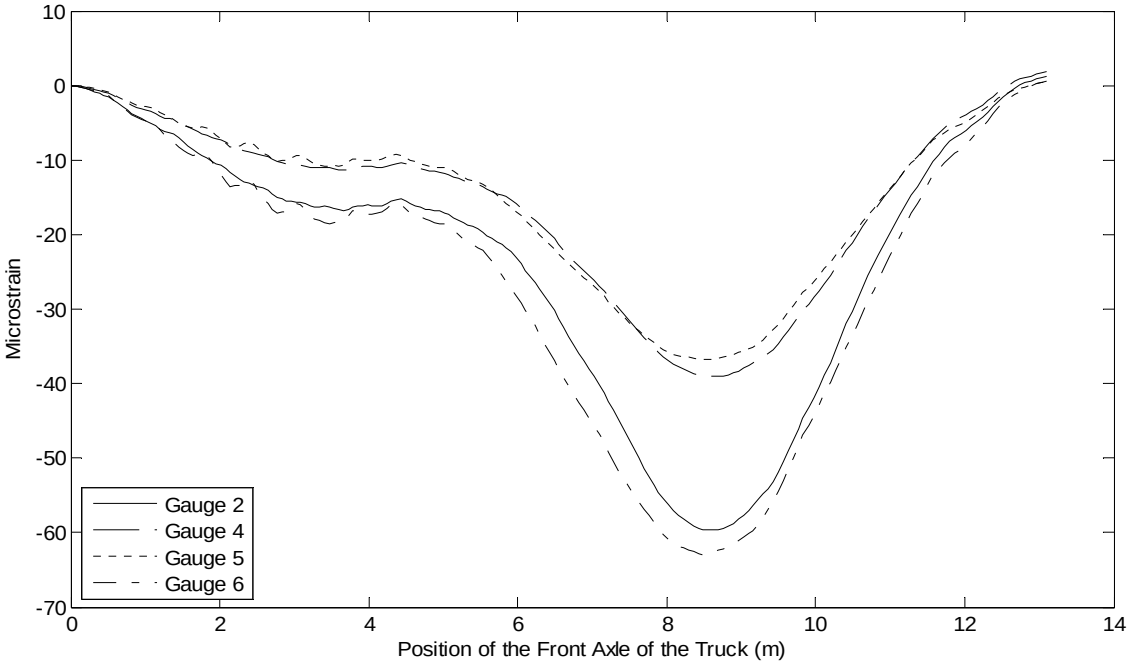

Figure D.41 – Resulting strains for the top gauges located at the centerline span for test 6

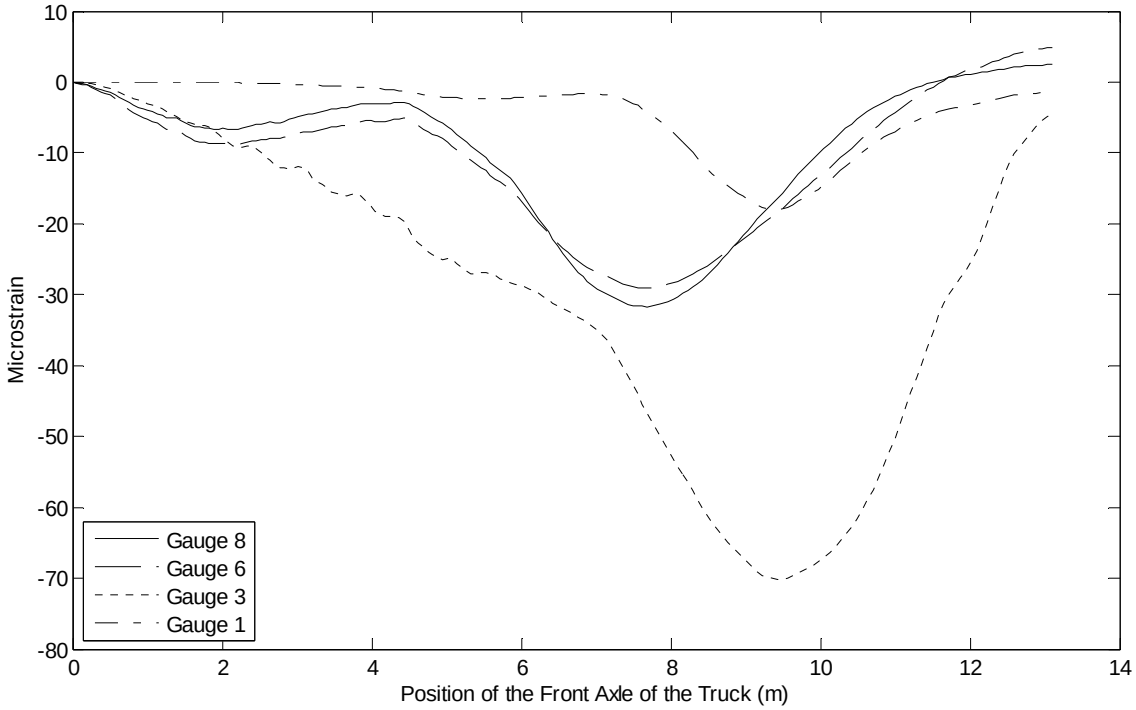

Figure D.42 – Resulting strains for the top gauges located along the quarter span for test 6

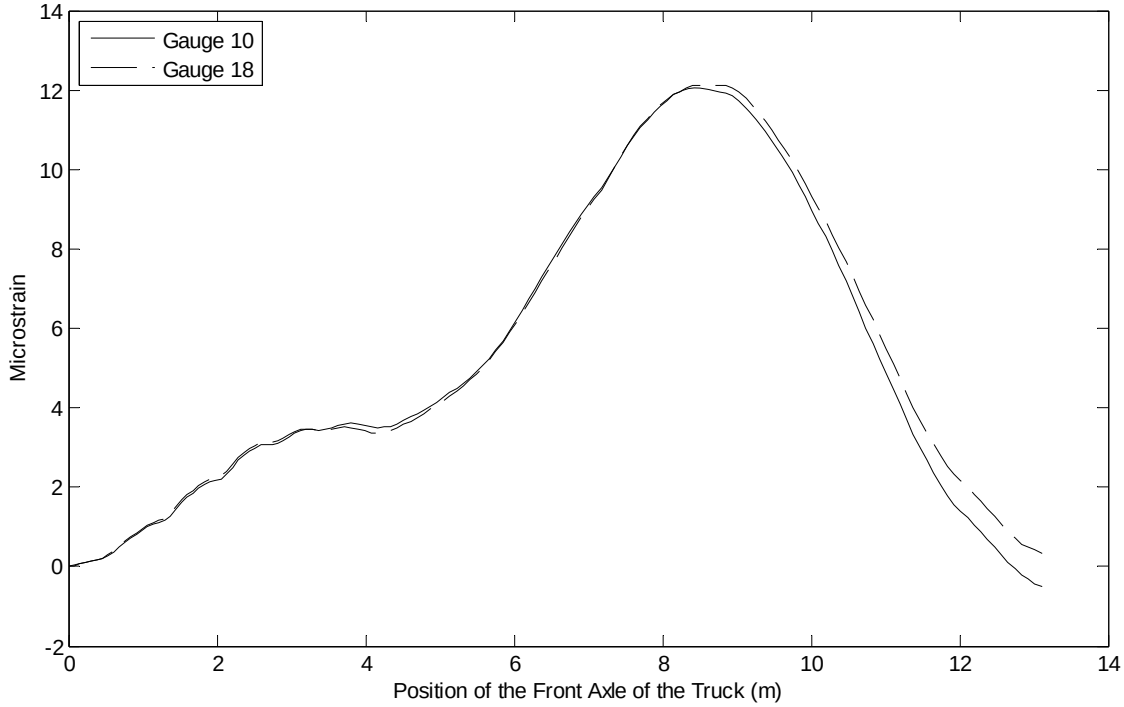

Figure D.43 – Resulting strains for gauges located under the curb along the centerline span during test 7

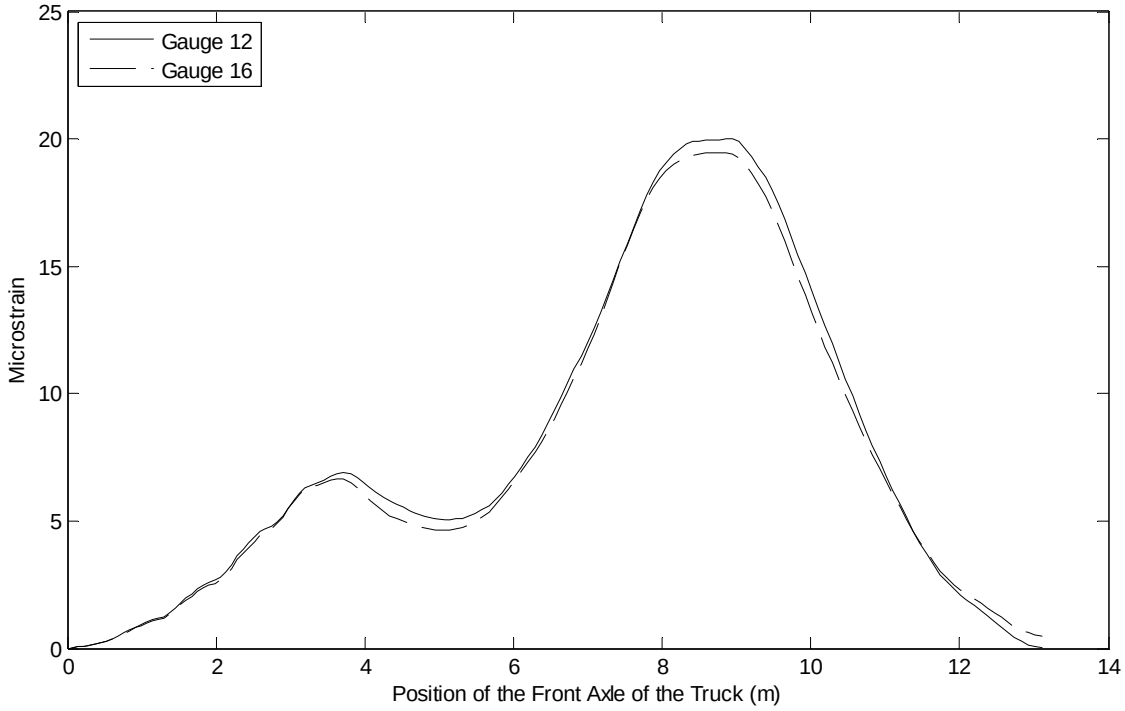

Figure D.44 – Resulting strains for gauges located at the transverse quarter points along the centerline span for test 7

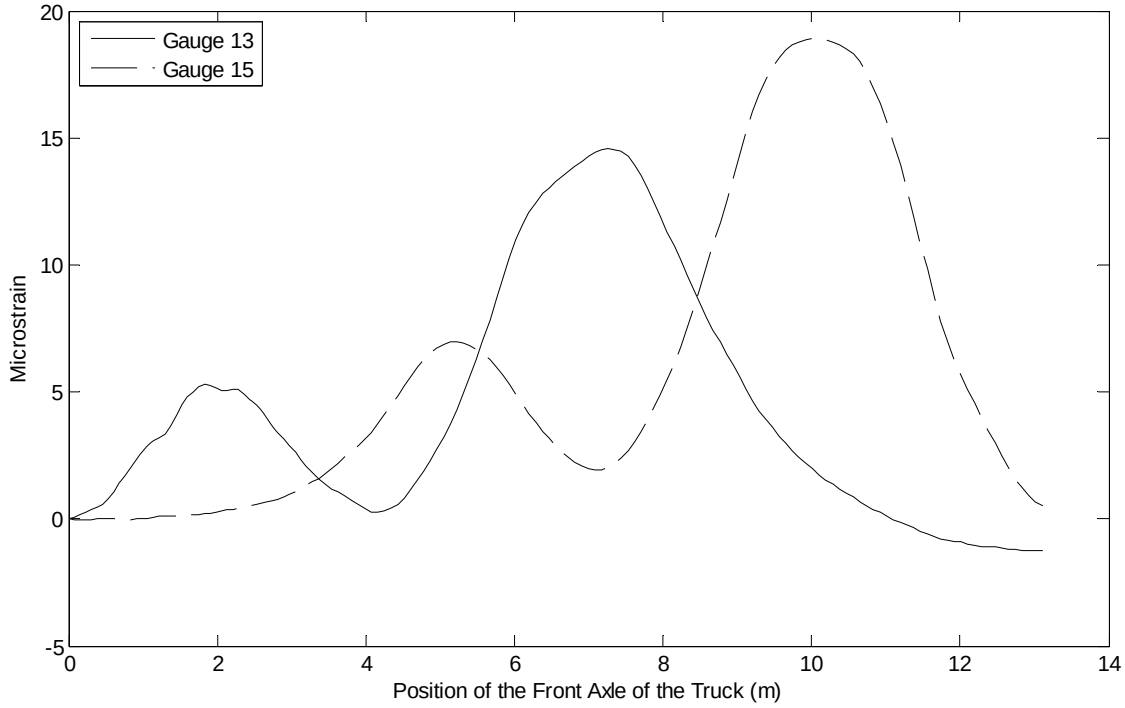

Figure D.45 – Resulting strains for bottom gauges located at the transverse centerline along the quarter span for test 7

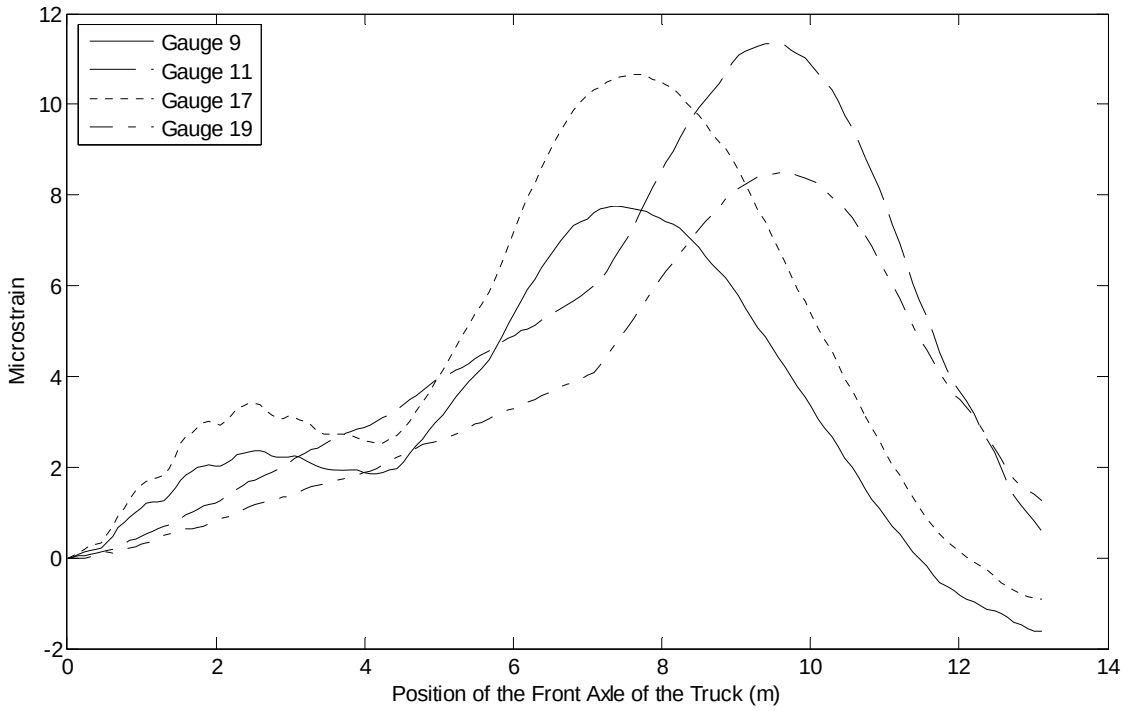

Figure D.46 – Resulting strains for the gauges located under the curbs along the quarter span for test 7

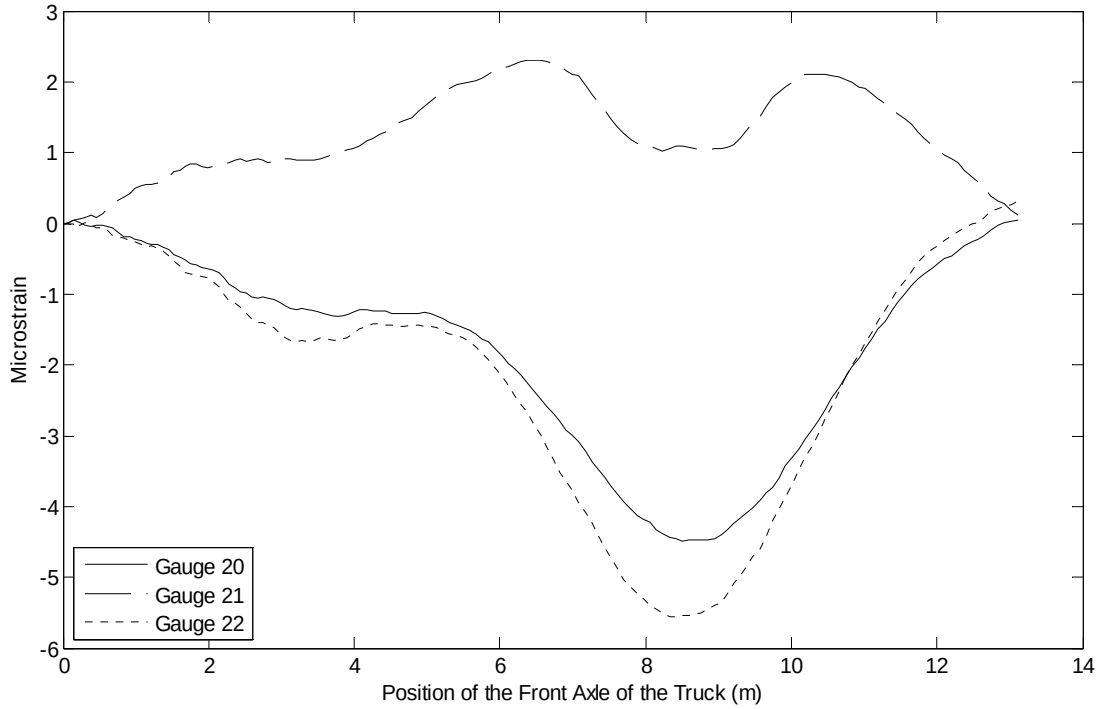

Figure D.47 – Resulting strains for the transverse gauges located along the centerline span for test 7

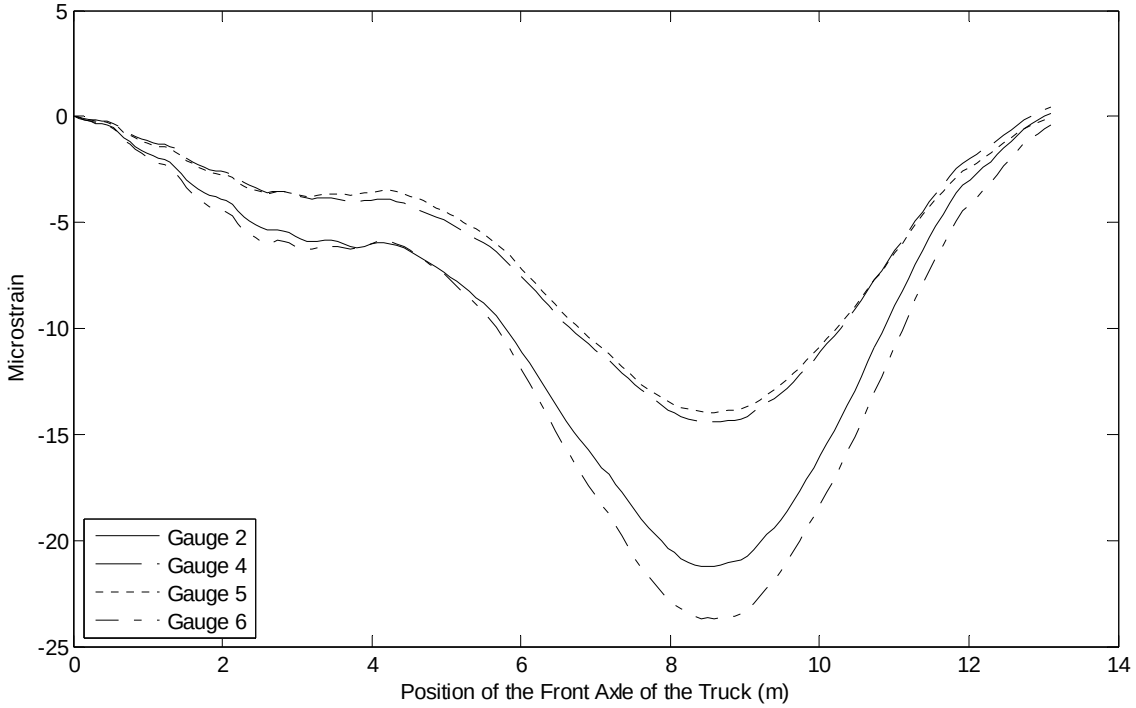

Figure D.48 – Resulting strains for the top gauges located at the centerline span for test 7

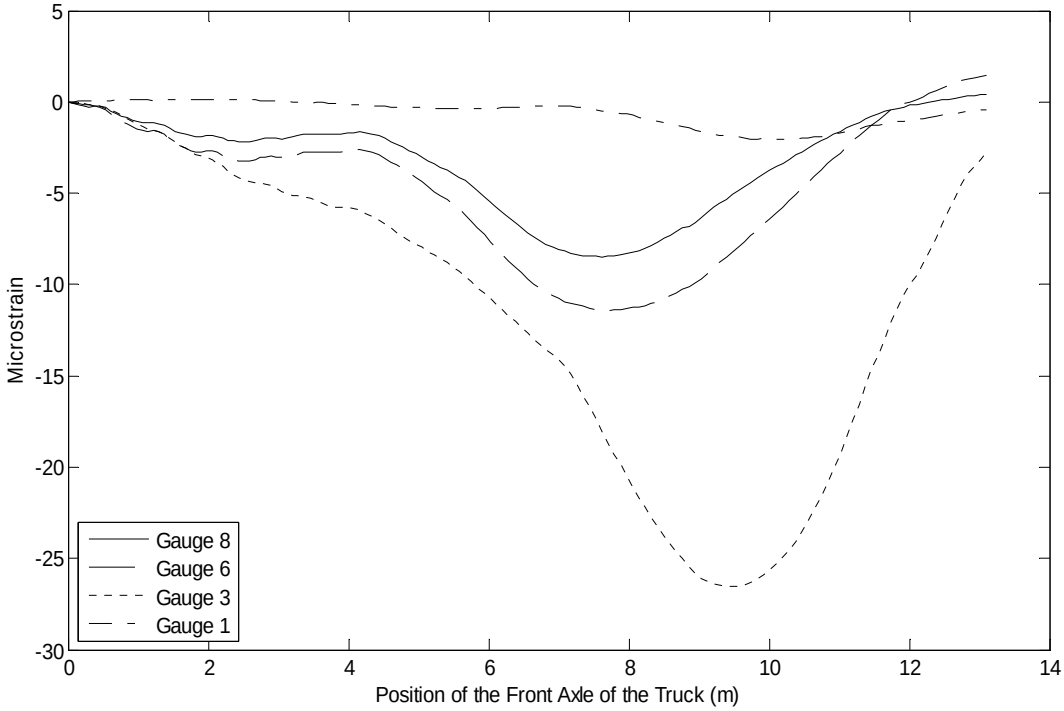

Figure D.49 – Resulting strains for the top gauges located along the quarter span for test 7

BIOGRAPHY OF THE AUTHOR

Timothy Poulin was born in Gorham, Maine on August 19, 1988. Son of Richard and Claire Poulin, Timothy grew up in Gorham and graduated from Gorham High School in 2006. He enrolled the University of Maine the fall of 2006 and graduated in the fall of 2010 with a Bachelor's degree in Civil and Environmental Engineering. Tim then entered the Civil Engineering graduate program at the University of Maine in the fall of 2010. Tim is a candidate for the Master of Science degree in Civil Engineering from the University of Maine in August, 2012.

Load Rating Guideline for Flat Slab Concrete Bridges Using the Strip Width Method and Finite–Element Method

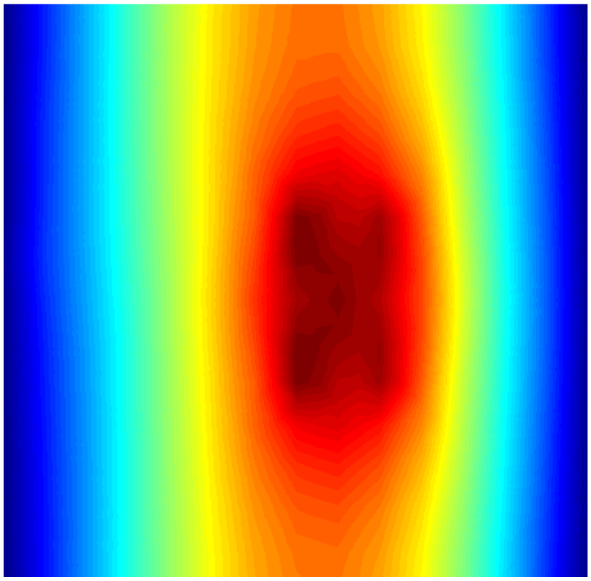

Authors:
William Davids Ph.D., P.E.
Timothy Poulin

1. Introduction

This document is a guide that draws on both accepted AASHTO and MaineDOT procedures and provides specific guidance for MaineDOT personnel and consultants performing load rating on flat concrete slab and rigid frame bridges. An overview of conventional load rating procedures is included as well as detailed guidance on the use of finite-element (FE) analysis techniques for concrete flat slab and rigid frame bridges. Examples of concrete slab bridge load ratings that demonstrate the application of conventional strip width and FE analysis methods are given at the end of the document.

Section 2 of this document overviews the conventional strip width method. These guidelines follow the 2008 edition of the AASHTO *Manual for Bridge Evaluation* (AASHTO 2008), along with the 2003 MaineDOT *Bridge Design Guide* with revisions from August 2008 (MaineDOT 2003). This document is to be used in conjunction with the current AASHTO *Manual for Bridge Evaluation*. This document also refers to specific sections in the AASHTO *Manual for Bridge Evaluation* for relevant information regarding the load rating of flat concrete slab bridges. The AASHTO *LRFD Bridge Design Specification* (AASHTO 2007) is also referred to extensively.

Section 3 provides guidance for the load rating of concrete slab bridges using finite-element analysis procedures. These guidelines are applied in conjunction with the 2008 edition of the AASHTO *Manual for Bridge Evaluation*.

Sections 4 and 5 of this document contain detailed examples of flat slab load rating using both the conventional strip width method and finite element analysis.

2. Conventional Slab Load Rating

Evaluation of Loads

General:

Loads for evaluation are determined with the use of section 6A.2 of the AASHTO Manual for Bridge Evaluation.

Only permanent loads and vehicular loads are considered to be of consequence in load rating. Environmental loads such as wind, ice, temperature, stream flow, and earthquake are usually not considered in rating except when unusual conditions warrant their inclusion. Creep and shrinkage also need not be evaluated if there is well-distributed reinforcement to control cracking (6A.2.3.8).

Dead Loads (DC and DW):

Dead loads should be computed in accordance to 6A2.2.1 of the AASHTO Manual for Bridge Evaluation.

DC: should be based on slab weight, curb weight and rail weight. The maximum moments at critical locations should be determined for a unit width. (i.e. units of kip-ft/ft, kN–m/m).
DW: should be based on the wearing surface and any utilities on the bridge. Maximum moments at critical locations should be determined per unit width (i.e. units of kip-ft/ft, kN–m/m).

Permanent Loads Other Than Dead Loads (P):

Permanent loads should be computed in accordance to 6A.2.2.2 of the AASHTO Manual for Bridge Evaluation.

Permanent loads P should be determined per unit width (i.e. units of kip-ft/ft, kN–m/m).

Transient Loads (LL):
Transient loads should be determined based on section 6A.2.3 of the AASHTO Manual for Bridge Evaluation.

The maximum moments should be determined by modeling the bridge as a beam, and dividing the maximum moment due to one lane of live loading by an equivalent strip width. Calculation of the equivalent strip width is discussed later in this document. If the bridge being rated is a simple span, Appendix E6A of the AASHTO Manual for Bridge Evaluation can be used to determine maximum moments for AASHTO trucks.

Design Live Loads: HL-93 Design Loads per the LRFD Design Specifications shall be used. The HL-93 loads include a design tandem, design truck and a lane load as well as an additional negative moment loading. The maximum moment caused by the design truck and design tandem must be multiplied by the Dynamic Load Allowance and added to the lane load moment, which does not include a Dynamic Load Allowance. The HL-93 truck axles and weights are given in appendix C6A.

Legal Live Loads: Legal live loads include AASHTO legal truck loads along with notional rating loads. The AASHTO legal truck loads are specified in Article 6A.4.4.2.1a of the AASHTO Manual for Bridge Evaluation, while the notional rating loads are specified in Article 6A.4.4.2.1b. All these loads will include dynamic load allowance factor. Axle spacing and weights can also be found in Appendix D6A of the AASHTO Manual for Bridge Evaluation.

Permit Live Load: Permit live loads are based on the specific permit truck.

Dynamic Load Allowance (IM):
Impact shall be evaluated as specified in Article 6A.2.3.3 of the AASHTO Manual for Bridge Evaluation.

The factor to be applied shall be taken as (1+IM/100), and is applied only axle loads, not lane loads. Generally IM shall be taken as 33% but can be modified according to C6A.4.4.3.

Evaluating Equivalent Strip

General:
Equivalent strip widths are determined in accordance with of the AASHTO LRFD Bridge Design Specifications.

The live load moments determined from the beam analysis must be divided by the equivalent strip width. The equivalent strip does not apply to the dead loads and the capacity of the bridge, but applies only to the live loads.

Skew Angle:
Equivalent strip widths for skewed bridges shall be reduced based on recommendations in the AASHTO LRFD Bridge Design Specifications.

Capacity of Bridge (Moment Resistance)
Concrete capacity shall be calculated in accordance with the AASHTO LRFD Bridge Design Specifications.

Maximum Reinforcement
The factored resistance of compression controlled prestressed and non-prestressed sections shall be reduced in accordance with the AASHTO LRFD Bridge Design Specifications.

Material Properties
If the concrete compressive strength f_c' is unknown then it may be estimated using Table 6A.5.2.1-1 of The AASHTO Manual for Bridge Evaluation. If the steel yield strength f_y is unknown, Table 6A.5.2.2-1 of the AASHTO Manual for Bridge Evaluation shall be used to determine a value for rating. Also section 6A.5 of the AASHTO Manual.

for Bridge Evaluation shall be used for reference for concrete. Alternatively, f_c' and f_y may be determined by testing material samples taken from the structure being rated. The strength reduction factor φ is determined by classifying sections as tension-controlled, transition, or compression-controlled.

Minimum Reinforcement
Concrete members that do not satisfy the minimum flexural reinforcement provisions of AASHTO LRFD Bridge Design Specifications shall have their strength reduced in accordance with 6A.5.7 of The Manual for Bridge Evaluation

Load Rating Equation

General:
The load rating should be determined in accordance of section 6A.4.2.1 of the AASHTO Manual for Bridge Evaluation. Equation 6A.4.2.1-1 shall be used to determine the rating factor, along with equations 6A.4.2.1-2 and 6A.4.2.1-3.

Rating factors shall be determined at critical locations. If the design level rating factors are below one, then the analyst must compute rating factors for the legal truck loads. If the minimum rating factors are still below one for legal loads posting must be considered per MaineDOT procedures.

Load Factors:
γ_{DC} shall be taken as 1.25 for reinforced concrete. (Table 6A.4.2.2-1). γ_{DW} shall be taken as 1.50, but if dimensions and materials are field verified 1.25 may be used. (Table 6A.4.2.2-1). γ_P shall be taken as 1.0 (Article 6A.2.2.3). γ_{LL} shall be taken from Table 6A.4.3.2.2-1. φ_C shall be determined from Table 6A.4.2.3-1 based on bridge inspections. 1.0 shall be used for φ_S (6A4.2.4-1). φ shall be determined as specified in AASHTO LRFD Design Bridge Design Specification as detailed above.

Design load factors for inventory and operating ratings are 1.75 and 1.35 respectively. Legal load factors shall be taken from Table 6A.4.4.2.3a-1 and be used for AASHTO truck loads and Table 6A.4.4.2.3b-1 for specialized hauling vehicles.

3. Slab Load Rating Using the Finite-Element Method

Construction of Finite Element Model

A finite element model of each bridge must be created. The finite element models can be created using solid, plate, or shell elements.

The model may assume

- Pin – pin boundary conditions,
- Linear elasticity
- Small deformations

Element performance should be verified by comparison with known analytical solutions for simple load cases. A Mesh refinement study must be performed to ensure convergence of the model. Skew angles may require the consideration of a combination of transverse and longitudinal bending moments

Extensive analyses have been done to verify these assumptions (Poulin 2012).

Evaluation of Loads

Same Loads will be evaluated as detailed in Section 2.

All loads should be determined with units of moment per length. (i.e. kN-m/m or lb-ft/ft

Application of Transient Live Loads

The application of vehicular live loads should be determined in accordance of section 6A.2.3.2 of the AASHTO Manual for Bridge Evaluation

Each axle loads should be evenly distributed between two wheel loads. Each wheel should be treated as a 10” by 20” uniform pressure.

Capacity of Bridge (Moment Resistance)

Capacity of the bridge is determined in the same manner as detailed in Section 2.

Load Rating Equation

The load rating equation is the same as detailed in Section 2.

4. Example Using Conventional Method

Flat Slab Concrete Bridge Example

Bridge Information:
Milford Bridge # 2070

Span Length:		27.349′ (centerline to centerline)
Span Width:		30.333′
Skew Angle:		15° (clockwise)
Slab Thickness:		16.5″
Wearing Surface Thickness:		4.5″ (concrete – average of 6″ and 3″ on drawings)
Curb Width:		14″ (both sides)
Curb Height (above slab):		12″ (both Sides)
ADTT(one direction):		unknown
Reinforcement:		#10 Bars (1.270″ diameter) at 6.5″ O.C.
Clear Cover:		1″
Material:	Concrete:	f'_c = 2.5 ksi (modular ratio of 10)
	Reinforced Steel:	f_y = 40 ksi (unknown bridge after 1954)

Dead Load Analysis

Components (DC)

Concrete slab

$$\frac{16.5}{12}\times 1\times 0.150 = 0.206 \text{ kip / ft}$$

Curb:

$$\frac{2\times\left(\frac{14}{12}\times\frac{12}{12}\right)\times 0.150}{30.33} = 0.012 \text{ kip/ft}$$

DC:

$$0.206 + 0.012 = 0.218 \text{ kip / ft}$$

M_{DC}:

$$M_{DC} = \frac{WL^2}{8} = 20.4 \text{ kip ft / ft}$$

Wearing Surface (DW)

Concrete wearing surface

$\frac{4.5}{12} \times 1 \times 0.150$ = 0.056 kip /ft

$M_{DW} = \frac{WL^2}{8}$ = 5.26 kip ft / ft

Live Load Analysis

Table 1 – Max Live Load Moments

Transient Load	Max Moment (M_{LL+IM})(Appendix E6A) kip-ft
Max Design Live Load (HL -93)	445
Type 3 truck unit	266
Type 3S2	259
Type 3-3	219
SU4	317
SU5	346
SU6	376
SU7	388
Notional Load	394

All values are maximum mid-span moments. Maximum design live load is the maximum moment cause by the either the truck or the tandem with dynamic load allowance factor. Lane load must be added to maximum moment, and the lane load does not include a dynamic load allowance factor.

Equivalent Strip Width

One Lane Loaded

$E = 10.0 + 5.0\sqrt{L_1 W_1}$

L_1 = Lesser of 27.3 ft or 60 ft = 27.4 ft

W_1 = Lesser of 30.3 ft or 30 ft = 30 ft

$E = 10.0 + 5.0\sqrt{27.3 \times 30}$

= 153 in

= 12.8 ft

Multilane Loaded

$E = 84.0 + 1.44\sqrt{L_1 W_1} \le \frac{12.0W}{N_L}$

L_1 = Lesser of 27.3 ft or 60 ft = 27.3 ft

W_1 = Lesser of 30.3 ft or 60 ft = 30.3 ft

$E = 84.0 + 1.44\sqrt{27.3 \times 30.3}$

= 126 in

= 10.5 ft

$N_L = \frac{30.3}{12} = 2$ Design Lanes

$\frac{12.0W}{N_L} = \frac{12.0 \times 30.3}{2} = 182 \text{ in} \geq 125 \text{ in}$ OK

Use E = 10.5 ft since 10.5 ft $\leq$ 12.8 ft

Skew Reduction Factor

$r = 1.05 - 0.25 \tan\theta$

$\theta = 15^{\circ}$ (clockwise)

$r = 1.05 - 0.25 \tan(15)$

$r = 0.983$

$E = r \times E$

$= 0.983 \times 10.5$

$= 10.3$ ft

Compute Capacity of Slab (Nominal Resistance)

$M_n = f_y \left(d - \frac{a}{2} \right)$

$c = \frac{A_s f_y}{0.85 f_c' b \beta_1}$

$A_s \quad \frac{1.27^2 \times \pi}{4} \times \frac{12}{6.5}$

$= 2.34 \text{ in}^2 / \text{ft}$

$\beta_1 = 0.85$

$b = 12$ in

$f_y = 40$ ksi

$f_c' = 2.5$ ksi

$c = \frac{2.34 \times 40}{0.85 \times 2.5 \times 12 \times 0.85}$

$= 4.3$

$a \quad \beta_1 c$

$= 0.85 \times 4.3$ in

$= 3.67$ in

d = Distance to CG of steel from compression face of concrete

$= 16.5 - 1 - \frac{1}{2} \times 1.27$

$= 14.9$ in

$M_n = 2.34 \times 40 \times \left(14.9 - \frac{3.67}{2} \right)$

= 1220 kip in / ft
= 102 kip ft / ft

Minimum Reinforcement (6A.5.7 of The Manual for Bridge Evaluation)
Amount of reinforcement must be sufficient to develop M_r equal to the lesser of:
$1.2M_{cr}$ or $1.33M_u$

M_r $= \varphi M_n = 0.90 \times 102$ kip ft
$= 91.4$ kip ft

1.) $1.33M_u$ $= 1.33 \times \left(1.75 \times \frac{445}{10.3} + 1.25 \times 20.4 + 1.25 \times 5.26 \right)$
$= 143$ kip ft > 91.4 No Good

2.) $1.2M_{cr}$ $= 1.2\left(S_c \left(f_r + f_{cpe} \right) - M_{dnc} \left(\frac{S_c}{S_{nc}} - 1 \right) \right) \geq 1.2\left(S_c f_r \right)$

Where a monolithic or composite section is designed to resist all the loads, S_{nc} is substituted for S_c. In this Case $f_{cpe} = 0$, therefore:

$1.2M_{cr}$ $= 1.2\left(S_{nc} f_r \right)$

S_{nc} $= \frac{I}{y_t}$

I = moment of inertia of uncracked section (neglecting reinforcement steel)
$= \frac{1}{12} \times 12 \times 16.5^3 = 4490 \text{ in}^4$

y_t = distance from neutral axis of the uncracked section to the extreme tension fiber
$= \frac{16.5}{2} = 8.25$ in

S_{nc} $= \frac{4490}{8.25} = 544 \text{ in}^3$

f_r $= 0.37\sqrt{f_c'} = 0.37\sqrt{3} = 0.585$ ksi

M_{cr} $= 0.585 \times 544 = 319$ kip in $= 26.5$ kip ft

$1.2M_{cr}$ $= 1.2 \times 26.5 = 31.9$ kip ft < 91.4 kip ft OK

The section meets the requirements for minimum reinforcement

Maximum Reinforcement (6A.5.6 of The Manual for Bridge Evaluation)
Current provisions of the LRFD specifications have eliminated the check for maximum reinforcement. Instead, the factored resistance (φ factor) of compression controlled sections shall be reduced in accordance with LRFD Design Article 5.5.4.2.1 This approach limits the capacity of over-reinforced (compression controlled) sections.

The net tensile strain ε_t is the tensile strain at nominal strength and determined by strain compatibility using similar triangles.

Given allowable concrete strain of 0.003 and depth to neutral axis c = 4.316 in (solved above):

$$\frac{\varepsilon_c}{c} = \frac{\varepsilon_t}{d-c}$$
$$\frac{0.003}{4.32} = \frac{\varepsilon_t}{14.9-4.32}$$

$\varepsilon_t = 0.00733$

For $\varepsilon_t = 0.00733 > .005$, the section is tension controlled and Resistance Factor φ shall be taken as 0.90

Shear

Concrete slabs and slab bridges designed in conformance with AASHTO specifications may be considered satisfactory for shear

Also shear need not be checked for design load and legal load ratings of concrete members.

General Load- Rating Equations (6A.4.2 of The Manual for Bridge Evaluation)

$$RF = \frac{c-(\gamma_{DC})(DC)-(\gamma_{DW})(DW)\pm(\gamma_P)(P)}{(\gamma_L)(LL+IM)} \qquad \text{Eq. 6A.4.2 – 1}$$

Evaluation of Factors (for Strength Limit States)

Resistance Factor, φ (LRFD Design 5.5.4.2)

φ = 0.90 For Flexure

Condition Factor, φ_c (6A.4.2.3)

φ_c = 1.0 No Deterioration

System Factor, φ_s (6A.4.2.4)

φ_s = 1.0 Slab Bridge

Design Load Rating (6A.4.3)

Strength I Limit State (6A.5.4.1)

$$RF = \frac{(\varphi)(\varphi_s)(\varphi_c)(R_n)-(\gamma_{DC})(DC)-(\gamma_{DW})(DW)\pm(\gamma_P)(P)}{(\gamma_L)\left(\frac{M_{LL+IM}}{E}\right)}$$

Load	Inventory	Operating	
γ_{DC}	1.25	1.25	
γ_{DW}	1.50	1.50	Asphalt was not field verified
γ_L	1.75	1.35	

Table 6A.4.2.2-1

Inventory:

$$RF = \frac{(0.9 \times 1.0 \times 1.0 \times 102) - (1.25 \times 20.4) - (1.50 \times 5.26) - (1.0 \times 0)}{\left(1.75 \times \frac{445}{10.3}\right)}$$

$$= 0.767$$

Operating:

$$RF = \frac{(0.9 \times 1.0 \times 1.0 \times 102) - (1.25 \times 20.4) - (1.50 \times 5.26) - (1.0 \times 0)}{\left(1.35 \times \frac{445}{10.3}\right)}$$

$$= 0.994$$

Service Limit State

No service limit states apply to reinforced concrete bridges.

As RF < 1.0 for HL-93, evaluate the bridge for Legal Loads.

Legal Load Rating (6A.4.4)

Live Loads: AASHTO Legal Trucks – Type 3, Type 3S2, Type 3-3

(6A.4.4.2.1) Specialized Hauling Vehicles – SU4, SU5, SU6, SU7, Notional Rating

E = 10.278

IM = 33% (Unknown riding surface)

	Type 3	Type 3S2	Type 3-3	SU4	SU5	SU6	SU7	Notional
M_{LL+IM} (kip ft)	266	259	219	317	346	376	388	394
$\frac{M_{LL+IM}}{E}$ (kipft/ft)	25.8	25.2	21.3	30.8	33.6	36.6	37.8	38.3

Strength I Limit State (6A.5.4.2.1)

For AASHTO Trucks:

ADTT =Unknown

γ_L = 1.80

$$RF = \frac{(0.9 \times 1.0 \times 1.0 \times 102) - (1.25 \times 20.4) - (1.50 \times 5.26) - (1.0 \times 0)}{\left(1.80 \times \frac{M_{LL+IM}}{E}\right)}$$

For Specialized Hauling Vehicles:
ADTT = Unknown
γ_L = 1.60

$$RF = \frac{(0.9 \times 1.0 \times 1.0 \times 102) - (1.25 \times 20.4) - (1.50 \times 5.26) - (1.0 \times 0)}{\left(1.60 \times \frac{M_{LL+IM}}{E}\right)}$$

	Type 3	Type 3S2	Type 3-3	SU4	SU5	SU6	SU7	Notional
RF	1.25	1.28	1.52	1.18	1.08	0.992	0.961	0.947

No Posting required as RF> 1.0 for all AASHTO Legal Loads

Service Limit State

No service limit states apply to reinforced concrete bridge members at the Legal Load Rating.

Shear

Concrete slab and slab bridges designed in conformance with AASHTO specifications may be considered satisfactory for shear. Shear need not be checked for legal loads

5. Example Using the Finite-Element Method

Flat Slab Concrete Bridge Example

Bridge Information:
Milford Bridge # 2070

Span Length:		27.3′ (Centerline to Centerline)
Span Width:		30.3′
Skew Angle:		15° (clockwise)
Slab Thickness:		16.5″
Wearing Surface Thickness:		4.5″ (Concrete Surface) (Average of 6″ and 3″)
Curb Width:		14″ (Both sides)
Curb Height (above slab):		12″ (Both Sides)
ADTT(one direction):		Unknown
Reinforcement:		#10 Bars (1.270″ Diameter Bars) at 6.5″ O.C.
Clear Cover:		1″
Material:	Concrete:	f'_c = 2.5 ksi (Modular Ratio of 10)
	Reinforced Steel:	f_y = 40 ksi (Unknown Bridge after 1954)

Finite Element Model Details
The finite element model was constructed with 8-noded, shear deformable plate elements which are described in some detail in Bhatti (2006). Quadratic shape functions were used to interpolate element displacements. Shear contributions to the element stiffness matrix are under-integrated using 2x2 Gaussian quadrature, and 3x3 Gaussian quadrature is used for integrating the bending contributions to the element stiffness matrix. An isoparametric element formulation was used to allow the use of non-rectangular elements and accommodate skewed supports. Pinned supports, linearly elastic materials and small deformations were assumed in the analysis.

A mesh refinement study was conducted to ensure convergent and accurate results. The mesh refinement study relied on uniform meshes, and examined the effects of both the number of longitudinal and transverse elements used in the model on the maximum live load moments due to the HL-93 tandem truck with lane load. The truck was placed at the position on the bridge that provided the maximum moment. Dead load moments converged at lower levels of mesh refinement than live loads.

Figure 1 shows a plan view of the finite-element mesh with 14 by 14 elements. The elements adjacent to the top and bottom slab edges are thinner because two elements are used from the slab edge to the point nearest the curb at which the load can be positioned. The top and bottom row of elements correspond to the curb width of 14 inches. The elements just inside of those correspond to the 24 inch width that the truck cannot be placed within to satisfy the AASHTO requirement that no wheel be placed closer than 24” from a curb. The rest of the elements have a width of 28.8 inches.

Figure 2 is a plot of max moments vs. number of transverse elements to ensure convergence of the model. Each line on the graph represents different amount longitudinal elements. As can be seen from the graph, the models converge to a consistent value around 14 longitudinal and transverse elements. All the mesh sizes more refined than 14 longitudinal and 14 transverse elements provide results within 0.5% of the 14 by 14 mesh. The skew angle of 15 degrees is considered small enough that the analysis can be based only on longitudinal bending moments.

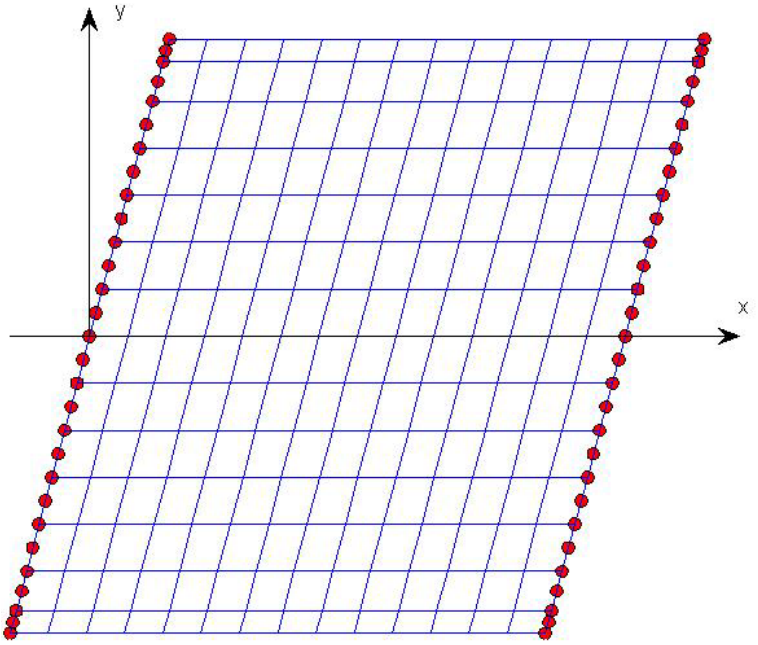

Figure 1 – Typical Finite-Element Mesh

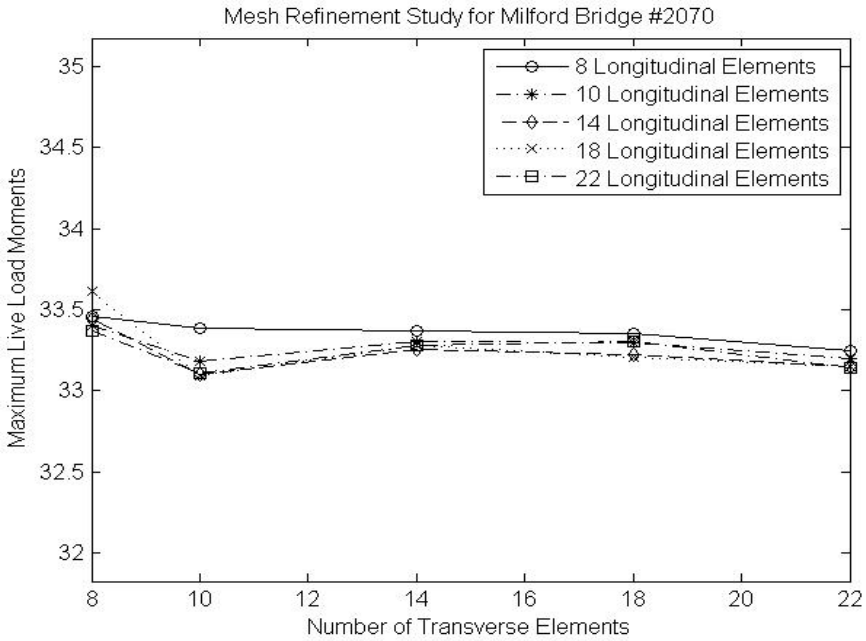

Figure 2 – Results of Mesh Refinement Study

Dead Load Analysis
The curb weights are treated as uniform pressures acting over the width of each curb along the span of the bridge. The slab weight was treated as a uniform pressure that acts over the entire bridge, and the wearing surface was treated as a uniform pressure acting between the curb faces.

Tables 2 and 3 give the dead load moments at the location of the maximum live load moment. These values are given for each rating vehicle because the location of maximum live load moment varies with truck type.

Table 2 – DC Moments at Location of the Maximum LL Moment

Transient Load	Max Moment (M_{DC}) kip-ft / ft
Max Design Live Load(HL -93)	19.0
Type 3 truck unit	19.0
Type 3S2	19.0
Type 3-3	19.7
SU4	19.0
SU5	19.0
SU6	19.7
SU7	19.7
Notional Load	19.7

Table 3 – DW Moments at Location of the Maximum LL Moment

Transient Load	Max Moment (M_{DW}) kip-ft /ft
Max Design Live Load(HL -93)	4.11
Type 3 truck unit	4.11
Type 3S2	4.11
Type 3-3	4.21
SU4	4.11
SU5	4.11
SU6	4.21
SU7	4.21
Notional Load	4.21

Live Load Analysis
Figure 3 shows the placement of the HL-93 Tandem Load which resulted in the maximum moment for all the different load combinations. Not shown is the lane load that acts over a ten foot loaded width positioned transversely within each lane. The center of the lane load is centered on the center of the truck. Each truck is considered to be a lane so there are two lane loads applied in Figure 3, one for each lane. The location to the center of the bottom truck's back axle is (103.0, -108.0) inches from center of the left pier in the *x*-*y* coordinate system indicated in Figure 3. The vertical spacing of the trucks is 6 ft from the center of the top wheels of the bottom truck to the center of the bottom wheels of the top truck. An *x*-position offset was used to place the truck at the same relative

distance away from the supports. This was done by placing the trucks at the same skew angle of the bridge.

Table 4 shows the maximum live load moments produced by each rating vehicle. The table provides the maximum moment, where the maximum moment occurs and the location and direction of the truck that produces the maximum moment.

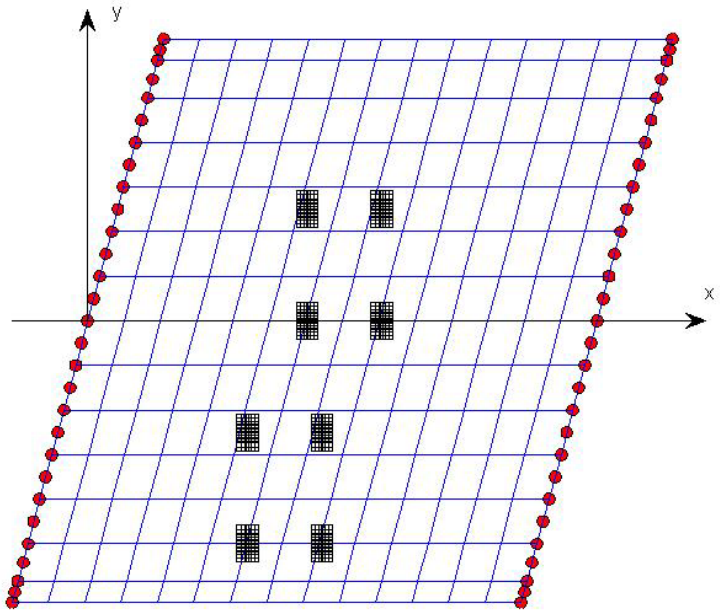

Figure 3 – Placement of the HL-93 Tandem to Maximize Live Load Moment

Table 4 – Maximum Live Load Moments including Dynamic Load Allowance

Transient Load	Max Moment (M_{LL+IM}) kip-ft / ft	Location of Maximum Moment (inches)	Location of Truck at Max Moment (inches)	Number of Lanes	Direction of Truck
Max Design Live Load (HL -93)	33.3	(149.0, -144)	(103.0, -108.0)	2	Right
Type 3 truck unit	19.7	(149.0, -144.0)	(148.6, -108.0)	2	Left
Type 3S2	19.0	(125.5, -144.0)	(-236.9, -108.0)	2	Right
Type 3-3	16.2	(140.6, -175.0)	(107.3, -108.0)	2	Right
SU4	23.3	(125.5, -144.0)	(73.2, -108.0)	2	Right
SU5	25.1	(125.5, -144.0)	(78.7, -108.0)	2	Right
SU6	27.2	(140.6, -175.0)	(48.4, -108.0)	2	Right
SU7	28.4	(140.6, -175.0)	(6.6, -108.0)	2	Right
Notional Load	28.5	(140.6, -175.0)	(298.0, -108.0)	2	Left

All loads reported generate the lowest rating factor for each specific truck type. The truck positions are the distance to the center of the back axle of the bottom truck to the center of the left pier. For the spacing of multiple trucks the center of the closest wheels are placed 6 ft away from each other per AASHTO. The trucks are also offset in the traffic

direction based on the skew of the bridge, which leads to each wheel being at the same relative distance away from the pier in the span direction.

Compute Capacity of Slab (Nominal Resistance)
Capacity calculations are given in section 4.

General Load- Rating Equations (6A.4.2 of The Manual for Bridge Evaluation)

$$RF = \frac{C - (\gamma_{DC})(DC) - (\gamma_{DW})(DW) \pm (\gamma_p)(P)}{(\gamma_L)(LL + IM)} \qquad \text{Eq. 6A. 4.2. } -1$$

Evaluation of Factors (for Strength Limit States)

Resistance Factor, φ (LRFD Design 5.5.4.2)

φ = 0.90 For Flexure

Condition Factor, φ_c (6A.4.2.3)

φ_c = 1.0 No Deterioration

System Factor, φ_s (6A.4.2.4)

φ_s = 1.0 Slab Bridge

Design Load Rating (6A.4.3)

Strength I Limit State (6A.5.4.1)

$$RF = \frac{(\varphi)(\varphi_S)(\varphi_C)(R_n) - (\gamma_{DC})(DC) - (\gamma_{DW})(DW) \pm (\gamma_P)(P)}{(\gamma_L)\left(\frac{M_{LL+IM}}{E}\right)}$$

Load	Inventory	Operating	
γ_{DC}	1.25	1.25	
γ_{DW}	1.50	1.50	Asphalt thickness not field verified
γ_L	1.75	1.35	

Table 6A.4.2.2-1

Inventory:

$$RF = \frac{(0.9 \times 1.0 \times 1.0 \times 102) - (1.25 \times 19.0) - (1.50 \times 4.11) - (1.0 \times 0)}{(1.75 \times 33.3)}$$

$$= 1.05$$

Operating:

$$RF = \frac{(0.9 \times 1.0 \times 1.0 \times 102) - (1.25 \times 19.0) - (1.50 \times 4.11) - (1.0 \times 0)}{(1.35 \times 33.3)}$$

$= 1.36$

Service Limit State

No service limit states apply to reinforced concrete bridges.

Since RF > 1.0 for HL-93, evaluation of the bridge for legal loads is not needed. Legal load rating is done here only as an example.

Legal Load Rating (6A.4.4)

Live Loads: AASHTO Legal Trucks – Type 3, Type 3S2, Type 3-3

(6A.4.4.2.1) Specialized Hauling Vehicles – SU4, SU5, SU6, SU7, Notional Rating

	Type 3	Type 3S2	Type 3-3	SU4	SU5	SU6	SU7	Notional
M_{LL+IM} (kip ft/ft)	19.7	19.0	16.2	23.3	25.1	27.2	28.4	28.5
M_{DC} (kip ft/ft)	19.0	19.0	19.7	19.0	19.0	19.7	19.7	19.7
M_{DW} (kip ft/ft)	4.11	4.11	4.21	4.11	4.11	4.21	4.21	4.21

Strength I Limit State (6A.5.4.2.1)

For AASHTO Trucks:

ADTT =Unknown

$\gamma_L = 1.80$

$$RF = \frac{(0.9 \times 1.0 \times 1.0 \times 102) - (1.25 \times M_{DC}) - (1.50 \times M_{DW}) - (1.0 \times 0)}{(1.80 \times M_{LL+IM})}$$

For Specialized Hauling Vehicles:

ADTT = Unknown

$\gamma_L = 1.60$

$$RF = \frac{(0.9 \times 1.0 \times 1.0 \times 102) - (1.25 \times M_{DC}) - (1.50 \times M_{DW}) - (1.0 \times 0)}{(1.60 \times M_{LL+IM})}$$

	Type 3	Type 3S2	Type 3-3	SU4	SU5	SU6	SU7	Notional
RF	1.72	1.78	2.06	1.64	1.52	1.38	1.32	1.32

No Posting required as RF> 1.0 for all AASHTO Legal Loads

An average increase in rating factor of 38.2% was seen going from the strip width method to the finite element method for this bridge. This was predominantly caused by the maximum live load moments decreasing by an average of 24.5% going from strip width method to the finite element models. Even though this specific bridge does not go from a rating factor below one for the strip width method to above one using the finite element method, it could happen with this larger increase in rating factors.

6. References

AASHTO (2008). *Manual for Bridge Evaluation*. American Association of Highway and Transportation Officials, Washington, D.C.

AASHTO (2007). *LRFD Bridge Design Specifications*. American Association of Highway and Transportation Officials, Washington, D.C.

Bhatti, A. (2006). *Advanced Topics in Finite Element Analysis of Structures*. John Wiley & Sons, New York, NY.

MaineDOT (2003), *Bridge Design Guide*. Maine Department of Transportation, Augusta, ME.

Poulin, T.J. (2012). "Development of Improved Load Rating Procedures and Retrofitting Techniques for Flat Slab Bridges." M.S. thesis, Dept. of Civil and Environmental Engineering, University of Maine.